The Middle Fork Plutonic Complex:

A plutonic association of coeval peralkaline and metaluminous magmas in the north-central Alaska Range

by

Diana Nelson Solie

Dissertation submitted to the Faculty of the
Virginia Polytechnic Institute and State University
in partial fulfillment of the requirements for the degree of
Doctor of Philosophy
in
Department of Geological Sciences

APPROVED:

A. K. Sinha

D. A. Hewitt

J. R. Craig

J. D. Rimstidt

S. E. Swanson

December 30, 1988

Blacksburg, Virginia

The Middle Fork Plutonic Complex:

A plutonic association of coeval peralkaline and metaluminous magmas in the north-central Alaska Range

by

Diana Nelson Solie

A. K. Sinha

Department of Geological Sciences

(ABSTRACT)

The 57 m.y. Middle Fork Plutonic Complex (MFPC) intrudes Paleozoic metasedimentary rocks south of the Farewell Fault zone in the north-central Alaska Range. Though spatially related to the late Cretaceous - Early Tertiary subduction-related Alaska Range batholith, MFPC is more characteristic of an extensional or anorogenic setting. A swarm of basalt, hawaiite and rhyolite dikes east of the complex intruded, and was intruded by, the plutonic rocks. Approximately 30% of the exposed rock in the 125 km² complex is hedenbergite - fayalite syenite, ≃20% is peralkaline arfvedsonite - biotite alkali-feldspar granite (AF granite), and ≤20% is pyroxene - olivine - biotite gabbro. The rest is a mixed unit including clinopyroxene - biotite - amphibole diorite, and hornblende - biotite granite (HB granite).

K-Ar and Rb-Sr radiometric dating of rock types shows that they are coeval. Their close spacial and temporal relationships led to complex magmatic interactions. Calculated initial $^{87}Sr/^{86}Sr$ for gabbro and diorite group around 0.705 to 0.706. HB granites are heterogeneous, but fall mostly around 0.707 to 0.708. Hypersolvus syenites and AF granites form an isochron with initial $^{87}Sr/^{86}Sr$ of 0.70965. These groupings suggest that at least three different magmas formed the MFPC; scatter of isotopic data reflects mu-

tual contamination and assimilation. Trends in whole rock and mineral chemistry also reflect interactions between the magmas.

Consanguinous hypersolvus syenite and AF granite mineralogy appears to be controlled by fluorine in the magma chamber. Magmatic mineral assemblages reflect increasingly reduced magmatic conditions; subsolidus oxidation, indicated by mafic mineralogy and cathodoluminescence, is due to magmatic process rather than introduction of external components.

Eruptive stratigraphy, as predicted by intrusive history of MFPC, compares favorably with volcanic stratigraphies of peralkaline volcanic systems worldwide, and MFPC may be modelled as the root zone of a peralkaline volcanic system. The common absence of mafic volcanism during peralkaline volcanic activity may be due to entrapment of mafic magmas within the peralkaline magma chamber. The result of this entrapment is seen at the present level of erosion of MFPC, as extensive mafic enclave swarms and pull-apart dikes within syenites in the pluton's core.

Acknowledgements

Thanks go to my committee chairman, A. K. Sinha, for his help and encouragement during this study, and also to my committee members, D. A. Hewitt, J. R. Craig, and S. C. Erikkson at Virginia Tech, and S. E. Swanson at the University of Alaska, Fairbanks. Thanks also to J. D. Rimstidt for filling in for S. C. Erikkson during her absence.

This study started as part of a mapping project with the Alaska Division of Geological and Geophysical Surveys, whose financial support is gratefully acknowledged. Special thanks go to project managers Wyatt Gilbert, Tom Bundtzen and Jeff Kline for their encouragement, help and friendship. Also, the field assistance of Kate Bull, Karen Clautice and Dan Solie was invaluable, and greatly appreciated.

Many people have been important to my graduate school experience. Among the most important, in terms of sharing knowledge, experiences and fun, have been my colleagues in 'Lab Central': Charlotte Allen, John Hogan, Rob Badger, Dave Wayne, Russ Guy, and Joe Jurinsky. Friends like Charlotte Allen and Julie Herman have been especially crucial in helping me maintain a balance between work and play, and I have greatly enjoyed their friendship. Other fellow graduate students, past and present, are also here thanked for their friendship, encouragement and moral support. Llyn Sharp was a wonderful help, not only in the photography lab, but as a friend who helped me

appreciate the beauties of southwestern Virginia. I also want to thank my musician friends, especially Jana Ruble and Linda Plaut, for the fun and great discussions, and for keeping me reminded that life is a multi-faceted adventure.

Thanks also go to Hal Pendrak for knowing how to do everything in the lab, and sharing his knowledge. Todd Solberg's assistance on the microprobe was helpful.

The help and encouragement of D. R. Wones, under whom this study was started, is gratefully remembered.

The friendship, understanding and patience of my husband Daniel throughout our time in graduate school has been above and beyond the call of duty, and I thank him. I also thank my parents for bringing me up to believe that I could do whatever I set out to do.

Table of Contents

List of Illustrations

List of Tables

Chapter 1: The Geology of the Middle Fork Plutonic Complex

Introduction

The early Tertiary Middle Fork Plutonic Complex (MFPC) in north-central Alaska Range (Figure 1) consists of a suite of diverse lithologies which include olivine - clinopyroxene ± orthopyroxene - biotite gabbro, clinopyroxene - biotite - amphibole diorite, faylalite - clinopyroxene syenite, peralkaline biotite - arfvedsonite - alkali-feldspar granite, metaluminous to peraluminous hornblende - biotite granite, alkali-feldspar quartz porphyritic rhyolite, and aphanitic to fine-grained basalt and hawaiite. The close spacial and temporal relationship between such widely diverse magmas led to a broad spectrum of magmatic processes. Rapid uplift and erosion of the MFPC has left more than 60% of the 125 km^2 complex exposed. This excellent exposure offers an unusual oportunity to study the petrogenetic relationships between coeval, contrasting magmas. In this study, rocks of the MFPC are characterized through bulk rock major and trace elements, Rb-Sr isotopic composition, and mineral chemistry to establish the petrogenetic relationships of the magmas within the complex.

The intrusive history and compositional range of rocks of the MFPC are the plutonic equivalent of a typical peralkaline volcanic suite. Silicic peralkaline volcanism

is commonly preceded by emplacement of mafic extrusives, with only minor volumes of mafic lavas associated with the main phase of peralkaline activity. The commingling nature of gabbroic/syenite contacts in the MFPC suggests that the mafic magma was intercepted within the magma chamber rather than erupted. Field, mineralogic and isotopic data from the MFPC yield information about the plutonic root zone of a model peralkaline volcanic system.

The MFPC is comparable lithologically and geochemically to anorogenic suites (Loiselle and Wones, 1979) in other parts of the world, such as the Younger Granites of Niger and Nigeria, the Pikes Peak batholith, Colorado, the Topsails igneous terrane, Newfoundland, and the A-type granites of Lachland Fold Belt, Australia. However, in contrast to the anorogenic setting typical of these suites, the MFPC was emplaced in a tectonically active region, contemporaneously with calc-alkaline magmatism of the Alaska Range - Talkeetna Mountains magmatic belt. The Tertiary age of the MFPC is also in contrast to most anorogenic suites, which are typically Precambrian.

The complex was first described as a composite intrusive containing granodiorite, quartz monzonite and syenite (Reed and Elliott, 1968). No further study was made of the MFPC until 1982, when the mapping project which resulted in Plate I was initialized by the Alaska Division of Geological and Geophysical Surveys. An open-file report (Solie, 1983) presents initial results from this study; the present study is an expansion of the earlier work (Solie, 1983). More detailed information about physiographic setting is given in Appendix A.

Host rocks of the MFPC are a low-grade meta-sedimentary sequence of deep-water turbidites and hemipelagic deposits characterized by graptolitic shale, calcareous sandstone, silty limestone, and laminated limestone of Cambrian to Devonian age (Gilbert and Solie, 1983; Gilbert and Bundtzen, 1983) (Plate I). The rocks in direct contact with the exposed plutonic rocks of the MFPC are predominantly Silurian to

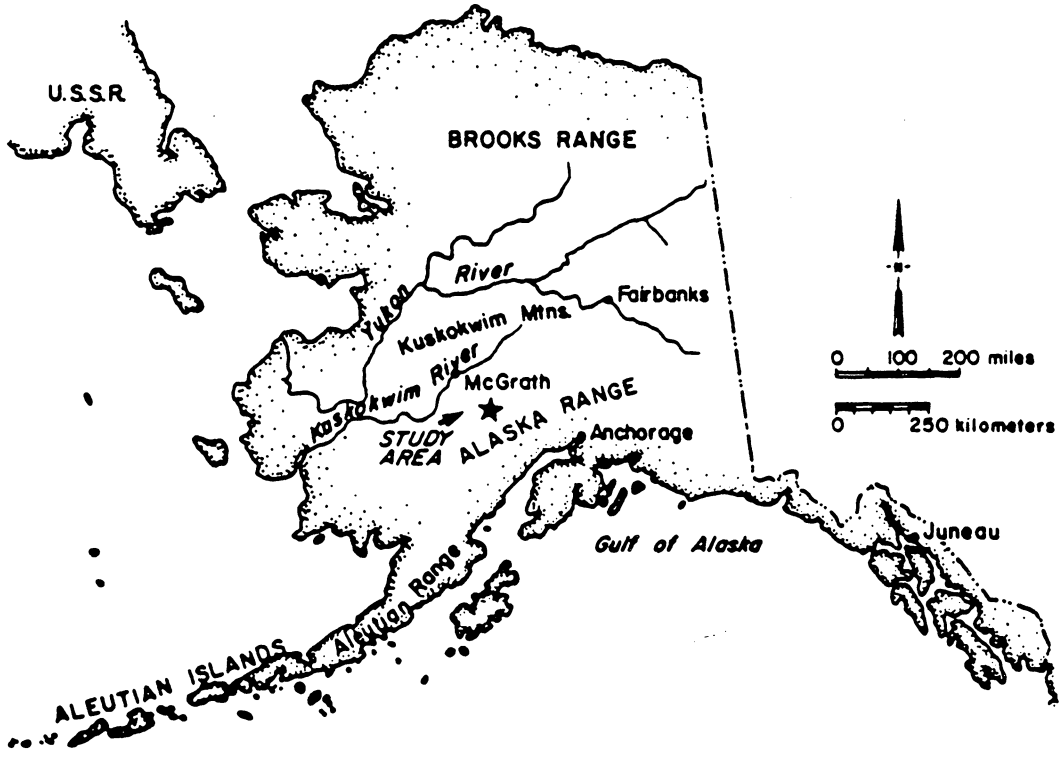

Figure 1. Location map: The Middle Fork Plutonic Complex is shown as a star, on the north flank of the Alaska Range.

Devonian phyllitic calc-sandstones and silty limestones. These very thin (≃1 cm) to very thick (≃5 m) bedded rocks locally contain subordinate amounts of black shale, grey marble, granule conglomerate, and siltstone. Many of the layers are now phyllite as a result of regional metamorphism. The plutonic rocks transect bedding planes of the host rocks. There is no noticeable increase in deformation of host rocks close to the plutonic contact. A contact aureole extends for about 200-300 meters, in which the metasediments are fine-grained hornfelses and recrystallized marbles. At the syenite-country rock (Ss; Plate I) boundary, the contact is very irregular, with syenitic dikes of varying sizes extending 1-2 km into the host rocks, crosscutting foliation. Extensive recrystallization of country rock to new assemblages, and small syenitic patches in the southwest contact area of the complex (Figure 2) suggests that syenite is present just below the exposed metasediments in that area.

Thickness of the total stratigraphic section intruded by the MFPC is estimated to be about 4 km (Gilbert and Bundtzen, 1983). Cross-cutting quartz and calcite veinlets are present throughout the section. Dikes of probable Tertiary age have intruded the Paleozoic rocks, and are randomly oriented except in the area of the east-west trending dike swarm on the east side of the MFPC. Quaternary drift deposits representing at least six episodes of late Cenozoic glaciation occur throughout the study area (Kline and Bundtzen, 1986).

Rocks underlying the Cambrian strata are not exposed. It has been suggested that the exposed Paleozoic host rock package has been "tectonically stripped from its original substratum" based on the pervasive northward-verging recumbent isoclinal folding in the region (Jones et al., 1982). This folding, which probably occurred during pre-Early Jurassic (Jones et al., 1982) leads to an estimated minimum of 50 km of crustal shortening from Post River to Big River (Bundtzen and Gilbert, 1983). Evidence of this shortening and consequent crustal thickening in the study area is the northwest-verging

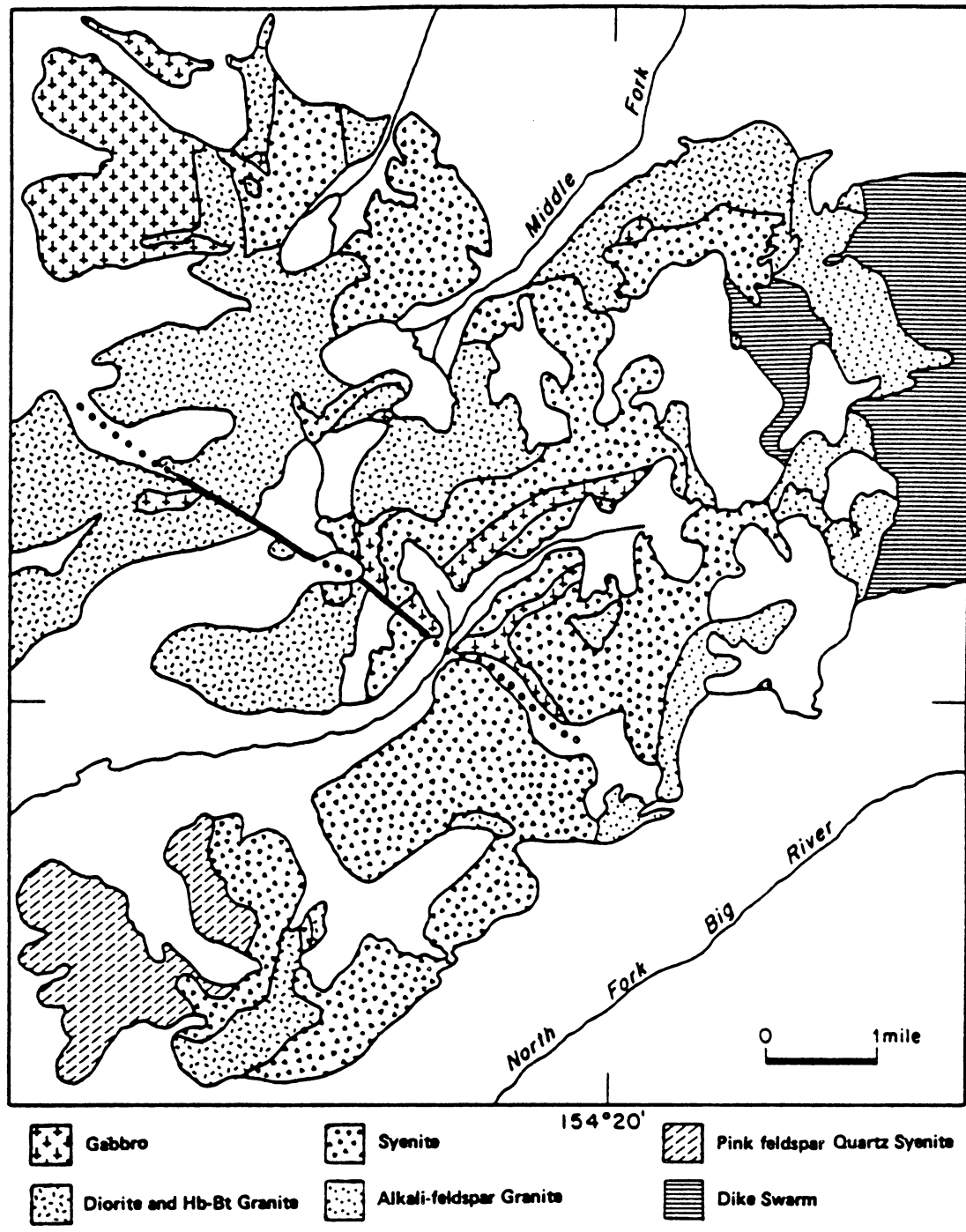

Figure 2. Generalized geologic map, Middle Fork Plutonic Complex (MFPC): Modified from Solie (1983).

nappe structure whose axial plane intersects the surface about 14 km north of the MFPC. Isoclinal folding at all scales is ubiquitous in the area. Related shears and thrust faults occur along bedding surfaces and within incompetent layers parallel to axial surfaces of large scale subisoclinal folds. A later folding event, whose fold axes are northeast-southwest, regionally warped the strata in broad open folds (Gilbert et al., 1982).

The Farewell fault zone, about 7 km north of the MFPC, is a segment of the Denali fault system which extends in a 2000 km arc across south central Alaska into southeastern Alaska (Figure 3). Cenozoic strike-slip movement on the Farewell fault system has been dextral. Total offset is not known, but is estimated to be at least 40 km, based on displacement of Tertiary clastic rocks from their source area (Dickey, 1984). Bundtzen (1982) states that offset on the Farewell segment probably was no more than 60 km; however, it may have been as much as 145 km, based on apparent offset of the Cretaceous-Paleozoic contact along the fault (Gemuts et al., 1983). Younger movement on the fault is vertical, south side upward, as evidenced by Holocene scarps.

The Big River fault, which truncates the MFPC on its west side, diverges from the Farewell fault system (Plate I). It can be traced southward for at least 30 km, and shows evidence of right lateral movement based on offsets of late Quaternary deposits, deflections in foliation attitudes and the apparent bend of ridges adjacent to the fault (Gilbert et al., 1989).

A northwest-southeast trending fault within the MFPC appears to downdrop the northeast side relative to the southwest based on the juxtaposition of a large (1.2 x 1.4 km) metasedimentary xenolithic block along the northeast side of the fault. Deformation is brittle where observed in outcrop, with brecciated plutonic rocks and abundant fractured surfaces with slickensides. No evidence for this fault was observed in the strata outside the plutonic complex, making the structure an intraplutonic feature. Thus, the

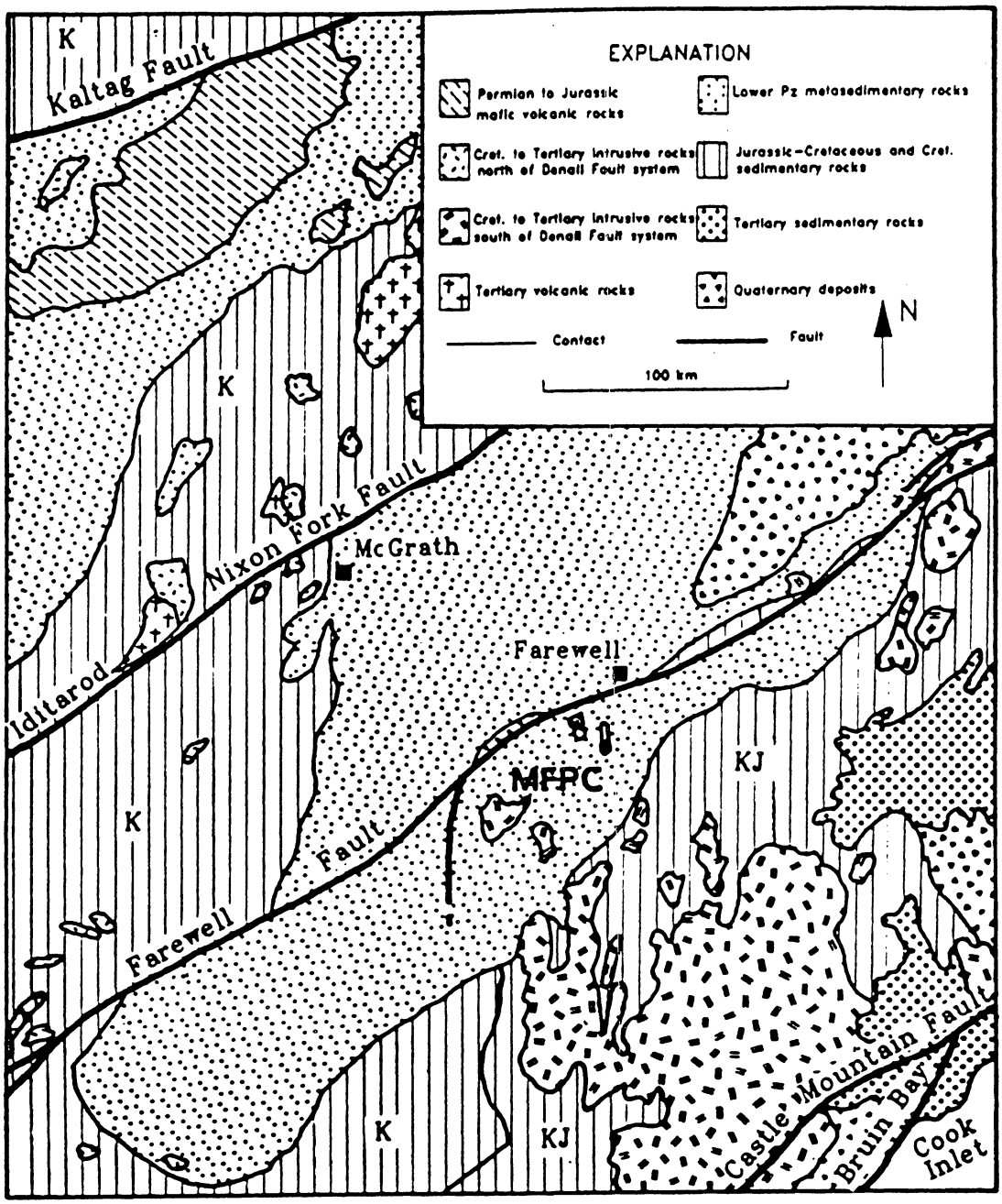

Figure 3. Geologic map of southwest portion of Alaska: Map is modified from Beikman (1980).

fault may reflect postmagmatic subsidence, perhaps in response to volcanic venting, possibly even caldera collapse.

Several other Tertiary intrusive bodies are present in close proximity to the MFPC (Plate I). A small ($\simeq$5 km^2) stock about 8 km north of the MFPC consists of fine- to medium-grained, hypidiomorphic-granular biotite quartz monzonite to granite. K-Ar age determinations on biotites yield results of 56.6 $\pm$ 1.7 m.y. (Gilbert et al., 1989) and 56.0 $\pm$ 1.6 m.y. (Reed and Lanphere, 1972). Just northwest of this stock, two small (each about 0.2 km across) monzonite plugs of presumed Tertiary age occur within a sheared fault sliver of Paleozoic or Mesozoic greenstone.

The Windy Fork pluton is an Oligocene peralkaline granite body about 10 km southeast of the MFPC (Reed and Miller, 1980). It is approximately 30 km^2 in exposed area. Directly south of the MFPC about 8 km is another small felsic intrusive body, presumed to be Tertiary (Reed and Elliott, 1970).

The Chip Loy prospect, 1.5 km north of the MFPC on Straight Creek, is a dioritic intrusion, first reported by Herreid (1968). A 12-m-thick sulfide-rich zone at the edge of the dike contains pyrrhotite, chalcopyrite, pentlandite and magnetite. This occurrence is thought to be Tertiary, based on similarities to Tertiary pyrrhotite-rich intrusions 25-35 km to the east (Gilbert et al., 1989).

As exposed, the MFPC itself consists of approximately 30% hedenbergite - fayalite syenite, and about 20% peralkaline sodic amphibole - biotite, alkali-feldspar granite. Less than 20% is augite - olivine - biotite gabbro. The rest of the complex, predominantly in the core and northern areas, is a mixed zone which includes meta- to peraluminous hornblende - biotite granite and quartz monzonite (hereafter collectively referred to as HB granites), and hornblende - biotite - augite diorite and monzodiorite (hereafter collectively referred to as diorites). A swarm of basalt to rhyolite dikes east of the complex intrudes, and is intruded by, the plutonic rocks (Figure 2 on page 5).

Both K-Ar and Rb-Sr data indicate similar ages for each of the major rock types in the MFPC. The median age is 58 m.y., and no age determination deviates more than 3 m.y. from this median. The contemporaneity of the magmas of the MFPC is also evident in the contact relationships between the rock types, as sharp intrusive relationships are rarely observed. More commonly, diffuse gradations and extremely irregular geometries between lithologies are characteristic, and suggest emplacement of magmas while in a semimolten state. Mafic enclaves are abundant in the diorites, syenites and hb-bt granites. Color index, mode and textures vary widely, particularly in diorites and HB granites at scales of outcrop to thin section. The complexity arising from this variability and the interactions between contrasting rock types leads to the questions: "How many different magmas were involved in the formation of the MFPC?" and "How do these magmas relate to one another?". In order to address these questions, a suite of samples from each of the most prevalent and homogeneous rock types was selected and characterized by major oxide, trace element and Rb/Sr isotope whole rock analyses. These data, in conjunction with mineral compositions and petrographic and textural information, were evaluated with respect to the relative effects of fractionation, contamination/assimilation and mixing on the the magmas of the MFPC.

Field Observations--Middle Fork Plutonic Complex

Mapping of the rocks of the MFPC by Solie is incorporated in the published colored map of the McGrath A-3 quadrangle (Gilbert et al., 1989) included in this report as Plate I. A generalized map of the MFPC is shown as Figure 2. On these maps, diorites and hornblende-biotite granites were lumped together as one map unit, due to the complex, close spatial interrelationship of the numerous varieties of these rocks.

Locations of samples which have been analysed for geochemical, petrologic, and isotopic data are shown in Figure 4. Additional samples which were used for field relationships and have not been analyzed are located on the overlay of Plate I (Plate II).

Intrusive relationships between lithologies are interpreted based on the presence of dikes, chill margins, brecciation, and inclusions. Mafic microgranitoid enclaves in contact zones between mafic and felsic lithologies are interpreted in some cases to suggest magma commingling. In other cases, contact relationships are ambiguous due to incomplete and/or inaccessible exposure, and the masking effect of superficial weathering patterns. A schematic summary of intrusive relationships between lithologies of the MFPC as interpreted from field observations is shown in Figure 5. Grain size terminology is after Williams et al., (1982) where fine-grained < 1mm, medium-grained = 1-5 mm, coarse-grained = 5 mm-3 cm, and very coarse-grained > 3 cm.

The term commingling is used herein, following the usage of Wiebe (1980), to indicate "mixing in which the original magmas (now rocks) retain their identities in the mixture at the outcrop scale." Hybridization, on the other hand, is taken to be "mixing in which the identities of the original magmas (now rocks) are obscured and/or in which a significant proportion of intermediate rock is apparent at the outcrop scale" (Wiebe, 1980, p. 197-8).

Field observations are discussed by map unit, from mafic to felsic in the following sections. These units are gabbro, diorite, hornblende-biotite granite, syenite, alkali-feldspar granite, pink-feldspar quartz syenite, and dike swarm. Of the approximately 125 km^2 of plutonic rocks exposed in the MFPC, about 30% is syenite, 20% is alkali-feldspar granite, and less than 20% is gabbro. The rest, more than 30%, consists of hornblende-biotite granite and diorite.

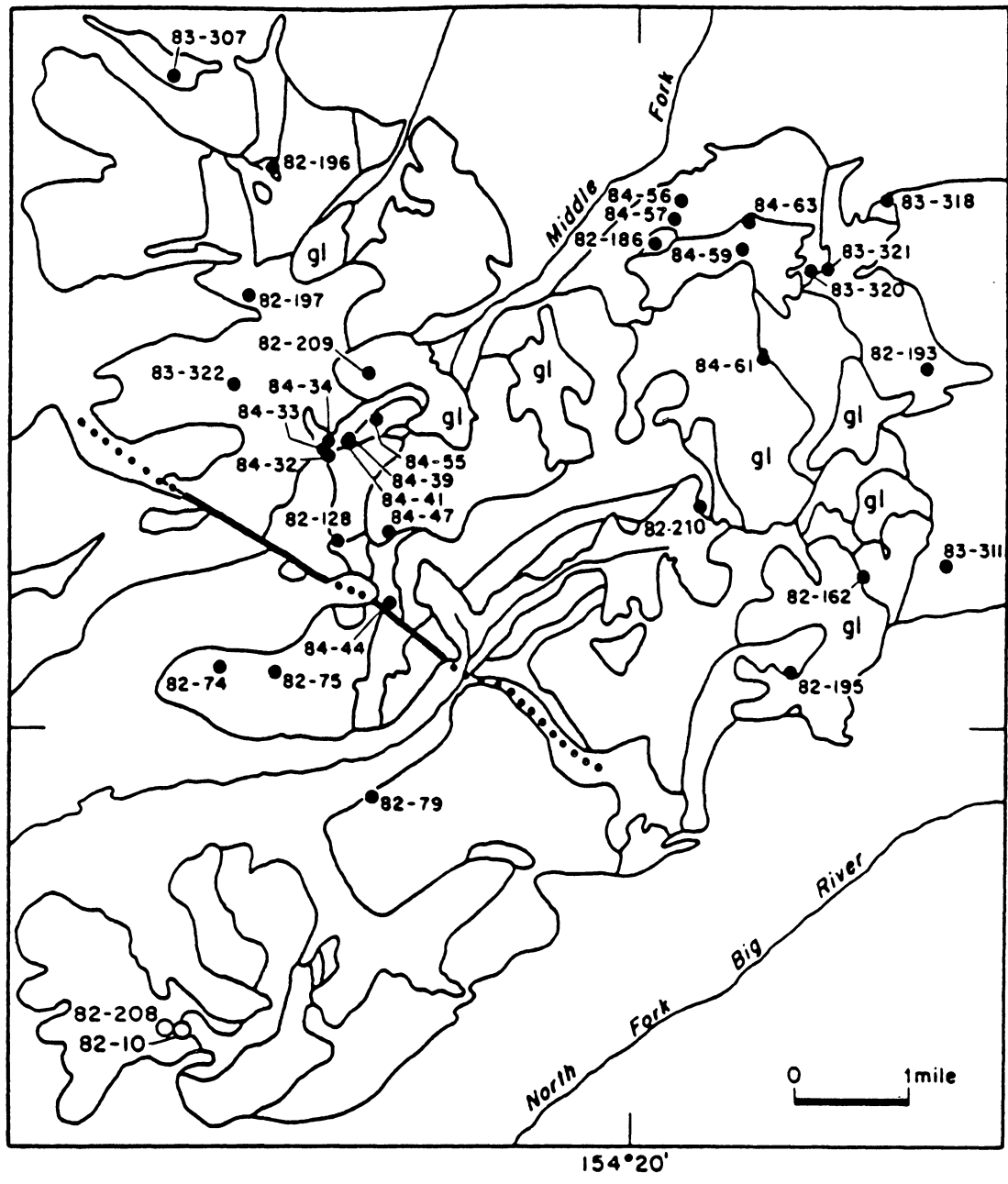

Figure 4. Geologic map showing locations of analyzed samples

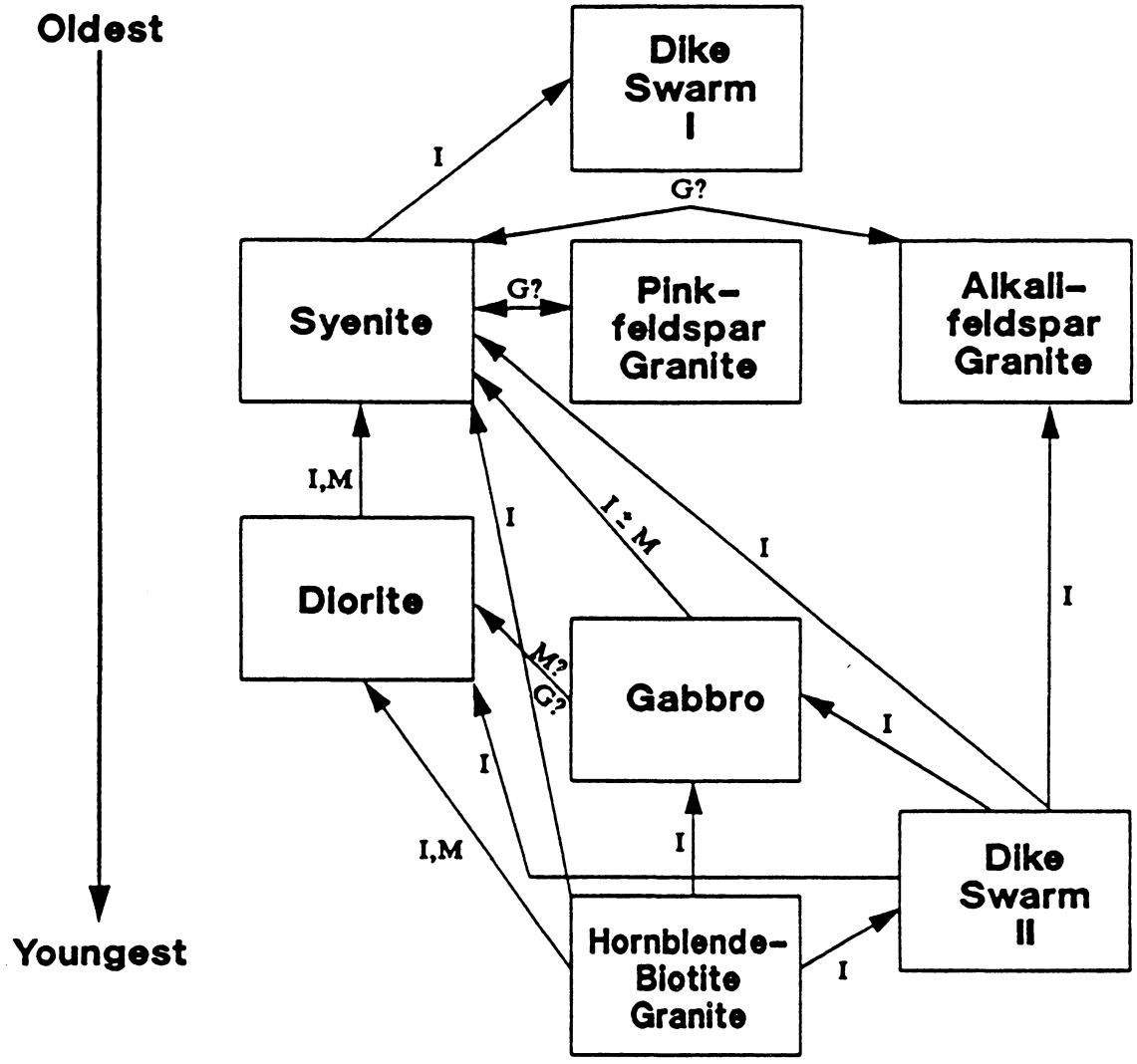

Figure 5. **Diagrammatic summary of intrusive relationships:** The first intrusive rocks, dike swarm I, is shown at the top of the diagram. Subsequent intrusive relationships are labelled; I = intrusive, M = mixing, G = gradational; queried where relationships are uncertain. The youngest dike swarm may also have occurred after HB granite emplacement.

Gabbro:

The gabbro of the MFPC mineralogically and compositionally overlaps the diorite suite. In the field, gabbros were distinguished from diorites by the higher color index and lower modal percentages of hornblende and plagioclase of the gabbros. However, the distinction is often equivocal.

Gabbro typically forms rounded, dark brown, grus-covered outcrops. The rocks are coarse- to medium-grained, contain plagioclase, olivine, pyroxene, and are always biotite-rich. Some varieties contain large multicrystalline biotite flakes nearly 2 cm in diameter. Rare disseminated iron sulfides have been observed in some gabbros.

Leucocratic net-veining of quartz, alkali feldspar, ± plagioclase, with minor biotite, opaque oxide, ± hornblende is common in the gabbro. These veins intrude the gabbro in random crosscutting patterns, and range in width from a couple mm up to about 20 cm. Contacts between the veins and gabbro are sharp, with no megascopic evidence for reaction rims adjacent to minerals. Due to the mineralogical similarity and physical connection, in places, of veins to larger granitic intrusions (e.g., 84DNS34; Figure 4) the net veins are considered as part of the HB granite suite.

Gabbroic rocks occur commonly in the northwest portion of the complex (Figure 6), where they are in close spatial association with diorite and HB granite. Cumulate-textured rhythmic layers in the gabbro are found at the locality of 82DNS174, and in a near-horizontal, roughly 150 m-thick sill which intrudes syenite (82DNS105, 83DNS305, 86DNS19; Plate II). The layers are on the order of 7-10 cm thick, with sharp interfaces, and are defined by abundance of mafic minerals. The relative abundances of these mafic minerals (olivine, pyroxene, biotite) were not noted to systematically vary vertically from band to band. Grain sizes are constant across the layers. A crude foliation, parallel to layering, is defined primarily by plagioclase, but is not present

throughout the layered outcrops. Nor is the layering consistent throughout the outcrops. Where observed near the southwest end of the gabbroic sill, layering is diffuse (86DNS19 locality, Plate II), with less color and mineralogic contrast between layers, and stronger foliation than observed elsewhere.

Contact relationships suggest that the gabbro intruded the syenite. The layered sill (described above), in sharp contact with syenite, is one example of this relationship (e.g., locality 82DNS105: Plate II). Further north and west in the core of the MFPC, relationships with syenite are more ambiguous, as other mafic rocks (i.e., mafic enclaves, diorites) are also in contact with the syenite, and not always distinguishable from the gabbro. However, unambiguous intrusion of biotite-rich gabbro into syenite is observed in places. For example, at locality 84DNS39 (Figure 7), the gabbro decreases from medium- to fine-grained over a 0.5 m interval near the gabbro-syenite contact, suggesting a chilling effect as the gabbro intruded syenite. Irregular wisps of the mafic magma intrude about 2 cm into the syenite at this location.

Within the gabbro in the northwest part of the complex, (Figure 6), areas of diorite occur as either irregular intrusions or lenses in the gabbro, comprising perhaps 20% of the ridges. Elsewhere, the interrelationship between gabbro and diorite is equally ambiguous, due to apparent textural gradations and lack of sharp defined contact relations. However, mafic enclaves within the diorite near a transition between diorite and a medium-grained biotite gabbro (location 86DNS23, Plate II) suggest possible commingling of gabbro and diorite over an area of several meters.

Contact relations between gabbro and peralkaline granite were not observed in the MFPC. There is, however, a clear-cut intrusive relationship of HB granite magma(s) intruding the gabbro. This is seen not only as the typical net-veining, but as larger brecciated zones where felsic magma intruded the already crystalline gabbro, as at lo-

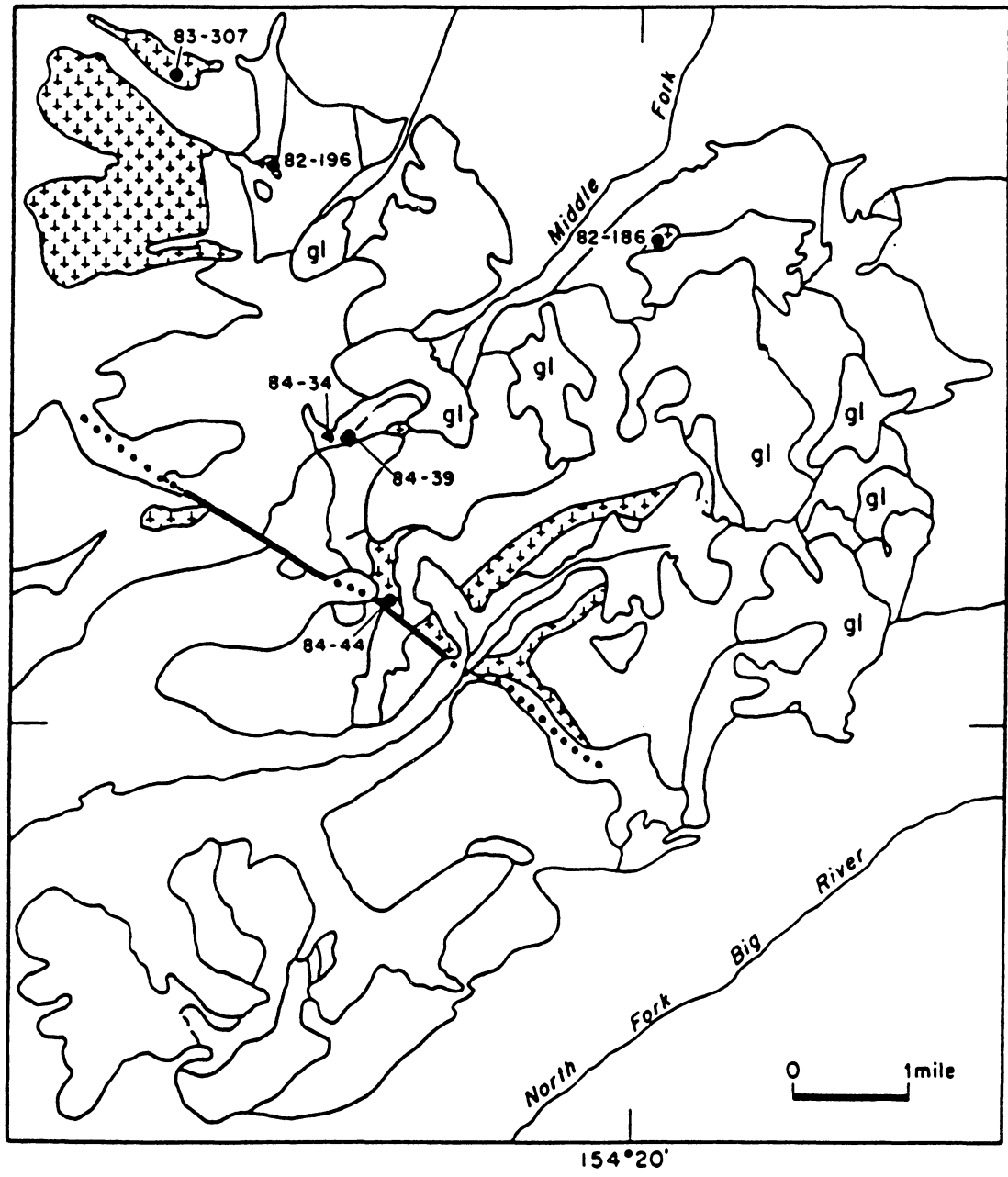

Figure 6. Geologic map showing location of gabbros (pattern) and samples: Gabbro as a mappable unit is most prevalent in the northwest portion of the MFPC, but also crops out in small areas throughout the core of the complex. Sample labels are abbreviated, with a hyphen replacing 'DNS'.

Figure 7. Photo of contact between gabbro and syenite: There is a chill margin in gabbro (under hammer) over several cm, toward contact with syenite. Location shown is 84DNS39.

cality 83DNS307 (Figure 8). Biotite- rich rims around some gabbro enclaves indicate reaction of these enclaves with the HB granite.

Gabbro is intruded by a few basaltic dikes, particularly near the northern margin of the pluton in the vicinity of 84DNS56 (Figure 6). The dikes are about 2 - 6 m in thickness, and are in sharp contact with gabbro. They are aphanitic to fine-grained; some contain randomly oriented 1 - 2 mm plagioclase phenocrysts. The dikes also intrude the other plutonic rocks in this area, and are probably part of the post-plutonic dike swarm event (dike swarm II, Figure 5).

Scattered metasedimentary xenoliths, ranging from about 2 cm to 1 m across, occur within the gabbro. Thin (mm to cm scale) relict sedimentary layering is present in the xenoliths; some layers are carbonate-rich and contain diopside and garnet. Other layers contain fine-grained plagioclase, biotite, opaque oxides, clinopyroxene, ± hornblende. Some xenoliths have become deformed, and appear to reacted with the gabbro. Felsic zones in the gabbro surrounding deformed xenoliths (Figure 9) suggest that material from the xenolith (either fluid or melt) was added to the enclosing gabbro. Compared to the rest of the plutonic units in MFPC, however, the gabbro contains relatively few visible xenoliths.

Diorite:

The designation 'diorite' is herein used to include rocks of diorite, quartz diorite, monzodiorite and quartz monzodiorite compositions. These rocks are included within the map unit Tgqm (Plate I) due to their close spatial interrelationships with one another and with the HB granites.

The diorites are coarse- to medium-grained. Their essential mineralogy is plagioclase, clinopyroxene, hornblende, biotite, ± alkali feldspar, and ± quartz. Color

Figure 8. Photo of gabbro included within HB granite: Sample locality 83DNS307, where HB granite is seen to have intruded gabbro. Rims around gabbro enclaves indicate reaction with granitic magma.

Figure 9. Photo of metasedimentary xenolith within gabbro: Bands of relict sedimentary bedding are visible in xenolith; textural variations and increased felsic mineralogy are present in gabbro in areas around xenolith. (Pen is 13.5 cm for scale).

ranges from green to green-grey to brown. Textures are very variable at hand speciman scale, with mottled patches of more felsic or more mafic areas, and differing grain size. Alkali feldspar forms rare phenocrysts up to about 1 cm long. Tourmaline is locally present, particularly on 'Tourmaline Ridge'(Figure 10), as both blooms and veins. HB granite is also prevalent on 'Tourmaline Ridge', as are sedimentary xenoliths, in both diorite and HB granite.

Felsic veining is common in the diorites. Thickness varies from mm scale (similar to net veining in gabbro) to dikes on the scale of meters. They are granitic and contain biotite and/or hornblende. Reaction rims between veining and diorite were not noted. Pegmatitic veins occur in the diorites in a few places, and consist of quartz, alkali feldspar and biotite. Miarolitic cavities occur in the felsic veins and also rarely in the diorite as vugs surrounded by coarse-grained minerals similar to the minerals found in the enclosing rock. Diorite enclaves are very common within dikes of HB granite. These granitic veins are included in the discussion of HB granite.

Contact relationships between diorite and syenite are not always unequivocal. In the more southern portion of the complex (e.g., 86DNS4; Plate II) there are contacts of fine-grained dioritic rock against syenite. The grain-size of these mafic rocks grades into medium-grained diorite away from the contact, indicating that in this locality, the diorite intruded the syenite and was chilled against the more felsic rock. In the core area of the complex (e.g., 86DNS24; Plate II), a mafic enclave swarm occurs in the contact area between diorite and syenite, with an increase in biotite content in the syenite within 1 - 2 m of the contact. These mafic enclaves, if part of the diorite magma, suggest a commingling relationship of diorite and syenite, not unlike the relationship between gabbro and syenite.

Other contacts are obscured by weathering or inaccessibility. The observed irregular distribution of rock types is not typical of the intrusion of one magma into a pre-

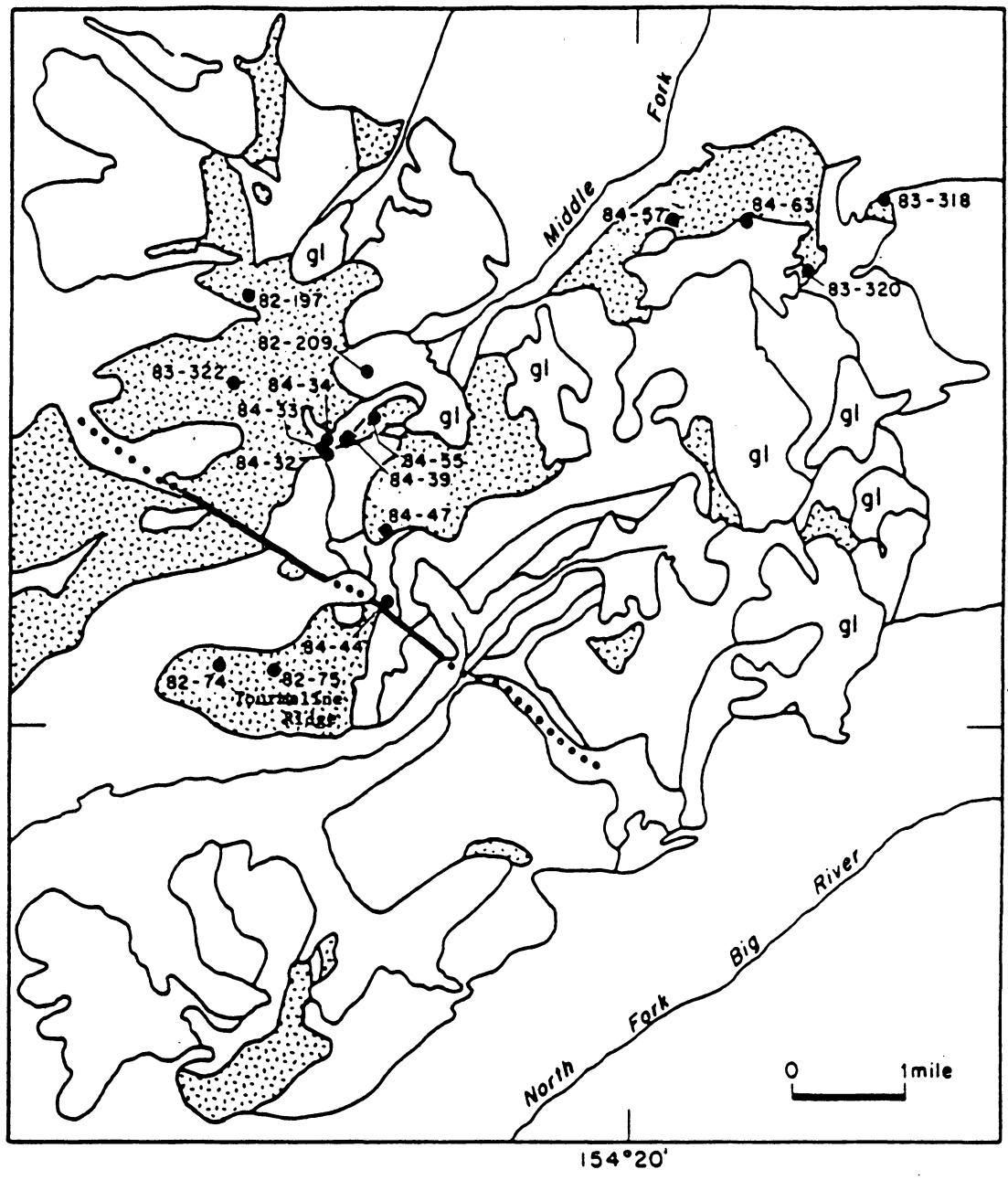

Figure 10. Geologic map showing patterned areas of diorite and HB granite: Locations of analyzed samples shown; labels are abbreviated with a hyphen replacing 'DNS'.

existing pluton to form another discrete pluton. Rather, the diorite occurs as outcrop-scale areas in ambiguous contact relationship with syenite throughout the central zone of the MFPC, suggesting intrusion of diorite magma into syenite magma.

Mafic enclaves locally occur in the diorite. It is not always clear whether these enclaves are related to the gabbro, to a later mafic intrusion (e.g., dike swarm II), or are mafic xenoliths. However, as discussed earlier, at least some enclaves appear related to the gabbro, based on spatial relationships.

Mafic dikes cut the diorite. Some are similar to those seen to intrude gabbro, and are probably part of the dike swarm II event. Others intruding diorite are part of composite dikes, which consist of a mafic dike later intruded by a felsic dike. Xenoliths are common in the the diorite, commonly with leucocratic rims surrounding them, as in the gabbros.

Hornblende-Biotite Granite (HB granite):

The HB granites are a heterogeneous rock unit. They are grouped with the diorites as map unit Tgqm (Plate I) due to the close spatial interrelationships of these rock types. HB granites occur as dikes (cm to m in thickness) in syenite and diorite, as veins and dikes in gabbro, as the felsic component of composite felsic/mafic dikes and, where intrusive relationships are not revealed, as small heterogeneous granitic rock with abundant enclaves and xenoliths.

HB granites commonly are fine-grained, but include a wide variety of textures from fine- to coarse-grained. Color index (0-30) and modal mineral percentages also vary, although the essential mineralogy is fairly consistent. Mafic mineralogy is hornblende and biotite, ± early clinopyroxene. All variants of HB granite have been grouped together for ease of discussion. It must be noted, however, that this is not meant to imply

that these rocks necessarily appear related in the field; they are each isolated entities without field relationships between them. Some HB granites are porphyritic, with alkali feldspar up to 5 mm in a fine-grained groundmass. Miarolitic cavities are common, with vuggy cores rimmed with quartz and alkali feldspar, ± chlorite. Angular metasedimentary hornfels xenoliths are typical within many of the HB granite dikes, and basaltic, gabbroic and dioritic enclaves are also common, either alone or accompanying xenoliths. Enclaves range from 1 mm to several cm, and contain plagioclase, diopside, iron oxides, ± chlorite, ± prehnite. An example of one of these HB granite dikes with enclaves is 84DNS63, a 12 cm thick granite dike in sharp contact with syenite. It contains both basaltic enclaves and hornfelsed metasedimentary xenoliths, as well as fragments of the host syenite, as illustrated in Figure 11.

Composite dikes up to about 1 m thick randomly intrude diorite, syenite and gabbro. These are aphanitic to very fine-grained basaltic dikes, either continuous or broken which HB granitic magma intruded (Figure 12). Basaltic pieces included in the HB granite are mineralogically similar (i.e., plagioclase, clinopyroxene, biotite, ± amphibole, epidote, and opaque oxide) to the basaltic enclaves illustrated in Figure 11.

Where HB granite intrudes diorite, it typically contains the diorite as enclaves. Where only minor granitic rock separates angular pieces, it can be seen how the pieces fit together prior to their brecciation, indicating brecciation of solid diorite. Elsewhere, the diorite blocks (about 1 to 20 cm) are subrounded, and appear to have been moved within the granitic magma (Figure 13). Reaction rims are not typical around the diorite blocks.

Leucocratic veinlets of HB granite are present pervasively in the gabbros and locally within diorites. Veins range from mm to several cm in thickness. They may be either straight dikes or randomly crosscutting veinlets. Graphic intergrowths of quartz and feldspar occur in some veins.

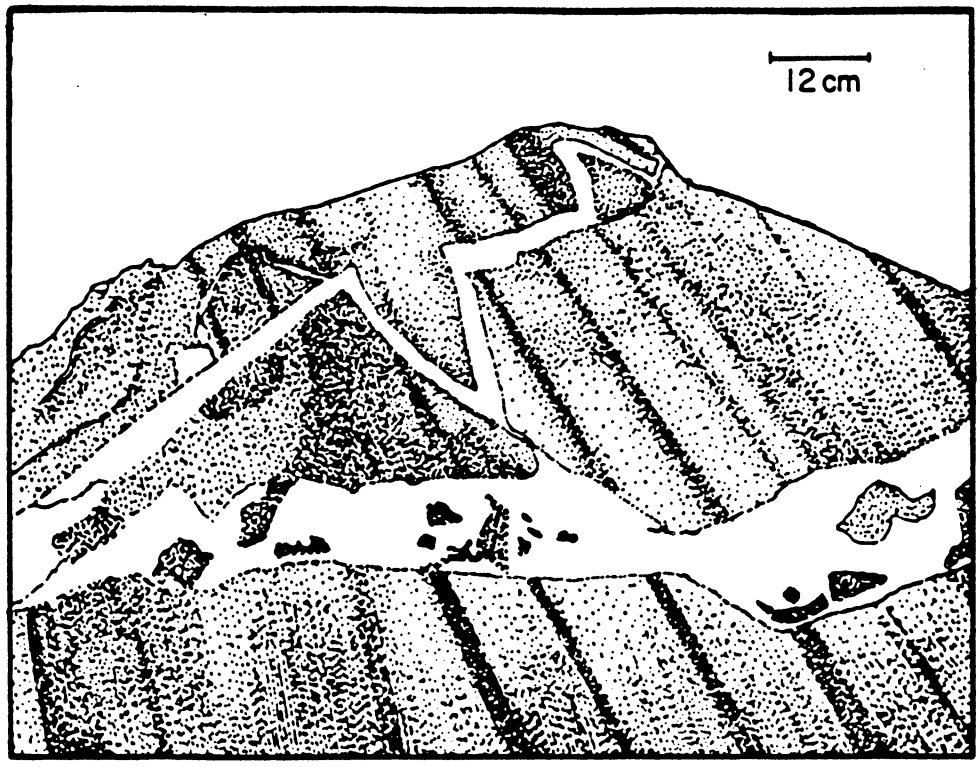

Figure 11. Sketch of HB granite dike intruding banded syenite: Included within HB granite are basaltic enclaves, hornfels xenoliths, and syenite clasts (sample location 84DNS63).

Figure 12. Photo of composite dike intruding syenite: HB granite intruded along margins of preceding mafic dike; note veinlets of HB granite which intruded mafic dike, and mafic blocks which were broken by granite emplacement. (Ruler is 6 inches long for scale).

Figure 13. Photo of HB granite within diorite: HB granite has brecciated diorite, and angular blocks of diorite are encompassed within the HB granite. Textural variations and miarolitic cavities are evident in the HB granite.

The most homogeneous samples of HB granite are found in the vicinity of peak 6780′, though even here enclaves and modal variations are present. Judging from rocks in talus and color variations observed on cliff faces, it is speculated that the tops of some of the taller peaks (e.g., 6780′, 6375′, 6240′; Plate I) in the study area are composed primarily of HB granite.

Syenite:

Syenite forms an irregular arcuate outcrop pattern along the eastern portion of the MFPC (Figure 14). It is typically medium- to coarse-grained, forming massive jointed cliffs. Iron-staining is pervasive on weathered surfaces and along fractures throughout the rock. About 80% of the rock is composed of alkali-feldspar crystals which range from 4 - 7 mm in length. Mafic minerals tend to be finer-grained ($\simeq$2-3 mm) and interstitial. Variable amounts of quartz are present. Preferred grain orientations are not characteristic of the syenite, though several outcrops were observed to have a subvertical igneous mineral alignment, defined primarily by alkali feldspars (e.g., 84DNS59, and enclave-rich 84DNS37 and 84DNS41; Plate I).

Metasedimentary xenoliths are common throughout the syenite, ranging from a few centimeters to large mappable blocks many meters across. They occur in seemingly random orientations and distribution. The larger metasedimentary xenoliths have a leucocratic reaction aureole within the surrounding syenite. Thickness of the aureole varies from 0 - 1 m across. The quartzofeldspathic material of the aureole locally intrudes the xenolith as small wisps. The leucocratic material grades irregularly into the syenite.

The actual contact zone between syenite and alkali-feldspar granite in most cases is in inaccessible terrain or covered by talus. No sharp intrusive contacts between the

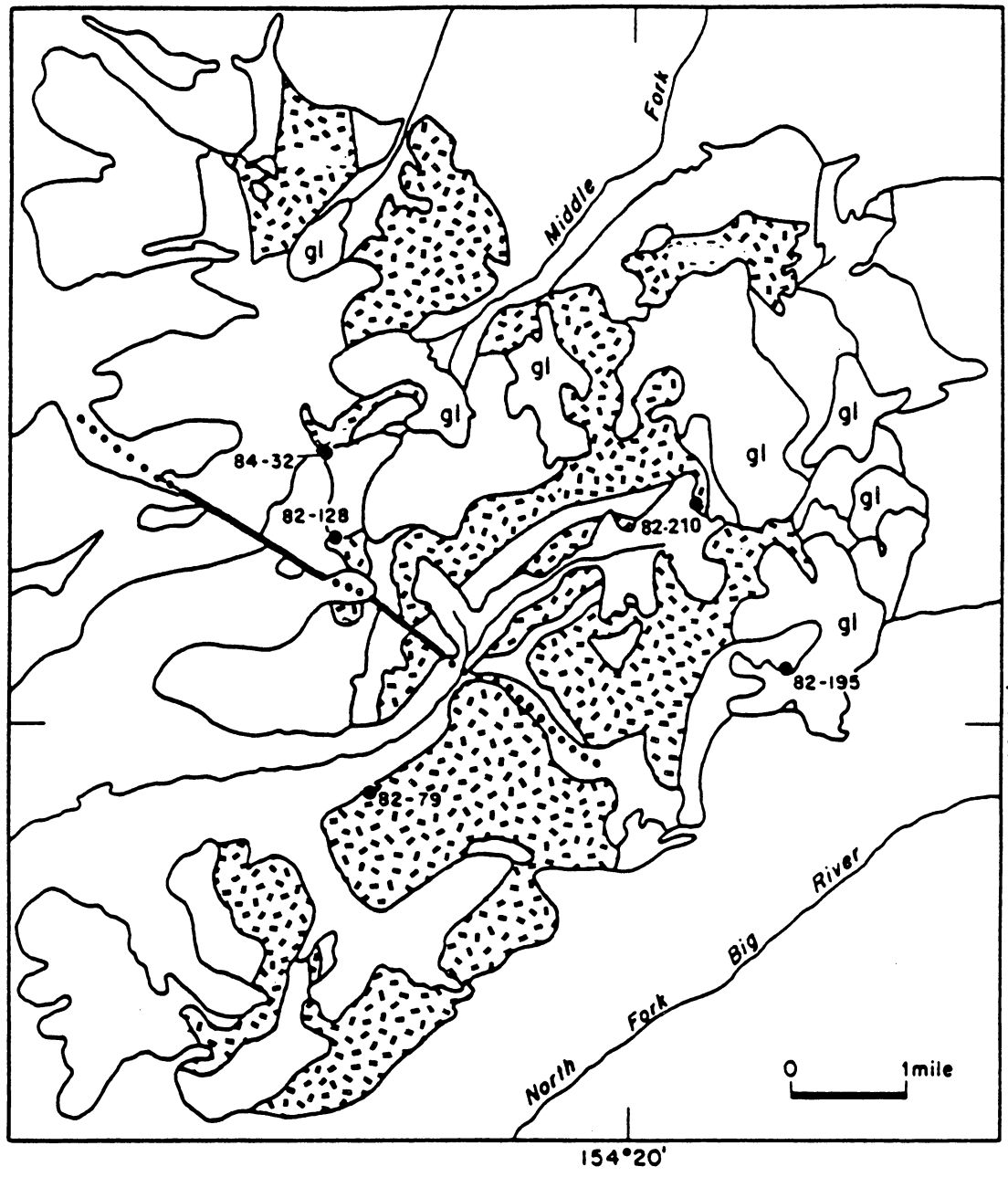

Figure 14. Geologic map showing locations of syenite (pattern) and samples: Syenite occupies the largest exposed area of the MFPC, in an arcuate pattern through the core of the complex. Sample labels are abbreviated, with a hyphen replacing 'DNS'.

two rock types were observed, although a slight increase in quartz content in syenite towards the contact area on the eastern margin of mapped syenite suggests a gradational contact. However, contact relations remain inconclusive based on field observations.

As discussed above, gabbro, diorite and HB granite have been intruded into syenite. Evidence for commingling of gabbro and diorite with syenite is also suggested from field evidence. Therefore, syenite (± alkali-feldspar granite) is interpreted as the earliest plutonic unit observed in the MFPC.

Vertical east-west trending mafic dikes from the dike swarm (dike swarm II; Figure 5) intrude the syenite on the northeast side of the complex. These dikes are in sharp chilled contact with the syenite. These dikes are not observed further west and south in the complex. However, in this core region, mafic enclaves become abundant in both syenite (Figure 15) and diorite. Two textures of mafic enclave have been noted within the syenite. The more common, typically within enclave swarms, is elongate with rounded edges, dark green-grey, and aphanitic with chlorite-rich clots about 2 - 4 mm in diameter. The other variety seems to form more randomly scattered rounded enclaves of very dark green, dense, fine-grained mafic rock. This latter variety is also present in the diorites. In the vicinity of the enclave swarms, hornblende ± biotite are present in the syenite in much more noticeable quantities, and these will be more fully described as subsolvus syenite in subsequent sections.

One locality (84DNS63; Plate II) of banded syenite was observed. This foliated syenite outcrop contains mafic bands with the same mineral assemblage, roughly oriented N20E 45SE. The bands are irregularly spaced, of variable thickness in the range of several cm, and are generally planar, though were also seen to coalesce. The outcrop is crosscut by composite dikes (Figure 11).

Figure 15. Photo of mafic enclave swarm within syenite: Mafic enclaves are most abundant within the core of the complex, where mafic dikes are absent.

Alkali-feldspar granite (AF granite):

Alkali feldspar granite outcrops along the easternmost margin of the MFPC, in a map pattern which rims the syenite (Figure 16). The rock is typically medium- to coarse-grained, whitish grey, with up to 75% perthitic alkali feldspar, 15 - 40% anhedral quartz, and 5 - 10 % mafic minerals. The AF granite is intruded by numerous mafic dikes from the adjacent dike swarm (dike swarm II, Figure 5), and by minor felsic dikes. Miarolitic cavities, with alkali feldspar and large euhedral quartz crystals in the vugs, are present though not abundant. Xenoliths very similar to the hornfelsed calcareous metasediments at the peripheral contact are common in the AF granite.

Pink-feldspar quartz syenite (PF quartz syenite):

Quartz syenite forms a set of ridges in the southwestern part of the complex (Figure 17). The syenite contains pinkish alkali feldspars and locally grades into granite. These rocks vary from fine- to coarse-grained, with color index of 15 - 25. Outcrops form barren, rounded grus-covered ridgetops. Small mafic enclaves are common. Quartz content is variable, and thus granite grades into syenite. The quartz syenite unit was distinguished from the syenite unit in the field primarily by its overall pink color, and higher quartz content. The intrusive relationship is not clear, but appears to be gradational with the syenite.

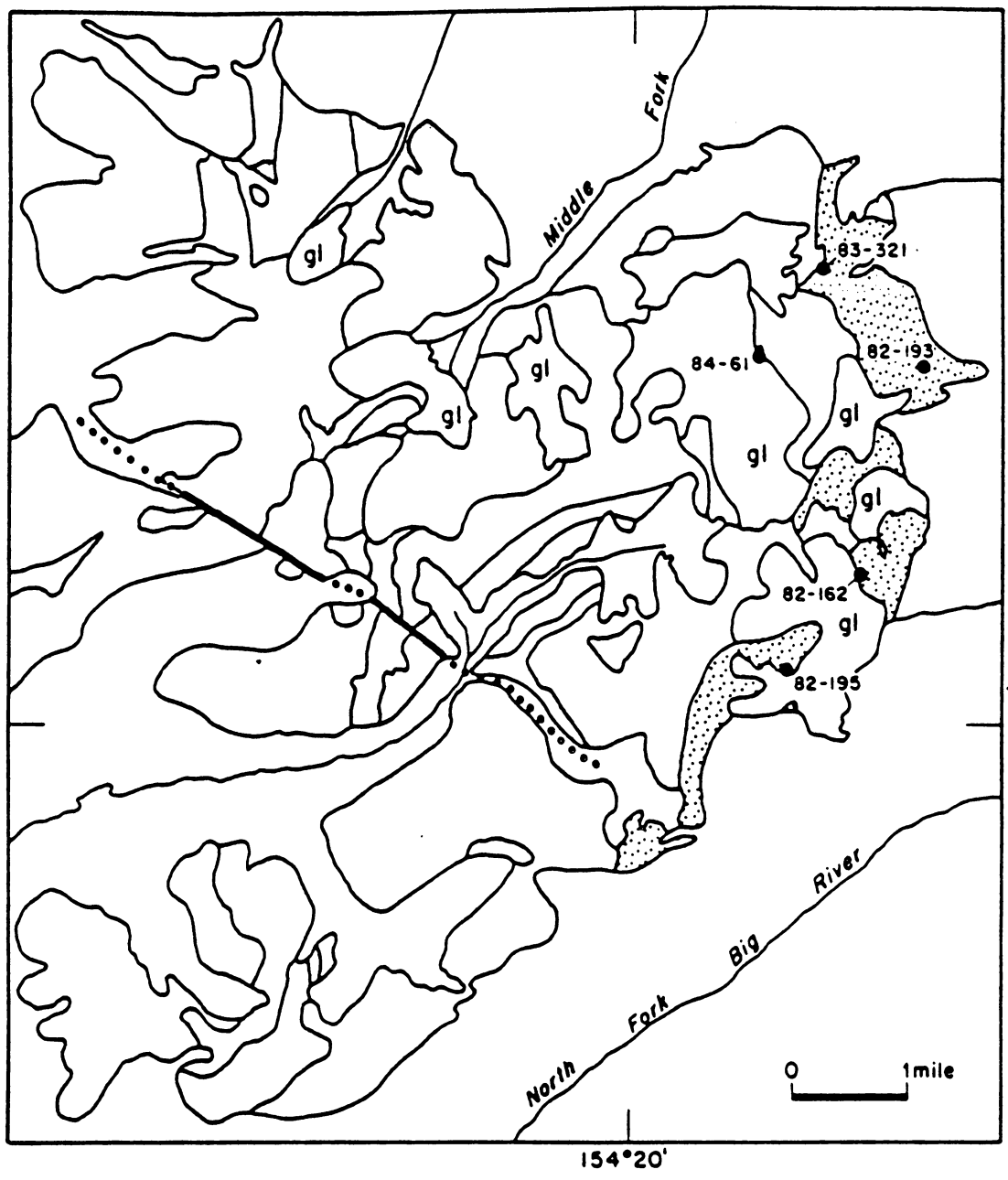

Figure 16. Geologic map with location of AF granites (pattern) and samples: AF granite crops out only along the eastern rim of the Middle Fork Plutonic Complex. Sample labels are abbreviated, with a hyphen replacing 'DNS'.

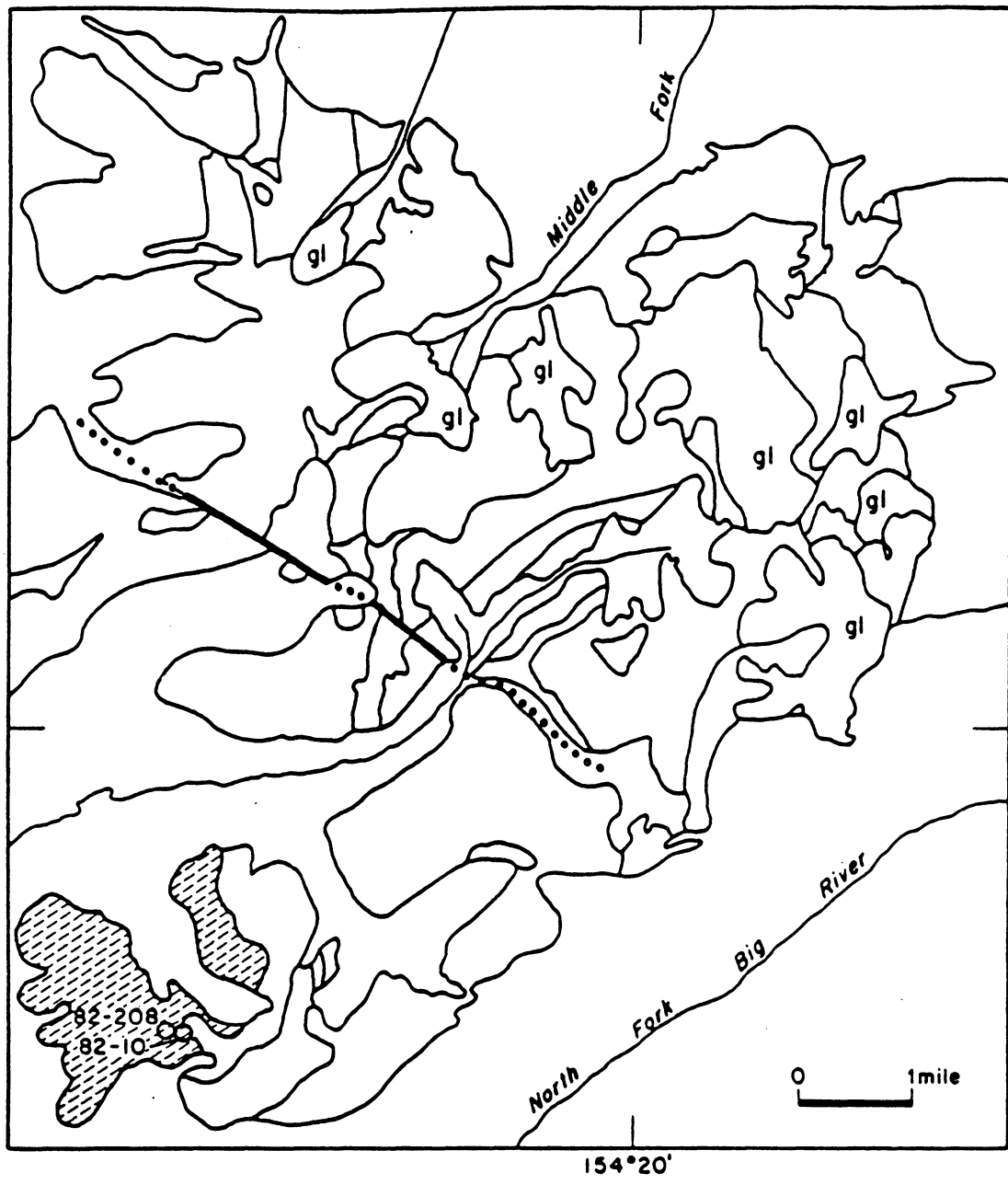

Figure 17. Geologic map showing location of pink-feldspar quartz syenites: PF quartz syenite crops out only in the southwest portion of the Middle Fork Plutonic Complex.

Dike swarm:

Outside the MFPC to the east is a swarm of nearly east-west trending dikes (Plate I). They are vertically dipping, about 2 m to 15 m thick, and near the plutonic complex are so numerous that little if any country rock is present between them. They thin and become less abundant to the east, and at about 20 km distance, the swarm is no longer discernible as a mappable unit. Randomly oriented dikes are ubiquitous throughout the region, but may be related to other magmatic events.

There is evidence for at least two generations of dike intrusion. A pre-plutonic generation was observed within a block of metasedimentary country rock which was subsequently incorporated as a xenolith in syenite. A post-syenite generation was observed as vertical east-west striking dikes which intruded syenite on the eastern side of the complex.

Basaltic dikes are predominant, though locally, up to 50% of the dikes are rhyolitic in composition. Intermediate compositions are minor. The basalts are dark grey, aphanitic to very fine-grained, equigranular, some containing phenocrysts of plagioclase. Basalts tend to weather in spheroidal shapes. Flow foliation and chill margins are not evident.

Rhyolite in dikes commonly contains quartz phenocrysts in an aphanitic light grey groundmass, and typically weather orange. Some felsic dikes contain mafic enclaves within 2 m margins along contacts with basaltic dikes. This suggests that the felsic intrusions post-date at least some basalt dikes, following along their pre-existing planar surfaces and partly brecciating the basalts. Composite dikes in which narrow felsic dikes intrude along both sides of a mafic dike are also present.

Modal Data -- Middle Fork Plutonic Complex

Modal data was derived from point-counts of a 1000-point grid on representative thin sections of each plutonic rock type of the MFPC. Point spacing was adjusted for each sample so that for the average grain size only one or at most two points fell within the same grain. The samples chosen as representative of the magmatic suite contained no enclaves or xenoliths, were relatively homogeneous and unaltered throughout, and contained textures and mineralogies most characteristic of the rock type, or of a commonly observed variant. Foliations and other preferred orientations were not present in the samples which were used for point counting. Therefore, the measured modal percent is estimated to be approximately equivalent to volume percent. These same samples were analyzed for whole rock major and trace element content, Rb-Sr isotopes, and selected mineral compositions, and form the basis for most of the discussion in this study.

The range of lithologies from the MFPC is shown in Figure 18, and follows the IUGS classification scheme (Streckeisen,1976). Rocks of the gabbro unit fall within the gabbro field, with one sample (84DNS39c) in the monzodiorite field. The diorite suite includes diorite, quartz diorite and quartz monzodiorite. HB granites include a granodiorite sample (84DNS34a), and the rest are granites. The alkali-feldspar granites range into the alkali-feldspar syenite field (82DNS195c). The syenites span the fields of alkali-feldspar syenite, quartz syenite and alkali-feldspar quartz syenite. The pink-feldspar quartz syenites spread over into the quartz monzonite field (82DNS64).

Most of the felsic rocks of the MFPC have less than 10% mafic constituents; all have less than 16%. The highest measured color index in the suite is about 85, in a gabbro (83DNS307). None of the point counted rocks can be considered ultramafic (i.e., color index $\geq$90). Modal data for each analyzed sample is presented in Appendix B.

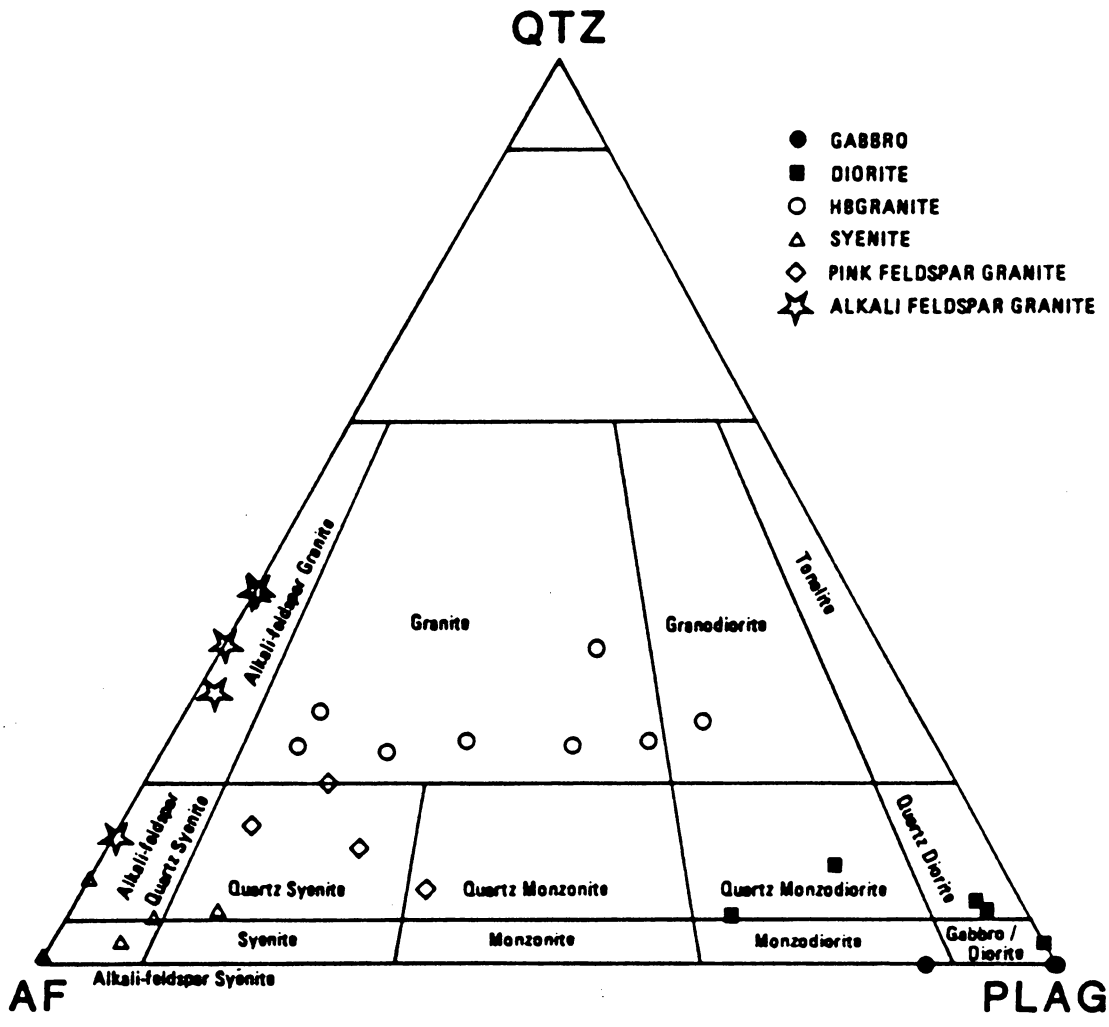

Figure 18. Quartz - Alkali feldspar - Plagioclase plot of modal data: Classification scheme from Streckeisen (1976). Includes all modal data from plutonic suite of MFPC, showing the spread in lithologies within each mapped rock type.

Petrography -- Middle Fork Plutonic Complex

Petrographic examination of the representative suites was made in order to determine mineral assemblages, textures, and crystallization sequences of the mineral phases. Criteria used to interpret crystallization sequence are: 1) included phases precede their host phase, 2) euhedral grains precede surrounding subhedral or anhedral phases, 3) porphyritic grains precede their groundmass, 4) a subhedral phase precedes the phase(s) against which its crystal faces are grown, 5) interstitial phases postdate surrounding phases, 6) rimming phases postdate their core, and 7) alteration minerals postdate their host. A generalized summary of crystallization sequences for each rock type is shown schematically in Figure 19. A more detailed description of each sample in the suite is included in Appendix B, and results of electron microprobe chemical analyses are presented in the section on mineral chemistry and in Appendix C.

Gabbro:

Seven representative samples were chosen to characterize the gabbros. Of these, four (83DNS307, 82DNS186, 84DNS44a, 82DNS196) have strongly poikilitic textures (Figure 20), suggestive of cumulate crystallization (Cox et al., 1979). Due to sampling problems, none of these cumulate samples are from the rhythmically layered gabbro localities. Olivine is an early-crystallizing, medium-grained ($\simeq$1 mm), subhedral, cumulate mineral. Some pyroxene grains are poikilitically enclosed within plagioclase, and may also be cumulate. Plagioclase and some pyroxene (both $\simeq$1 mm) are ophitic intercumulates, enclosing earlier cumulate minerals. Biotite ($\simeq$1-1.5 mm) occurs as intercumulate or as adcumulate rims, especially on opaque minerals. The opaque minerals are

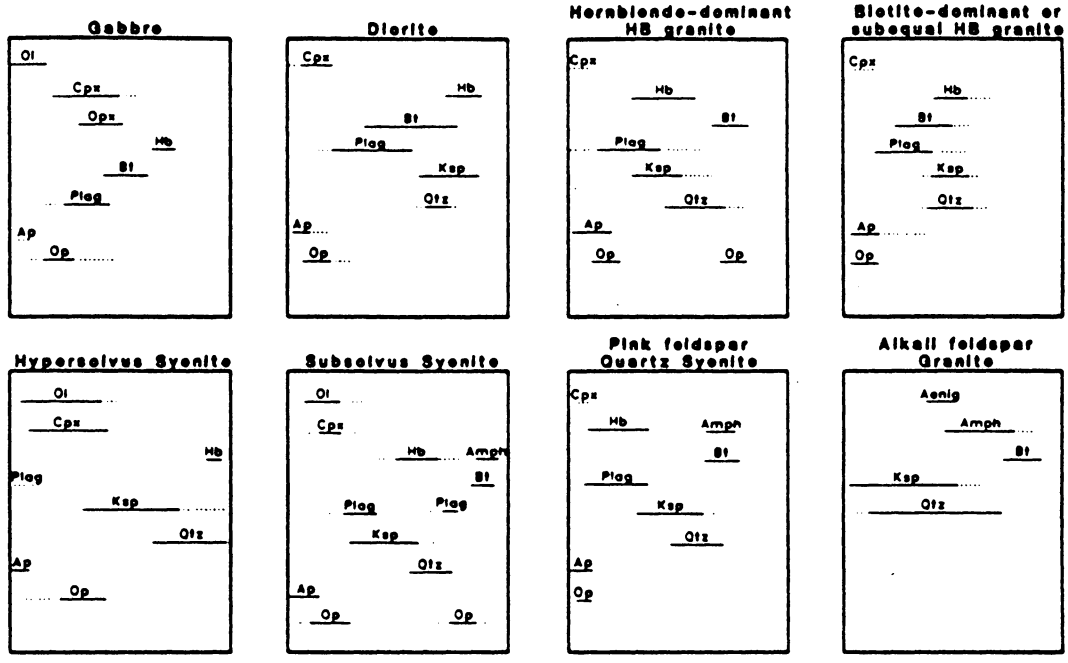

Figure 19. **Schematic representation of crystallization sequence:** Interpretive sequence characteristic of each plutonic lithology of the MFPC. Ol = olivine, cpx = clinopyroxene, opx = orthopyroxene, hb = hornblende, am = amphibole, bt = biotite, aen = aenigmatite, plag = plagioclase, ksp = alkali feldspar, qtz = quartz, ap = apatite, op = opaque. Each diagram represents progressive crystallization from early on left to late on right.

primarily ilmenite ±iron sulfides. They range from 0.2-0.5 mm, are early-crystallizing, and may be cumulate. Apatite or other accessory phases in the cumulate samples are rare. Both orthopyroxene and clinopyroxene are present as intercumulates in two of the samples (82DNS186, 82DNS196). Late amphibole is present in three of the cumulate samples, rimming and/or replacing pyroxene and rimming biotite. Biotites are strongly pleochroic from orange to very pale orange. In 82DNS186, ilmenite grains look like they have been resorbed, with rounded embayed forms, rimmed by biotite.

Chlorite (≤2%) and opaques (≤1%), ± trace amounts of calcite are the dominant alteration minerals, and are commonly derived from olivine and pyroxene. Patches of plagioclase are altered to sericite, but not pervasively. Opaque-filled fractures cut sample 83DNS307.

In the non-cumulate gabbro samples (84DNS34d, 84DNS39a, 84DNS39c), textures are hypidiomorphic, medium-grained, and equigranular. Early-crystallized olivines are sparse (≤1%) and highly altered. Neutral greenish-brownish clinopyroxene is the most abundant mafic mineral, but is replaced by hornblende in places. Some clinopyroxene contains exsolution lamellae. Biotite is orange-brown and late-crystallizing. Ilmenite grains are subhedral, and less than 1 mm in diameter. Apatites are included in all other mineral phases, and contain rod-shaped inclusions within them. Plagioclase is concentrically zoned, ranging from labradorite to andesine. Alkali feldspar is present in small amounts in samples in close contact with syenite. In 84DNS39a, which is 15 m from the syenite contact, alkali feldspar rims plagioclase. In 84DNS39c, <6 cm from the contact, alkali feldspar crystallized early, is coarse-grained and myrmekitic.

Figure 20. Photomicrograph showing poikilitic textures in gabbro: Sample 82DNS186, olivine grains enclosed within plagioclase. Field of view is about 5 mm across.

Diorite:

The fine- to medium-grained diorites have a color index of 30 - 50. Clinopyroxene ($\leq$1 mm) is present as up to 20% of the rock, but is commonly altered to hornblende $\pm$ biotite. Color zonation in clinopyroxene of some samples, in tones of tannish-pinkish, indicates compositional zoning. Hornblende ($\simeq$1 mm) forms about 10% of the diorites, and is olive to tan in pleochroism. About 10% biotite ($\simeq$1 mm) is present as unaltered subhedral grains. It forms after clinopyroxene, and is pleochroic from orange-brown to tan. Ilmenites ($\simeq$0.5 - 1 mm) are lath-shaped, but commonly rounded, and surrounded by biotite. Rounded embayments in some opaque oxides suggest resorption in response to a changing magmatic environment. This is particularly evident in 83DNS320d, where embayments in ilmenite are filled with late stage alteration minerals. Apatite is an abundant early-crystallizing accessory ($\simeq$1%), found within all other mineral phases. It occurs as both thick stubby grains and thin elongate needles, in the same samples. Rod-shaped inclusions within some apatite grains may be either fluid inclusions or an earlier generation of apatite. Plagioclase ($\simeq$1 - 2 mm) forms approximately 50% of the rock, is rarely cumulate, and is commonly normally zoned in the range of An_{30-55}, based on the Michel-Levy determination method. Alkali feldspar and quartz, when present, are in relatively small % (quartz <5%, alkali feldspar <15%), and are late-crystallizing interstitial grains. Accessory minerals include zircon, titanite, and allanite(?) in trace amounts. Secondary minerals, which in some samples comprise up to 15% of the rock, are chlorite, sericite, iron oxide and actinolitic amphibole. Tourmaline, which is present particularly along 'Tourmaline Ridge', appears to be a secondary mineral forming anhedral clots (up to 5%). The tourmaline is concentrically zoned in colors of blue to brown to tan pleochroism. Surrounding the tourmaline clots are rims, 1-3 mm thick, of intense hydrothermal alteration in the diorite.

Hornblende-Biotite granite (HB granite):

The HB granites contain >20% quartz, and varying amounts of plagioclase and alkali feldspar. Most grain sizes range between about 0.5 to 1 mm; alkali feldspar in some samples may be up to 2 mm. Mafic minerals include hornblende (≃0.5-1 mm) and biotite (≃0.25-0.75 mm). However, relative amounts of these minerals vary widely, ranging from dominantly hornblende with minor late (secondary?) biotite (82DNS75d, 83DNS307d, 84DNS63a), to dominantly biotite with minor amounts of hornblende (83DNS322a, 84DNS33a, 84DNS34a). Other samples contain subequal amounts of hornblende and biotite. Relict, altered, clinopyroxene cores are not uncommon within hornblendes; some have a pinkish-greenish color. Hornblende is dark to light olive green or brown pleochroic in the hornblende-dominant samples. Where the amphibole is a minor phase, it is light tan to pale green. Biotite is dark brown to light orange-brown or tan.

Accessory phases include opaque oxides (ilmenite and/or magnetite), apatite, zircon, ± allanite, ± titanite, ± fluorite. Apatite in at least one sample, (83DNS307d), contains rod-shaped inclusions. Euhedral to subhedral tourmaline with blue to brown pleochroism is present on 'Tourmaline Ridge' in thin (2-5 mm) veins of HB granite between abundant hornfelsed metasedimentary xenoliths. These xenoliths are subangular to subrounded, and range from very small (mm scale) to several cm in diameter.

Alteration products comprise from <1 up to ≃8 vol.% of the HB granites. Alteration minerals are dominantly chlorite (after biotite), and sericite (largely after plagioclase), with some calcite, epidote and opaque oxides. Alkali feldspars are generally somewhat turbid. In sample 82DNS75d, there is a secondary fibrous amphibole with green to blue-green pleochroism.

In general, the HB granites are hypidiomorphic and fine-grained. Zoning, both normal and reverse, is present in the plagioclase, based on patterns of extinction angles upon rotation of thin section under crossed polarizers.

Subhedral plagioclase is the earliest crystallizing felsic mineral in each sample, followed by alkali feldspar and quartz in that order, except in 83DNS322a where quartz grains appear to precede interstitial alkali feldspar. Apatite and opaque are early, crystallizing before or with plagioclase, based on their euhedral shape and inclusion in later phases. Hornblende crystallized after plagioclase, and before biotite, in the hornblende-dominant granites. In all the other samples, however, biotite started crystallizing before hornblende, on the basis of rimming relationships of hornblende around biotite.

Syenite:

Mineralogically, the syenites can be grouped into two suites: a hypersolvus and a subsolvus suite. These two groups are difficult to distinguish in the field, and were not mapped separately. Petrographic observations suggest that the subsolidus suite occurs primarily in areas where mafic enclaves are present, especially in the core area of the complex (e.g., 84DNS32).

Hypersolvus syenite:

Of a suite of six representative syenite samples from the MFPC, three are hypersolvus with virtually no plagioclase except albite as perthitic exsolution lamellae (Figure 21). Mafic mineralogy consists of hedenbergite (approximately 6%), about 2% fayalite ($Fo_{<1}$), 2% ilmenite, 1 - 6% quartz, $\leq$1% zircon, a trace of early crystallizing

apatite, minor fluorite, and minor late crystallizing hornblende and rare biotite. No silica undersaturated syenites have been observed in the MFPC.

The hypersolvus syenites are medium- to coarse-grained, with subhedral perthitic alkali feldspar grains up to about 6 mm. Most other grains are smaller and subhedral to anhedral; rounded hedenbergite is not uncommon. Hedenbergite contains a subtle, mottled color zonation from pinkish-tan to pale green. Though not consistent, there is a tendency for the pyroxene rims to be greener than the cores. The alkali feldspars are turbid to varying degrees, with turbidity most prevalent in areas containing late or secondary minerals. Secondary minerals include carbonate, mica and aggregates of a brown, iron-rich mineral. Iron-rich alteration products are common in fractures in the fayalite. A film of iron oxide is present in post-magmatic brittle fractures, and appears to mobilize from altered fayalites.

Subsolvus syenite:

The other three samples in the suite are subsolvus, containing about 8 - 12% fine-grained oligoclase (An_{10-15}), in addition to albite exsolved from perthitic alkali feldspars (Figure 22). Early-crystallizing fayalite (Fo_{2-5}) in these samples is largely altered, and up to 10% ferro-edenitic hornblende with green to tan color zonations and 1 - 2% biotite have crystallized late, partly at the expense of early hedenbergite. The opaque phases are ilmenite; accessory minerals include zircon and apatite. Small amounts of secondary actinolite are also present in these three samples.

Figure 21. Photomicrograph of hypersolvus syenite sample 82DNS195b: Field of view is about 6 mm by 4 mm.

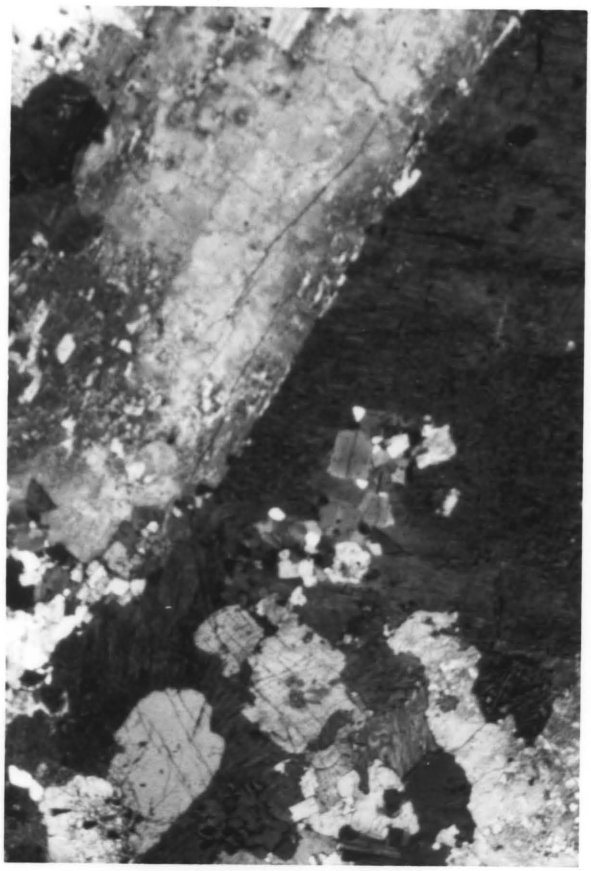

Figure 22. Photomicrograph of subsolvus syenite sample 82DNS210: Field of view is about 6 mm by 4 mm.

Alkali-feldspar Granite (AF granite):

The AF granite is typically medium- to coarse-grained, with up to 75% perthite, and 15 - 40% anhedral quartz. Mafic mineralogy, which comprises 5 - 10% of the rock, consists of late-crystallizing sodic amphibole in all samples, and annite-rich biotite and aenigmatite in some samples. Accessory minerals include fluorite, ilmenite, zircon, and a brown Ce-rich mineral, probably chevkinite.

The alkali feldspars are coarsely perthitic, and turbid in patches. Granophyric intergrowth of quartz and alkali feldspar occurs locally in some samples. Sutured grain boundaries are common, as is undulatory extinction and some subgrain development in quartz. Alkali feldspar was typically the first phase to crystallize. There are two distinct groups of amphibole compositions, the earlier crystallizing amphiboles greenish-tan to dark green (ferrorichterites), the later (riebeckites, arfvedsonites) having light to dark blue and greenish blue pleochroism. In samples in which the amphibole is largely or totally arfvedsonite, the accessory zircon grains are subhedral, and possibly resorbed. Otherwise zircon is euhedral. Biotite, when present, crystallized after amphibole. Fluorite crystallized during the late stages of feldspar formation.

Pink-feldspar quartz syenite:

Hornblende is the dominant mafic mineral in the pink-feldspar quartz syenite, comprising about 10% of most samples. The hornblende crystallized early relative to alkali feldspar and quartz, and is euhedral to subhedral. It is olive green to brown pleochroic; some grains have textures in their cores in which pleochroism and birefringence are different from the surrounding grain, and may indicate relict pyroxene.

Sample 82DNS64 contains clinopyroxene which crystallized before hornblende, and is concentrated in irregular finer-grained areas. Accessory phases include apatite, opaques and zircon, all of which crystallized early. The zircons tend to be fairly large ($\simeq$0.1 mm) euhedral squares, as in the syenites. Plagioclase appears to have crystallized at about the same time as the hornblende. It occurs as small rectangular grains within alkali feldspar, and as larger, zoned, highly altered and slightly resorbed grains. Alkali feldspar, which constitutes the bulk of the rock, is typically the largest phase in the rock. It is anhedral, and may rim plagioclase grains. The alkali feldspars are turbid, as they are in the syenites and AF granites, but do not have the extensive perthitic exsolution textures that are present in these other lithologies. In some places, alkali feldspar and quartz are in graphic intergrowth. Quartz is interstitial.

Secondary amphibole growth is present to varying degrees in all pink-feldspar quartz syenite samples. This amphibole varies from green to blue-green to blue. It rims and replaces hornblende, and in places forms fibrous sprays within quartz. Small amounts (<2%) of orange-brown biotite also grow within and around the hornblende. Calcite occurs interstitially in pockets of secondary minerals. In sample 82AR9, small unaltered grains of albite are present interstitially, and rim larger feldspars.

Dike Swarm:

Mafic dikes generally have a felted groundmass of plagioclase laths. Some may have small (1-2 mm) plagioclase and/or clinopyroxene phenocrysts (Figure 23). Clinopyroxene is present in all thin sections except 82DNS107, which is a thin dike in the dike swarm east of the Windy Fork River (Plate I). Clinopyroxene is neutral to slightly pinkish, and is typically about the same size as the plagioclase laths. Plagioclase is commonly slightly normally zoned and is randomly oriented. Opaque oxides, both

elongate and equant forms, are abundant (about 10%), and probably crystallized early. Biotite tends to be smaller, subhedral to anhedral, brown to tan grains and is present in all thin sections. Olivine was observed only in section 84DNS59a, one of the vertical dikes which intrude syenite.

Alteration products vary from almost none to ≥50% of the mafic dike rocks. They include epidote, chlorite, calcite, and olive green cryptocrystalline masses, possibly celadonite.

In the felsic dikes, quartz, plagioclase and alkali feldspar phenocrysts are common (Figure 23). Quartz has the euhedral form of β-quartz. Some phenocrysts of plagioclase and alkali feldspar are grown together, in a glomeroporphyritic texture. Virtually no mafic phases are present as phenocrysts; only one small grain which has been altered to iron oxides was observed. Also, a small lath of biotite is present as an inclusion in a quartz phenocryst (84WG2). Opaque phases are present in small amounts (<3%), mostly in the groundmass. The groundmass is predominantly an equigranular microcrystalline mass of indeterminate felsic grains, with small amounts (≤5%) of a colorless, high birefringent mineral that appears to be a white mica.

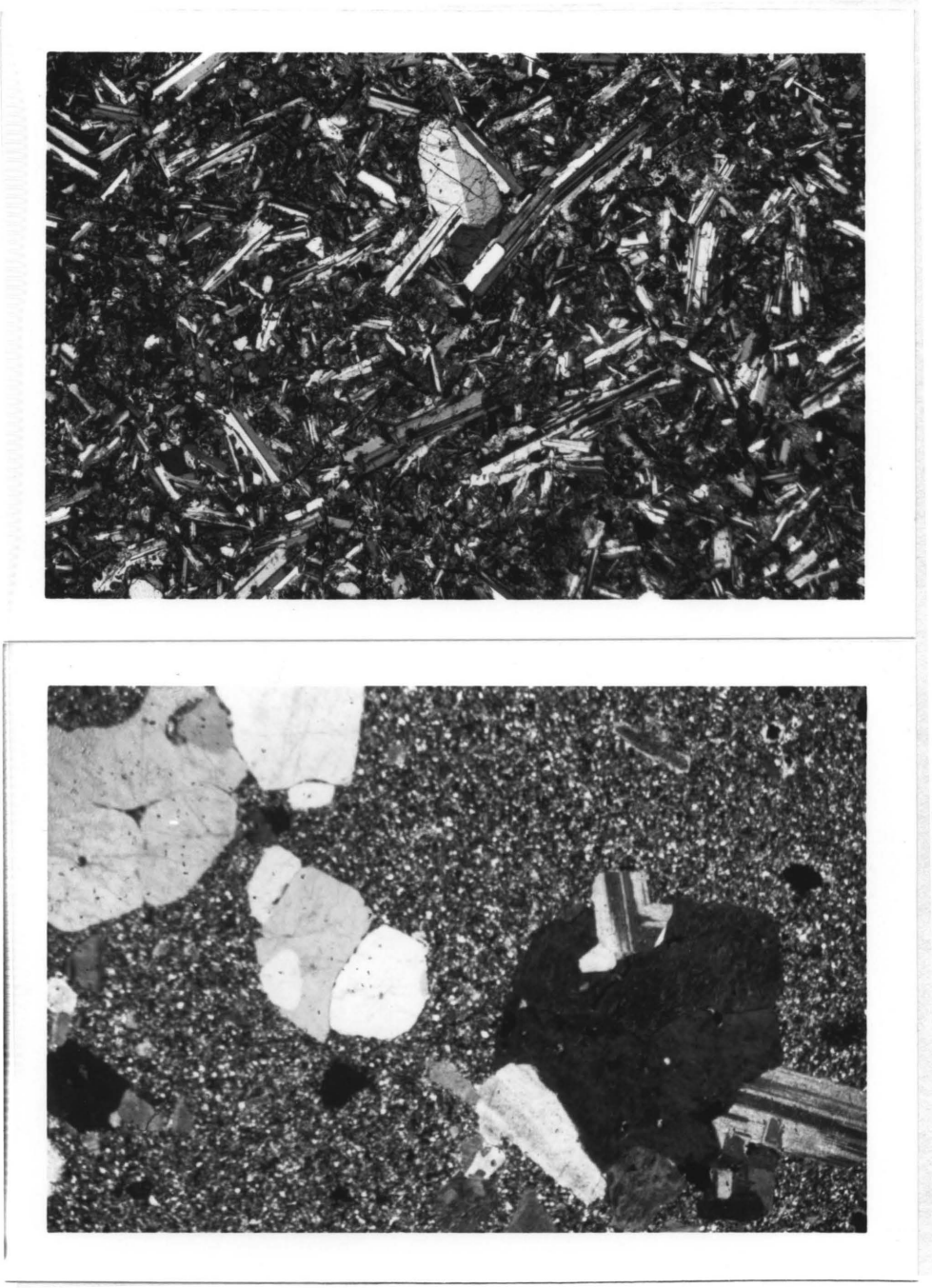

Figure 23. Photomicrographs of mafic and felsic dikes: Top photo is basaltic dike (84DNS59a); bottom photo is felsic dike (84WG4). Field of view for both is about 6 mm by 4 mm.

Chapter 2: The Geochemistry of the Middle Fork Plutonic Complex

Introduction

Several samples of each rock type in the MFPC were analyzed for bulk rock major oxide and selected trace element composition. Major oxide analyses include samples analyzed at Virginia Tech, as part of the representative suite described in Chapter 1. This suite was also analyzed for trace element, Rb-Sr isotopic, modal, and selected mineral compositions. The trace elements determined were Ba, Rb and Sr. Additional samples (ADGGS suite) were analyzed for major element chemistry only, at the Alaska Division of Geological and Geophysical Surveys, Fairbanks, Alaska (Appendix B). Thin sections of these latter samples were studied, and included in the petrographic characterization of rock units (Chapter 1), but no further analyses of these samples were done. A discussion of comparison between results from the two different labs, as well as analytical techniques, is included in Appendix D.

Major and Trace Element Geochemistry

Major oxides plotted against SiO_2 (Harker diagrams) are commonly used as a geochemical overview of the compositional trends in an igneous suite. Increasing silica content represents increasingly evolved rocks. The Harker diagrams in the following figures contain analytical results from the MFPC suite (Figure 24, Figure 25, and Figure 26). One of the first points to be made from these diagrams is the bimodality of the suite. There is a compositional gap in the data between 53.2 and 60.4 wt.% SiO_2. This is within the andesite compositional range, taken as (53 - 63 wt% SiO_2; Gill, 1981). Although three analyses fall within this compositional gap (a dike, a mafic enclave, and a country rock), none of the three are thought to necessarily represent an uncontaminated magma composition.

This observed silica gap has been reported from numerous other plutonic and volcanic suites of alkaline affinity (as discussed by Macdonald, 1974), and overlaps the so-called 'Daly gap' (53-57 wt% SiO_2) seen by Chayes (1963) in oceanic island volcanic rocks. Possible mechanisms which could cause this gap are: 1) preferential exposure of rocks due to igneous and/or weathering processes, 2) geometry of the pertinent phase equilibria which could create a jump in silica composition during fractionation, 3) different magma sources and/or histories for rocks on either side of the gap, and 4) biased sampling.

Biased sampling of exposed rocks can probably be discounted as the causative mechanism for bimodality in the MFPC. A specific effort was made to find and sample rocks of intermediate composition in order to bridge the 'Daly gap', but none were found. It is difficult to evaluate the effects of igneous processes which may leave the intermediate compositions unexposed or allow them to vent to the surface; thus this ef-

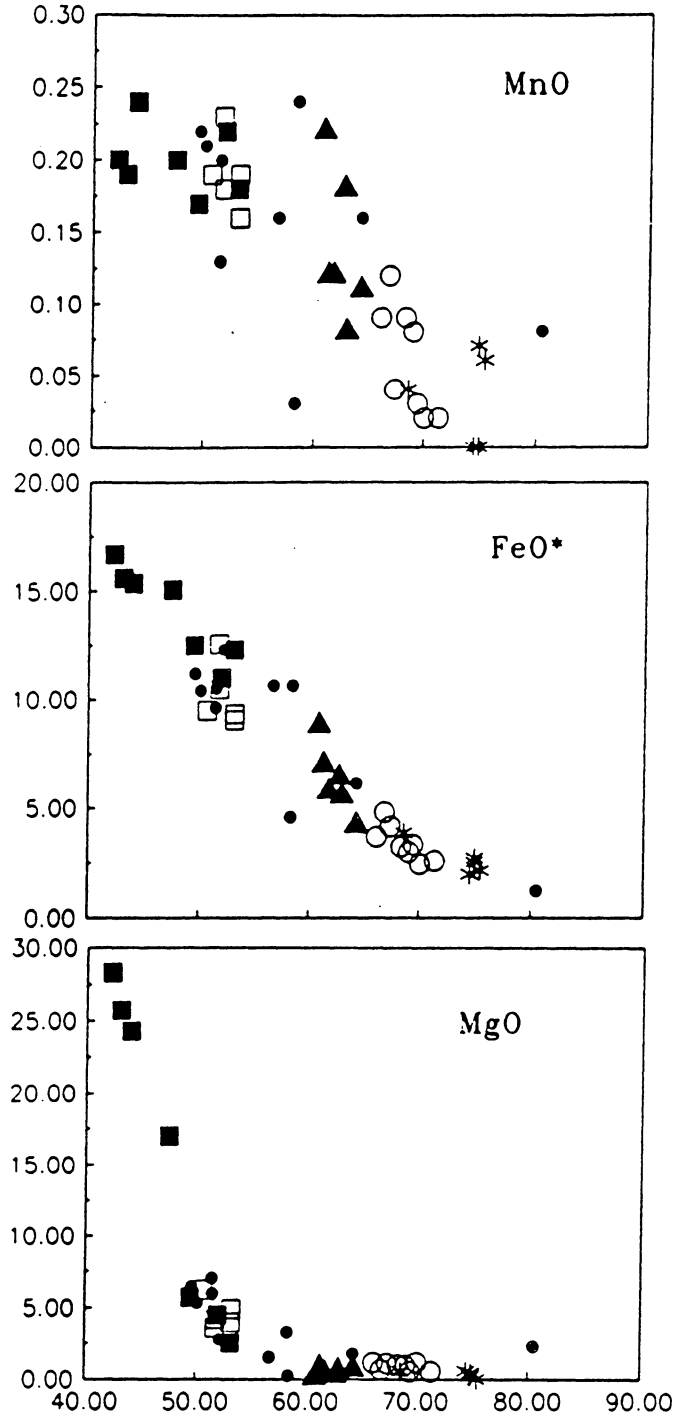

Figure 24. **Harker diagrams of major oxides vs silica (wt%):** Closed square = gabbro, open square = diorite, triangle = syenite, open circle = HB granite, star = AF granite, dot = dikes, enclaves and country rocks.

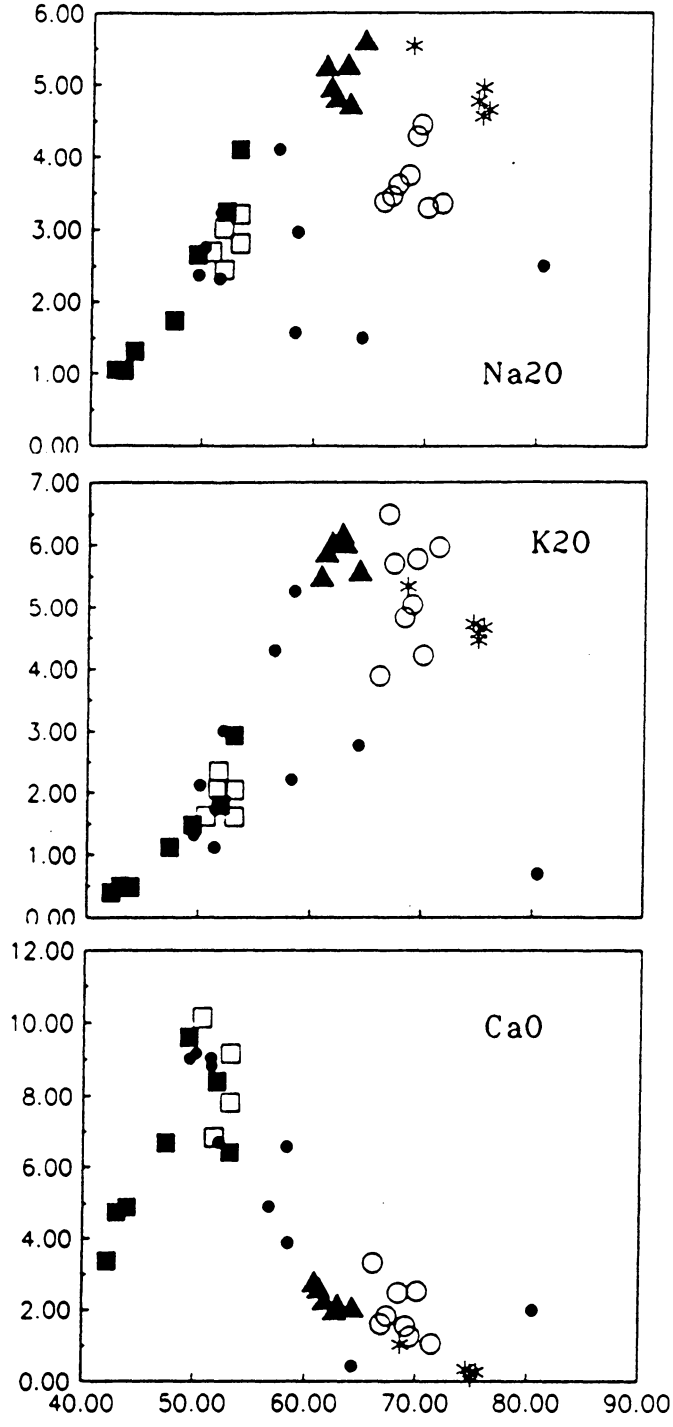

Figure 25. **Harker diagrams of major oxides vs silica (wt%):** Closed square = gabbro, open square = diorite, triangle = syenite, open circle = HB granite, star = AF granite, dot = dikes, enclaves and country rocks.

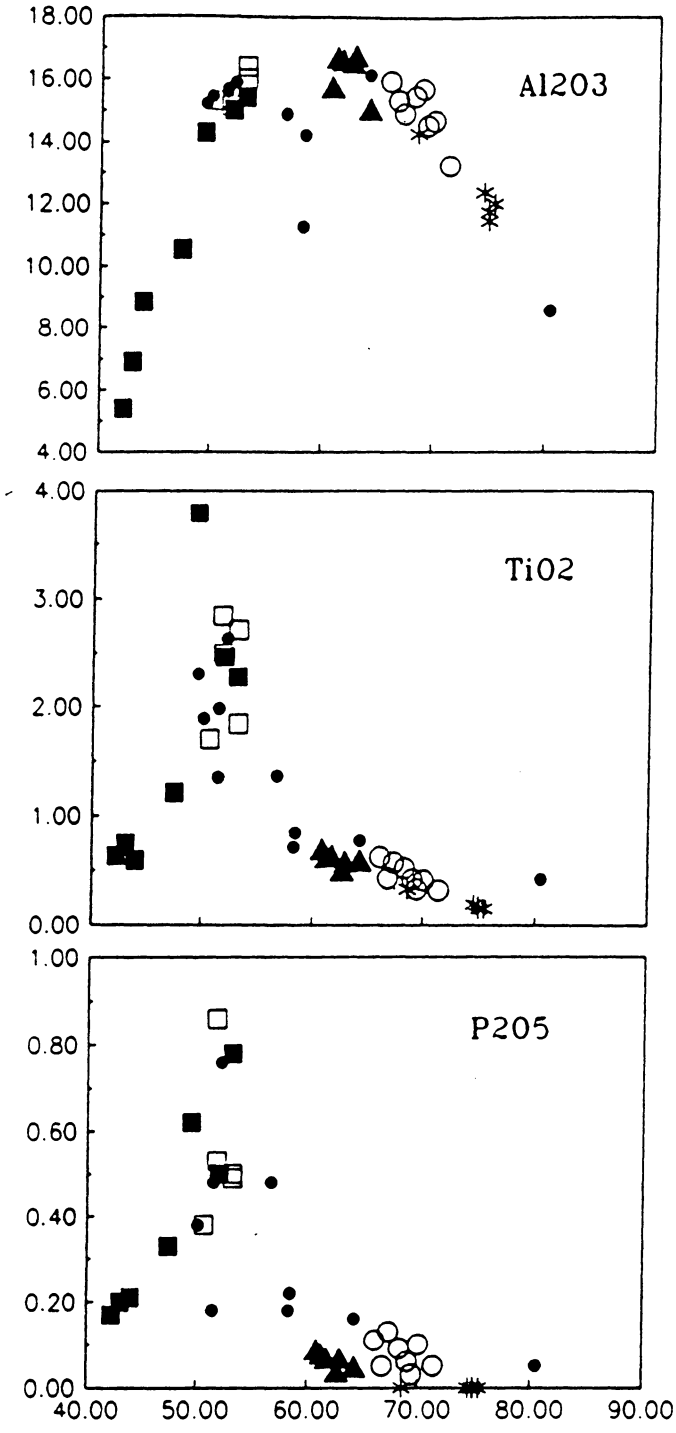

Figure 26. **Harker diagrams of major oxides vs silica (wt%):** Closed square = gabbro, open square = diorite, triangle = syenite, open circle = HB granite, star = AF granite, dot = dikes, enclaves and country rocks.

fect may never be totally ruled out. However, the following discussion of the petrogenesis of the MFPC will address the effects of fractionation and the possible sources and differing histories of the exposed rocks, to assess whether these processes could account for this observed silica gap within the MFPC.

Another silica gap is also evident in the MFPC data. This is between the most mafic gabbro samples (42 - 44 wt% SiO_2) and the other gabbros and diorites (47 - 53 wt% SiO_2). This gap reflects the difference between the low-silica cumulate gabbros and the other mafic rocks.

Comparing the composition of the suite of MFPC samples with standard volcanic classification schemes, the suite plots along the line dividing tholeiitic and calc-alkaline trends on the AFM diagram, within the field of alkaline suites (Irvine and Baragar, 1971), (Figure 27). According to the Peacock index, the suite is alkali-calcic.

A plot of $(FeO^* + MgO + CaO) - (Na_2O + K_2O) - (Al_2O_3)$ illustrates the inter-relationship of most of the rock-forming oxides. These trends superimpose directly on the plotted data compiled from the Nigerian Younger Granite suite (Jacobson et al., 1958; Bowden and Turner, 1974; Bowden et al., 1987), considered to represent an ideal Mesozoic anorogenic magmatic suite (Figure 28). As seen in Figure 28, there are two exceptions to the fit of this overlap. The $(FeO^* + MgO + CaO)$-rich samples from the MFPC are cumulate gabbro samples, and are not represented in the Nigerian suite. The $(Na_2O + K_2O)$-poor samples in the Nigerian set represent anorthosites. Anorthosites are not exposed in the MFPC. However, due to the close parallel in other rock assemblages, it is possible that anorthosite exists at depth in the MFPC.

The mafic suite of the MFPC consists of gabbros, with both cumulate and noncumulate textures, and diorites. The felsic suite consists of both subsolvus and hypersolvus syenites, pink-feldspar quartz syenite, alkali-feldspar granite, and hornblende-biotite-

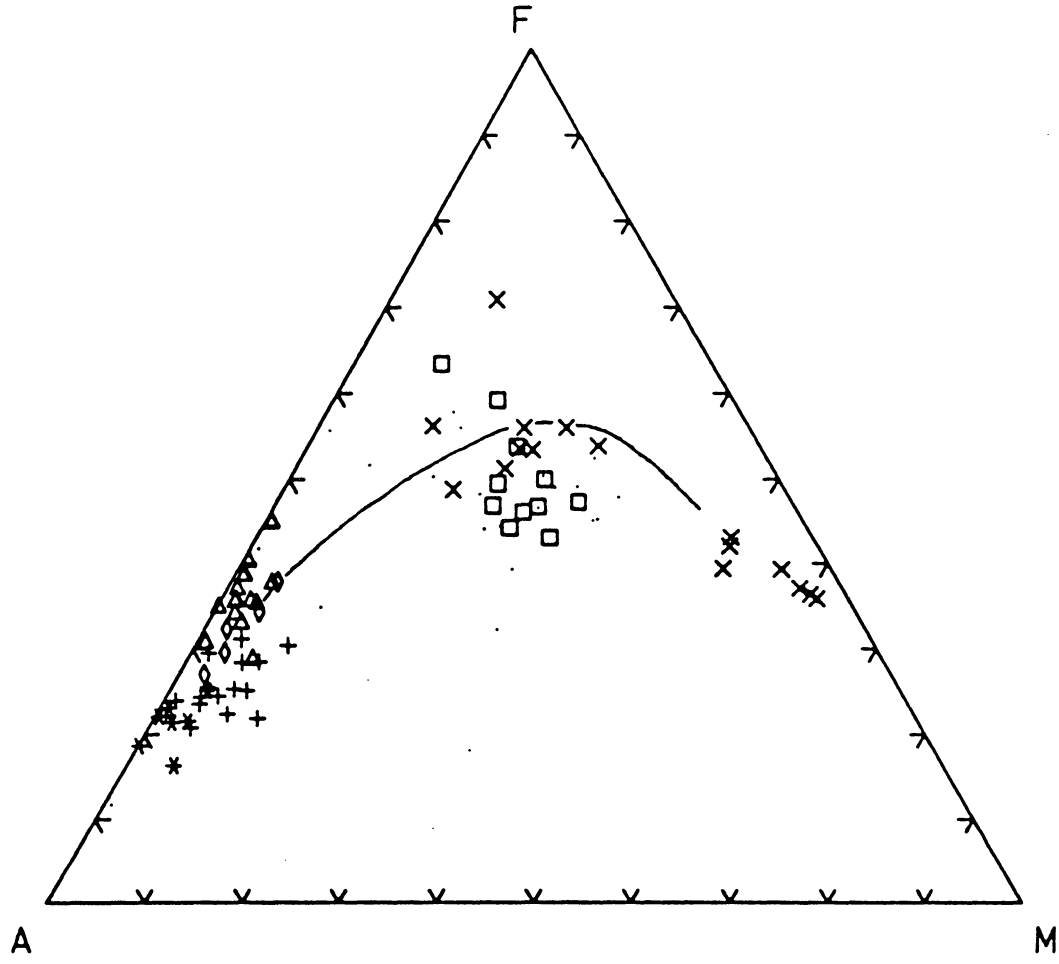

Figure 27. **AFM diagram showing all analyzed samples from the MFPC:** Tholeiite - calc-alkaline dividing line from Irvine and Baragar (1971). x = gabbro, square = diorite, + = HB granite, triangle = syenite, diamond = PFqtz syenite, * = AF granite, dot = dikes, enclaves and country rocks.

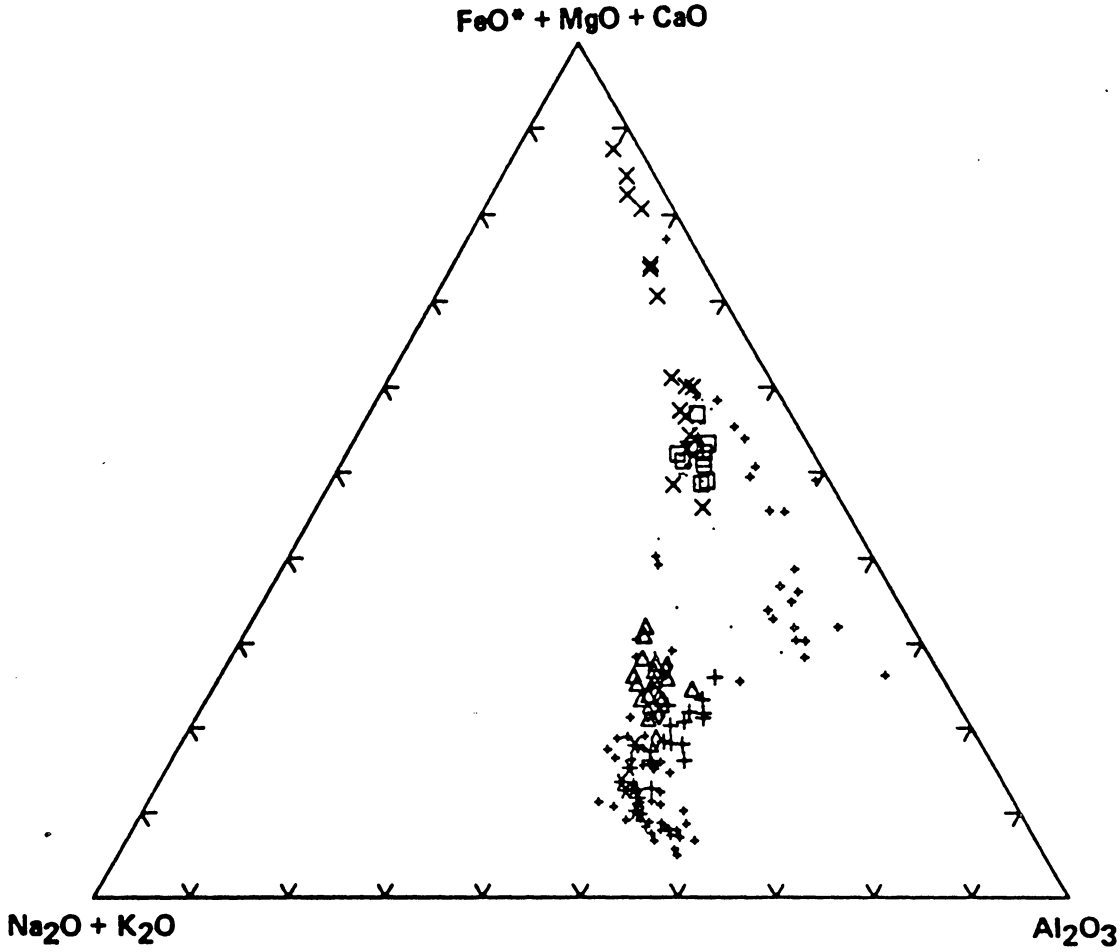

Figure 28. **Comparison of MFPC with Younger granites of Nigeria:** Plotted in terms of (FeO* + MgO + CaO) = F + M + C, vs (Al_2O_3) = Al2O3, vs (Na_2O + K_2O) = A. References for Nigerian data are listed in text. Small + = Nigerian data; larger symbols are MFPC data: x = gabbro, square = diorite, + = HB granite, triangle = syenite, diamond = PFqtz syenite, * = AF granite.

granites. Each of these rock types falls within compositional groupings which are distinct from one another. This grouping is particularly distinct in terms of some elements, such as Sr (related to plagioclase content) vs FeO* (related to mafic mineralogy) (Figure 29). With regards to other elements, though they are still grouped, there is overlap between rock types, particularly between gabbro and diorite, and between syenite and pink-feldspar quartz syenite. In order to maximize objectivity as to the genetic relationships between suites and members of suites, the following discussions will first focus on each rock type individually.

Gabbro:

The least siliceous rocks analyzed are gabbros with cumulate texture. These four samples form curvilinear trends on the Harker diagrams and are different from the trend of the other MFPC rocks in the case of Sr, Al_2O_3, CaO, P_2O_5 and TiO_2. In all cases, whole rock chemical composition of the gabbro is controlled by modal mineralogical content. This is illustrated for some of the major elements in Figure 30. Modal olivine content decreases sharply with increasing SiO_2, from about 60% to $\leq$2%. Concomitant with this modal change is a decrease in bulk rock FeO* and MgO, as seen in Figure 30, describing a compositional path away from the olivine composition field (which was determined using microprobe data from selected gabbro samples). Textures indicate that olivine is the dominant cumulate phase, with possibly some clinopyroxene cumulates. The continual extraction of the olivine composition from a fractionating magma would create a trend as seen in Figure 30.

The forsterite content of olivines in analyzed gabbros decreases with increasing wt% SiO_2 (Figure 31), and also with decreasing modal % olivine. The En content of clinopyroxene similarly decreases with increasing silica content of the rock (Figure 31).

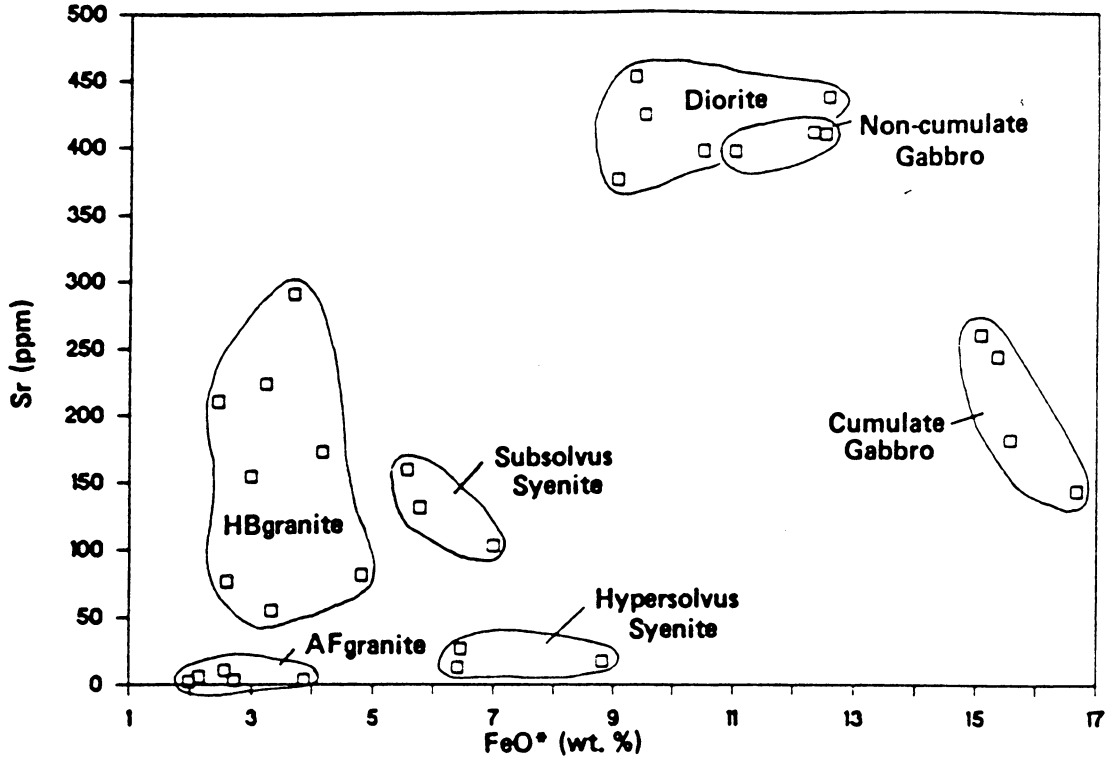

Figure 29. Plot of Sr (ppm) vs FeO* (wt%) for all MFPC analyses: Plot illustrates compositional grouping of different plutonic lithologies.

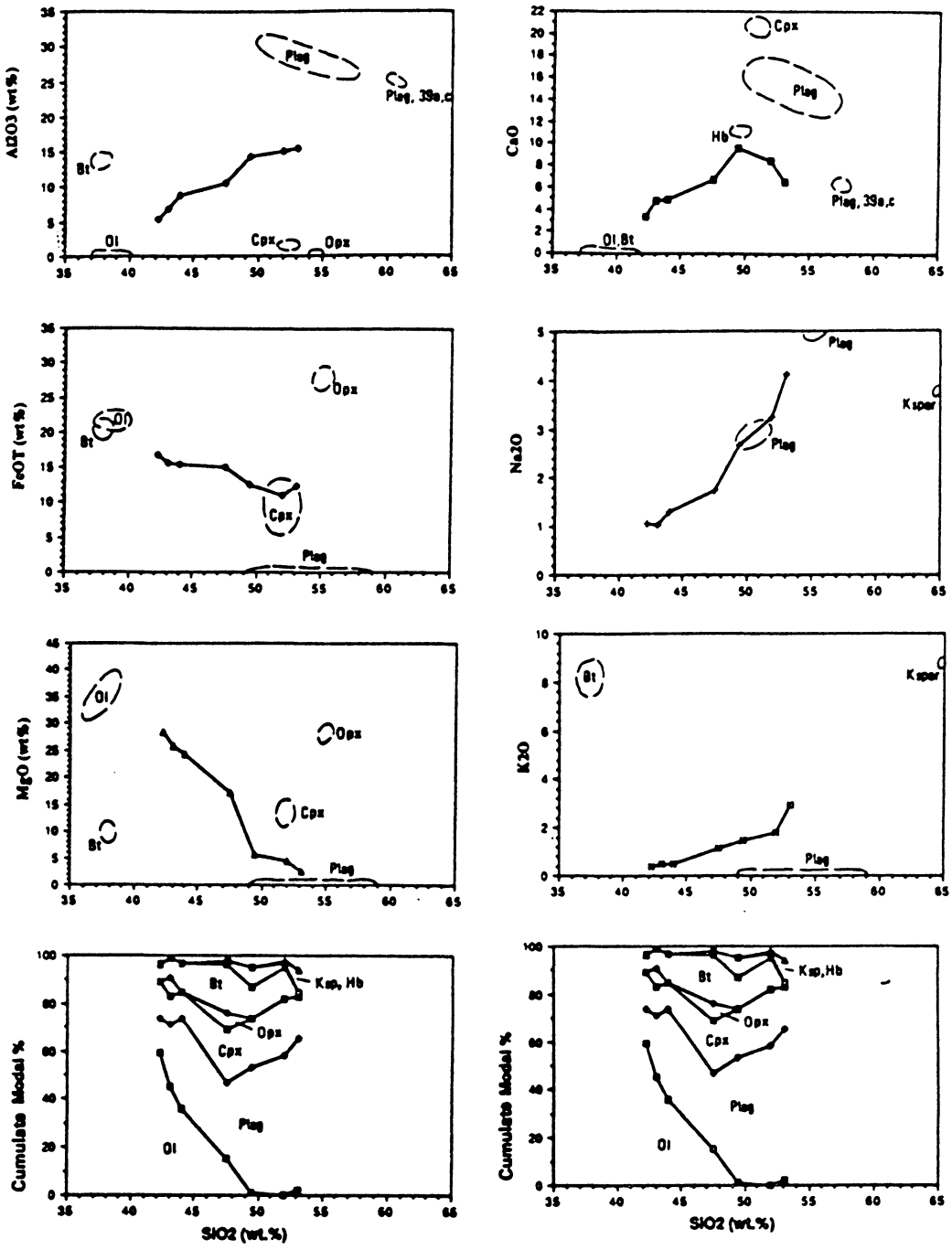

Figure 30. **Gabbro silica vs major oxides (wt%) and mineral compositions:** Mineral compositional fields are from analyses of minerals in gabbro modes. Lower plots are cumulate modal percentages in each whole rock sample vs silica in whole rock. Trends illustrate control of modal mineralogy on whole rock composition.

Modal clinopyroxene increases but does not track quite as systematically with decreasing En. This supports the interpretation that olivine was an early crystallizing phase in fractionating mafic magma; the most Mg-rich olivine accumulations were the first to crystallize. As olivine became less stable, clinopyroxene became relatively more abundant, and as would be expected, Fe/Mg increased in the crystallizing phases.

In the plots of Al_2O_3, CaO, and Na_2O against SiO_2 (Figure 30), bulk composition can be clearly seen to evolve towards the plagioclase composition field, consistent with the overall increase in modal plagioclase. Plagioclase An-content decreases with increase in both modal proportion of plagioclase, and wt% SiO_2, again suggesting the evolution of a fractionally crystallizing magma.

Samples 84DNS39a and c, which are from near a gabbro-syenite contact (highest silica gabbro samples), clearly show independent trends in Figure 30, especially 84DNS39c. These samples contain plagioclase which is markedly less calcic than in the cumulate samples, and alkali feldspar. It is these mineral compositions which largely control the inflection in the compositional trends, and are interpreted to be the result of contamination due to proximity to syenite.

Pyroxene, plagioclase, olivine and biotite are the most prevalent phases in the cumulate samples. Of these, the CIPW norm (Appendix B) accounts for all but biotite. The prescribed apportionment of major oxides to their normative mineral assemblages in the norm calculation allows for direct mineralogic comparison of disparate rock types, regardless of their modal differences. The CIPW norm is also useful as a means of comparing natural assemblages with experimental systems (Morse, 1980). To qualitatively examine the fractional crystallization process represented by the cumulate samples, their norms are plotted on the Px-Ol-Plag phase diagram in Figure 32. Normative pyroxene (En + Fs + Wo), olivine (Fo + Fa) and plagioclase (An + Ab) comprise over 88% of the normative phases in the cumulate samples, and thus, error

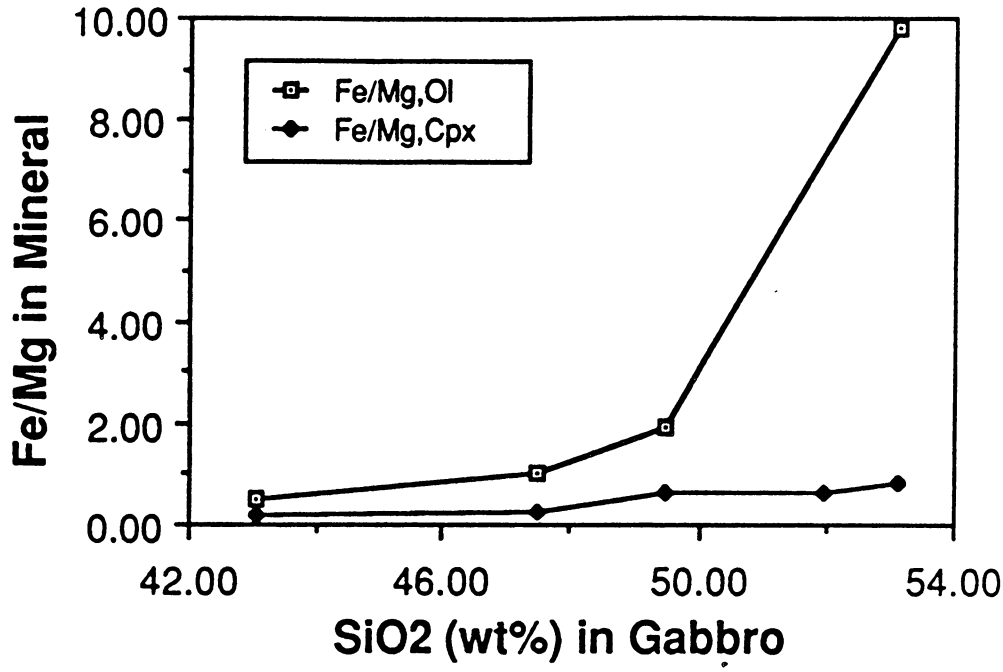

Figure 31. Gabbro silica vs Fe/Mg in olivine and clinopyroxene: Mineral data from probe compositions, showing increase in Fe/Mg with increasing SiO_2 in bulk gabbros.

caused by other components and by the projection through silica is minimal. Samples 83DNS307 and 82DNS186 (the lowest silica samples) could easily be derived from the same parent liquid, representing differing mixes between fractionated crystals (with collective compositions on the Fo-Di tieline) and resultant liquid (with composition on path away from Fo and on the cotectic). 84DNS44a has a greater percentage of plagioclase component, and cannot have the same parent composition in the simplified system being used, since it falls on the other side of the line between Fo and the eutectic. This could indicate 1) different parent liquid 2) local addition of plagioclase component, as fractional crystallization progressed 3) local contamination from external source, either pre-, syn- or post-crystallization 4) inapplicability of plotting norms from rocks with hydrous phases. Although none of these possibilities can be ruled out, the third is preferred based on the potential for contamination observed in field relationships, and the scatter in isotopic signatures which will be discussed later in this chapter.

Sample 82DNS196 plots very close to the eutectic in the Ol-Di-Pl system. Texturally, this sample contains resorbed cumulate olivine crystals, possibly some cumulate pyroxene crystals, and some intercumulus pyroxene. Plagioclase is subhedral, not ophitic. These textures are consistent with the interpretation of 82DNS196 as a mix of about 1 - 2% cumulate crystals and 98 - 99% eutectic liquid. This would provide a mode of roughly 9% olivine, 42% plagioclase and 49% pyroxene in this ternary system. Comparing this to the observed mode of 15% olivine, 32% plagioclase, 29% pyroxene, and 20% biotite, the presence of water, as evidenced by presence of biotite, would affect the eutectic temperature, and crystallization temperature was probably lower than the 1270°C indicated on the phase diagram.

Alternatively, each of these points may be considered as a separate bulk liquid composition. Since the analyzed samples are not stratigraphically related, systematic variation cannot be rigorously tested. However, due to the cumulate nature of the

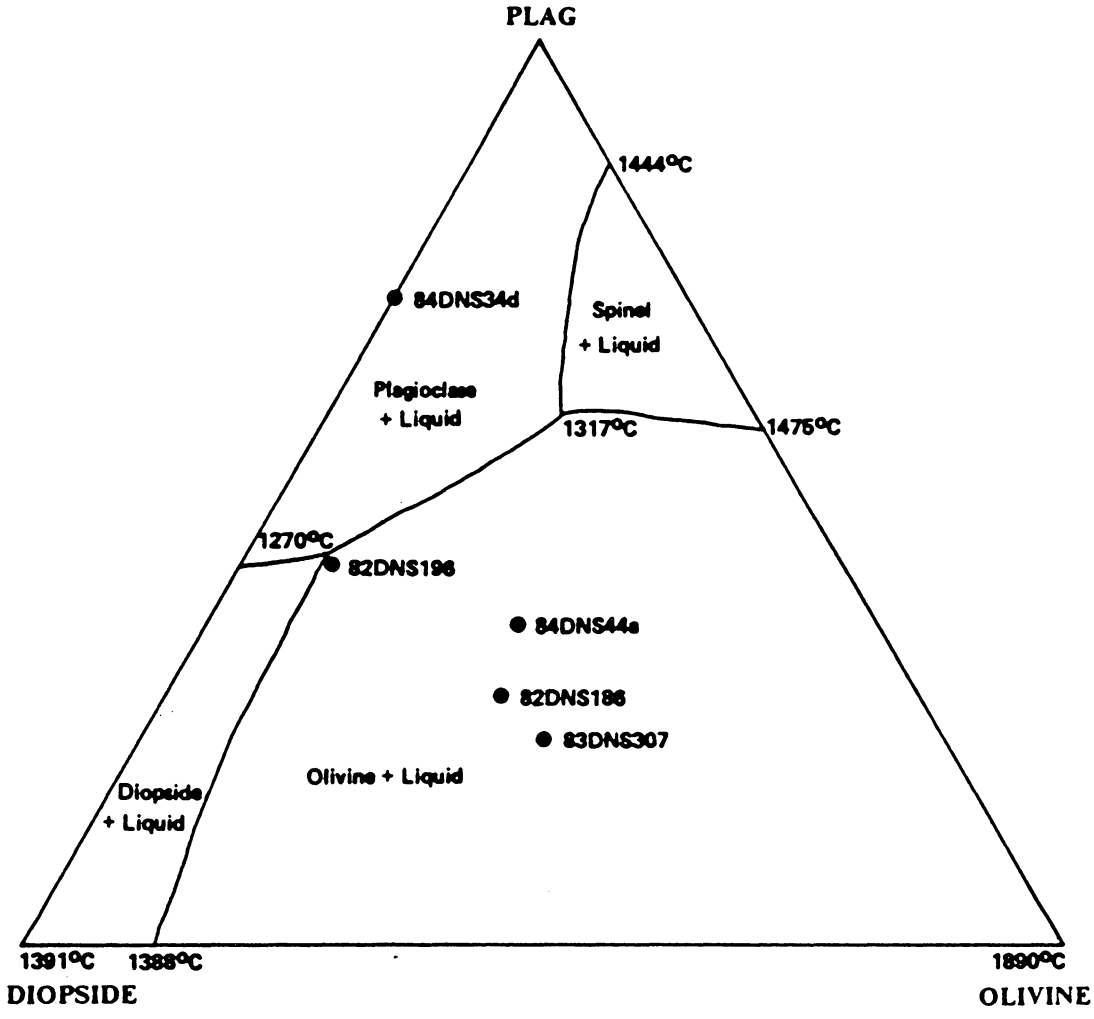

Figure 32. Di - Ol - Plag, norms of cumulate gabbros: Phase diagram taken from Morse (1980), P = 1 atm. (see text for discussion).

olivines, the bulk rock does not represent the bulk liquid from which the other minerals crystallized. Hence, calculation of bulk distribution coefficient (D) does not yield true information about the parent magma. Mineral-liquid distribution coefficients (K_d) will be discussed in the section on mineral chemistry. Sample 82DNS196 is the most promising candidate for representing the liquid at a single stage of its evolution, due to its normative composition at the eutectic of Di-Ol-Pl (Figure 32). Calculation of D for Rb and K in the hypothetical liquid from which 82DNS196 would have crystallized, (using values for K_d from Arth (1976), Nelson et al (1987) and Cox et al (1979)), yields results of 1.90 wt% K_2O, 49.27 ppm Rb, and K/Rb = 320.7, as shown in Appendix E. These values fall within the range of alkali basalts (Engel et al., 1965). The relatively high TiO_2 and LILE enrichment (evidenced by Ba/Y > 100) of the non-cumulate gabbro suite are also suggestive of alkali olivine basalt magma (Engel et al., 1965).

Diorites

It is reasonable to test the hypothesis that the diorites are more evolved fractionates of the gabbro, given the importance of fractionation in the gabbroic rocks of the MFPC. The diorites seem to follow fractionation trends for Al_2O_3, MgO, FeO*, MnO, Na_2O, P_2O_5, and TiO_2 (Figure 24, Figure 25, and Figure 26). Using gabbro sample 84DNS34d (SiO_2 = 49.47 wt%) as a starting composition (due to its noncumulate texture and relative lack of evidence for contamination), the program XLFRAC2 (Stormer and Nicholls, 1978) was used to test the possibility of deriving diorite compositions by fractionation. For example, to derive the most siliceous diorite (84DNS47c) from 84DNS34d, 46.7% of the magma must be crystallized, in the proportions 16.8% plagioclase, 12.8% clinopyroxene, 7.7% olivine, 5.0% ilmenite, and 4.4% biotite (sum of the squares of the residuals = 0.2334). The resulting cumulate rock, with modal

assemblage 36.0% plagioclase, 27.4% clinopyroxene, 16.5% olivine, 10.7% ilmenite, and 9.4% biotite, is a plausible, though unobserved, assemblage and is permissive that fractionation may be active. However, Harker diagrams show exaggerated increase of K_2O and Rb over the limited silica range of the diorites, and decrease in Sr, CaO, and Ba, relative to the trend seen for the gabbro samples (Figure 25 on page 54and Figure 33). These trends indicate that some other process may also have played a role in the paetrogenesis of the diorite.

The trends in these elements do not track directly with increasing SiO_2 ; in fact, the incompatible elements K and Rb are highest in the less siliceous samples 83DNS318b and 83DNS320d. These anomalous elements are all controlled by feldspar crystallization, and reflect the modal abundance of late crystallizing alkali feldspars in the diorites. The apparent late growth of the alkali feldspars in diorites, and the unsystematic increase of alkalis with silica suggest that there may have been a fluid-enhanced alkali exchange between diorite and some external source. The source could be 1) syn- or early post-crystallization fluid influx from HB granite, 2) syn- or early post-crystallization fluid influx from xenoliths/country rocks, or 3) late post-crystallization deuteric alteration by diorite magma fluids. Due to the anhydrous nature of the syenite and AF granite, they are unlikely sources of the altering fluids. The major and trace element data alone do not define the timing or source of the fluids. Further constraints will be discussed under mineral chemistry and isotopes.

HB granites

The HB granites fall in the subalkaline field of $Na_2O + K_2O$ vs. SiO_2 of MacDonald and Katsura (1964). Three samples (83DNS307d, 84DNS57a, 84DNS63a) are metaluminous (i.e., $(CaO + Na_2O + K_2O) > Al_2O_3 > (Na_2O + K_2O)$). The rest

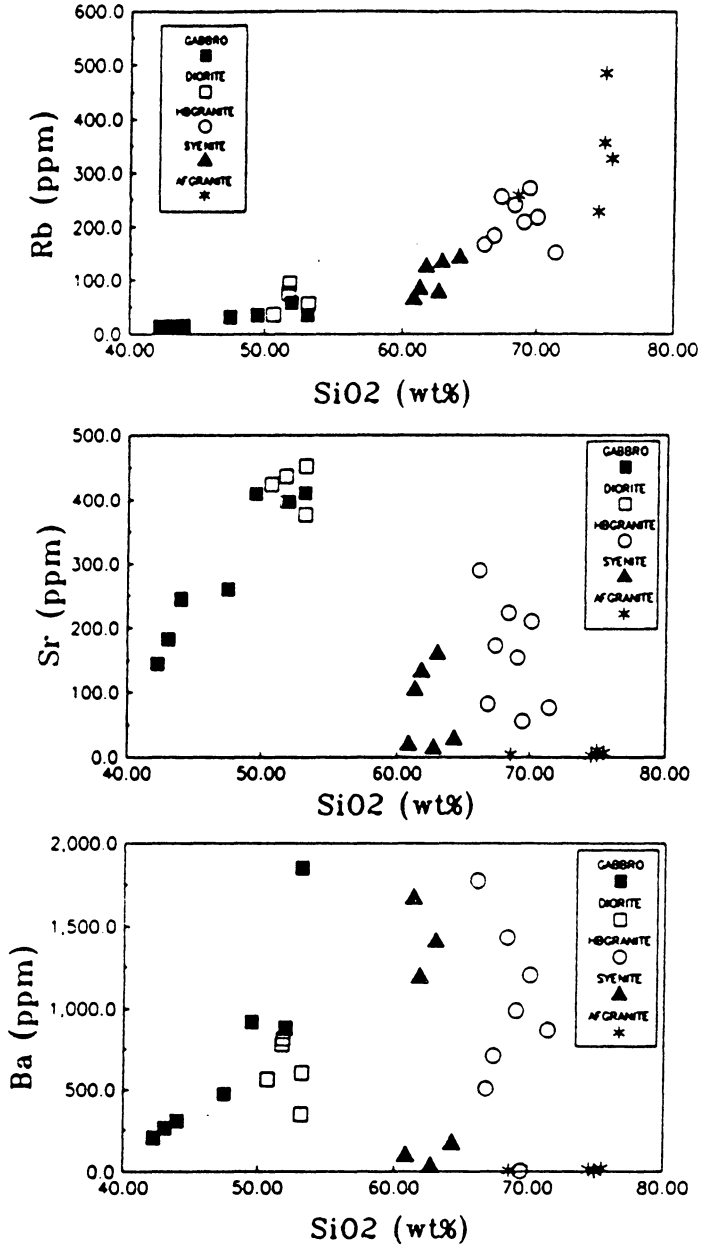

Figure 33. **Variation diagrams, SiO_2 vs. Ba, Sr and Rb:** Symbols as indicated.

are peraluminous (i.e., Al_2O_3 > (CaO + Na_2O + K_2O)). HB granite compositions plot between syenite and AF granite for most elements, suggesting a continuous fractionation trend (Figure 24, Figure 25 and Figure 26). However, the deviation from this trend in terms of K_2O, and Na_2O versus silica argues against a simple fractional relationship between these rock types, as does the intrinsic difference in mineralogic character of the HB granites from the more alkaline, more anhydrous syenites and AF granites. On a plot of normative Q-Ab-Or, the HB granites fall in a scatter away from the minimum towards the Ab-Or tieline (Figure 34) and thus do not represent minimum melts.

On the basis of field relations and textural homogeneity, sample 82DNS197 is probably representative of the largest mass of HB granite in the MFPC. All other samples in the analyzed suite have particular field relations which could lead to compositional variations (e.g., proximity to contacts, inclusion of mafic enclaves and/or xenoliths, modal and textural variations). Although each individual sample was collected and processed with care in an attempt to maximize homogeneity, the inter-sample chemical variability probably reflects a unique set of conditions for each sample.

Modelling of derivation of HB granite 82DNS197 from the most silica-rich unaltered diorite (84DNS47c) was attempted, using Stormer and Nicholl's (1978) XLFRAC2 program, with many permutations of added and subtracted mineral assemblages. The most feasible solution (SRR = 1.55) requires the removal of 90.5% of the diorite melt, in the assemblage 43.5% plagioclase, 29.5% hornblende, 12.7% biotite, and 4.76% clinopyroxene. This assemblage is not found in the MFPC. Therefore, fractionation of HB granite from diorite is considered unlikely, especially because of the quantity of the removed assemblage which is required by the model.

Analyzed silica contents of HB granites range from 66 to 73 wt% (Appendix B), reflecting the modal spread from granodiorite to granite (Figure 18 on page 36). Over this silica range, they follow fairly systematic trends of decreasing Al_2O_3, TiO_2, P_2O_5 ,

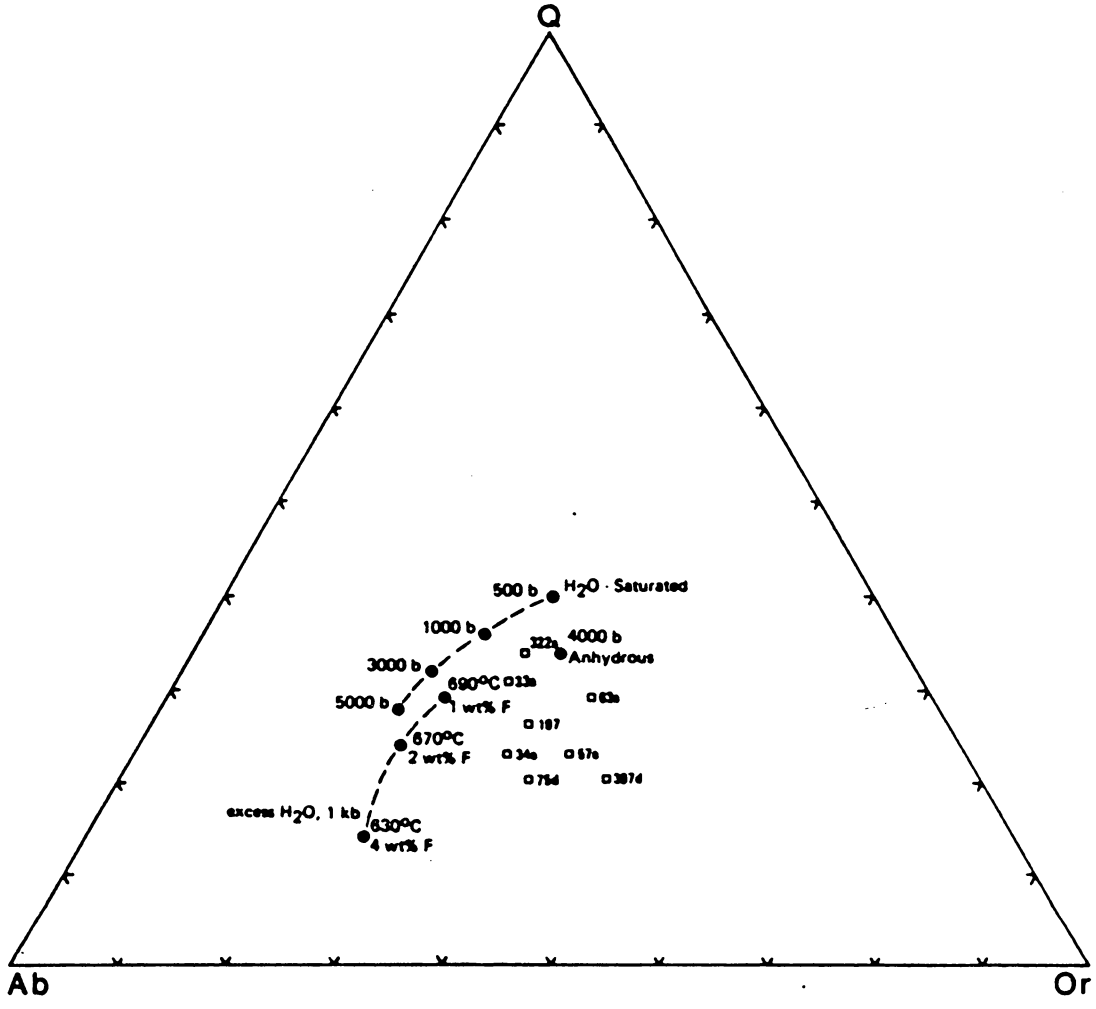

Figure 34. Normative Q - Ab- Or plot, showing HB granite compositions: HB granites do not plot as minimum melt compositions. Sample numbers are labelled. Anhydrous datum from Steiner et al (1975), F-bearing data from Manning and Henderson (1981), H_2O- saturated data from Tuttle and Bowen (1958; 0.5 - 3 kb) and Luth et al (1964; 5kb).

MgO, MnO, and FeO*. However, in terms of the alkalis (K, Na, Ca) and trace elements, they scatter unsystematically. This could be due to one or more of the following: 1) differing initial bulk compositions 2) varying degrees of mixing with a)syenite b)AF granite c)diorite d)gabbro e)country rock/xenolith, or 3)fluid exchange with the preceding possibilities.

Syenites

Analyzed syenite samples range between 60 and 66 wt% SiO_2 (Appendix B). This is more siliceous than the average syenite (SiO_2= 58.58wt%) of LeMaitre (1976), and reflects the silica oversaturated nature of these rocks. None are nepheline-normative. Two samples (82DNS128, 82DNS210) are silica-saturated, with normative olivine and hypersthene, the others are silica-oversaturated, with normative quartz and hypersthene.

The syenites represent the most alkali-rich rocks of the MFPC. Na-metasilicate (Na_2SiO_3) occurs only in the norm of 82DNS195b. This sample is peralkaline (molecular proportion $Na_2O + K_2O > Al_2O_3$), the other samples are metaluminous. Sr values are low (12.8 to 26.6 ppm), and Rb values are moderate (64.3 to 141.4 ppm). Wet chemical analysis, using the method of Whipple (1974), of whole rock sample 82DNS195b yielded a weight percent FeO of 4.10-4.31 on duplicate runs. The resultant Fe^{2+}/Fe^{3+} of 1.68 is considerably more reduced than the average ratio of 1.03 for 512 syenites reported by LeMaitre (1976). This is clearly a function of the f_{O_2} of the magma, and is discussed in a later section.

The hypersolvus and subsolvus syenites are distinguished compositionally by distinctly higher concentrations of Sr, Ba and Al_2O_3 and lower Na_2O in the subsolvus samples. All other analyzed elements overlap between the two types of syenite. Mineralogically, the subsolvus suite could be more evolved than the hypersolvus suite,

because of the late crystallization of hornblende at the expense of hedenbergite in the subsolvus samples (Figure 19). However, this contradicts the compositional distinctions, since Sr, Ba and Al_2O_3 are typically lower and Na_2O higher in more evolved rocks. Indeed, using XLFRAC2 (Stormer and Nicholls, 1978) modelling to derive the subsolvus (84DNS32a) from the hypersolvus (82DNS79), 3.9% oligoclase (of analyzed composition from subsolvus sample 82DNS210) must be added (SSR = 0.5376) to the hypersolvus composition. This is in accordance with the apparent late-crystallization of plagioclase in the subsolvus samples. Thus, the observed crystallization sequence and analytical data suggest the addition of components to the hypersolvus syenite to derive the subsolvus syenite. The late crystallization of oligoclase following an early history of hypersolvus alkali feldspar crystallization in the the subsolvus suite suggests that one of these components was probably H_2O. Higher water content in the melt is known to depress the temperature of the solidus so that it intersects the solvus, allowing crystallization of two feldspars (Tuttle and Bowen, 1958). Introduction of water late in the crystallization history of hypersolvus syenite would thus not only explain the observed texture, but would facilitate migration of the feldspar components (i.e., Sr, Ba, Al_2O_3, Na_2O) which distinguish the two types of syenite. The presence of abundant mafic enclaves in the vicinity of subsolvus syenite sample sites suggests that the fluid source was the mafic magma. The presence of biotite in the mafic enclaves indicates that water was present in the mafic liquid. Evidence for isotopic contamination will be discussed in a later section.

AF granites

The AF granites are peralkaline, with agpaitic index (Al_2O_3 /(Na_2O + K_2O)) ranging from 1.04 to 1.13. Silica values range from 68.63 to 75.48 wt%, the highest in the

MFPC. CIPW norms of the five representative samples analyzed contain only quartz, orthoclase, albite, Na-metasilicate, diopside, and ilmenite. Relative to the other felsic rock types of the MFPC, AF granites have lower content of all major oxides except SiO_2. Fluorine content ranges from over 900 to over 3000 ppm. Ba content is low (4 - 19 ppm), as is Sr (2.4 - 10.8 ppm); Rb (227.0 - 494.3 ppm) and Y (117 - 416 ppm) are high.

AF granite can be derived from syenite compositions, according to XLFRAC2 modelling (Stormer and Nicholl, 1978), by removal of about 60% of the syenite melt in proportions similar to syenite modal assemblage. Alternatively, a total of about 7% alkali feldspar and clinopyroxene can be removed with concurrent addition of about 10% quartz in order to form AF granite (82DNS195c) from hypersolvus syenite (82DNS195b).

Pink-feldspar Quartz Syenite (PF quartz syenite)

All PF quartz syenite analyses are from the ADGGS suite, and include only major oxide data. These data generally group with the syenite compositions (eg, Figure 24), with approximately a 2 wt% shift in average composition to higher SiO_2, and an overall slight decrease in alkalis. These shifts follow the trend of both HB granites and AF granites, and are related to the modal increase in quartz and decrease in alkali feldspar which sets the PF quartz syenites apart from the syenites. However, the overall chemical similarities and field relationship with the syenite suggest that the PF quartz syenites are a locallized, genetically related variant of the syenites.

Discussion

On the basis of bulk chemistry, a number of conclusions have been proposed with regard to the interrelationships between the rock types of the MFPC. Fractionation is thought to have played an important role in the evolution of the gabbros, with bulk composition largely controlled by modal mineralogy. Fractionation of gabbro to form diorite may have occurred. However, superimposed upon this process was a fluid influx which mobilized elements which are controlled largely by feldspars (i.e., K, Rb, Ca, Sr, Ba). The metaluminous to peraluminous HB granites are probably not fractionally related to other rocks of the MFPC, and therefore are thought to represent at least one other independent magma. The syenites are the most alkali-rich rocks of the MFPC. Addition of water caused the hypersolvus syenites to crystallize plagioclase, forming subsolvus syenites in areas where mafic enclaves are numerous. The peralkaline AF granites are the most siliceous rocks in the complex; their genetic relationship to other rock types cannot be determined solely on the basis of bulk composition, though fractionation from syenitic magma is feasible. The PF quartz syenites are thought to be a locallized, genetically related variant of the syenites, based on chemical similarities.

Isotope Geochemistry

In order to explore the age and history of the MFPC rocks, isotopic analytical studies of the Rb-Sr and K-Ar systems were undertaken. All K-Ar analyses were done in the geochronology laboratory at the Geophysical Institute, University of Alaska, Fairbanks. Rb-Sr analytical work was done in the isotope geochemistry lab at Virginia Tech. Analytical procedures by which these data were collected are reported in Appendix D.

K-Ar Age Determinations

K-Ar age determinations (Gilbert et al, 1989) are summarized and compared to Rb-Sr determinations on Table 1. The K-Ar ages of all analyzed plutonic rocks fall between 55.6 ± 1.7 and 57.7 ± 1.5 m.y., all within overlapping errors. This includes biotite and hornblende ages for HB granite sample 82DNS197 which are concordant within error. This lends support to the interpretation that the measured K-Ar ages reflect the time of crystallization without subsequent resetting. The slightly older measured age of the hornblendes (both 82DNS197 and 82DNS193) than biotites in the complex is probably a measure of hornblende's higher (and thus earlier and older) blocking temperature (Dodson, 1973). The small differences between hornblende and biotite ages indicates rapid cooling of the magmas from which the minerals crystallized. This suggests that the magmas were emplaced at a shallow level. in order to cool quickly. Volatile loss also promotes rapid crystallization, and could possibly be related to volcanic eruption.

Table 1. Radiometric age determinations from the MFPC

	K-Ar	Rb-Sr
Syenite	No data	Age: 56.3+2.6 Isochron: Whole rock, 3 points MSRS: 1.7710 SIR: 0.71018
AFgranite	Age: 57.7+1.5 Sample: 82DNS193 Type: Na-amphibole Age: 55.6+1.7 Sample: 82DNS195c Type: Na-amphibole	Age: 57.5+3.0 Isochron: Whole rock, 4 points MSRS: 0.18 SIR: 0.71185
Syenite + AFgranite		Age: 58.5+0.2 Isochron: Whole rock, 7 points MSRS: 2.967 SIR: 0.70965
Gabbro	Age: 56.1+1.7 Sample: 82DNS196 Type: Biotite	Age: 60.8+1.0 Isochron: 82DNS196;Pl,bt,wr MSRS: 3.471 SIR: 0.70585
Diorite	Age: 56.6+1.7 Sample: 82DNS209 Type: Biotite	Age: 57.2+0.6 Isochron: 83DNS320d;Ap,pl,bt,hb,wr MSRS: 11.020 SIR: 0.70689
HBgranite	Age: 56.5+1.7 Sample: 82DNS197 Type: Biotite Age: 57.2+1.7 Sample: 82DNS197 Type: Hornblende	Scatter
Dike Swarm	Age: 55.0+1.6 Sample: Type: Whole rock Age: 54.1+1.6 Sample: Type: Whole rock	Scatter

Two mafic samples from the dike swarm to the east of the MFPC yield K-Ar ages of 54.1 ± 1.6 and 55.0 ± 1.6 m.y.. The errors on these analyses overlap errors of plutonic rock analyses. However, their overall younger mean age, in conjunction with field evidence that some of the dike swarm postdates plutonic crystallization, suggests that the two sampled dikes are from the post-plutonic generation of dike intrusion.

Rb-Sr Determinations

The Rb-Sr isotopic data are presented in Table 2, and are discussed by rock types. The initial $^{87}Sr/^{86}Sr$ (SIR) calculated for individual samples uses the age of 57 m.y.

Gabbro

An isochron plot of $^{87}Rb/^{86}Sr$ vs $^{87}Sr/^{86}Sr$ for whole rock gabbro samples is shown in Figure 35, and scatter in the data yield no age information. Since there is no systematic pattern in the scatter with respect to the amount of petrographic evidence for alteration, it seems unlikely that the scatter was imposed entirely by secondary processes.

It is assumed on the basis of evidence for fractionation discussed in a preceding section, that the gabbros are comagmatic. Therefore, they either initially had uniform $^{87}Sr/^{86}Sr$ ratios, or were derived from a inhomogeneous parent magma. If initially uniform, then they have experienced different degrees of contamination. Locallized magmatic contamination at the time of crystallization (i.e., at the time of setting of the Rb-Sr 'clock') would be indistinguishable from evolution from a inhomogeneous parent magma.

Initial $^{87}Sr/^{86}Sr$ ratios (SIRs) calculated to 57 m.y. for the gabbros yield values of 0.7053 to 0.7059 (Figure 36). These are moderately high for primitive gabbroic rocks

Table 2. Whole rock plutonic Rb - Sr isotopic data

SAMPLE	Rb	Sr	$^{87}Rb/^{86}Sr)_{meas}$	$^{87}Sr/^{86}Sr)_{meas}$	+/-	SIR	$^{87}Sr/^{86}Sr)_{corr.}$
GABBRO:							
83DNS307	13.6	144.0	0.26919	0.70586	8	0.70551	0.70573
82DNS186	14.8	182.7	0.23434	0.70566	9	0.70534	0.70553
84DNS44a	15.0	244.6	0.17741	0.70620	10	0.70593	0.70607
82DNS196	31.5	260.3	0.35008	0.70619	9	0.70578	0.70606
84DNS34d	34.7	409.4	0.24519	0.70598	8	0.70565	0.70585
84DNS39a	57.1	396.9	0.41618	0.70604	12	0.70558	0.70591
84DNS39c	34.9	410.6	0.24589	0.70622	8	0.70589	0.70609
DIORITE:							
82DNS74b	36.0	432.7	0.24066	0.70523	8	0.70491	0.70510
83DNS320d	74.6	436.5	0.49447	0.70737	9	0.70684	0.70724
83DNS318b	93.8	397.2	0.68323	0.70701	12	0.70633	0.70688
82DNS209	55.5	376.5	0.42644	0.70617	9	0.70570	0.70604
84DNS47c	55.2	452.0	0.35331	0.70688	11	0.70647	0.70675
HBGRANITE:							
84DNS33a	166.3	290.4	1.65702	0.70853	7	0.70706	0.70840
83DNS307d	183.2	81.5	6.50720	0.71313	12	0.70773	0.71300
84DNS57a	254.5	172.5	4.27083	0.71284	8	0.70925	0.71271
82DNS197	239.5	223.2	3.10531	0.71002	8	0.70738	0.70989
84DNS34a	207.7	154.0	3.90330	0.71053	9	0.70724	0.71040
82DNS75d	270.5	54.8	14.29604	0.71791	10	0.70620	0.71778
83DNS322a	216.5	210.0	2.98412	0.71199	8	0.70945	0.71186
&4DNS63a	151.0	76.4	5.72107	0.71237	9	0.70761	0.71224
SYENITE:							
82DNS210	82.6	102.7	2.32712	0.70802	9	0.70601	0.70789
84DNS32a	124.0	131.2	2.73477	0.70859	9	0.70625	0.70846
84DNS32b	133.7	159.4	2.42694	0.70817	10	0.70608	0.70804
82DNS128	83.4	17.8	10.46550	0.72120	10	0.71260	0.72107
82DNS79	91.1	12.8	17.21124	0.72686	20	0.71279	0.72673
82DNS195b	174.9	26.6	15.40698	0.72546	8	0.71285	0.72533
AFGRANITE:							
82DNS195c	257.3	3.8	199.12070	0.87537	14	0.71398	0.87521
84DNS61a	226.5	2.4	279.20312	0.93785	40	0.71160	0.93768
82DNS193	356.1	10.7	97.07899	0.79141	18	0.71266	0.79127
82DNS162b	486.3	3.6	403.27393	1.03300	82	0.70627	1.03281
83DNS321d	326.6	6.0	159.56047	0.84192	16	0.71257	0.84177
COUNTRY ROCK:							
84DNS64	91.3	98.0	2.70067	0.72727	12	0.72495	0.72714
85DNS206	93.6	85.8	3.15786	0.71262	14	0.70993	0.71249
82DNS202	24.0	132.2	0.52553	0.71302	9	0.71247	0.71289

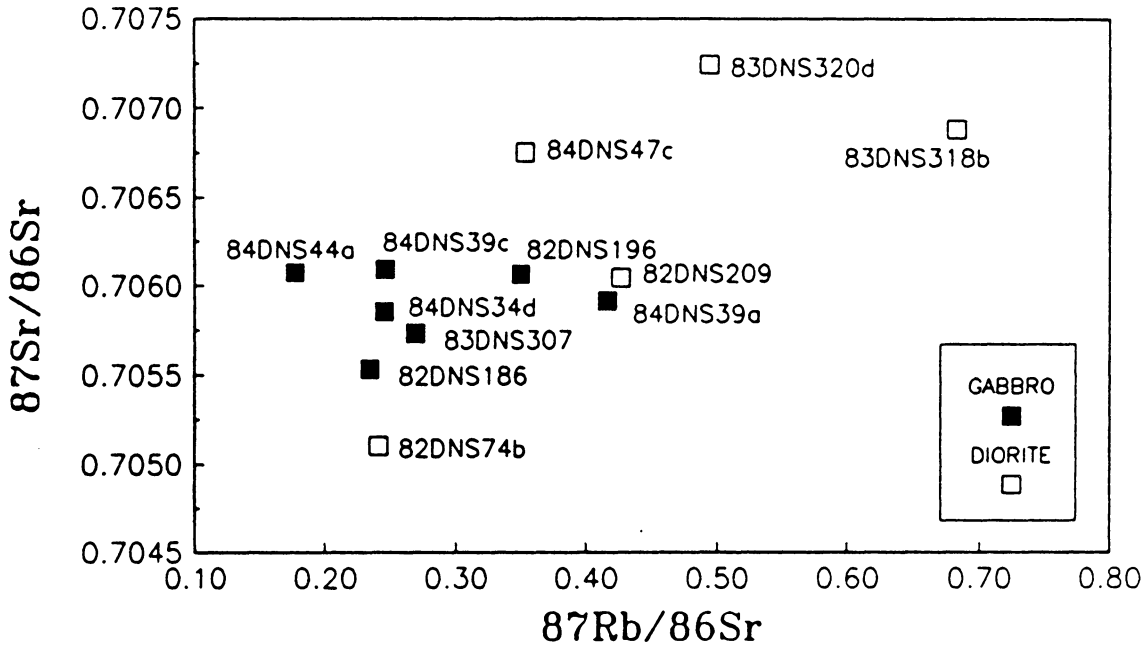

Figure 35. Radiogenic Rb-Sr plot, whole rock gabbros and diorites: $^{87}Rb/^{86}Sr$ vs measured $^{87}Sr/^{86}Sr$ diagram, showing scatter of data.

(e.g., Faure and Powell, 1972), suggesting either derivation from an enriched mantle source or contamination by a crustal component. If they were uncontaminated products of an enriched mantle melt, then all samples must have the same SIR. Because of scatter in the data it seems likely that the Sr isotopic system of the MFPC gabbros has been affected by contamination from crust or other magmas. When and where this occurred prior to crystallization is indeterminate from the data available.

In order to confirm the coeval nature of rocks of the MFPC, as suggested by the field relations and K-Ar data, a Rb-Sr isochron age using mineral separates from sample 82DNS196 (biotite and plagioclase) was obtained (Table 3). This sample was chosen as a representative gabbro due to its unaltered mineralogy. Plagioclase and biotite were selected to yield a wide spread in $^{87}Rb/^{86}Sr$, and to represent early- and late-crystallizing phases respectively. The results show that these two minerals and the whole rock were of uniform isotopic composition at the time of crystallization, and have not been subsequently altered. They form a three point isochron (MSRS of 3.47) with SIR of 0.7058 and an age of 60.8 ± 1.0 (2σ) m.y.. This age is somewhat older than other age determinations from MFPC rocks (Table 1), though it is within error limits and not necessarily older. Field evidence precludes the gabbros from being the oldest rock type within the MFPC. Indeed, the differences in age are slight, lending support to the interpretation of synchroneity of magmatism in the MFPC.

Diorites

Rb-Sr isotopic data from the five representative diorite samples yield results which overlap the gabbro data but have a broader scatter (Figure 35; Figure 36). These samples have been argued on a major and trace element basis (preceding section) to be fractionally related to the gabbros, with a compositional overprint due to fluid influx.

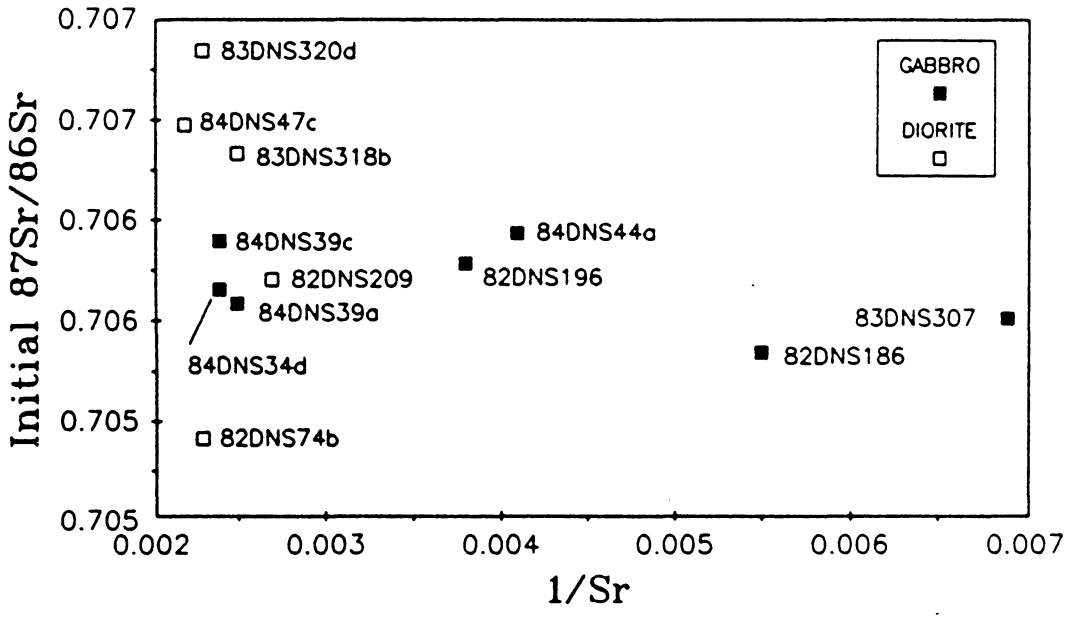

Figure 36. SIR vs 1/Sr diagram for whole rock gabbros and diorites

Table 3. Rb - Sr isotopic data, gabbro 82DNS196

SAMPLE	Rb	Sr	$^{87}Rb/^{86}Sr)_{meas}$	$^{87}Sr/^{86}Sr)_{meas}$	+/-	SIR	$^{87}Sr/^{86}Sr)_{corr.}$
WHOLE ROCK	31.5	260.3	0.35008	0.70619	9	0.70578	0.776062
BIOTITE	219.5	36.8	17.28000	0.72093	19	0.70694	0.720800
PLAGIOCLASE	2.5	918.2	0.00788	0.70608	10	0.70607	0.705952

The increased scatter, and the large amount of hydrothermal alteration in some diorite samples suggest that subsolidus processes have affected the Rb-Sr systematics.

The Rb-Sr isotopic data can provide some constraints on the timing and source of the altering fluids in the diorites. On a plot of SIR vs 1/Sr, the diorites with highest SIR are shifted nearly vertically with respect to the gabbro field (Figure 36). This implies that Sr concentration was not the controlling factor in the SIR increase. On Figure 37 is shown the correlation between SIR and K/Rb, Rb, Sr, Loss on Ignition (LOI- as a measure of hydrothermal alteration), Ba, modal quartz and modal alkali feldspar. Although high SIR samples 83DNS318b and 83DNS320d are heavily altered, the correlation of SIR with LOI is low due to the relatively small amount of alteration in high SIR sample 84DNS47c. The geologically significant correlations seem to be the greater amount of alkali feldspar (correlation coefficient = +0.75) and Rb content (correlation coefficient = +0.62) with increasing SIR. Thus, the scatter in increasing SIR can be attributed to the interplay of these factors: 1) the amount of fluid that infiltrated the diorite 2) the amount of alkali feldspar that crystallized (implying that the alkali feldspar components are at least in part from an external source), and 3) the amount of Rb which was introduced into the diorite. The abundance of secondary minerals is not a controlling factor. Therefore, any late removal of Rb or addition of Sr, which would lead to miscalculation of SIR, is probably not a relevent problem in this case.

Either the HB granites or some composition of country rock would be viable fluid sources since both have SIR higher than the diorites. K/Rb decreases with increasing SIR, with a shift toward HB granite (Figure 38). Moreover, the ubiquitously intimate relationship between diorite and HB granite (Figure 39) suggests that the most probable fluid source is the HB granite.

To gain some constraints on the timing of alteration, mineral separates from sample 83DNS320d (most altered, highest SIR) were analyzed. The data (Table 4) from

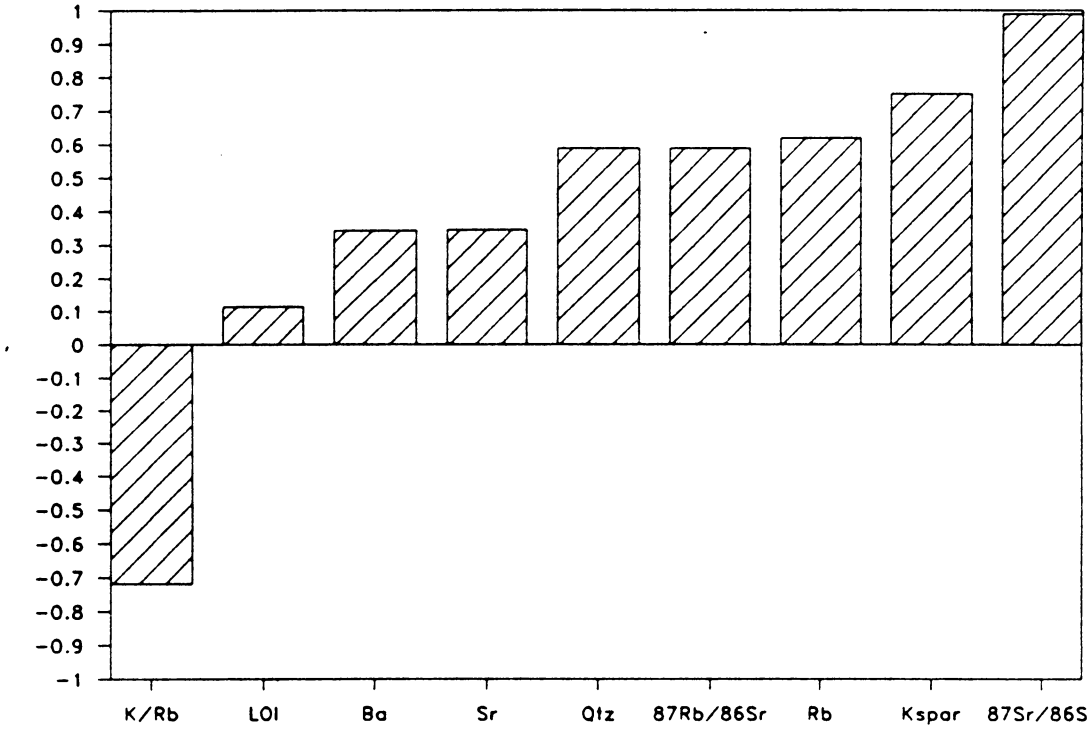

Figure 37. Correlation of compositional factors with SIR in diorites: Degree of alteration, as measured by LOI (loss on ignition) does not control SIR; K/Rb, modal alkali feldspar, and whole rock Rb are the most closely correlated factors with diorite SIR.

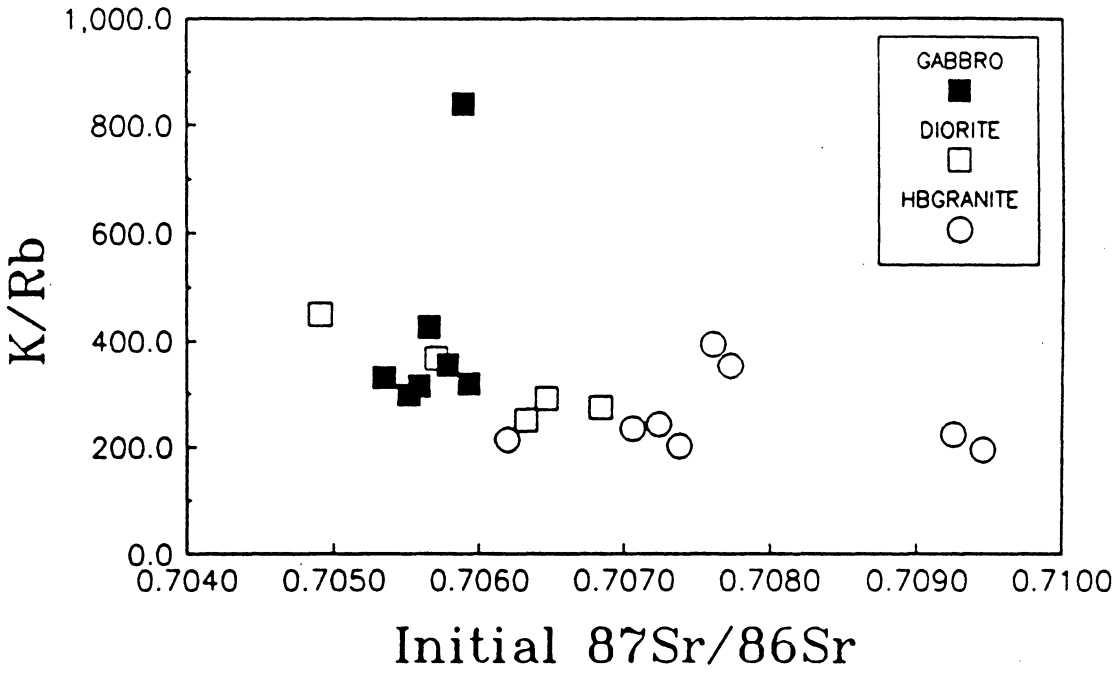

Figure 38. **K/Rb vs SIR - gabbros, diorites and HB granites:** There is a general decrease in K/Rb with increasing SIR in gabbro and diorite toward HB granite field.

Figure 39. Photo of HB granite brecciating and intruding diorite: The close association of these two rock types helps explain scatter in diorite isotopic data (see text).

apatite, plagioclase, biotite, secondary amphibole and whole rock form a five-point isochron, age 57.2 m.y. ± 0.6 (2σ), with MSRS of 11.02. This indicates that the magma from which these minerals, including the amphibole, crystallized was in isotopic equilibrium. Its SIR was 0.70689. This places an important constraint on the timing of the fluid influx. The fluid must have been introduced prior to crystallization of the minerals analyzed, or during their crystallization. The conclusion based on data presented thus far, is that the diorites, in very early stages of crystallization, were variably flooded by alkali-bearing fluids. The alkali-addition scattered the whole-rock Rb-Sr systematics, but preserved mineral data. Therefore, variable amounts of residual water hydrothermally altered the diorites in a closed system, maintaining isotopic equilibrium.

The sample with the lowest SIR in the MFPC, 84DNS74b, is texturally and mineralogically very similar to the other diorites, but with very little alkali feldspar. The alkali-bearing fluids must not have come in contact with this rock, although the post-crystallization, residual fluid did. This sample was run in duplicate with good reproducibility, and must simply be a fractionate of a particularly uncontaminated magma.

HB granites

Eight samples of HB granite were analyzed for Rb-Sr isotopes. The scatter in the resultant data can be fitted with regression lines (York, 1969, Model 2) yielding isochrons of two different slopes (Figure 40). One, a three-point line, (84DNS34a, 82DNS197, 82DNS75d), indicates an age of 49.7 m.y. ± 1.2 (2σ), MSRS = 0.29. The other is a four-point isochron (84DNS33a, 82DNS197, 84DNS63a, 83DNS307d) of age 66.1 m.y. ± 2.6 (2σ), MSRS = 0.92. When sample 84DNS34a is included in this latter group, the resultant age is very similar; 66.2 m.y. ± 2.6 (MSRS = 1.86). From all other

Table 4. Rb - Sr isotopic data, HB granite 83DNS320d

SAMPLE	Rb	Sr	$^{87}Rb/^{86}Sr)_{meas}$	$^{87}Sr/^{86}Sr)_{meas}$	+/-	SIR	$^{87}Sr/^{86}Sr)_{corr.}$
PLAGIOCLASE	67.5	868.9	0.22475	0.70706	11	0.70687	0.70692
BIOTITE	384.1	19.2	58.14581	0.75441	12	0.70733	0.75427
APATITE	1.6	246.4	0.01897	0.70738	22	0.70736	0.70725
HORNBLENDE	43.1	46.9	2.65924	0.70904	12	0.70689	0.70891
WHOLE ROCK	74.6	436.5	0.40447	0.70737	9	0.70684	0.70724

indications, including K-Ar data, and both whole rock and mineral separate Rb-Sr data (Table 1 on page 76), the MFPC is about 57 m.y. old; somewhere between the two diverse isochrons. Therefore, the geologic significance of ages yielded by these possible isochrons must be questioned.

Field evidence is clear that HB granites are intrusive into the other rock types. Therefore, the 66.1 m.y. age is unlikely to represent crystallization of the HB granites, unless all the other ages were the product of later resetting. This is ruled out for two reasons: 1) it is highly improbable that all other age indicators would be uniformly and completely reset, and 2) if such a thorough resetting event did occur, then the HB granites should also have been affected.

The younger isochron would make the HB granites about 8 m.y. younger than the other rock types. Although this is a possibility, the geologic evidence for the three samples on the line being cogenetic and uncontaminated is tenuous. They occur in three very different field settings: 82DNS197 is from what appears to be the most large-scale representative area of HB granite, 84DNS34a is from felsic dikelets and veins in gabbro, and 82DNS75d is from Tourmaline Ridge where mafic enclaves (diorite) and metasedimentary xenoliths abound.

The younger isochron could represent a thermal event which reset the Rb-Sr systematics. However, the concordant K-Ar age on both biotite and hornblende in 82DNS197 argues against this.

Due to the overall scatter of the data, the very different field settings of the individual samples, the field relationships between units, and the small number of points on the line, it is concluded that neither regression line is indicative of crystallization age. To evaluate the possibility that they are mixing lines, a plot of SIR vs 1/Sr is shown (Figure 41). On the basis of the isotope data, several models are possible. Since field evidence does not necessitate a common origin for all samples, the data could represent

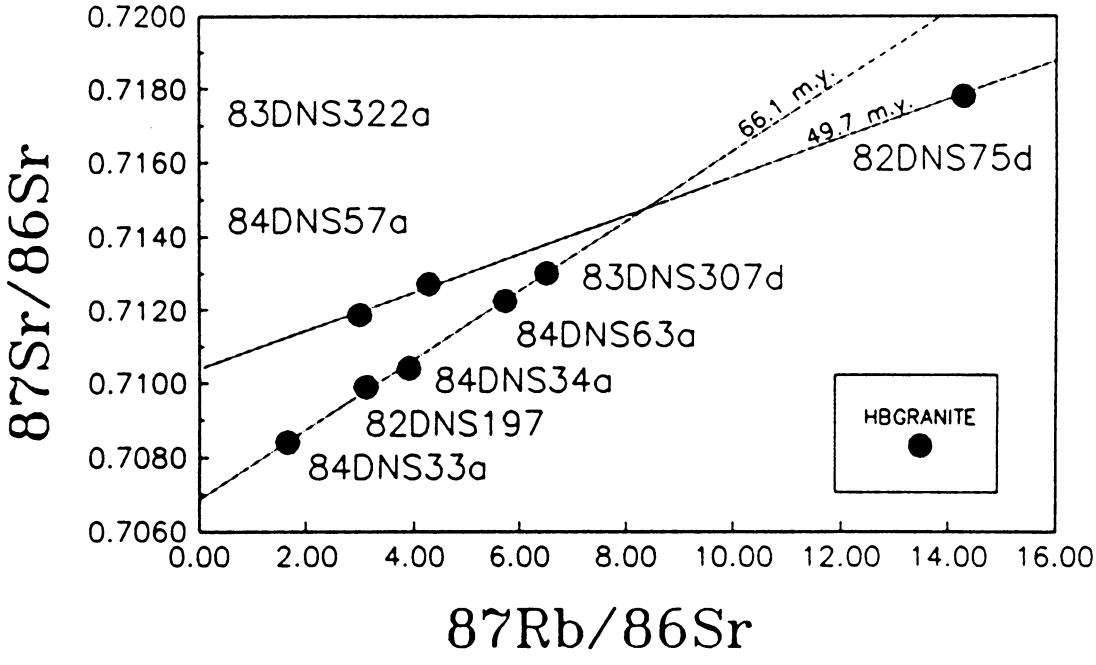

Figure 40. Radiogenic Rb-Sr diagram - whole rock HB granites: Two isochrons, yielding ages of 49.7 m.y. and 66.1 m.y., are not consistent with field associations, as discussed in text.

up to eight different magmas (since there are eight samples). Any superimposed fractionation and/or mixing would then obscure the original character of each magma(s). There seem to be three general ranges of calculated SIR (Figure 41); one around 0.7062, between 0.7071 and 0.7077, and one between 0.7092 and 0.7095. These may suggest several different sources which yielded HB granites; the scatter within these ranges could be due to inhomogeneity of source and/or later contamination.

Samples 82DNS197 (relatively homogeneous granite), 84DNS33a (dike in syenite, with sharp contacts and syenite inclusions), and 84DNS34a (veining in gabbro) group together with relatively high Sr concentration and low calculated SIR. These three sample sites do not contain metasedimentary xenolithic inclusions or mafic enclaves, and are taken to probably represent the least contaminated HB granite samples in the suite. Samples 83DNS307d and 84DNS63a fall within the same SIR range as these samples (0.7071 - 0.7077), but with lower Sr content, suggesting a possible fractionation relationship.

These two latter samples (83DNS307d and 84DNS63a) contain mafic enclaves and xenoliths, as do samples 83DNS322a, 84DNS57a and 82DNS75d. These five enclave-bearing samples form a linear pattern (-- Figure id " unknown -- refid= SSrHb page= no.) suggesting a mixing line. The upper end of this possible mixing line is in the approximate compositional range of observed country rocks. However, the lower SIR endmember, with low Sr concentration, is an unlikely and unobserved composition. It is suggested, therefore, that the linearity of these samples is fortuitous, and that the two high SIR samples (Figure 41) are the result of country rock contamination. This is a striking example of a case in which field observations and corraborative data must be used to evaluate the validity of what appears at first glance to be an obvious mixing relationship.

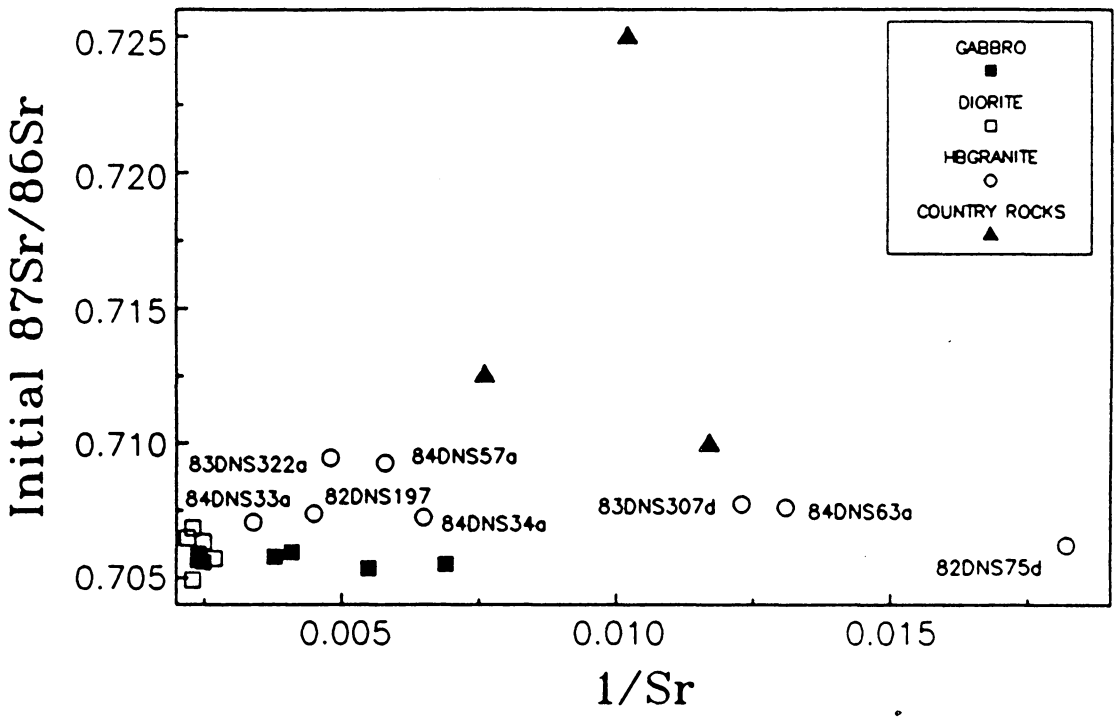

Figure 41. **SIR vs 1/Sr - HB granites, gabbros, diorites and country rocks:** Lack of isochron in HB granites is probably due to varying amounts of contamination from observed mafic enclaves and country rock xenoliths.

Sample 82DNS75d must be considered individually, because of it enigmatic composition. As will be presented in a following section, 82DNS75d contains mineralogy which is significantly different from the other HB granites, with strong trends toward syenitic compositions. The high measured $^{87}Sr/^{86}Sr$ is in keeping with contamination by syenite. However, the sample's low SIR does not support this interpretation. The best explanation for the anomaly is a relatively recent Rb addition or Sr loss in 82DNS75d, causing overcorrection for age in the calculated SIR. Although there is no specific evidence for late alteration in thin section, the cores of plagioclases are heavily corroded, and could have resulted in Sr loss.

Syenites

The distinction between hypersolvus and subsolvus syenite is readily apparent in the Rb-Sr isotopic data for the six analyzed samples (Figure 42). The three hypersolvus samples, with higher $^{87}Rb/^{86}Sr$ and $^{87}Sr/^{86}Sr$, form a three-point isochron with an age of 56.3 m.y. ± 2.6 (2σ), and SIR of 0.71018 $\pm .00033$, (MSRS = 1.77). This regression uses whole rock data, with Rb concentration values from the XRF and Sr concentration values by isotope dilution. The age is interpreted as the time of crystallization of the syenite.

The subsolvus syenites are lower in both $^{87}Rb/^{86}Sr$ and $^{87}Sr/^{86}Sr$, and fall in a group below the hypersolvus isochron. On a plot of SIR vs. 1/Sr, the three subsolvus samples fall along a trend between the hypersolvus syenite and the gabbro fields. In light of their field occurrence in areas of high mafic enclave incidence, and the compositional evidence for contamination, the trend is probably best interpreted as a mixing relationship between hypersolvus syenite and gabbro and/or diorite.

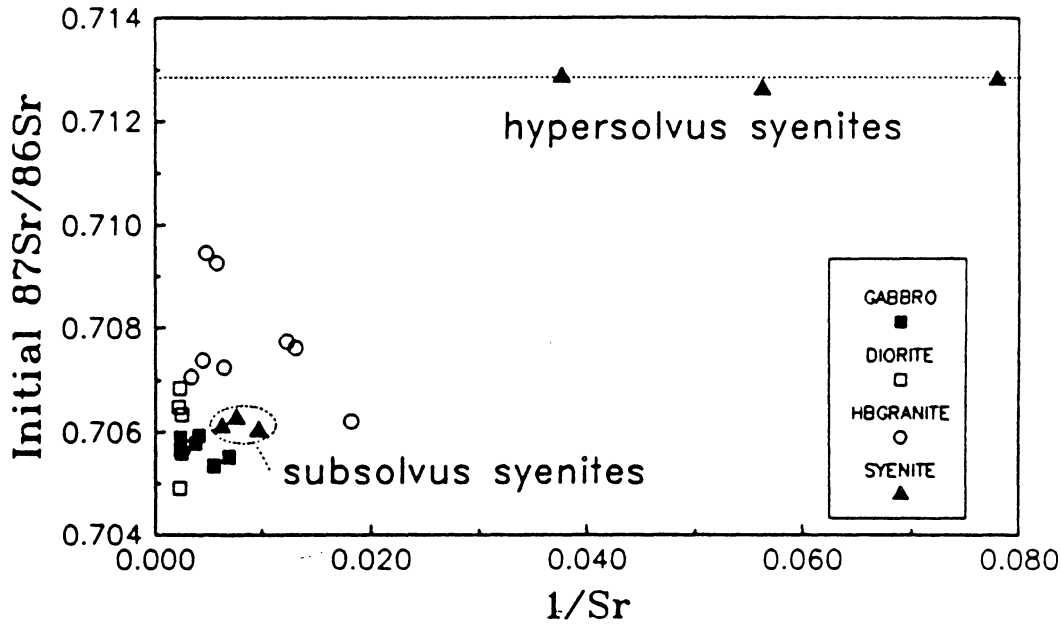

Figure 42. SIR vs. 1/Sr - syenites: Showing difference between hypersolvus and subsolvus syenites and their relation to gabbros, diorites and HB granites.

AF granites

Five AF granite samples were analyzed for Rb-Sr isotopic composition. Of these, four form an isochron, with an age of 57.5 m.y. ± 3.0 (2σ); MSRS = 0.18, and SIR of 0.71185 ±0.00336. Sample 82DNS162b, with the highest $^{87}Rb/^{86}Sr$, falls to the right of the isochron (Figure 43). When corrected back to 57 m.y., the calculated SIR of 82DNS162b is 0.70627, much lower than the other AF granites. With such a high Rb/Sr value (135.1) in the sample, the sensitivity to Sr loss is most acute. This is likely to be the cause of the sample's isotopic disequilibrium, though no specific textural evidence explains the Sr loss.

The similarity between SIR for the four-point AF granite isochron (0.71185) and the isochron for the three hypersolvus syenites (0.71018), and the apparent gradational contact betwen these rock types suggests that they may be comagmatic. When the isochrons are combined (4 AF granites and 3 hypersolvus syenites), they form an isochron (Figure 43) with resultant age of 58.5 m.y. ± 0.2 (2σ), MSRS = 3.0, and SIR of 0.70965 ±0.00008. This age of 58.5 m.y., which is slightly older than age determinations from other rock types (Table 1 on page 76), may help to confirm the syenite and AF granite as the oldest rocks in the complex. The isochron implies that these two rock types are related to one another through fractional crystallization. Their SIR of 0.70965 ±0.00016 (2σ) suggests an evolved crustal source and is distinctly different from calculated SIR of gabros and diorites (0.705 - 0.706) and the relatively uncontaminated HB granites (0.707 - 0.708). Further implications regarding source and petrogenesis will be discussed in a later section.

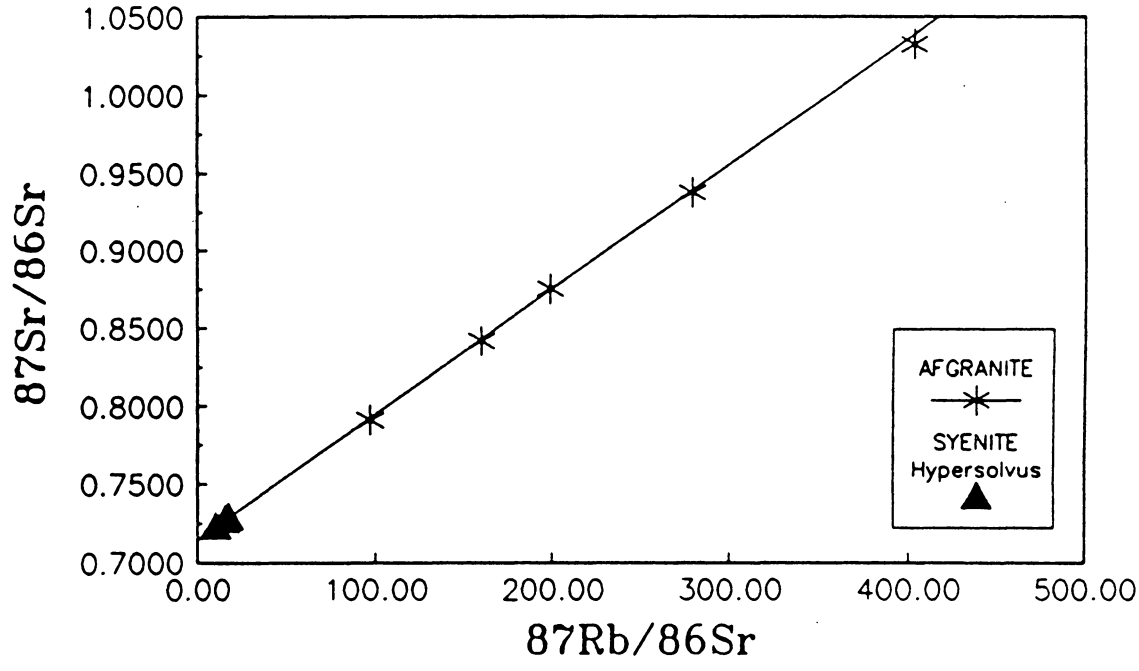

Figure 43. **Radiogenic Rb-Sr diagram - Hypersolvus syenites and AF granites:** Isochron yields age of 58.5 m.y., SIR of 0.70965 ±.00008. See text for discussion regarding combination of two rock suites.

Mineral Geochemistry

Electron microprobe analyses of minerals in thin section from each of the rock types of the MFPC provide information on mineral compositions. Analytical techniques are discussed in Appendix D. The mineral data, presented in Appendix C, will first be discussed for each rock type individually.

Mafic Suite: Gabbros and Diorites

Olivines - Gabbros:

Olivine analyses show a range in Fo content from 77.5 to 63.0 in cumulate gabbro samples 82DNS186 and 82DNS196 respectively. Fo content is around 15 in 84DNS39c, which is a gabbro sample from near a contact with syenite. The highest measured value ($Fo_{77.5}$)is from an olivine rimmed by clinopyroxene in 82DNS186. Although Fe/Mg in olivine increases with increasing SiO_2 in the rock suite (Figure 31), in two grains in sample 82DNS186 there is a suggestion of very slight increase in Mg from core to rim (e.g., $Fo_{76.5}$ - $Fo_{76.8}$). If this reverse zonation trend is real, it may reflect the onset of Fe-Ti oxide crystallization, which would preferentially deplete the liquid in Fe relative to Mg. If the K_D for $(Fe/Mg)_{olivine}/(Fe/Mg)_{liquid}$ is 0.3, as determined by Roeder and Emslie (1970), then for $(Fe/Mg)_{olivine}$ = 0.54 in gabbro, the approximate Fe/Mg in the melt during crystallization of olivine was about 1.8. This value is much higher than a primitive mantle-derived magma would be and suggests either fractional or assimilational effects in the gabbroic magma.

The fayalitic nature of olivine in 84DNS39c reflects the close proximity of this sample to a syenite contact. As shown previously, its bulk composition diverges from the gabbro trend toward syenitic composition. The high Fe content of the olivine must result from a marked increase in Fe/Mg in the gabbroic magma at the contact with syenite, as a result of locallized magma mixing.

MnO content of the analyzed cumulate-rock olivines range from 0.34-0.61 wt%. This is in keeping with the trends described by Simkin and Smith (1970) in which Mn is closely correlated with the Fe content of the olivine, a function of magma composition. Similarly, the Fe-rich olivine in 84DNS39c contains correspondingly high amounts of Mn, around 1.30 wt%. Calcium contents of the gabbroic olivines of the MFPC are low (0.06 - 0.16 wt% CaO). Chromium was not present above detection limits. Ni was not in the analytical scheme, but did not show on the energy dispersive unit screen.

Orthopyroxenes - Gabbros:

Orthopyroxenes from cumulate-textured samples 82DNS186 and 82DNS196 were found to contain calculated ferrosillite (Fs) component ranging from 19 to 28%, and are classified as bronzites (i.e., Fs 12-30, optic sign negative) (Deer et al., 1976). The absence of exsolution lamellae preclude their being inverted pigeonite, as does their low (1.1-1.2 wt%) CaO content. They coexist in seeming equilibrium with clinopyroxene and olivine in both samples.

Clinopyroxenes - Gabbros and Diorites:

Clinopyroxenes in two cumulate gabbro samples (82DNS186, 82DNS196), three non-cumulate gabbro samples (84DNS34d, 84DNS39a and 84DNS39c) and two diorite

samples (84DNS47c and 82DNS209) were analyzed (Appendix C). Compositionally they are all augites, with the pyroxenes of 84DNS39c ranging into the ferroaugite field in the pyroxene quadrilateral (Figure 44). This follows a trend toward compositional similarity of 84DNS39c with syenite pyroxenes, with which it is in contact, and similar to the trend seen in olivines for this sample.

The augites coexisting with orthopyroxene are the most Mg-rich clinopyroxenes analyzed. This supports the interpretation that these samples are relatively early crystallizing cumulates.

Titanium contents range from 0.2 to 1.4 wt% TiO_2,but the values are too low to make these titanaugites. Their neutral color in thin section also confirms low Ti contents. Ssodium contents are low in the gabbro and diorite clinopyroxenes, averaging from 0.15-0.32 wt% Na_2O. Aluminum content decreases from an average of 2.24 in 82DNS186 to 0.58 in 84DNS47c. This trend correlates directly with increasing bulk rock SiO_2. On a plot of wt% SiO_2 vs. Al_2O_3, the gabbro and diorite clinopyroxenes fall in the subalkaline field of La Bas (1962).

In Figure 44, the approximate traces of pyroxene compositions for the Skaergaard intrusion (a tholeiitic body), the Kungnat Fjeld intrusion and the Iskou ring complex (both mildly alkaline complexes with oversaturated differentiation products), and the Shiant Isles sill (a mildly alkaline, undersaturated intrusive) are shown. The variation in Ca levels has been shown to be a function of the silica activity of the magma from which the pyroxenes crystallized (Larsen, 1976). The compositions of the MFPC clinopyroxenes overlap those of the Kungnat Fjeld and Iskou complexes, as suggested by their similarities in rock types.

Another approach toward comparing pyroxenes which crystallized from mafic magma is through a plot of normative pyroxene compositions. The norms of the MFPC clinopyroxenes all are quartz-absent, and diopside-rich. They fall within the overlap of

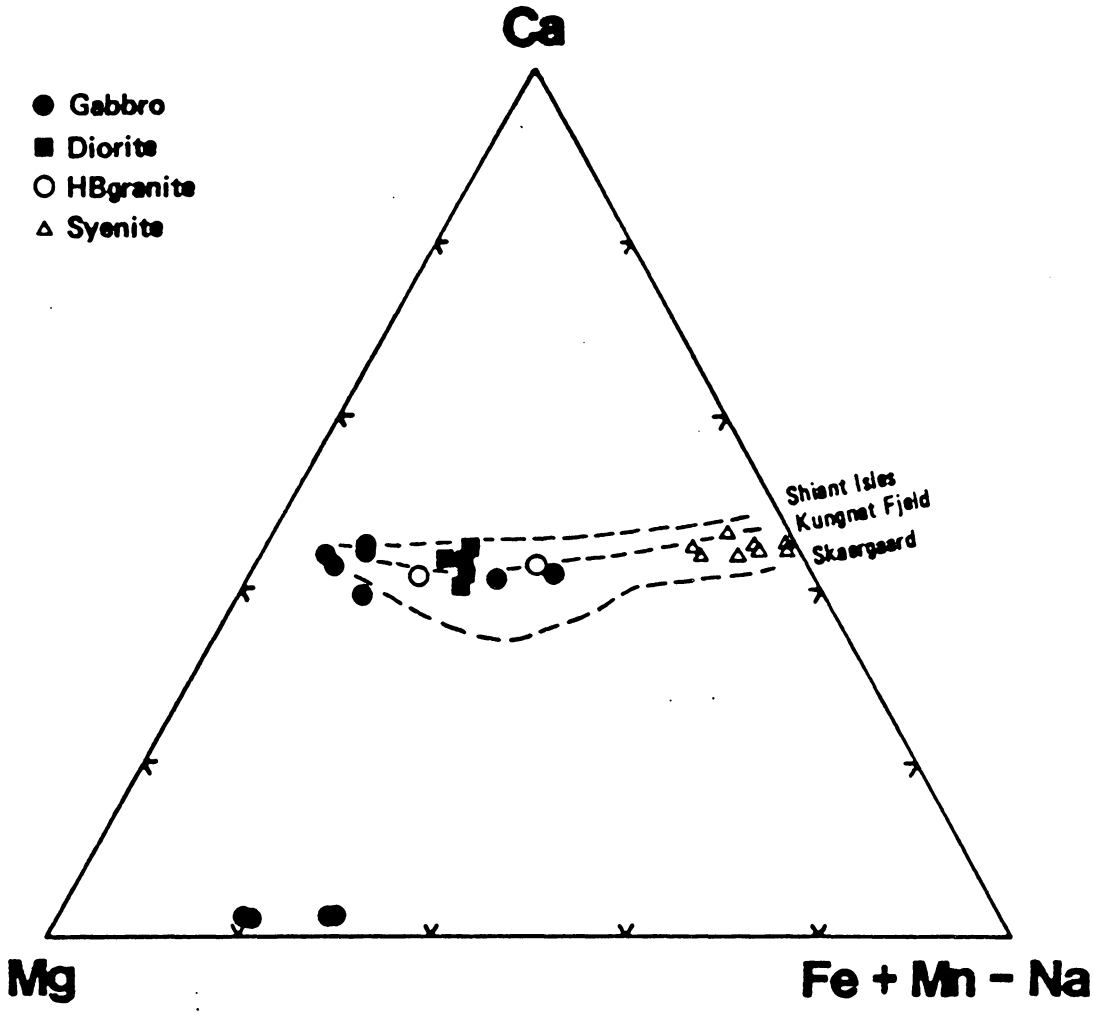

Figure 44. Pyroxene compositional field, with all MFPC analyses: Trends of suites from other igneous complexes shown for comparison (from Larsen, 1976).

alkali basalt and tholeiitic basalt fields (Coombs, 1963). Again, conclusions as to magma type are ambiguous based on clinopyroxene analyses.

To examine the equilibrium between minerals and melt, and the cogenetic relationship between samples, a plot of the limited data pairs for coexisting olivine and clinopyroxene was made for Fe and Mg (Figure 45). On this, the three more mafic samples (84DNS34d, 82DNS186, 82DNS196) form a line with respect to Mg in clinopyroxene and olivine. This suggests that these three samples formed in equilibrium from a single evolving magma. Samples 84DNS39a and c are not on this line, which is predictable due to their proximity to a syenite contact, and contamination by syenite as previously noted. In the plot of FeO*, the samples are scattered. If samples 82DNS186 and 82DNS196 are used as a reference line, then the clinopyroxene in 84DNS34d is highly enriched in FeO* relative to them. This may reflect the difference between remnant cumulus olivines in 84DNS34d and pyroxenes crystallizing from a magma not in equilibrium with those olivines.

Biotites - Gabbros and Diorites:

Spot analyses of biotites from five gabbro samples show that the biotites from cumulate samples 82DNS186 and 82DNS196 have higher Mg/(Mg+Fe) (i.e., Mg#) than the other biotites of the MFPC (Figure 46). Their Al^{IV} contents of 2.4 and 2.5, and Mg#s of 0.81 and 0.74 respectively, places them between the phlogopite and eastonite endmember compositions. Their recalculated formulae, to 22 oxygens, contain only up to 0.22 pfu (per formula unit) Al^{IV}. The rest of the gabbro biotites cluster around 0.5 Mg, with 2.4 to 2.6 Al^{IV}. Sample 84DNS39c falls outside this grouping, with only 2.26 Al^{IV}, again reflecting the compositional influence of the syenite with which this sample is in contact.

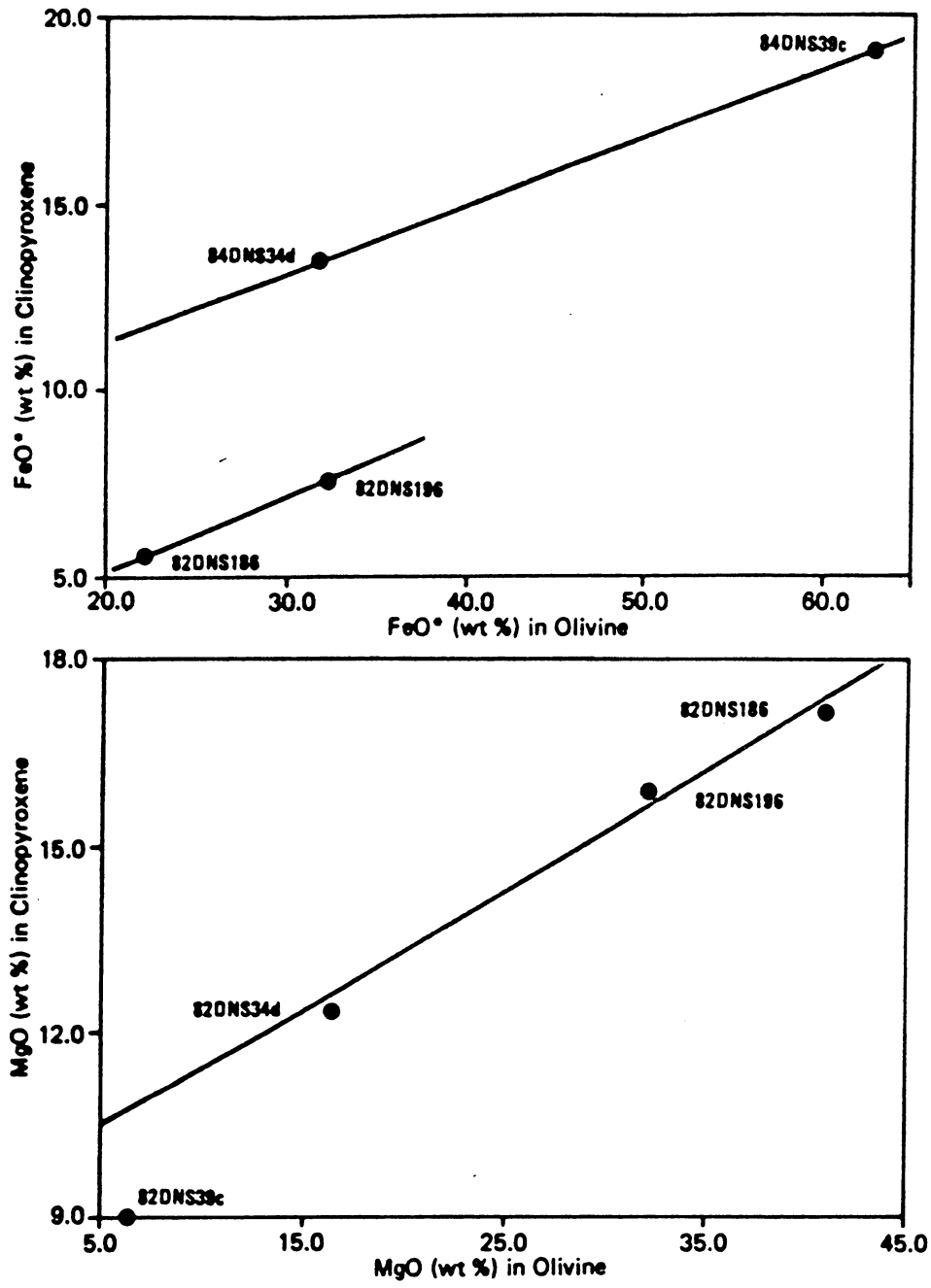

Figure 45. MgO and FeO (wt%) in coexisting gabbro olivines and pyroxenes: Samples which crystallized in equilibrium from a single liquid would form a straight line. Samples from the MFPC do not form consistent equilibrium patterns.

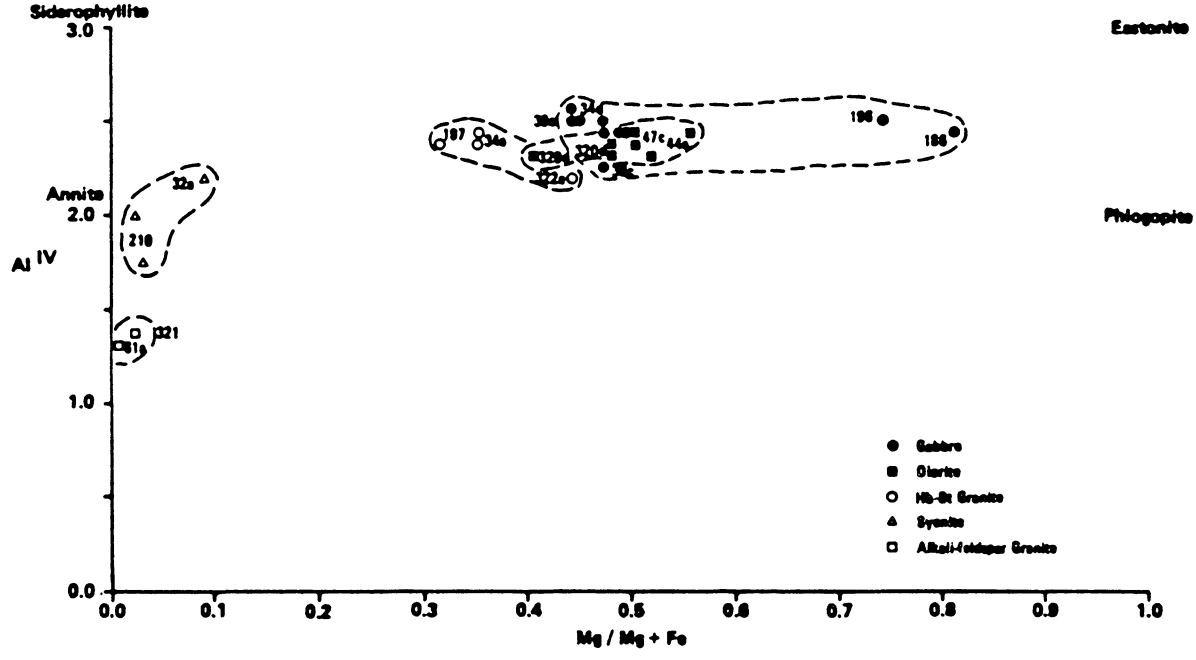

Figure 46. Mg# vs. aluminum in biotites, all rock types: Dashed circles encompass analyses from each rock type.

Ti contents range from 0.48 (84DNS39c) to 0.80 (84DNS34d), with no systematic variation with Mg#. The cumulate samples are relatively rich in Na compared to the other biotites, with 0.21 - 0.32 pfu Na. The highest Ba content of all biotites from plutonic rocks in the MFPC is in 84DNS34d (0.088 pfu). The Ba content in the gabbro biotites has a wide spread, down to 0.015 pfu (82DNS196). Even within 84DNS34d itself, Ba is as low as 0.029 pfu. This variation in Ba between grains may reflect locallized growth conditions, depending on the amount of Ba available within the melt adjacent to the crystallizing biotite. F content is low but present in the gabbro biotites. It averages about 0.21 pfu, and is slightly higher (0.46 pfu) in 84DNS39c.

Several microprobe analyses from biotites in diorites show that they are compositionally similar to the gabbro biotites, but with slightly lower Al^{IV} (Figure 46). The average F content is 0.24 pfu, similar to that of the gabbro biotites.

Amphiboles - Gabbros and Diorites:

Amphiboles, when present in the gabbros, are minor and secondary. Analysis of an amphibole from 84DNS39a (sample close to syenite contact) shows it to be an actinolitic hornblende, according to the classification modified from Leake (1978) (Figure 47). This confirms the subsolidus nature of these amphiboles, as the products of reaction with clinopyroxene. The analysis is low in F (0.15 wt%), and similar in composition to amphiboles in the diorites.

Amphiboles from two diorite samples were analyzed. The amphiboles are classified as actinolite 84DNS47c) and ferroactinolite (83DNS320d). They are probably not magmatic amphiboles (Leake, 1971), and are probably reaction products of clinopyroxene, which they texturally replace. On the basis of isotopic analysis of mineral

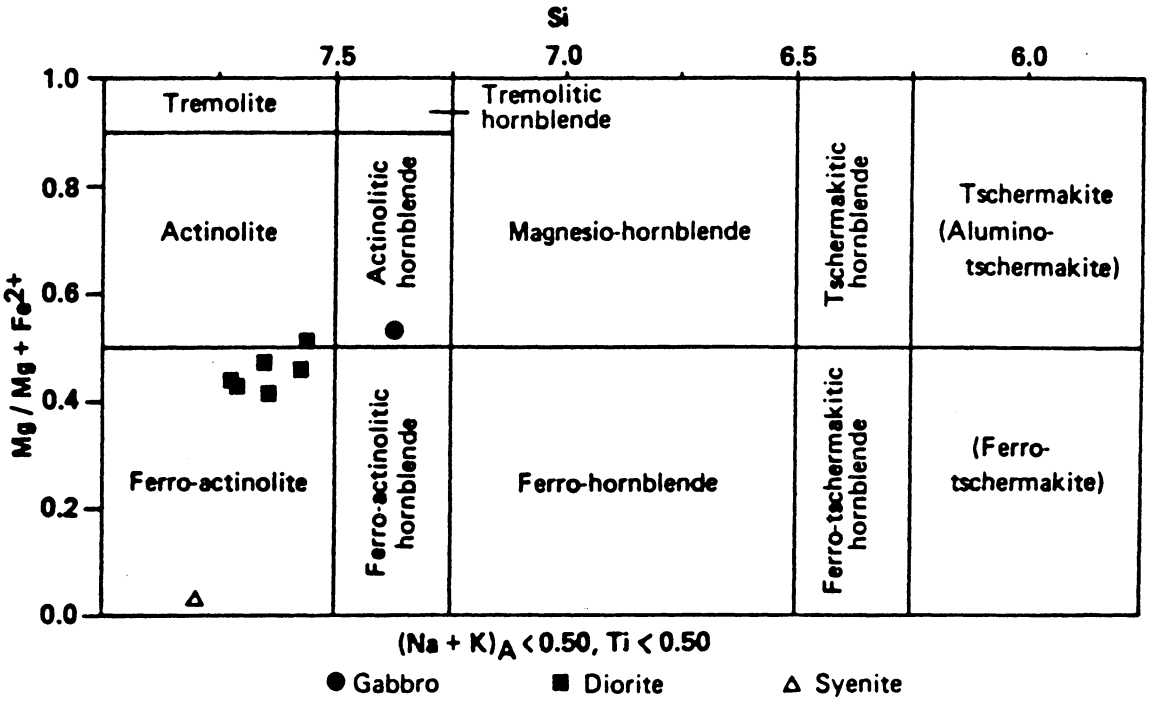

Figure 47. Calcic amphibole classification, (Na + K) < 0.5: Figure includes all suitable MFPC analyses (after Leake, 1978).

separates from 83DNS320d, it was concluded that the secondary amphibole growth occurred very shortly after crystallization, and involved magmatic fluids.

Feldspars - Gabbros:

The most calcic plagioclases analyzed from the MFPC gabbro are in cumulate sample 82DNS186. These range within the bytownite field, from An_{69} to An_{79} (Figure 48). Within the compositional range of labradorite (An_{50-70}) are the cores of plagioclases in 84DNS34d. These range down to An_{32} (andesine) at the edge of grains. Spot analyses of plagioclases from 82NDS196 and 84DNS39a also fall within the andesine range. Sample 84DNS39c, which is consistently closer to the syenite composition, is predictably somewhat less calcic (An_{28}). The normal zonation in 84DNS34d may be a result of fractionation of the gabbro magma. However, An_{32} is significantly more sodic than typical gabbro plagioclase, and may represent some magmatic contamination from the HB granite felsic veining (84DNS34a) which penetrates it. The low-Or rim analysis is very similar in composition to plagioclase of HB granite 84DNS34a.

An alkali feldspar from 84DNS39c is the most calcic analyzed from the MFPC ($Or_{59}An_5Ab_{36}$). In comparison to alkali feldspars from syenites, it is also slightly more aluminous, and Ba-rich. This suggests that it is not a xenocryst from the syenite which it intrudes, but rather a magmatic product of a K_2O-enriched gabbro.

Feldspars - Diorites

Analyzed plagioclase from diorites 83DNS320d and cores in sample 82DNS209 are labradorite. Analyses from rims of these normally zoned grains are andesine, with a spread in Or content (Figure 48). The two analyses from 84DNS47c are andesine, as

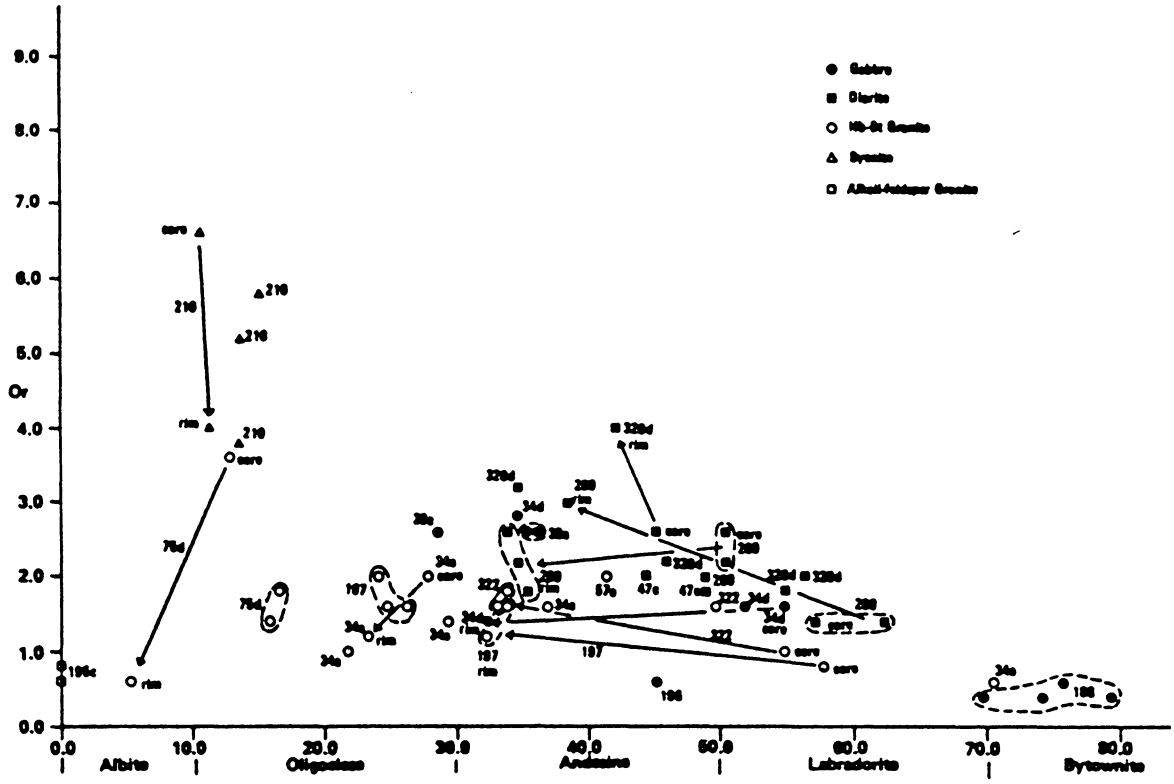

Figure 48. Plagioclase analyses plotted as Or vs. An: Figure includes analyses from all rock types of the MFPC. Sample numbers are labelled; arrows point from cores to rims of the same grain. Dashed circles encompass analyses from one grain.

are some plagioclases in 83DNS320d. Plagioclases in 83DNS320d contain the most Ba of plagioclases from the MFPC, with up to 0.20 wt%.

The overall increase in Or-content with decreasing An in the diorites as a whole could result from fractionation or may reflect the infiltration of alkali-bearing fluids from HB granite magma during crystallization of the diorites. That the plagioclases in diorites and gabbros (except 82DNS196) are slightly more Or-rich than plagioclases in the HB granites is probably a function of higher temperature of crystallization of the mafic rocks. At higher temperature, the slope of the ternary feldspar solvus allows for incorporation of more K in the plagioclase structure (e.g., Fuhrman and Lindsley, 1988).

Two analyses of alkali feldspar from 84DNS47c give an average of $Or_{78.6}$. The Ba content is up to 0.91 wt%, the highest observed in MFPC feldspars.

Fe-Ti Oxides and Accessories - Gabbros and Diorites:

Accessory minerals are not common in the gabbros; even the almost always ubiquitous apatite was not observed in two of the cumulate samples (82DNS186, 82DNS196). It is present in the other samples, and zircon is present in 84DNS39a and possibly in 84NDS39c. Iron sulfide (pyrite or pyrrhotite) was identified on the energy dispersive unit on the microprobe, in samples 82DNS186 and 82DNS196. These coexist with ilmenite. Ilmenite is the only Fe-Ti oxide that has been identified in gabbro thin sections, and ranges from Ilm_{95-98}. No exsolution lamellae have been observed in reflected light.

Apatite is present in all diorite samples, and two were probed in 83DNS320d. These grains are F-rich, with over 3 wt%. An iron-sulfide, probably pyrite, is present in 84DNS47c. Other identified opaque phases are ilmenite, with no observed exsolution lamellae.

HB granites

Clinopyroxenes - HB granites:

Clinopyroxene occurs within HB granite only as relict cores which have not reacted to form amphibole. These cores were observed in samples 82DNS197 and 82DNS75d. Limited electron microprobe analysis suggests that these clinopyroxenes overlap the gabbro and diorite augites in composition.

On the pyroxene quadrilateral (Figure 44 on page 101), 82DNS197 falls between the cumulate gabbros and the other mafic samples. The low Fe ratio of this analysis, from a clinopyroxene in a felsic rock, and the extensive reaction rims around the grains, suggest that the clinopyroxenes are not in equilibrium with the magma from which the rest of the rock crystallized. Since the isotopic data reveal that 82DNS197 is not comagmatic with the mafic rocks, the pyroxene cores are not relicts of pure fractionation of HB granite from diorite/gabbro. It is suggested that the pyroxenes are xenocrysts incorporated into the HB granite when it intruded the diorite. There is no evidence for any other xenocrystic phase in the syenite.

Pyroxene from sample 82DNS75d plots between the mafics and syenite-contaminated 84DNS39c. This is typical of 82DNS75d, in that both its bulk and its mineral chemistries tend toward syenitic and AF granite compositions. This pyroxene analysis also has the highest proportion of Na of all analyzed MFPC pyroxenes. This is a characteristic of highly evolved rocks with peralkaline tendencies, again reflecting this sample's chemical affinities for the more alkaline rock types.

Biotites - HB granites

The analyzed biotites from three HB granite samples have about the same Al^{IV} content as biotites from gabbro and diorite, but the HB granite minerals tend to have slightly lower Mg#. 83DNS322a overlaps the Fe-rich mafic samples (Figure 46). They are most different from the mafic rock biotites in their F content. The HB granites contain from 0.38 - 0.60 pfu F. All other elemental contents overlap those of the gabbros and diorites.

Amphiboles - HB granites

Amphiboles from five HB granite samples were analyzed. All analyzed grains are calcic amphiboles within the range of 6.50 - 7.24 formula units Si, and 0.00 - 0.50 Mg/Mg+Fe. They all contain low Ti (0.14 -0.21 pfu), and an average of 1.7 pfu Ca. The range of total (Na+K) is from 0.55 - 0.83 pfu. The differentiating factor between ferroedenite and ferrohornblende in the classification scheme modified from Leake (1978) is the lower (<0.5 pfu) sum of Na+K in the A-site in ferrohornblende. In the HB granite amphiboles, when the atoms are apportioned such that they stoichiometrically fill the structural sites according to the method outlined by Robinson, (1982), the remaining Na+K in the A-site ranges from 0.55 to 0.83 pfu. Thus, the analyzed amphiboles of the HB granites are ferroedenites (82DNS197, 83DNS322a, 84DNS34a and 82DNS75d) and ferroedenitic hornblende (84DNS57a) (Figure 49). Fluorine content ranges from 0.22 - 0.68 pfu; Cl is ≤ 0.03 pfu.

Although edenites and ferroedenites are generally considered to be metamorphic amphiboles which are unstable at magmatic temperatures (Graham and Navrotsky, 1986), the MFPC analyses do not approximate endmember edenitic composition [(

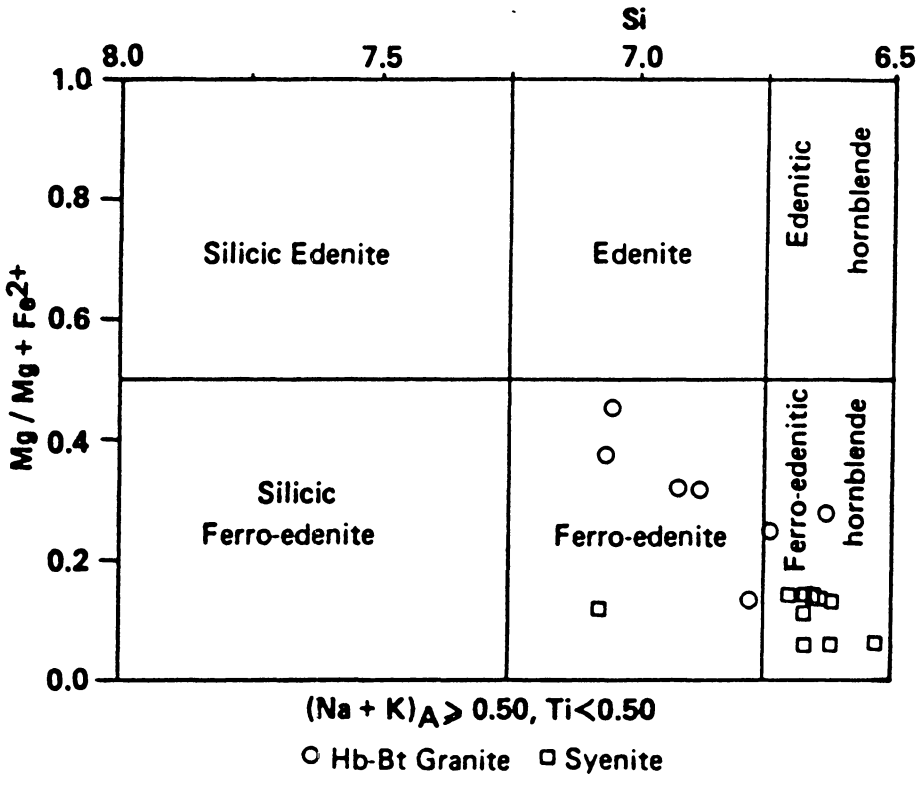

Figure 49. Calcic amphibole classification, (Na + K) > 0.5: Figure includes HB granite and subsolvus syenite amphibole analyses (after Leake, 1978).

$NaCa_2(MgFe)_5Si_7AlO_{22}(OH)_2]$. They do, however, plot within Leake's (1971) field of 1467 magmatic amphibole compositions. Therefore, it is interpreted that the HB granite ferroedenites crystallized directly from the magma, as is supported by their texture.

Clinopyroxene cores, present in analyzed amphiboles of 82DNS197 and 82DNS75d, do not seem to systematically affect the composition of the surrounding amphibole. The irregular anhedral shape of the pyroxene is probably due to interaction with the magma; the rimming amphibole was subsequently derived from the magma.

Ferroedenites from the two samples in which biotite is dominant and early relative to amphibole (83DNS322a and 84DNS34a) are slightly more actinolitic (higher Si, lower Al, lower $(Na + K)_A$) than the other ferroedenites. This may reflect a lower temperature environment of amphibole growth (Leake, 1971).

Feldspars - HB granites

The HB granites contain a wide range of plagioclase compositions (Figure 48 on page 108). The most calcic is from 84DNS34a, a grain with An content (An_{71}) in the range of cumulate gabbro. This grain, in a granite with whole rock SiO_2 of 69 wt%, must be out of equilibrium. Since this sample is of felsic veining which invades gabbro 84DNS34d, the most likely explanation is that the plagioclase core is a xenocryst derived from the gabbro. Similarly, labradorite cores from 82DNS197 and 83DNS322 are likely to be gabbroic xenocrysts. An alternative explanation is that they are restite. They could also be residual early fractionates, suggesting that the HB granite fractionated from the gabbro. However, isotopic evidence previously discussed precludes simple fractionation.

Most of the analyzed HB granite plagioclases are oligoclase and andesine. All zoning appears to be normal. They contain overall less Or (0.01 - 0.02 pfu) than the

mafic rock plagioclases, probably due to lower temperature of crystallization (Figure 48). Their tetrahedral Si content tends to be higher than in the gabbro and diorite plagioclases, due to the higher bulk rock SiO_2 content. Ba contents are low, the highest being in 82DNS197, up to 0.11 wt%.

The plagioclases of 84DNS75d are unlike the others from the HB granites. They are more Ab-rich (An_{16}- An_5); the most albitic rims a core that is similar in composition to plagioclase in subsolvus syenite 82DNS210. This follows the consistent trend in bulk and mineral chemistry in which this sample mimics syenite composition.

Alkali feldspar from samples 84DNS34a and 84NDS57a are considerably different, with Or_{97} and Or_{73} respectively. 84DNS34a also contains more Ba, with 0.88 wt%.

Fe-Ti Oxides and Accessories - HB granites:

The only analyzed Fe-Ti oxides in HB granites are ilmenites from 84DNS34a and 84DNS57a, with composition around Ilm_{91}. Magnetite is also present as an anhedral secondary mass in 84DNS57a. A small miarolitic cavity in 84DNS34a contains calcite, ilmenite rimmed by titanite (with 1.31 wt% F), biotite, plagioclase, apatite and a Ce-rich allanite.

Syenites

Olivines - Syenites:

A limited number of analyses from both hypersolvus and subsolvus syenites reveal that the olivines are very fayalitic (Fo 0.3-3.2). This is typical of olivine-bearing syenites (e.g., Larsen, 1976; Stephenson and Upton, 1982). The fayalites are Mn-rich (1.96-2.30

wt% MnO), which is predictable in light of their Fe content (Simkin and Smith, 1970). CaO contents are 0.24-0.29 wt%, substantially higher than that of the gabbro olivines, but still in the range typical of plutonic rocks (Simkin and Smith, 1970).

Clinopyroxenes - Syenites:

The pyroxenes in both hypersolvus and subsolvus syenites closely approximate endmember hedenbergite compositions, and compare closely to pyroxenes from other silica-saturated alkaline provinces, as illustrated in Figure 44 on page 101. The analyzed pyroxenes contain more Mn than Mg, though both elements are present at less than 1 wt%.

The typical trend in most alkaline complexes is toward Na-enrichment in pyroxenes (e.g., Neumann, 1976 (Oslo, Norway); Brooks and Gill, 1982 (Kangerdlugssuaq, East Greenland); Stephenson, 1972 (South Qoroq Centre, south Greenland); Stephenson and Upton, 1982 (Kungnat Fjeld, south Greenland); Larsen, 1976 (Ilimaussaq intrusion, south Greenland); Platt and Woolley, 1986 (Mulange complex, Malawi); Mitchell and Platt, 1978 (Coldwell alkaline complex, Ontario)). This Na enrichment is generally assumed to be accompanied by Fe^{3+} enrichment, as part of the increasing acmite component ($NaFe^{3+}Si_2O_6$). As discussed by Ferguson (1978), the Na increase is manifested mineralogically by a sequence of increased Na in a Ca-pyroxene (hedenbergite), then an alkali amphibole, followed by a Na-pyroxene (aegirine). In the syenites of the MFPC, neither Na-amphibole nor aegirine are observed. However, there is the suggestion, based on analysis of cores and rim of pyroxenes in subsolvus syenite 82DNS210, that Na content increases slightly toward the rim. Zonation is indeterminate from the other analyses. The trend of pyroxene compositions for the entire MFPC suite, shown in Figure 50, is toward Fe enrichment, with little indication of Na enrichment. However,

as will be discussed below, the trend toward increased Na is taken over by amphiboles in the AF granite.

Biotites - Syenites:

The biotites of subsolvus syenite samples 82DNS210 and 84DNS32a are minor in modal percent (< 1%). Reconnaissance analysis of these biotites shows them to be very ferruginous, with an average of about 2 pfu Al^{IV}. Though Fe^{2+}/Fe^{3+} is not known, these biotites can probably be considered as close to annite in composition. Their Ba content is low to nil. They have appreciable Cl (Cl peak observed on 'Kevex' energy dispersive unit display screen when not in analytical scheme, measured up to 0.44 pfu in 82DNS210). They contain variable but low F (0.05 - 0.13 pfu). Ti is fairly low, at an average of 0.25 pfu.

Amphiboles - Syenites:

Amphiboles are present in greater than trace amounts only in the subsolvus syenites (82DNS210, 84DNS32a and 84DNS32b). Analyses of the samples show them to contain ferroactinolite (82DNS210), ferroedenite (84DNS32b), and ferroedenitic hornblende (82DNS210, 84DNS32a, 84DNS32b) (Figure 47;Figure 49). The latter are dark green grains, which texturally appear magmatic. The ferroactinolite and ferroedenite both texturally appear to be alteration products, with lighter green coloration and a more fibrous morphology. These secondary amphiboles are present only in amounts < 1vol.%. The ferroedenitic hornblendes contain F ranging from 0.4 - 0.6 pfu. The ferroactinolite contains only 0.02 - 0.03 pfu F. The ferroedenite contains 0.27 pfu

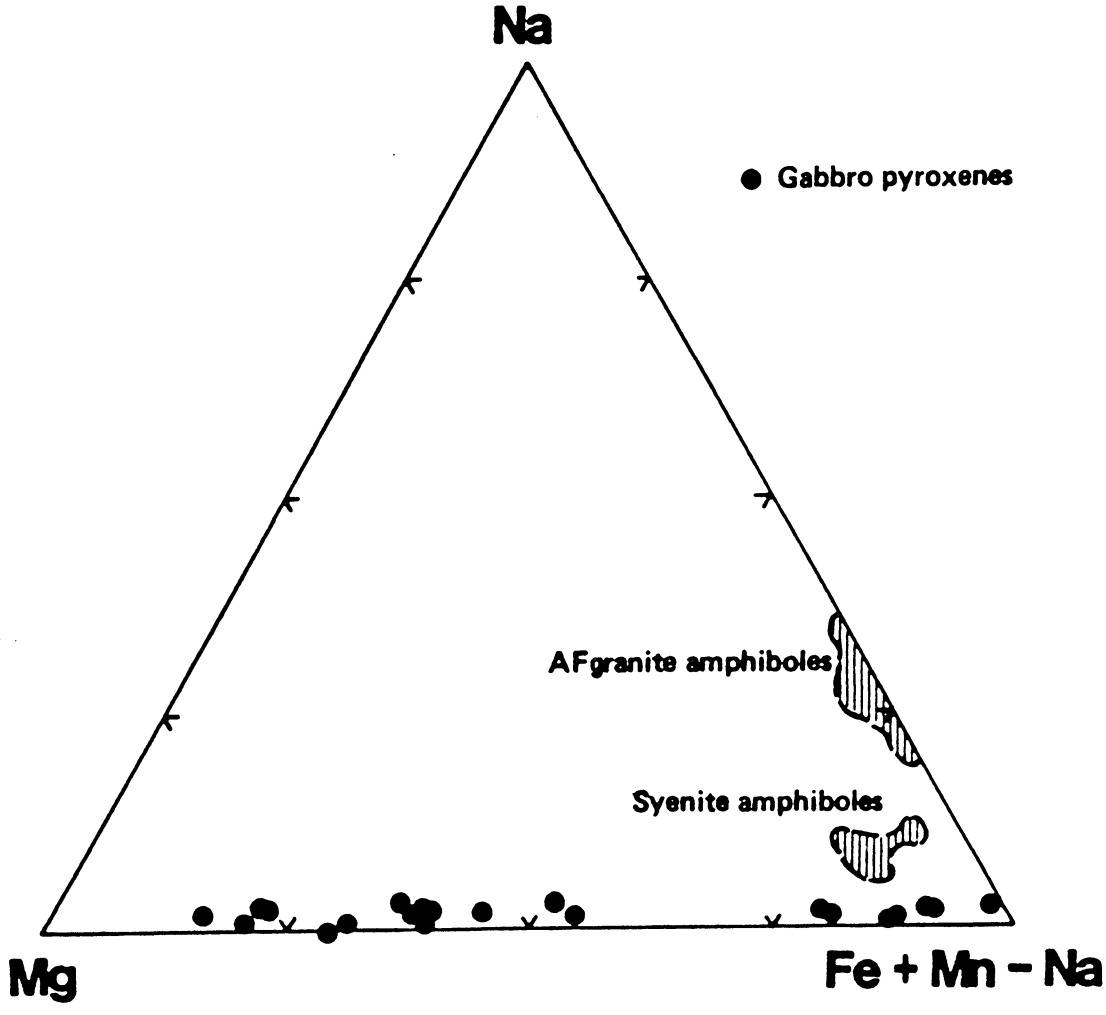

Figure 50. Pyroxene analyses, in terms of (Na) - (Mg) - (Fe* + Mn - Na): Gabbro pyroxenes are shown as closed circles. Fields of analyses for amphiboles from syenite and AF granite are shown, illustrating that Na enrichment in mafic mineralogy of the peralkaline suite is seen in the amphiboles rather than in pyroxenes.

F, with a strong Cl peak visible on the 'Kevex' energy dispersive unit display screen, though Cl was not in the analytical scheme for this analysis.

Plagioclases - Syenites:

Plagioclase (other than exsolved albite in perthite) is present in significant amounts only in the subsolvus syenites. Analyses from 82DNS210 reveal that these minerals, which occur both as grains within alkali feldspar and as small grains between alkali feldspars, are oligoclase (An_{11-15}). This suggests that these plagioclases are not the result of albitization, because albitization products have higher Ab content (L. Fox, pers. comm., 1988). These grains are also the most Or-rich analyzed plagioclases within the MFPC. There is evidence of zonation, with less Or toward the rims. This may be the effect of a change in bulk magma composition, decreasing activity of silica (Tuttle and Bowen, 1958), or an increase in P_{H2O} (Bowen and Tuttle, 1950). The occurrence of discrete feldspars is indicative of crystallization under relatively high P_{H2O} conditions, such that the solidus intersects the solvus and causes crystallization of two feldspars, in rocks such as these syenites with low normative An content (Tuttle and Bowen, 1958).

Alkali Feldspars - Syenites:

Due to the coarsely perthitic nature of the alkali feldspars in the syenites and alkali feldspar granites, spot analyses cannot be representative of the mineral composition. An experimental procedure to homogenize feldspars by heating is described in Appendix G. Grains from hypersolvus syenite sample 82DNS195b were homogenized, and the average results are included in Table 5. There appear to be at least two populations of alkali feldspar in the sample. One has an average composition of about Or_{42}. These

grains become deep red when heated in the furnace. The other, which remains white when heated, has composition of about Or_{83}. This may be the result of large scale exsolution and segregation of phases, creating populations of widely varying Or/Ab ratios. Though a complementary Ab-rich population was not observed in this homogenization study, these grains may simply not have been among those picked for heating, although one unheated grain did have an average composition of Or_{30}, and may represent a more albitic endmember. The high Or composition grains also contain moderately high Ba, averaging 1.02 wt%, and very little Fe (hence their white coloration).

Alternatively, the Or-rich grains could be argued to be metasomatic. However, it is unlikely that metasomatic feldspars would contain significant Ba. Also, it seems that metasomatic feldspars are characterized by the presence of ferric iron (Mariano, 1978a), and Fe is notably low in these grains.

Fe-Ti Oxides and accessories - Syenites

No exsolution lamellae were observed in the opaque phases of the syenite. Analyzed Fe-Ti oxides are all ilmenite (around Ilm_{97}). Zircons are large ($\leq$0.5 mm) and commonly squarish in thin section. Apatites were observed in samples 82DNS210, 84DNS32a and 82DNS195b. A Ce-rich allanite was analyzed on the probe, from sample 84DNS32b. Though Ce was not in the analytical scheme, its peaks were large on the energy dispersive unit. The analytical total, including F, is about 73 wt%. If the remaining 27 wt% is Ce, then this is an extremely REE-rich allanite. For comparison, the highest REE in allanite reported by Gromet and Silver (1983) was 20.5 wt%.

Table 5. Average compositions of unheated and heated alkali feldspars

	1	2	3	4	5	6	7
SIO2	66.73	66.28	66.27	66.79	63.52	66.21	66.36
AL2O3	18.69	18.72	18.75	18.96	18.34	18.98	18.89
NA2O	5.95	6.67	6.61	7.43	1.80	6.19	7.00
K2O	8.31	7.25	7.33	6.20	13.77	7.50	6.67
MGO	0.02	0.02	0.02	0.02	0.03	0.01	0.02
CL	0.0	0.0	0.0	0.0	0.0	0.0	0.0
FEO	0.38	0.35	0.43	0.32	0.23	0.30	0.42
MNO	0.0	0.0	0.0	0.0	0.0	0.0	0.0
CR2O3	0.0	0.0	0.0	0.0	0.0	0.0	0.0
TIO2	0.0	0.0	0.0	0.0	0.0	0.0	0.0
BAO	0.04	0.03	0.03	0.05	0.54	0.05	0.03
F	0.0	0.0	0.0	0.0	0.0	0.0	0.0
CAO	0.04	0.06	0.06	0.11	0.07	0.13	0.07
P2O5	0.0	0.0	0.0	0.0	0.0	0.0	0.0
SRO	0.0	0.0	0.0	0.0	0.0	0.0	0.0
SUM	100.16	99.38	99.50	99.88	98.30	99.37	99.46
-O= F+CL	0.0	0.0	0.0	0.0	0.0	0.0	0.0
SUM	100.16	99.38	99.50	99.88	98.30	99.37	99.46

SI	2.999	*	2.993	*	2.991	*	2.990	*	2.980	*	2.989	*	2.989	*
AL	0.990	*	0.996	*	0.997	*	1.000	*	1.014	*	1.010	*	1.003	*
TI	0.0	3.989	0.0	3.989	0.0	3.988	0.0	3.990	0.0	3.994	0.0	3.999	0.0	3.991
FE	0.014	*	0.013	*	0.016	*	0.012	*	0.009	*	0.011	*	0.016	*
CA	0.002	*	0.003	*	0.003	*	0.005	*	0.004	*	0.006	*	0.003	*
BA	0.001	*	0.001	*	0.001	*	0.001	*	0.010	*	0.001	*	0.001	*
NA	0.519	*	0.584	*	0.578	*	0.645	*	0.164	*	0.542	*	0.611	*
K	0.476	*	0.418	*	0.422	*	0.354	*	0.824	*	0.432	*	0.383	*
SR	0.0	1.013	0.0	1.020	0.0	1.021	0.0	1.018	0.0	1.012	0.0	0.993	0.0	1.015
O	8.000	*	8.000	*	8.000	*	8.000	*	8.000	*	8.000	*	8.000	*

AN	0.19	0.29	0.29	0.52	0.35	0.64	0.34
AB	51.98	58.11	57.62	64.16	16.35	55.24	61.23
OR	47.76	41.55	42.04	35.22	82.30	44.03	38.38
CN	0.07	0.05	0.05	0.09	0.99	0.09	0.05

1 82DNS61A-UNHEATED(n = 150)
2 82DNS61A-HEATED 7 DAYS(n = 160)
3 82DNS61A-HEATED 14 DAYS(n = 140)
4 82DNS195B-UNHEATED(n = 119)
5 82DNS195B-WHITE GRAINS(n = 74)
6 82DNS195B-HEATED 7 DAYS(n = 108)
7 82DNS195B-HEATED 14 DAYS(n = 85)

AF granites

Biotites - AF granites:

Biotites in the AF granites 83DNS321d and 84DNS61a are ferruginous, Al-deficient, and F-rich. Because of their low Mg (0.004-0.02 pfu) and low Al^{IV}, they most closely approximate annite compositions. Ti content is variable, from 0.04 pfu in 83DNS321d to 0.51 pfu in 84NDS61a. Ba content is negligible. F is present from 1.6 to 1.9 pfu.

Amphiboles - AF granites:

The AF granites contain both sodic-calcic amphiboles and alkali amphiboles, when formulae are calculated according to the method of Robinson (1982). Analyzed amphiboles from four AF granite samples include ferrorichterites (82DNS195c), riebeckites (82DNS195c and 82DNS162a - not 82DNS162b for which bulk analyses were done), and arfvedsonites (82DNS195c, 83DNS321d, 82DNS162a, and 84DNS61a). These compositions are not plotted on the classification diagrams of Leake (1978) because they require information on the Fe^{3+} content, which is not available. However, an alternative plot (modified from Giret et al., 1980) is useful in depicting the compositional variation of alkali-rich amphiboles is Al^{IV} + Ca vs. Si + Na + K (Figure 51). On this diagram classification boundaries are somewhat different from the Leake classification, in that some ferrorichterites plot as winchites, and others fall just on the other side of dividing lines. However, the trend toward increasing Si + Na + K with decreasing Ca + Al^{IV} is readily apparent. This evolutionary trend can be seen within 82DNS195c, in which rims are more sodic. The riebeckite appears to have formed after

the ferrorichterite. The one arfvedsonite analysis in 82DNS195c is of a small, very blue grain adjacent to a flake of white mica (zinnwaldite?). It is interstitial, and appears to be a very late stage amphibole.

In 82DNS195c, the riebeckites have lower F/OH (0.1 pfu) than the ferrorichterites (0.3 pfu). The arfvedsonite has F/OH of 0.2 pfu. The sodic amphiboles from the other samples are more F-rich, with F/OH of 0.4 - 1.3 pfu. Thus, it appears that the most sodic amphiboles, which seem to be late-crystallizing, are associated with a F-enriched fluid. The lower F in the riebeckites of 82DNS195c may represent a changing volatile environment during crystallization, during which F migrated toward the top and edges of the cooling magma chamber. Though the trends followed by the AF granite amphiboles do not move strongly in the oxidizing direction suggested by Strong and Taylor (1984), the suggestion of increased f_{O_2} concurrent with decreasing F/OH is in keeping with this oxidizing trend (Figure 51). The rest of the samples follow Strong and Taylor's (1984) magmatic/subsolidus trend, in which substitutions of the type Al^{IV} + Ca = Si + (Na,K) under reducing conditions lead to arfvedsonite amphiboles. These trends have been documented in other silica-oversaturated peralkaline complexes such as at Kerguelen and at Oslo, Norway (Giret et al., 1980), the Mulanje complex, Malawi (Platt and Woolley, 1986), and the St. Lawrence and Topsails suites, Newfoundland (Strong and Taylor, 1984). Data for F is not given in the above references, but the MFPC AF granite amphibole data lends insight into relative oxidation and reduction of the trends as a function of F content in the fluid phase accompanying amphibole crystallization. This relationship was also noted by Scofield and Gilbert (1982), in which subsolidus riebeckitic amphiboles contain less F than higher temperature, more reduced arfvedsonitic amphiboles.

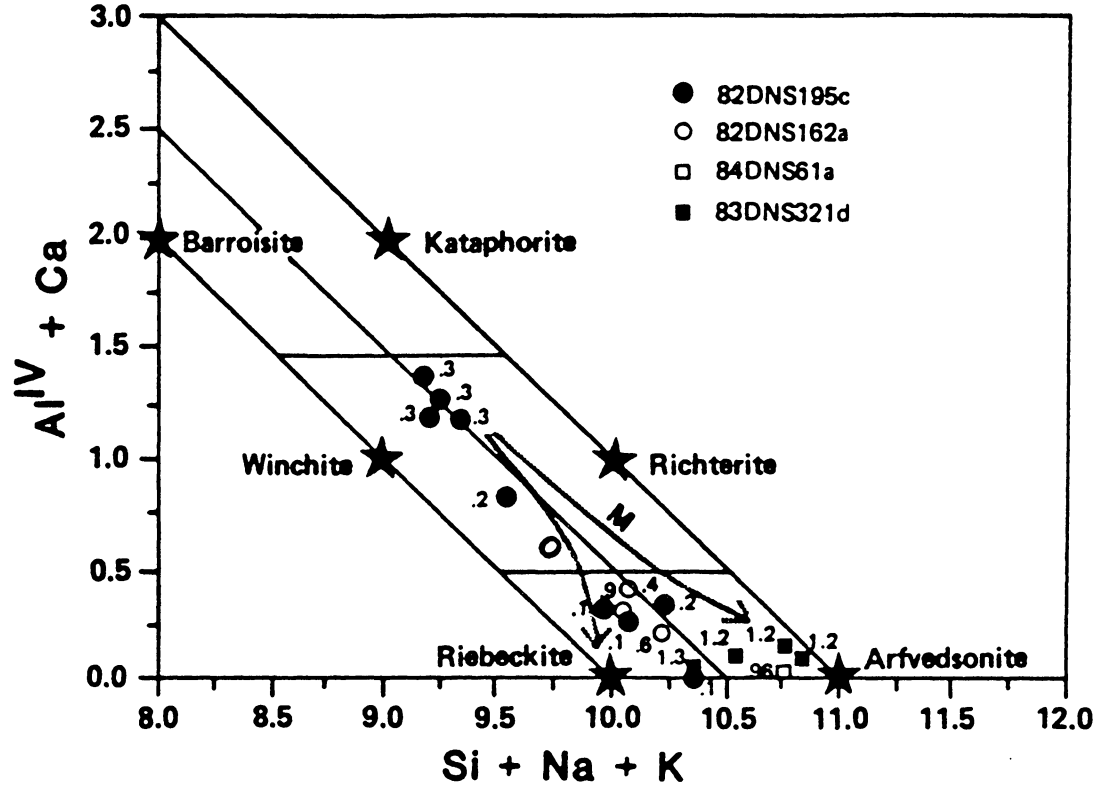

Figure 51. AF granite amphibole analyses: Plotted in terms of (Ca + Al^{IV}) vs. (Si + Na + K), modified from Giret et al (1980), and showing oxiding trends (O) and magmatic/subsolidus trends (M) of Strong and Taylor (1984). MFPC AF granite amphiboles are shown, with F/OH for each analysis.

Alkali Feldspars - AF granites:

Homogenized alkali feldspar grains (Table 5) from 84DNS61a indicate an average Or content of 42. Ba content is negligible (0.03 wt%). An analysis fo 82DNS162b yields Or_{37}. Spot analyses were also done on small individual, non-turbid albite grains in 82DNS162b, 82DNS195c and 83DNS321d. These contain $Or_{1.4}$, $Or_{0.7}$, and $Or_{0.9}$ respectively.

Single crystal precession X-ray photography of a perthite from sample 82DNS61a was done to ascertain the structural state of the phases within the feldspar grain. By measuring the α^* angles on the photograph (b^* angle c^* of the reciprocal lattice) it was determined that a nearly pure low albite phase, and a low microcline phase (with probably about 5 - 10 wt% Na_2O) are both present. No pericline twinning occurs in the X-rayed grain; the low albite is twinned on the albite law. This confirms that the feldspar originally crystallized as a microcline structure, and has since undergone ordering and exsolution.

Fe-Ti Oxides and Accessories - AF granites:

Ilmenite, with no exsolution lamellae, is the only opaque phase that has been observed from the AF granites of the MFPC (around Ilm_{97-98}). Zircon and fluorite are both present in most samples.

Aenigmatite occurs in sample 84DNS61a, within amphiboles. In sample 82DNS195c are brown-colored Ce-rich minerals. If the analytical total is brought to 100 wt% by adding Ce, then the resultant recalculated mineral formula is close to what is reported as the chevkinite composition (Fleischer, 1987). Also in this sample are a few late-stage white micas. Analytical totals from these grains are low, about 92 wt%, in-

dicating the substantial presence of an element(s) not included in the analytical scheme. A likely possibility is that Li occurs in these micas. If so, then the white mica laths are probably zinnwaldite. Zinnwaldite is known to occur in late stage differentiates and pegmatites of anorogenic suites (Cerny and Burt, 1984) with which the MFPC suite is comparable. These micas are extremely F-rich (about 3.0 pfu), and are probably the products of very late-stage volatile-rich magmatic fluid.

Eudialyte (a REE-bearing hydrous Na- Ca- Fe- Zr-silicate) has been identified from a piece of granitic talus in the syenite - AF granite contact zone. This mineral is generally found in late stage pegmatites, and represents the high degree of evolution of the AF granite. A complete crystal structure and compositional study is in progress by Johnson, Gunter, Wayne and Solie at Virginia Tech.

Chapter 3: Petrology and Petrogenesis

Conditions of Crystallization

Estimates of intensive variables in plutonic rocks are generally made on the basis of stable mineral assemblages. Physical aspects of the contact zone and its mineralogy, and stratigraphic level of emplacement are useful in constraining pressure estimates. Based on the mutual stabilities of coexisting minerals under different conditions, or on the amount of a given component in certain mineral structures, some constraints on such parameters as temperature, pressure, f_{O2}, and f_{H20} are possible. Several geothermometers and geobarometers, and P-T phase diagrams, have been applied to minerals of the MFPC in an attempt to quantify the conditions under which the various magmas crystallized. As always, when applying geothermometers and geobarometers, the inherent limitations of the method must be kept in mind. These include 1) assumptions involving mixing in the solid or vapor solutions, 2) the need to know (or assume) pressure in order to estimate temperature (or vice versa), 3) the simplicity of the model system versus the effect of other components in the real system, 4) the lack of precision which may be present in analyses, and 5) the assumption of equilibrium between minerals in the assemblage.

Pressure

Constraints on pressure are difficult to ascertain in many petrologic assemblages. Estimated thickness of originally overlying strata is roughly 4 km (Gilbert and Bundtzen, 1983). If this stratigraphic thickness formed the cover sequence at the time of emplacement, then the lithostatic pressure (with approximate gradient of 300 b/km) was about 1.2 kb. If the stratigraphic column were doubled in thickness to match the mapped nappe structure to the north (Gilbert et al., 1982), the pressure would be about 2-3 kb.

The contact area itself is only about 200-300 m wide. This suggests a combination of shallow emplacement and/or relatively low water content of the intrusion. Other characteristics of the MFPC which are suggestive of epizonal emplacement (up to 6, possibly 10 km) according to the classification of Buddington (1959) are: discordance of intrusions with host rock; composite character of plutonic rocks due to successive intrusions; abundance of country rock xenoliths ± roof pendants; plutonic foliation absent or restricted to border areas; local occurrence of granophyre and miarolitic cavities.

Observed mineralogy from the metasedimentary contact rocks includes diopside, calcite, plagioclase, ± prehnite, ± wollastonite, ± spinel, ± alkali feldspar, ± quartz. Garnet is present only in calcareous xenoliths, not in the contact zone. Ba-rich micas, similar to kinoshitalite in composition, have been described from the contact area (Solie and Su, 1987) (Appendix F). Pressure constraints are not offered by these assemblages.

Hammarstrom and Zen (1986) developed an empirical geobarometer based on the Al content in hornblendes. Their proposed correlation, however, is only applicable to rocks with the mineral assemblage plagioclase (andesine-oligoclase), alkali feldspar, quartz, hornblende, biotite, titanite, magnetite (or ilmenite), with particular emphasis that the hornblende be primary and not altered. The only sample in the MFPC suite

which fills these requirements is 82DNS197, although titanite is very rare even in this sample. Hammarstrom and Zen (1986) use the label hornblende loosely, to include edenitic compositions such as that in 82DNS197. The total Al contents from the two hornblende analyses from 82DNS197 are 1.245 and 1.263. Using the linear regression equation of Hammarstrom and Zen (1986) calculated pressure estimates from the MFPC hornblendes are between 2.34 and 2.43 kb. However, this result is not necessarily meaningful, since the stated uncertainty from the geobarometer is ±3 kb (Hammarstrom and Zen, 1986). Hollister et al (1987) refined this geobarometer decreasing the error to ±1 kb. Using their linear fit equation, calculated P = 2.26 to 2.36 kb, ±1 kb. Although based on only two analyses, it is likely that pressure of crystallization was between 1 and 3 kb, implying a depth of emplacement between 3 and 9 km.

Temperature

Electron microprobe analyses of coexisting pyroxenes from cumulate gabbro samples 82DNS186 and 82DNS196 were evaluated using the two-pyroxene geothermometer described by Lindsley and Anderson (1983). A computer program, from Lindsley and Anderson, was used to recalculate pyroxene compositions, correcting for non-endmember components. Plotting on the polythermal quadrilateral phase relation diagram yields single grain temperatures (at <2 kb) between 800 and 951 °C. An orthopyroxene-clinopyroxene pair from 82DNS186 plots on the 900°C isotherms. Clinopyroxenes from 82DNS196 plot at lower temperature than orthopyroxenes, suggesting that these pairs are not in thermal equilibrium with each other. The 900°C determination is low for magmatic pyroxenes (Lindsley and Anderson, 1983), and suggests

that these cumulate pyroxenes continued to react during slow cooling. Therefore, 900°C can only be considered a minimum temperature of gabbro crystallization.

The olivine-clinopyroxene assemblage is present in the gabbros and syenites. Using the Powell and Powell (1974) formulation, which uses the Fe-Mg exchange reaction between olivine and Ca-rich clinopyroxene, samples 82DNS186, 82DNS196, 82DNS210 and 82DNS79 were evaluated. The geothermometer is not extremely pressure dependent; the estimated dependency is 5°C/kb (Powell and Powell, 1974). As a first approximation, 3kb was used for pressure (P) in the calculation for MFPC samples. The method requires knowledge of ferric and ferrous iron content in the minerals. Since this is not known from the probe data from MFPC gabbros and subsolvus syenites, the calculation yields unreasonably high temperature estimates (1560 - 1800°C). Assuming that all Fe is ferrous in hypersolvus syenite 82DNS79, calculated T, at 3 kb, is 930°C. This seems to be a reasonable estimate, based on the low pressure solidus temperature of the assemblage (which is present in 82DNS79) of hedenbergite + fayalite + quartz, which is about 950°C (Lindsley and Munoz, 1969).

Stormer and Carmichael (1971) proposed a geothermometer based on the F-OH exchange in apatite and biotite. This approach was tried for the MFPC, using apatite and biotite analyses from diorite sample 83DNS320d. The resultant T was < 127°C, obviously not a crystallization T. The apatite is F-rich ($F/F+OH = 0.97$) whereas the biotite analyses contain $F/F+OH < 0.1$. This disparity suggests that the biotite and apatite formed under different magmatic conditions, or that the biotite has undergone post-crystallization F loss, or post-crystallization F - OH exchange with fluids, possibly those fluids which have affected the diorite's isotopic and bulk compositions.

Water Content

The presence of biotite in the gabbros, and biotite and hornblende in the diorites suggests the presence of H_2O in the mafic magma(s), though there is no textural evidence of water saturation. Miarolitic cavities have been observed in HB granites, implying that they reached vapor saturation at some point in their crystallization. Pegmatites and miarolitic cavities in other rock types are absent, suggesting relatively dry magmas.

The anhydrous mineralogy of the hypersolvus syenite indicates crystallization from magma with very low water content. Furthermore, the hypersolvus nature of these syenites and AF granites suggests dry conditions of crystallization (Tuttle and Bowen, 1958).

Experimental studies of the crystallization sequence of granitic liquids with relation to T, P and water content are applicable to the HB granites. Naney (1983) found, for a granodioritic composition, that at higher wt% H_2O ($\geq$ about 5 wt% H_2O at 200 MPa) hornblende was on the liquidus, but not at lower wt% H_2O. From these observations, it can be deduced that the hornblende-dominant HB granites, in which hornblende crystallized before biotite, contained more water than did the biotite-dominant HB granites. In the biotite-dominant HB granites, biotite crystallized before hornblende. This suggests that crystallization began in a lower H_2O magma, and that saturation occurred during crystallization, placing amphibole on the liquidus. Since the composition of the rocks used in the experimental work by Naney (1983) does not match that of any of the HB granites, no precise H_2O or T estimate can be derived from his results.

Oxygen Fugacity

Temperature and oxygen fugacity (f_{O_2}) of the magma during crystallization of hypersolvus syenite are reflected by the assemblage fayalite + quartz; of AF granite by the assemblage arfvedsonite/riebeckite + quartz. The experimentally determined fields of stability for these assemblages are shown in Figure 52 (Ernst, 1963). The absence of magnetite in all observed rocks places crystallization conditions below the quartz - fayalite - magnetite buffer curve. The composition range of ilmenite (Ilm_{97-99}) further constrains the conditions of crystallization (Buddington and Lindsley, 1964), (Figure 52). The MFPC peralkaline AF granite assemblage falls within the area $\leq$600°C with log f_{O_2} in the range of -29 to -24, as illustrated in Figure 52.

The syenite field, defined by observed mineral assemblage in Figure 52, falls below the QFM buffer curve at a significantly higher log f_{O_2} than the granite, in the range of -16 to -19. The T range from the syenite field is between about 780 and 830°C. A general reducing trend is indicated during the crystallization history of the magma, with observed sequences of mineral growth following the predicted trend. Thus, the crystallization sequence of mafic minerals ilmenite-aenigmatite-arfvedsonite-annite (Figure 53) represents decreasing oxidation with decreasing temperature.

Fluorine Content

Concentration of F in the MFPC hypersolvus samples of syenite and AF granite is typical of similar rocks worldwide (Koritnig, 1978). Bulk rock compositions range from 710 to 3800 ppm F (Appendix B). The presence of F in the melt manifests itself in the AF granites in the crystallization of fluorite (generally as inclusions in mafic

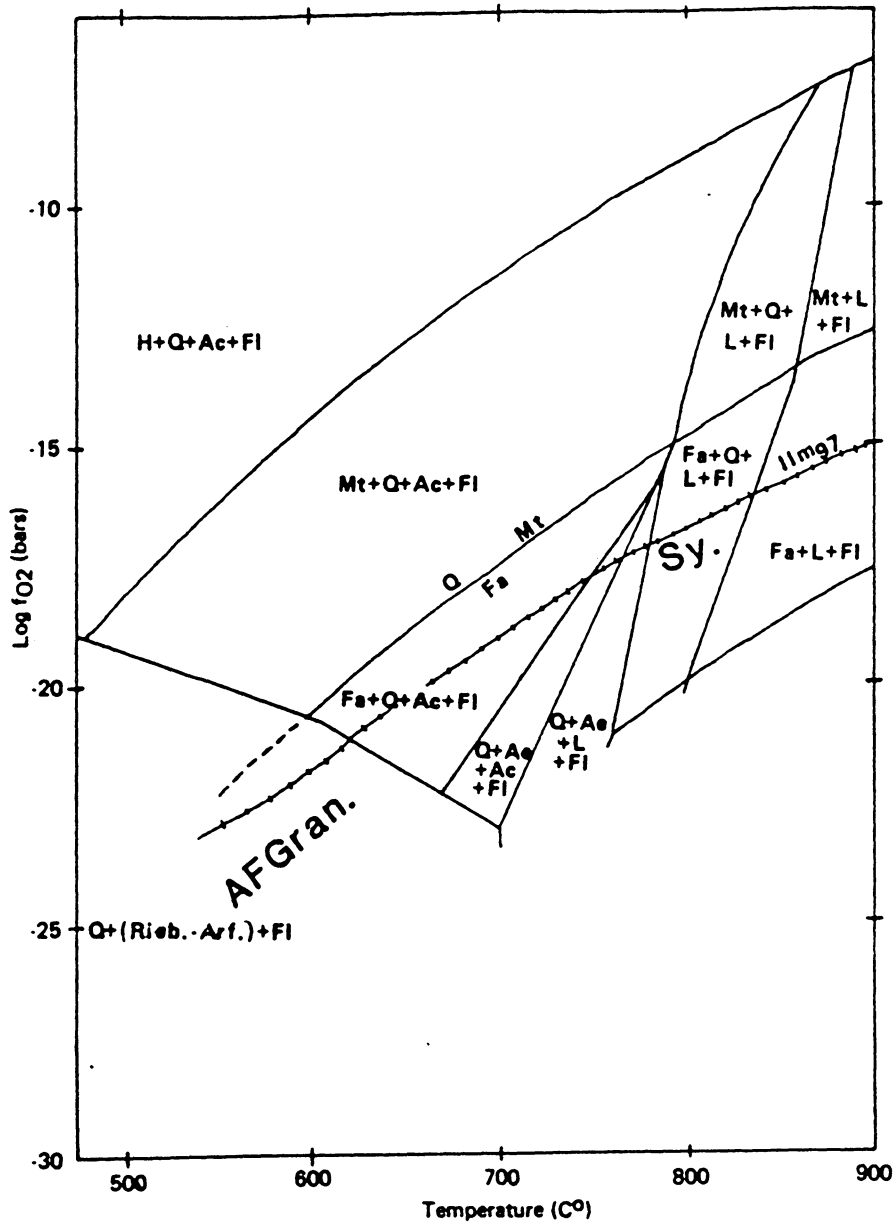

Figure 52. Log oxygen fugacity vs Temperature: "AFgran." and "Sy." labels show approximate fields of crystallization conditions for AF granites and hypersolvus syenites, based on mineral assemblages. Sources of stability curves given in text. Q = quartz, Rieb = riebeckite, Arf = arfvedsonite, Fl = fluid, H = hematite, Ac = acmite, Mt = magnetite, Fa = fayalite, Ae = aenigmatite, L = liquid.

Figure 53. Photomicrograph of mafic mineral asssemblage in AF granite: Crystallization sequence interpreted as ilmenite - aenigmatite - arfvedsonite - annite. Photo from sample 82DNS61a, field of view is about 3.25 mm across, plane polarized light.

minerals), particularly in the lower SiO_2 AF granite samples, which also have slightly higher CaO (up to 1.04 wt%). Fluorite is present in at least trace amounts ($\leq$1 modal %) in all AF granite samples; villiaumite (NaF) has not been noted. Thus F is saturated in all the AF granites. However, the whole rock concentration of F does not directly correlate with the observed amount of modal fluorite, as F is also present in biotite and amphibole. F concentration is greatest in those samples closest to the contact of granite against country rock, where magmatic fluids might be expected to concentrate. The decreased viscosity of F-rich melts (Dingwell et al, 1985) and the lower solidus temperature (Manning, 1981) could enhance the migration of F upward and outward in a magma chamber.

Alternatively, since during crystallization of the magma chamber F would be enriched in the melt relative to a H_2O-rich fluid (Manning and Pichavant, 1983), crystallization from the roof inward would lead to a peralkaline F-rich melt in the chamber. This might then have remobilized outward, to form the AF granite which is now exposed at the rim of the complex.

Not surprisingly, F goes into the hydrous minerals, with a general correlation between bulk F content and total modal mafic mineral content. F:OH ratios are greater than 0.5 in all analysed biotites and amphiboles, with higher ratios in the amphiboles. Cl content is negligible. Experimental work has shown that the presence of F in a melt expands the quartz field in the Q-Ab-Or system (Figure 54), shifting the minimum toward the Ab component (Manning, 1981). The difference between observed modal quartz and calculated normative quartz then might be a measure of the influence of F on the crystallization assemblage, and indeed, all of the AF granite samples have a greater modal percent of quartz than the norm would predict. However, the difference is not a systematic function of bulk rock F content in these five samples (Figure 55). In fact, the sample with the greatest difference between modal and normative quartz has

the lowest bulk F (84DNS61a); it also has the most abundant modal biotite. This is probably due to the lower SiO_2 content in biotite than in normative minerals (such as pyroxenes), resulting in norms with lower quartz content than the rock. Therefore, the difference between modal quartz and normative quartz is not a reliable measure of the influence of F on the felsic mineral assemblage.

Sample 82DNS195c is representative of the least evolved granite, in which a residuum of fluid at the end of its crystallization history did not escape, but formed late volatile- and trace element-rich minerals. These include a F-rich white mica (F:OH≃2.5), which is probably lepidolite or zinnwaldite, and a Ce-rich brown pleochroic mineral, possibly chevkinite. It is probably this late phase fluid which contributed to the least evolved sample having a high concentration of F. The other samples with higher F concentration (82DNS193 and 82DNS162b) have higher modal concentrations of amphibole and annite, and it is probably this which controls their whole rock F concentration.

All of the granites, except 82DNS195c, are close to minimum melt compositions, based on CIPW norm calculations (Figure 54). The highly evolved AF granite samples formed from fractionation of the syenite, following a path down the thermal trough of Figure 54 to a minimum approximately between 1 kb, H_2O - saturated, and 1 kb, 1 wt.% F, but shifted toward the anhydrous minimum. Though not quantitative, this minimum probably does reflect the conditions of final crystallization, and suggests fractional crystallization as the controlling factor in changes in bulk chemistry. However, the late crystallization of annite in samples not necessarily the most evolved in terms of Q - AB-Or indicates that other factors influenced the crystallization path.

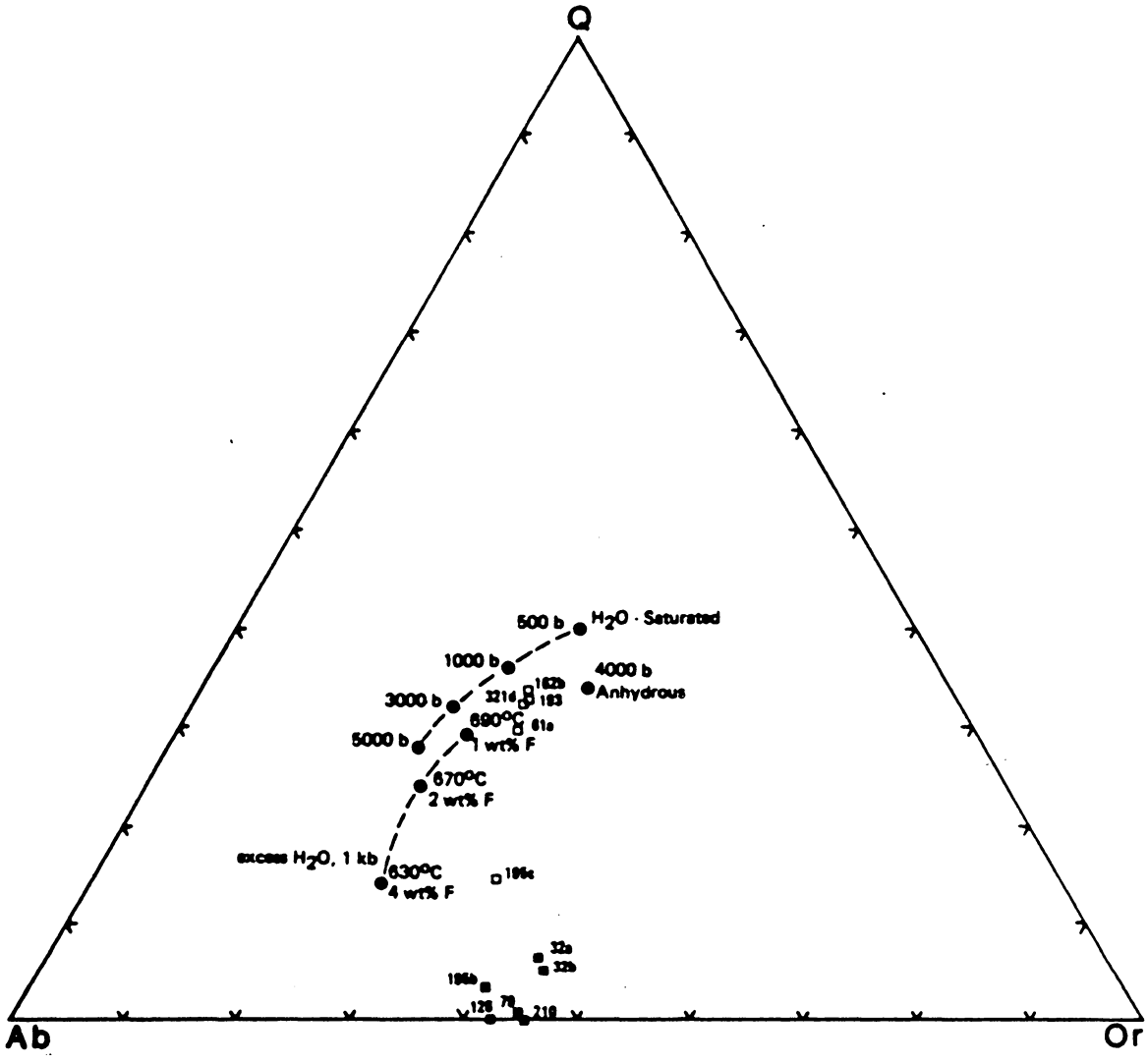

Figure 54. Q - Ab - Or plot for syenites and AF granites: Showing several minimum melt locations at different water and F contents, at different pressures. Sample numbers are labelled. Anhydrous data from Steiner et al (1975), F-bearing data from Manning and Henderson (1981), H_2O-saturated data from Tuttle and Bowen (1958; 0.5 - 3 kb) and Luth et al (1964; 5 kb).

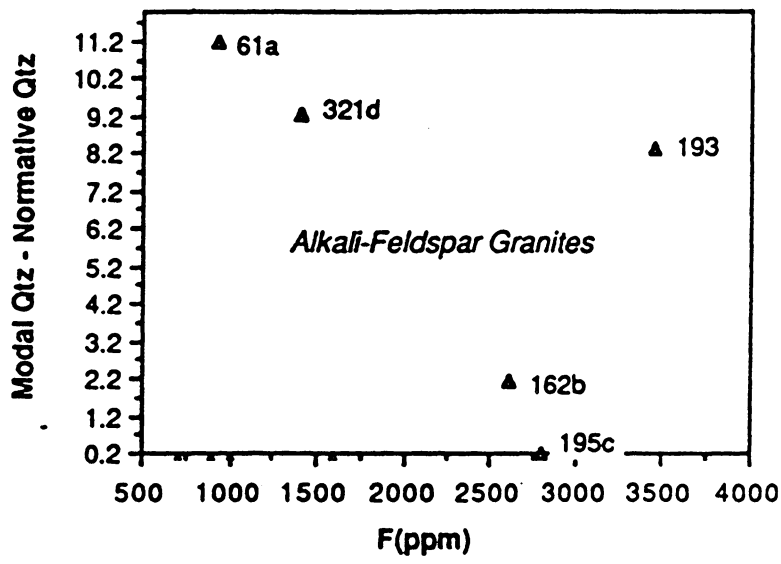

Figure 55. **(Modal quartz minus normative quartz) as function of F (ppm):** The difference between modal quartz and normative quartz is probably due in large part to presence of modal biotite, which is not included in the norm.

If F is added to a bulk composition with the relatively unevolved syenite mineralogies, a reaction such as the following can be written which forms the mineralogies of the peralkaline granites:

2 Fayalite + 7 Hedenbergite + 2 Orthoclase + 3 Albite + 17 HF + $3K^+$ =

Arfvedsonite + Annite + 8 Quartz + 3 Orthoclase + 5 H_2O + 2 H_2 + 7 Fluorite.

This reaction requires an open system (as for the addition of $3K^+$ to the left side of the equation) in order to balance the reaction. Thus, it is not tightly constrained, and may be written a number of different ways. Also, it assumes that all F is added as HF, which may or may not be realistic. However, the purpose of presenting this equation is not to define an actual reaction, but to illustrate the close compositional similarities between the mineral assemblages in hypersolvus syenite and AF granite, and the resultant controlling influence of volatiles on mineral assemblage. Moreover, it illustrates a mechanism for late-stage oxidation of the magma chamber, by loss of H_2 formed in the reaction. Evidence for subsolidus oxidation of the AF granite is seen in the late growth of riebeckite (as discussed in Chapter 2), and in the red luminescence of alkali feldspar (discussed in the following section). If this type of fluoridizing reaction operates in conjunction with fractionation, it may be expected that in some cases, reaction rate would differ from fractionation rate, and mineralogy would not always correspond directly to degree of fractionation.

A sample of calc-phyllite country rock from about 10 km north of the MFPC yielded a bulk F concentration of 3500 ppm. This value is considerably higher than typical sedimentary rocks (Koritnig, 1978). A representative thin section of this sample reveals only muscovite as a F-bearing phase. There is roughly 5-10 modal percent muscovite. Other minerals present are quartz, calcite, feldspar, and tourmaline. Electron microprobe analyses of muscovite yield $\leq$0.1 wt.% F. This is not sufficient to account for the whole rock concentration of F. Perhaps there are layers of F-rich min-

eralogies, perhaps the ubiquitous quartz and calcite stringers contain F-bearing minerals, or perhaps the one whole rock analysis is not reliable. It is not clear whether this high F concentration resulted from a fluid flux outward from the pluton, or if it is inherent in the sediments. If the latter, the sediments must be considered as a potential, though unlikely, source of F which could have fluxed into the pluton during and/or after emplacement.

Cathodoluminescence

Uncovered thin sections from syenite and AF granite were observed using a cathodoluminescent microscope (Appendix D). Luminescence is due to excitation of electrons in trace elements within minerals; non-luminescence is due to the total absence of luminescing ions, or the overriding presence of quenchers (i.e., elements which absorb excitation energy without emitting radiation). Colors of luminescence cannot be used unequivocally to define chemical composition, due to the complex interplay of relative amounts of various quencher and activator elements. However, cathodoluminescence is very useful in making visible any compositional zoning within minerals, and in some cases may indicate compositional constraints (Nickel, 1978).

Accessory minerals

Under cathodoluminescence, MFPC syenite zircons commonly show zonation patterns, in luminescent colors of dull grey to yellow grey and blue grey. These concentric zonations indicate a probable change in composition. Apatites, where observed in syenites, have yellowish luminescence which is indicative of the absence of Eu^{2+}, and

possibly the presence of Mn^{2+} (Mariano, 1978a). The core of apatite in 82DNS210 is non-luminescent, probably due to presence of Fe^{2+} (Mariano, 1978a).

The AF granite zircons are dull in cathodoluminescence, except 82DNS195c, which is concentrically dull in the center, then bright yellow, with a dark gray rim. If Fe^{2+} is responsible from quenching luminescence (Mariano, 1978a), then these zircons may be recording an increase and subsequent decrease in oxidation during crystallization. Luminescence of fluorite is variable, from milky purplish (82DNS195c, 84DNS61a, 83DNS321d) to bright yellow green (82DNS192, 82DNS162b); 83DNS321d fluorites have a light blue luminescent rim.

Alkali feldspars

When viewed under cathodoluminescence, the alkali feldspars in the syenites luminesce royal blue to bluish-black. AF granite sample 82DNS195c, the least evolved peralkaline granite, contains blue luminescing feldspars with bright red rims. Areas of most pervasive turbidity are reddest, though turbidity is also present in the blue cores and in the blue syenite feldspars. The feldspars of the other peralkaline granites all luminesce bright red, with the brightest coloration in areas of most intense turbidity. Apparently it is Fe^{3+} which causes the red luminescence in feldspars (Mariano, 1978a,b). Since the oxidized iron is present in feldspars which crystallized early under very reduced conditions, as described above, and is seen to occur as a rimming phenomenon in at least one sample, it is clear that the Fe^{3+} represents post-crystallization oxidation within the feldspar, probably due to late infiltration of either deuteric or meteoric fluids. Since these oxidizing fluids are influenced by the degree of turbidity, they must infiltrate after the turbidity occurred, penetrating along microfractures and lamellae interfaces.

Mariano (1978a) states that "all feldspars forming from fenitization can be recognized from their [red] luminescence behavior, even in the most subtle petrographic conditions". While this is probably true with respect to metasomatic feldspars, it is important to note that not all feldspars which luminesce red are necessarily metasomatic. Rather, as in this case, they can also be caused by infiltrating oxidizing fluids after feldspar crystallization.

Petrogenesis - Summary and Discussion

The following is a list of pertinent points made in the preceding sections of Chapters 2 and 3, in order to summarize the discussions which have been presented. These points will be the basis for the following petrogenetic discussion.

Summary

1) The MFPC suite is bimodal, with gap between 53.2 and 60.4 wt% SiO_2 .

2) Peacock index indicates alkali-calcic classification of suite.

3) Bulk chemistry of cumulate gabbros represents mix of crystals and liquid. Mineral compositions control compositional trends.

4) Calculated parental gabbroic magma composition suggests alkali olivine basalt parent.

5) Fractionation played a role in diorite-gabbro relationship.

6) A hydrous fluid which mobilized K, Rb, Ca, Sr and Ba seems to have affected the diorites. The HB granites are the most likely source of this fluid.

7) HB granites are metaluminous to peraluminous.

8) HB granite heterogeneity is most apparent in alkalis and trace elements, and may be due to differing initial bulk composition, mixing, or fluid exchange.

9) Syenites are all silica saturated to oversaturated, metaluminous to peralkaline.

10) Subsolvus syenites contain higher Sr, Ba, Al_2O_3, and lower Na_2O than hypersolvus syenite, and are products of contamination.

11) AF granites are peralkaline.

12) Pink-feldspar quartz syenites largely overlap syenite compositions, but are slightly more siliceous.

13) K-Ar data indicate ages between 55.6 and 57.7 m.y. for all plutonic samples.

14) Gabbro and diorite Rb-Sr isotopic data are scattered, but overlap, probably due to varying degrees of contamination.

15) Calculated SIR (at 57 m.y.) for gabbros and diorites are 0.705 - 0.706, due to contamination.

16) In diorites, higher SIR correlates with more modal alkali feldspar, Rb content, and lower K/Rb. Scatter is probably due to interplay of amount of contaminating fluid, amount of alkali feldspar crystallized, and K/Rb ratio of contaminating fluid.

17) Mineral separates from diorite 83DNS320d yield an isochron of age 57.2 m.y.. Secondary amphibole falls on the isochron, indicating that contaminating fluid influx occurred prior to or during crystallization.

18) Rb-Sr isotopic scatter in the HB granites suggests multiple sources, with possible superimposed fractionation and/or mixing. SIR (at 57 m.y.) ranges from 0.706 - 0.709.

19) Subsolvus syenite trends toward gabbros and diorites on a SIR vs. 1/Sr plot, suggesting mixing with the mafic rocks with which they are associated.

20) Hypersolvus syenite and AF granite form a seven-point isochron, 58.5 $\pm$0.2 m.y. (2σ), SIR = 0.70965, indicating comagmatic lithologies, fractionally related, which have remained isotopically undisturbed since crystallization.

21) Earliest-formed olivines in gabbro are not indicative of primitive mantle-derived magma, suggesting fractional crystallization or assimilational effects.

22) Gabbro sample 84DNS39c, from a contact with syenite, contains minerals (olivine, clinopyroxene, biotite, plagioclase, alkali feldspar) which are all shifted toward syenite compositions, indicating contamination by syenite.

23) Rim plagioclase composition of 84DNS34d gabbro is very similar to plagioclase composition of intruding HB granite veinlet sample plagioclase, 84DNS34a.

24) Relict augite cores in HB granites are similar in composition to augites in gabbros and diorites.

25) Plagioclase grains in subsolvus syenite are magmatic, not albitization products. Presence of two feldspars indicates higher P_{H2O} than in hypersolvus syenites.

26) Pressure at level of crystallization is probably between 1.5 - 3.0 kb.

27) Minimum gabbro crystallization temperature was about 900°C; maximum temperature of crystallization was roughly 1200°C. An approximate temperature of crystallization for syenite is 930°C. A reasonable estimate for temperature of crystallization of HB granite is 750 - 850°C.

28) HB granite magma(s) were most hydrous of the MFPC magmas; hornblende-dominant HB granites contained more H_2O than biotite-dominant HB granites.

29) AF granite crystallized at $\leq$600°C, with log f_{H2O} between -29 and -24. Syenite crystallized between log f_{H2O} -16 and -19, between 780 - 830°C; oxygen fugacity decreased during crystallization.

30) F concentrated in the outer portions of the magma chamber during fractionation of syenite to AF granite. F is incorporated as fluorite and in hydrous phases in AF granite.

31) Addition of HF to mineralogies of hypersolvus syenite can form the mineralogies observed in AF granite.

32) The country rock could be the source of F in the magma, or F could be inherent to the magma itself.

33) Red luminescing alkali feldspars in AF granites are a result of late oxidizing fluids.

A petrogenetic model for the MFPC must take into account all of the above petrologic points, as well as all field observations as described in Chapter 1. The complexity of the MFPC, as observed at its present level of erosion, is due to the interaction of at least three magmas from nearly simultaneous intrusive events. These were emplaced at a fairly shallow level, of about 3 - 8 km, where numerous blocks of stoped country rocks occur as xenoliths. Down-faulting of a large block of host rock suggests post-intrusion subsidence in the center of the complex. The juxtaposition of these various dynamic processes leads to variable degrees of hybridization, commingling, and contamination between observed endmember gabbros, syenites, hornblende-biotite granites and metasedimentary wallrock, in addition to any pre-emplacement contamination and fractionation which may have occurred.

The hypersolvus fayalite-hedenbergite alkali-feldspar syenite is the earliest observed intrusion in the complex, and occurs in its most homogeneous form near the south and east margins of the complex. In what appears to be a gradational contact with the syenite, along the east margin of the pluton, is hypersolvus annite-arfvedsonite AF granite. The AF granite is related to the syenite through fractional crystallization, and formed from a magma with SIR of 0.7096. Superimposed on the fractionation process are the observable effects of F migration toward the outer margin of the pluton. The addition of F leads to mineralogic reactions forming the AF granite lithologies.

Mafic magma intruded the syenite, and formed locallized cumulate zones of olivine-pyroxene-biotite-plagioclase gabbro. These gabbros fractionated towards dioritic composition. This process was locally disrupted by subsequent intrusive pulses of metaluminous felsic magma(s) and possibly additional gabbroic magma(s). The HB

granites, derived from heterogeneous local melts, were the source of an alkali-rich hydrous fluid which infiltrated the diorite and to some extent the gabbros, scattering their isotopic signatures and changing their bulk composition. Where the diorite was largely crystalline, the HB granite brecciated it, and mingled with it to form heterogeneous enclave-rich mixed rocks. Some hybridization of the HB granites from mixing with the diorite is suggested by the occurrence of cores of clinopyroxene and plagioclase of dioritic composition within HB granites. Isotopic scatter of all the mafic and HB granite samples is further evidence for their mutual contamination.

In addition, each of the aforementioned magmatic pulses locally became contaminated by syenite which was only partially crystalline (or remolten) toward the center of the complex. Mafic enclaves in the syenite, and amphibole-bearing subsolvus syenites are products of mingling and contamination of syenite with one or more mafic magmas. Xenolith assimilation/contamination locally lends further variability to the plutonic lithologies.

Discussion

Any petrogenetic model must include some discussion as to possible sources of heat and magma. Though SIRs of the mafic rocks are not unequivocally primitive, the presence of more than one pulse of mafic magmatism (dike swarms, gabbro and diorite) suggests a mantle source. The potential for contamination of these magmas is too great to attempt to model parental composition, although there is some evidence, based on trace element chemistry, that they were alkali olivine basalts.

The AF granites are typical of so-called A-type granites (Loiselle and Wones, 1979). The AF granite - syenite - gabbro association is typical of what are thought of

as anorogenic suites throughout the world (e.g., Barker et al., 1975; Kinnaird et al., 1985; Loiselle, 1978).

The magma from which the syenites and AF granites crystallized has an SIR of 0.7096, clearly not a mantle signature. This is in contrast to many similar anorogenic suites which yield low SIR values. For instance, the 35 m.y. Kialineq centre, East Greenland contains quartz syenite and granite with SIR = 0.70385. These are thought to be fractionated from magma of mantle origin (Brown and Becker, 1986). Similarly, Bonin et al., (1978), report SIR of 0.7034 for the Permian anorogenic granites of Evisa, Corsica, and suggest mantle derivation. Low SIR in the Topsails complex, Newfoundland is suggested to be due to the metasomatic influx of mantle-derived fluids (Taylor et al., 1981).

However, the high SIR from the MFPC is within the range of reported values from other similar complexes. These include the Davis Inlet--Flowers Bay suites, Labrador, with a syenite-peralkaline granite SIR of 0.7076 (Collerson, 1982), the Pikes Peak batholith, with SIR of 0.7072 (Hedge, 1970), and the granites of the East Antarctic shield, which have an SIR of 0.7184 (Sheraton and Black, 1988).

Four possible methods of deriving a high SIR are: 1) by reaction melting of radiogenic crust and contamination during fractionation of a mantle melt (e.g., Blaxland et al., 1978; Foland and Friedman, 1977; Barker et al., 1975; Collerson, 1982); 2) by partially melting radiogenic crust (e.g., Sheraton and Black, 1988); 3) by metasomatic alteration of isotopic composition (e.g., Currie et al., 1986); 4) by partially melting a very old enriched mantle (Brown et al., 1984).

There is not much difference between the first two processes, in that in either case there is a large (or total) crustal component to the magmas as seen at the level of emplacement. In either case, a heat source is requisite for melting the crust. In the MFPC, where mafic magmatism is shown to be coeval with felsic magmatism, it is rea-

sonable to call upon heat from these mafic magmas, and the heat of crystallization released during their crystallization to melt the crust.

The third process listed above (metasomatic resetting of chemistry) is difficult to verify, unless it occurred as a post-crystallization phenomenon, and left chemical and textural evidence which could be correctly interpreted. As stated by Whalen et al., (1987), the large scale homogeneity of A-type granites and lack of chemical and mineralogical evidence for late-stage metasomatism refutes this as a causative process for petrogenesis of A-type granites. In the MFPC, it is extremely unlikely that metasomatism at the level of emplacement could have resulted in such thorough and homogeneous alteration that a high SIR isochron, including two different lithologies, could be formed. Therefore, this model is ruled out.

Metasomatism prior to emplacement is more difficult to rule out, since time and emplacement could have provided the means for homogenization. Bailey (1974) suggests that a flux of mantle-derived volatiles induces lower crustal melting. This model cannot be refuted, and it stands as a possible process in the derivation of A-type granites.

Partial melt of a very old enriched mantle is a viable method to explain high SIR and elevated LIL and HFS element abundances (Brown et al., 1984). However, this model would imply fractionation from a mafic melt. In the MFPC, it is evident that the A-type suite is not comagmatic with the mafic rocks. Also, intermediate compositions, which might be expected in a fractionally related mafic to felsic suite, are absent. Thus it seems improbable that this model holds for the MFPC.

The most likely model for the derivation of the MFPC AF granite - syenite magma is some combination of the first two processes listed. The mantle magma, which is integral to the first process, is required in the MFPC model as a heat source for melting radiogenic crust. Whether, during crystallization of that mafic magma, any part of its

fractionate mixed with the crustal partial melt is a moot point. The overwhelming compositional influence on the derived magma was probably the crustal source.

Several protoliths have been suggested as the radiogenic crustal source of A-type magmas. These sources must allow for the production of relatively dry, high temperature, Cl(?)- and F-rich magmas, with enrichment in such elements as Rb, Y, Ce, and Zr. Many authors, as recently summarized by Whalen et al., (1987), propose variations of the model suggested by Barker et al., (1975), of a dehydrated residual lower crustal source, which has been previously melted. The different lithologies observed by Barker et al., (1975), in the Pikes Peak batholith, are explained by fractionation of the derived syenitic magma to form fayalite granite and riebeckite granite, and consequent contamination due to reaction melting at other crustal levels to form fayalite-free granite and aplites. Collins et al., (1982), ascribe the high halogen content in the melts as resulting from the high temperature breakdown of F- and Cl-rich amphiboles and biotites, which are residual from the previous melting event. Breakdown of refractory accessory minerals in the source may contribute elements such as REE and Zr to the melt. The halogens might alternatively come from mantle-derived volatile flux, which promotes crustal melting (Bailey, 1974). The above model fits the data from the MFPC, and is considered as most likely for the petrogenesis of the syenite and AF granite magma.

The source of the HB granites was probably different from that discussed from the syenite-AF granite suite. If the latter is a partial melt of previously melted lower crust, then the hydrous, metaluminous to peraluminous HB granites might be either the early partial melt of the lower crust, or a shallower - level partial melt. Since HB granite is the youngest of the plutonic lithologies, it is unlikely that it was the first partial melt of lower crust. The more likely model is that the HB granites are partial melts of middle to upper crust, in response to high heat flow, and possibly locallized pooling of mafic magma.

Martin and Bowden (1981) describe peraluminous biotite granites in the nonorogenic Ririwai ring-complex, Nigeria. They conclude from their study that the biotite granite is the result of subsolidus interaction of hypersolvus granite with fluid. The biotite granites which they describe have < < 1 wt% CaO (compared to 1 - 3 wt% CaO in HB granites), no amphibole, biotite compositions between annite and zinnwaldite, hydrothermal mineralization of columbite and cassiterite, and alteration textures which in many instances obliterate the magmatic assemblages. None of these characteristics are present in the HB granites, and Martin and Bowden's (1981) model, in which Na-for-K exchange and alkali removal cause peraluminosity, are not considered important in the generation of the HBganites of the MFPC.

The MFPC: root zone of a peralkaline volcanic system

The lithologies and textural relationships of the MFPC may be viewed as the root zone of a peralkaline volcanic system. The pre-plutonic dike swarm, the presence of comagmatic syenite-peralkaline granite, the mingling intrusion of mafic magma into the magma chamber, the fault-controlled subsidence of a large block of country rocks into the core of the complex, and the continued magmatism, both felsic and mafic, all equate with shallow-level characteristics of peralkaline volcanism. To explore this relationship further, a brief description of a model peralkaline extrusive system must be developed.

There are four compositional groups of silicic (quartz normative) peralkaline ($Na_2O + K_2O > Al_2O_3$) volcanic suites: comendites, pantellerites, comenditic trachytes and pantelleritic trachytes (Macdonald, 1975a), defined on the basis of Al_2O_3 vs. Fe as FeO (wt%). The comenditic suite is generally less peralkaline, and transitional towards the non-peralkaline rhyolites. The peralkaline trachytes (comenditic and pantelleritic) are typically porphyritic, with ubiquitous alkali feldspar (Or_{36} - Or_{43}) ± hedenbergite or

aegirine ± opaque oxides ± fayalitic olivine phenocrysts (Sutherland, 1975). Aenigmatite, pyroxene (hedenbergite, aegirine, sodic ferrohedenbergite), quartz, feldspar, opaque oxides (magnetite, ilmenite), and amphibole (kataphorite, barkevikite, arfvedsonite) may all occur in the groundmass of the trachytes (Sutherland, 1975). In the pantellerites, alkali feldspar phenocrysts (Or_{30} - Or_{44}), sodic pyroxene (aegirine, minor sodic ferrohedenbergite), minor fayalite, aenigmatite, amphibole (ferrorichterite, arfvedsonite), minor opaque oxides, and quartz are common, and in the comendites, alkali feldspar, aegirine and sodic ferrohedenbergite, minor oxyhornblende, quartz, minor biotite, riebeckite and arfvedsonite, and opaque oxide (Ti-magnetite, hematite) occur (Sutherland, 1975).

These assemblages have strong common characteristics with those of syenite and AF granite in the MFPC (Figure 56). The MFPC syenites (plutonic equivalents of trachytes) (Figure 57) contain the mineralogies seen as phenocrysts in peralkaline trachytes. Quartz in the syenites is late crystallizing, and therefore not likely to occur as phenocrysts. The MFPC AF granite resembles comendite mineralogy in that the most abundant peralkaline volcanic phenocrysts are alkali feldspar and quartz, which are early crystallizing phases in the AF granite. The hydrous mafic minerals in the AF granite are the hydrous equivalents of the pyroxenes commonly observed in peralkaline comendites. amphibole and biotite. Aenigmatite is not an unusual phase in volcanic peralkaline rocks. The presence in many of the extrusives of magnetite ± hematite indicates a significantly higher f_{O_2} than that of the MFPC (Figure 52); this may be due to their extrusive environment of crystallization.

Compositionally, the AF granites of the MFPC plot in the comendite field. The syenites (except 82DNS195b), though not strictly peralkaline on the basis of A/CNK, plot as comenditic trachytes (Figure 57). Trachytic rocks in peralkaline vocanoes are

MINERAL ASSEMBLAGES	PHENOCRYST ASSEMBLAGES
Middle Fork Plutonic Complex	**Peralkaline Volcanic Complexes**
Syenite: **fay -- hed -- ilm -- kspar -- qtz**	**Peralkaline Trachytes:** **kspar - pyx (hed) - fay - ilm**
Peralkaline Granite: **kspar -- qtz -- aenig -- arfved -- bt**	**Comendites:** **kspar - qtz - pyx (hed, aeg-aug)**

Figure 56. Comparison of plutonic and volcanic peralkaline assemblages: The peralkaline volcanic equivalents of hypersolvus syenite and AF granite are peralkaline trachyte and comendite. Their typical phenocryst assemblages (Sutherland, 1975) are compared to the mineralogy of observed plutonic rocks of the MFPC. The early crystallizing alkali feldspar in AF granite is the most abundant phenocryst in comendites.

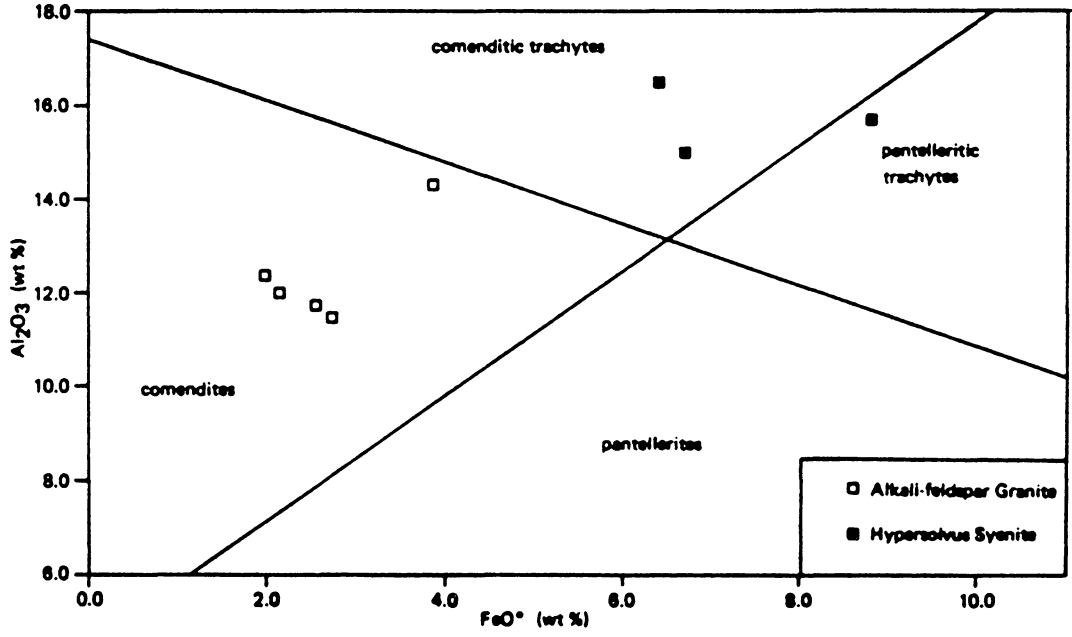

Figure 57. **Peralkaline volcanic classification scheme:** Plot of hypersolvus syenite and AF granite compositions, using classification from Macdonald (1975a).

not always peralkaline. For instance, Kenya Rift salic eruptive rocks are described as ranging from metaluminous to peralkaline (Baker, 1987). No volcanic rocks exist at the present-day erosional surface of the MFPC, so it is not demonstrable whether the peralkaline magma vented to the surface. However, mineralogically and compositionally, it is permissive that the proposed volatile-rich flux in the MFPC, which enhanced the development of the AF granites, may have vented to form a peralkaline volcano. The syenite presently exposed in the MFPC can best be considered as the denser, noneruptive portion of the magma, although portions of it may also have erupted to form trachytes.

One of the typical features of peralkaline volcanism is the absence or subordinate volume of basaltic activity during silicic eruptions, even though there is commonly extensive basaltic volcanism preceding silicic shield building (Mahood, 1984). Mahood (1984) refers to this as a 'shadow zone', in which basalts do not erupt due to the presence of magma reservoirs which intercept them. In the MFPC, this interception of mafic magmas is preserved in the mingled textures which characterize the complex. The mafic dikes of the dike swarm which preceded plutonic emplacement may well have manifested themselves at the surface as basalt flows. The mafic dikes are mostly hawaiites, with some basalts and some mugearites, according to the classification of Baker et al., (1974). This classification defines hawaiite as having a Thornton and Tuttle (1960) differentiation index (D.I. = $\sum$normative q + or + ab + ne + lc + kp) between 30 - 45, and normative plagioclase composition An_{30-50}. Mugearite has D.I. = 45 - 65, and normative plagioclase $< An_{30}$; basalt has D.I. < 30 and normative plagioclase $> An_{50}$. These mafic rock types are commonly cited as being associated with silicic peralkaline volcanism (e.g., Paisano volcano, Texas (Parker, 1983); Aden, South Arabia (Cox et al., 1970); Anahim volcanic belt, British Columbia (Bevier et al., 1979; also Macdonald,

1975b). All of the analyzed mafic rocks of the MFPC dike swarm are quartz saturated to oversaturated.

Basaltic eruptions associated with the peralkaline shield, if present, are found only from low-lying flank vents (Mahood, 1984). Late basaltic satellite eruptions from fissures have been reported from peralkaline volcanoes of the Kenya Rift (Baker, 1987). Such late mafic events on the periphery of the silicic activity, are correlative with mafic dikes which intrude the plutonic rocks on the eastern margin of the MFPC. These dikes are not seen through the central and western portions of the complex, and are thought to be, in part, the intermingled mafic magmatism which forms the mafic enclaves and gabbro(s)/diorite(s) in the central and western areas. Due to the complexity of field relationships and compositional heterogeneities of the mafic rocks, it is impossible to precisely determine how many mafic intrusions are present in the MFPC. However, the concept of the "basalt shadow", the arrestment of mafic pulses within a semicrystalline magma chamber sheds light on the process which led to the observed complexity. Where the syenite was already crystalline, mafic magma was able to intrude and form cumulate layering in a relatively quiescent environment. Where syenite was still semicrystalline (or perhaps it was even partially remolten by influx of heat and water), mafic magma formed pull-apart dikes, enclave swarms and irregular contacts. Introduction of water and some chemical exchange with the syenite allowed crystallization of the subsolvus syenite.

In support of this model are crystalline nodules reported from the volcanics of the Kenya Rift. These include dioritic nodules with biotite and andesine, (no olivine), from Silali volcano (Macdonald, 1987), and layered plagioclase - clinopyroxene - magnetite cumulate nodules from Emuruangogolak (Weaver, 1976-77). Syenite and granitic xenoliths are commonly observed in peralkaline volcanic (Mahood, 1984).

There are two notable differences between the MFPC and typical peralkaline volcanic systems. These are 1) equivalents to the metaluminous to peraluminous

rhyolite dikes and HB granites of the MFPC are not always present in strongly peralkaline volcanic suites, and 2) many studies of peralkaline volcanics have concluded that the trachyte - pantellerite/comendite sequence is a result of fractionation from a mafic magma (e.g., Boina Centre, Ethiopia (Barberi et al., 1975); Ningi-Burra complex, Nigeria (Turner and Bowden, 1979); Jebel al Abyad, Saudi Arabia (Baker et al., 1973)).

The brecciating nature of the HB granite suggests that its emplacement was forceful and could have vented to the surface. Its emplacement late in the sequence of the MFPC means that it would have erupted at the top of the volcanic pile. The surficial expression of this siliceous hydrous magma would probably be as volcaniclastic rocks. Therefore, the likelihood of preservation would be relatively low due to erosion, and thus may not be observed in present-day volcanic exposures elsewhere.

However, subalkaline rhyolites are not always absent from peralkaline centers. For example, subalkaline rhyolites associated with probable caldera collapse are reported from the Black Mountain volcanic center, southern Nevada (Noble and Parker, 1975). Subalkaline rhyolites on S. Pietro Island (type-locality of comendites) are coeval with the silicic peralkaline volcanics there (Arana et al., 1975).

Fractionation from a trachyte to pantellerite or comendite is commonly proposed in peralkaline volcanic suites (e.g., Gibson, 1975; Parker, 1983). The evolution proposed for the syenites and AF granites of the MFPC fits such a model. However, derivation of this peralkaline liquid by extensive fractionation of a basaltic liquid, as is proposed for many peralkaline volcanic centers, is not permitted by the isotopic data of the MFPC. Macdonald (1987) also points out that isotopic and geochemical evidence do not always support a fractionation model for volcanic centers, and it may be that a model such as that proposed for the MFPC is more applicable than presently recognized in volcanic studies.

Peralkaline volcanism is universally attributed to dominantly tensional stresses. Within this context, however, are several diverse tectonic settings in which peralkaline volcanism occurs. These settings are outlined by Macdonald (1975b) as: 1) continental areas of rift formation and/or epeirogenic uplift with no previous orogeny; 2) the later stages of orogenic cycles; 3) oceanic islands; 4) as isolated occurrences in active mobile belts; and 5) in areas of extensional tectonics at or near continental plate margins. It has been pointed out by Mahood (1984) that peralkaline magmas are generally associated with zones with relatively small extension rates, whereas areas of rapid extension are lacking in peralkaline magmatism. The presence of peralkaline volcanic rocks in zones of local extension in convergent margins is an example of this observation (Mahood, 1984). It is this setting which best describes the occurrence of the MFPC, as will be discussed in the section of Alaska magmatism.

Chapter 4: Regional Tectonic and Magmatic Setting

Regional Tectonics, southern Alaska

The accretion of 'suspect terranes' (Coney et al., 1980) to the southern margin of Alaska, with concomitant subduction, obduction and transform faulting, is generally thought to be the driving force behind folding and faulting in the McGrath quadrangle. Debate continues as to the significance, inter-relationship, and timing of the various tectonostratigraphic terranes in Alaska, but a brief discussion of pertinent terranes may be useful in presenting the origin of magmas in the study area.

The Paleozoic strata intruded by the MFPC are part of the Dillinger terrane as defined by Jones et al., (1981, 1982) (Figure 58). The rocks of this terrane are interpreted as basinal fan turbidites and foreslope deposits, and probably represent a single stratigraphic succession with the adjacent shallower water Mystic terrane (Gilbert and Bundtzen, 1984). To the southwest and across the Farewell fault zone to the northwest, the Nixon Fork terrane is juxtaposed against the Dillinger (Coney et al, 1980). This terrane consists of PreCambrian metamorphic basement overlain by Paleozoic carbonate and clastic rocks, and may represent a shallow water platform environment syndepositional with the Dillinger sediments (Churkin et al., 1984). Thus, these three

so-called 'suspect terranes' (i.e., Dillinger, Mystic and Nixon Fork) may simply be telescoped and translated facies equivalents from the Paleozoic cratonic North America margin.

Alternatively, they may be 'exotic' crustal segments which have been "swept from far reaches of the Pacific Ocean before collision into the Cordilleran margin" (Coney et al., 1980). However, close fossil fauna affinities suggest that the Nixon Fork terrane was in close proximity to western Canada during the Devonian (Blodgett, 1983). Paleomagnetic data from the Nixon Fork terrane suggest little northward displacement, with a counterclockwise rotation during latest Cretaceous and early Tertiary time, thus arguing against the model of this being a far-travelled 'exotic' terrane (Coe et al., 1985). It is suggested that the counterclockwise rotation was a local effect taken up by individual blocks; the data are permissive of lateral translation from western Canada (Coe et al., 1985).

Offset of the offshore facies of the Nixon Fork, Dillinger and Mystic terranes probably resulted from movement along the Tintina fault (a major fault to the north which roughly parallels the Denali fault system) and the Denali fault system. Estimates of lateral movement on the Denali fault system as a whole generally range between 300 to 400 km (e.g., Forbes et al., 1973; Lanphere, 1978; Stout and Chase, 1980; Kozinski, 1986; Aleinikoff et al., 1987).

Timing of the offset along the Denali system is equivocal, though it is generally agreed that major offset occurred during Late Cretaceous to Cenozoic time (e.g.,Patton and Gilbert, 1982; Box, 1985). Lanphere (1978) suggests major movement between 55 and 38 m.y. ago, with subsequent offset being less than 40 km. This latter constraint is based on an apparent 38 km offset of the 38 m.y. Foraker and McGonagall plutons along the McKinley segment of the fault, about 200 km northeast of the MFPC (Reed and Lanphere, 1974). Wallace and Engebretson (1984) suggest that onset of right-lateral

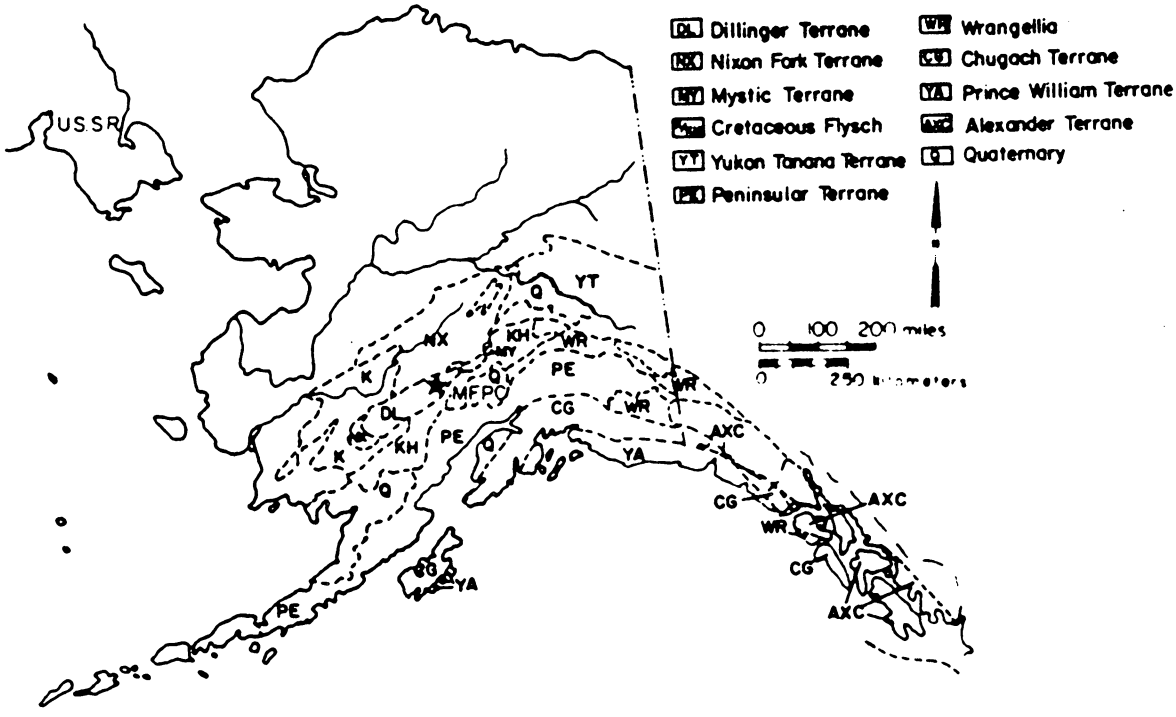

Figure 58. **Tectonostratigraphic terranes of southern Alaska:** (Modified from Jones et al., 1981). The MFPC (indicated by star) is located within the Dillinger terrane (DL), which is bounded by the Cretaceous flysch terranes (K and KH) and the Nixon Fork terrane (NX).

motion was at about 56 m.y., in response to an increase in velocity of the subducting Kula plate with respect to North America, and an increase in the component of motion parallel to movement. The assumption that the Alaska Range and Coast Mountain plutonic belts were a single continuous belt (Figure 59) places the MFPC just east of the present-day Canadian border, in pre-Eocene time.

South of the present-day Dillinger Terrane is a terrane of deformed Juro-Cretaceous flysch deposits (KJf of Jones et al., 1981). These black marine clastic and volcaniclastic rocks represent deposition in an ocean basin located between the North American continental margin and the northward moving 'exotic' Peninsular and Wrangellia terranes. These latter have been collectively called the Talkeetna superterrane. The intervening subduction zone is apparently now covered by the obducted terranes; thrusting and intense deformation resulted from the convergence of the blocks. Accretion is thought to have been complete by mid-Cretaceous (Csejtey et al, 1982; Coe et al., 1985). Paleomagnetic data suggest that these blocks were then also laterally transported on strike-slip faults before 52 m.y. (Coe et al., 1985). At some time in Late Cretaceous or early Tertiary, the locus of subduction must have migrated outboard, as additional 'exotic' terranes (including Chugach, Prince William, Alexander terranes) accreted to the southern margin of Alaska via obduction and/or right lateral displacement.

Oroclinal bending through southcentral Alaska may have occurred in mid-Tertiary, (Nokleberg et al., 1986), causing or enhancing the arcuate curve of the Denali fault, and further deforming the rocks of the region. Late Cenozoic block faulting along the Denali fault system formed horsts, grabens, and tilted fault blocks (Gilbert, 1975). Basinal Tertiary deposits are presently preserved in these grabens along the Farewell segment of the fault, north of the MFPC. Provenance studies of these sediments suggest a

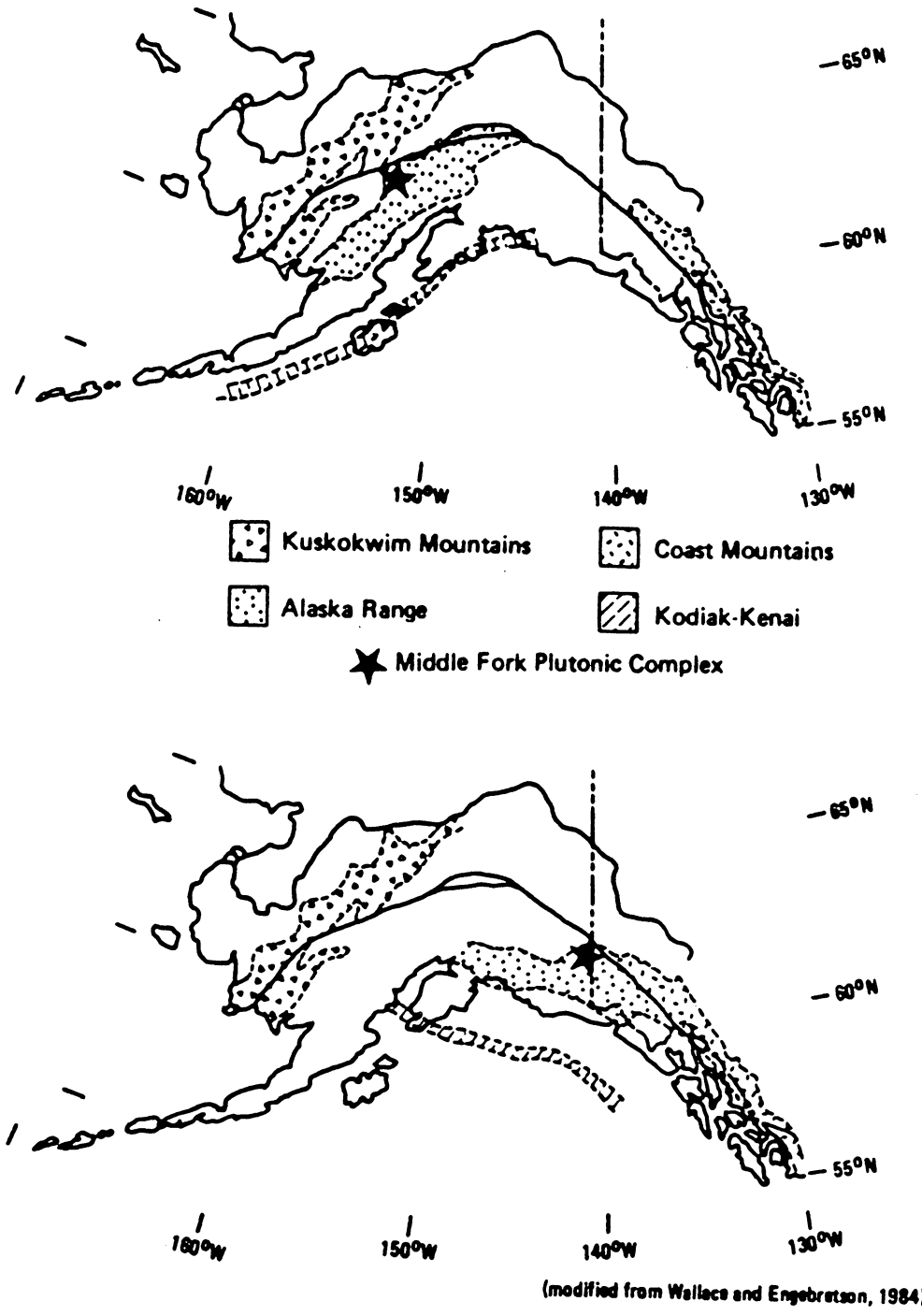

Figure 59. Reconstruction of Alaska Range prior to movement on Denali Fault: The upper figure shows the present-day position of the magmatic belts. The lower figure is a reconstruction, assuming that the Alaska Range and Coast Mountain magmatic belts were a single continuous belt prior to displacement on the Denali Fault. The star indicates position of the MFPC relative to the Alaska Range belt.

northern source area prior to lateral strike-slip translation in lower to middle Tertiary, and a subsequent upper Tertiary source from the uplifing Alaska Range to the south (Dickey, 1984).

The Alaska Range is presently being uplifted at an estimated rate of about 0.9 mm/year in the Mount McKinley area, based on fission track studies of apatite and zircon (Plafker et al., 1984). Subduction continues at the Aleutian trench, with accompanying active arc magmatism. The present position of the subducting slab below the MFPC is greater than 150 km, based on seismic hypocenter depth contours (Stone and Wallace, 1987).

Regional Magmatism, southern Alaska

Mesozoic and Cenozoic igneous rocks of Alaska are generally grouped into magmatic belts which are roughly subparalled to the present continental margin. Following the terminology of Hudson (1979), the plutonic belts in southern Alaska are, from oldest to youngest: 1) Kodiak-Kenai belt (Sanak-Baranoff belt of Moll-Stalcup (in press)) 2) Aleutian Range-Talkeetna Mountains belt 3) Tonsina-Chichagof belt 4) Nutzotin-Chichagof belt and 5) Alaska Range-Talkeetna Mountains belt (AkR-TM). In addition, Moll-Stalcup (in press) describes the 6) Kuskokwim Mountains (KM) and 7) Yukon-Kanuti belts north of the AkR-TM belt (Figure 60 on page 163). The MFPC is located within the AkR-TM belt, near the northwestern boundary, which is defined by the Denali fault system. Therefore, this discussion will focus on magmatism of this belt and its relation to the adjacent belt to the north (KM belt) and to the regional tectonics. Characteristics of these two belts are summarized in Table 6.

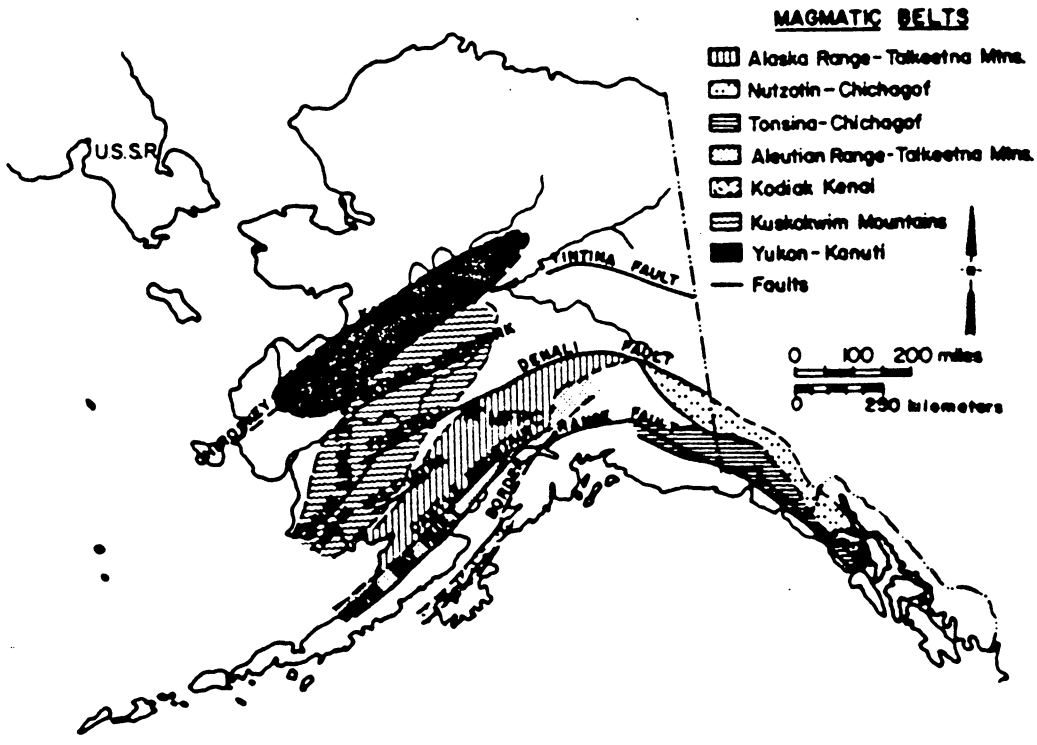

Figure 60. **Location of magmatic belts of Alaska:** (Modified from Hudson, 1979, and Moll-Stalcup, in press; fault locations from Beikman, 1980). The MFPC is included as part of the Alaska Range - Talkeetna Mountains magmatic belt.

Table 6. Summary of characteristics of magmatic belts

	ALASKA RANGE–TALKEETNA MOUNTAINS BELT					KUSKOKWIM MOUNTAINS BELT
Epoch	Late–Cretaceous–Paleocene				Eocene–Oligocene	Late Cretaceous
Age Range (my)	83–55				40–26	72–60
Overall Style	Generally larger batholiths, elongate N–S, cutting regional structural grain. Minor associated volcanics				Tend to be scattered, isolated plutons. Minor associated volcanics	Includes large volcanic fields and volcanoplutonic complexes as well as individual scattered volcanics
Age (my) Subgroups	83–81	74–55	67–62	60–55	Merrill Pass sequence Styx River Northeast prong of Tired Pup, Jimmy Lake Windy Fork Pluton Foraker McGonagall	Northern volcanic fields: Sischu, Dishna, Nowitna Northern volcanoplutonic complexes: Page Mtn, Cloudy Mtn, Candle Mtn, Takotna Mtn, Mt. Joaquin Northern plutons, dikes and sills: VanFrank, Stone Mtn. intrusives Volcanic & plutonic rocks of Sleetmute–Nyac area: Chuilnuk, Kiokiuk Plutonic rocks of southern Kuskokwim Mtn. region. Bristol Bay Volcanic series
Igneous Rocks Included in subgroup	Knutsen Bay Intrusive	Summit Lake Intrusive	Mt. Estelle Hartman Seq. Yentna Seq.	Tired Pup Crystal Creek McKinley Seq. MFPC		
Tectono-strati-graphic Terranes Intruded	Jurassic plutonic, and older volcanics & sediments of Peninsular terranes		Paleozoic Dillinger & Mystic terranes & Cretaceous flysch deposits		Paleozoic Dillinger & Mystic terranes, and Cretaceous flysch deposits	Northern portion intrudes Ruby, Innoko, Nixon Fork, Minchumina, Southern portion intrudes Dillinger, Tikchik Lake, Nyac, Kilbuck, Togiak, Goodnews.
Rock Types Reported	Tonalite, grano-diorite, quartz diorite	Tonalite, grano-diorite, quartz diorite	Qtz. monz. qtz. diorite, grano-diorite, composite plutons	Quartz monz., granite	Quartz monzonite, granite	Plutons: Monzonite, Monzodiorite, qtz. monzodiorite, qtz. monzonite, granodiorite, granite, minor gabbro. Volcanics: Rhyolite, dacite, andesite, minor basalt.
SiO_2 (wt%) contents reported	70–72	54–70	~58–68	66–77	~62–78	52–78
References	Reed & Lanphere, 1969	Reed & Lanphere, 1974	Reed & Lanphere, 1973	Reed & Lanphere, 1973	Reed & Lanphere, 1973	Moll–Stalcup, in press.

Alaska Range-Talkeetna Mountains (AkR-TM) belt:

There were two broadly defined episodes of magmatic activity in the AkR-TM belt; a Late Cretaceous to early Tertiary episode, and a younger middle Tertiary episode (Reed and Lanphere, 1969 and 1973). The older plutons form the bulk of the larger batholiths, while the younger episode resulted in the formation of isolated plutons. Associated volcanic rocks of both age ranges, including mafic and felsic flows, tuffs and tuff breccias, are scattered throughout the belt (Reed and Elliott, 1970).

During the Late Cretaceous - early Tertiary episode (83 - 58 m.y.), several sequences of granitoids were emplaced (Figure 61). The Knutson Bay intrusive, at the northeast end of Iliamna Lake, is the oldest known, with coexisting hornblende-biotite ages of 83.4 and 80.7 m.y. respectively (Reed and Lanphere, 1969). Between 74 and 55 m.y. ago, the granitoids of the Summit Lake group intruded the northwest margin of the Jurassic Aleutian Range-Talkeetna Mountains belt. The other rocks of this age range can be subdivided into two groups, one ranging in age from 67 to 62 m.y., and the other from 60 to 55 m.y. (Reed and Lanphere, 1973).

Plutonic rocks of Late Cretaceous - early Tertiary age intrude diverse tectonostratigraphic terranes. The Knutson Bay and Summit Lake rocks intrude the Jurassic plutonic and older volcanic and sedimentary rocks of the Peninsular terrane (part of the Talkeetna superterrane). The other two age subgroups intrude the late Jurassic to early Cretaceous flysch deposits and the Paleozoic rocks of the Dillinger and Mystic terranes.

The map patterns of the Late Cretaceous - early Tertiary plutons tend to be elongate, with a north-south trend, contrary to the prevailing NE-SW structural fabric of southwest and central Alaska. Chill margins are present; contacts with country rock tend to be sharp and discordant (Reed and Lanphere, 1973).

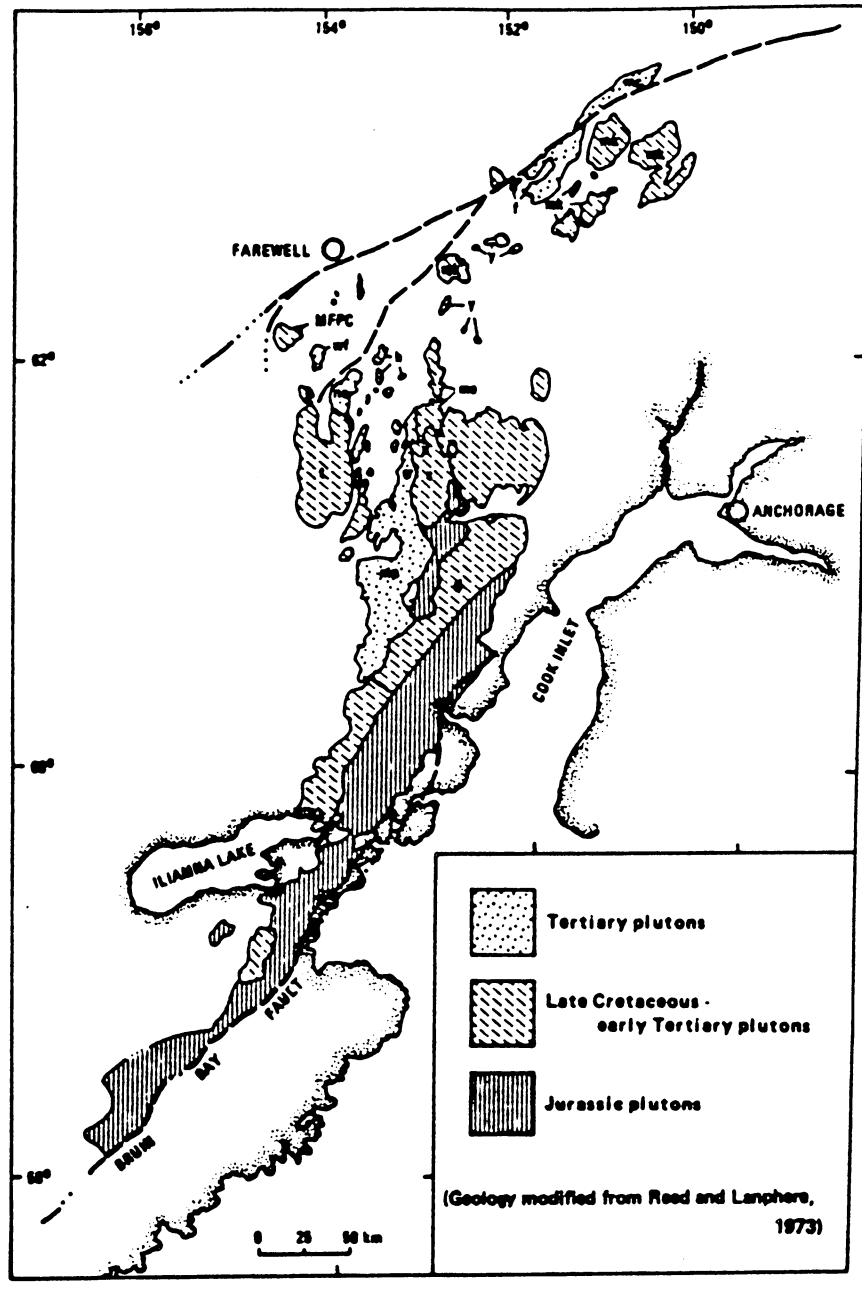

Figure 61. **Map of igneous rocks of Alaska Range-Talkeetna Mtn. belt:** (Modified from Reed and Lanphere, 1973). Igneous bodies mentioned in text are labelled: wf = Windy Fork pluton, mc = McGonagall batholith, f = Mt.Foraker pluton, mk = McKinley sequence, y = Yentna sequence, h = Hartman sequence, t = Tired Pup batholith, ne = Northease Prong of Tired Pup batholith, me = Mt.Estelle pluton, jl = Jimmy Lake pluton, c = Crystal Creek sequence, sr = Styx River pluton, mp = Merrill Pass sequence, sl = Summit Lake sequence.

Compositionally, the granitoids of the Late Cretaceous to early Tertiary group show a fair amount of diversity based on reconnaissance sampling and mapping (Reed and Elliott, 1970; Reed and Lanphere, 1969 and 1970). The Summit Lake and Knutson Bay rocks range from tonalite to granodiorite, with some granite. Major oxide analyses show these rocks to be generally lower in K_2O than other granitoids of this general age (Reed and Lanphere, 1974). They are generally most similar to the Jurassic Aleutian Range-Talkeetna Mountains belt granitoids, and are probably also a part of the allochthonous Talkeetna superterrane.

Of the two younger groups of Late Cretaceous - early Tertiary rocks, the older (67-62 m.y.) plutons tend in a very general way to be more mafic quartz diorites and granodiorites, compared to quartz monzonites and granites of the 60-55 m.y. group (Reed and Lanphere, 1973). The older group includes the granodiorite of Mt. Estelle, and the stocks of the Hartman sequence (Reed and Lanphere, 1973). The Yentna sequence, approximately 65 m.y. old, includes a group of composite plutons with a range of lithologies from peridotite to granite (Reed and Nelson, 1980). Quartz syenite is reported from the Upper Yentna pluton, and some of the ultramafic rocks of the group contain alkali feldspar (Reed and Nelson, 1980).

The younger age group includes the biotite granite of the Tired Pup batholith, the quartz monzonite and granite of the Crystal Creek sequence, and the peraluminous McKinley sequence. A large group of as yet unassigned plutons north of Chakachamna Lake may be included in this age group (Reed and Lanphere, 1973). The MFPC falls within this 60 - 55 m.y. age group, though it is lithologically distinct in its alkaline tendencies from the bulk of coeval AkR-TM magmatism. There is a temporal break in magmatism between 55 and 40 m.y..

The youngest episode of AkR-TM belt plutonism occurred between 40 and 26 m.y. ago. The greatest volume of these middle Tertiary granitoids is along a north-south

trend south of Farewell. They include the Merrill Pass sequence granites and quartz monzonites, which range from 33.7 to 40.8 m.y. (Reed and Lanphere, 1973). The rocks in the northern part of the Merrill Pass sequence are somewhat younger (33.7 - 36.7 m.y.) than those in the southern part (37.6 - 40.8 m.y.), and differ from the more southern rocks of the sequence in their scarcity of hornblende and slightly higher K_2O content (Reed and Lanphere, 1973).

Along roughly the same north-south trend with the Merrill Pass sequence are several other bodies of middle Tertiary granitoids. These include the Styx River biotite granite, the Northeast Prong of the Tired Pup batholith, the Jimmy Lake biotite granite stock, and the Windy Fork pluton (Reed and Elliott, 1970). The Northeast Prong of the Tired Pup batholith is a hornblende-biotite granite which is megascopically very similar to the Tired Pup itself (Reed and Miller, 1980). The Windy Fork pluton is a peralkaline granite located about 10 km southeast of MFPC. Its mineralogy is similar to the peralkaline granite of the MFPC, and consists of perthitic alkali feldspar (40-60%), quartz (25-45%), sodic amphibole (15-10%), with minor plagioclase, biotite, and opaques, zircon, apatite, fluorite, and carbonate (Gilbert and Solie, 1983). K-Ar dating yields ages of the Windy Fork pluton of 30.1 $\pm$0.9 m.y. (on biotite separate), 29.0 $\pm$0.9 m.y. (on amphibole separate) (Reed and Lanphere, 1972), and 23.5 $\pm$0.7 m.y. (on aegirine-augite separate from a dike associated with the pluton) (Gilbert et al., 1989).

The Middle Tertiary Foraker and McGonagall biotite hornblende granodiorites occur to the northeast along the Denali fault zone (Reed and Miller, 1980). In the southwest part of the Alaska-Aleutian Range batholith, straddling the Bruin Bay fault, is a group of middle Tertiary quartz diorite and granodiorite intrusions. These latter rocks yield two age ranges, one from 26 to 28 m.y., the other about 36 m.y., with no apparent lithological differences between the two magmatic pulses (Reed and Lanphere, 1973).

Middle Tertiary volcanic complexes and breccia pipes of intermediate composition are present in the central part of the Alaska Range, between the Tired Pup batholith and Farewell. Samples from three of the volcanic centers plot on a calc-alkaline trend based on major element chemistry, and include compositions ranging from rhyolite to basalt. K-Ar ages from the Windy Fork volcanic complex and the Sheep Creek volcanic complex range from 49.0 to 37.2 m.y. (Solie et al., 1982).

The AkR-TM belt is a direct, albeit complex, magmatic response to the collisional tectonic history of the southern margin of Alaska. Differing rates and angles of subduction, accretion of 'exotic' terranes, probable movement of trench zones, lateral strike-slip movement, and varying amounts, compositions and temperatures of subducted rocks all contribute to the complexity of regional magmatism. Compositionally, most of the AkR-TM belt igneous rocks are calc-alkaline on the basis of the Peacock diagram, with low TiO_2, moderate K_2O, and a lack of Fe-enrichment typical of orogenic regions (Moll-Stalcup, in press). The mid-Tertiary rocks are thought to be the result of a crustal melting event due to high heat flow in a post-magmatic arc and/or post-accretion setting (Hudson, in press).

Kuskokwim Mountains (KM) belt:

The main magmatic pulse in the KM belt occurred between 60 and 72 m.y., simultaneously with the older late Cretaceous - Early Tertiary magmatism of the AkR-TM belt. Volcanic and plutonic rocks of the KM belt include moderate-K alkali-calcic to calc-alkalic to shoshonitic suites. Volcanic rocks range in composition from minor basalt to abundant andesite and rhyolite. Most of the intrusions are pyroxene-hornblende monzonite, monzodiorite, quartz monzonite, granodiorite, and biotite-hornblende granite with minor pyroxene syenite (Moll-Stalcup, in press).

Volcano-plutonic suites in the Innoko area of the KM belt (Iditarod and Ophir quadrangles) are commonly zoned from alkali gabbro to monzodiorite to quartz syenite and monzonite. The Peacock index for these suites defines them as alkali-calcic. Also present are peraluminous garnetiferous rhyolites (Bundtzen and Swanson, 1984 and in press).

The overall more alkalic trends of the KM belt compared to the coeval AkR-TM belt rocks may be attributed to 1) development of a back-arc extensional regime; 2) fault-controlled magmatic emplacement within a transitional tectonic setting caused by differential movement along Farewell-Denali, Nixon-Iditarod, and Tintina-Kaltag fault systems (Bundtzen and Swanson, in press); 3) increasing depth to a shallowly dipping subducting slab within a wide (400-900 km) arc setting, with increasing degrees of interaction with old enriched crust or mantle (Moll-Stalcup, in press; Bergman and Doherty, 1986; Smith et al., 1986). It has also been suggested that the KM belt could be a separate arc associated with a subduction zone along which the Talkeetna superterrane was accreted (Wallace and Engebretson, 1984). Due to the temporal and present-day spatial proximity, and the greater compositional similarities of the MFPC to the KM belt, it is possible that the MFPC could be better linked to that belt than to the AkR-TM belt. Therefore, each of the above possibilities will be considered. However, if large-scale offset on the Denali fault zone occurred post-MFPC-emplacement, then the spatial relationship argues against an identity of the MFPC with the rocks of the KM belt.

Although the heightened alkalinity of the KM belt and its inland position relative to the present-day trench are suggestive of back-arc magmatism, the timing is not conducive to such an interpretation. Development of back-arc magmatism is late in the evolution of collision zones (e.g., Brown et al., 1984); simultaneous late Cretaceous - Early Tertiary activity occurs throughout the AkR-TM and KM belts, with a spatial as well as temporal overlap of calc-alkaline and alkali-calcic magmatism. Temporally it

would be easier to attribute the mid-Tertiary intrusions to back arc activity. However, this interpretaion does not hold spatially, as there is no mid-Tertiary activity in the more inland KM belt. If the trench migrated seaward, then the KM belt should be more typical of a near-trench calc-alkaline arc, not a back-arc.

A regional tensional environment, created by differential movement along parallel faults seems plausible, especially if the greatest offset on the Denali fault zone was late Cretaceous - Early Tertiary as proposed earlier. Such an environment could allow for mantle upwelling and crustal heating, with emplacement along deep-seated structures. Indeed, it is widely observed that emplacement of alkaline complexes is related to changes in the stress field along strike-slip faults (Black et al., 1985). Emplacement of the late Cretaceous - Early Tertiary igneous rocks does coincide with the proposed timing of greatest movement on the strike-slip faults. The geochemical interpretation of the Innoko suite of KM rocks as being alkalic and bimodal (Bundtzen and Swanson,in press) has been disputed on the basis of classifying the rocks as shoshonitic instead of alkalic, and recalculating major oxide chemistry on an anhydrous basis, such that the mafic rocks become intermediate and thus not part of bimodal suites (Moll-Stalcup,in press). The ambiguity of the geochemistry cannot at this point rule out the second model, and thus it remains a plausible hypothesis. This model encompasses the MFPC in terms of the complex's proximity to the intersection of the Denali and Big River faults, and its connection with a brittle extensional crustal break associated with the east-west trending dike swarm.

Alternatively, the KM belt rocks can be considered shoshonitic in composition (Moll-Stalcup,in press). Shoshonites are characterized by high Al_2O_3, Fe_2O_3/FeO, total alkalis, K_2O and LILEs (P, Rb, Sr, Ba, Pb, LREE), low TiO_2 , and low silica saturation (Morison, 1980). The tectonic implication is of younger rocks which occur above a deeper Benioff zone within an evolved orogenic setting (Morrison, 1980). As pointed

out above, there is no systematic temporal and spatial progression of magmatism northward; the KM belt is contemporaneous with much of the AkR-TM belt magmatism. Thus, this model seems somewhat difficult, though it may be tenable considering the effects of crustal contamination, and the complexities of possible trench migration (Csejtey et al., 1982; Smith et al., 1986).

In summary then, KM magmatism could be the result of either 1) magma generation in a structurally controlled continental trans-tensional regime or 2) inboard magmatism of a wide arc related to a shallowly dipping subducting slab. However, the MFPC could only be a product of the first model. It does not geochemically fit the characteristics of arc magmatism (i.e., it is not shoshonitic or calc-alkaline). Therefore, either the first model is correct, or the MFPC is not related to the KM belt (or the AkR-TM belt).

The presence of the Windy Fork peralkaline granite 10 km southeast of MFPC, compositionally very similar to the peralkaline granite of MFPC but about 30 m.y. younger, suggests that similar melting events, presumably from a similar source, occurred at distinctly different times. This implies that perhaps the source has a more overriding influence on magmatism that the specific magmatic setting. Indeed, Arth (in press) found, based on a compilation of initial strontium ratio (SIR) values from all Alaska, that the nature of the deep continental crust can be inferred from its magmatism. He groups the SIR data into three groups, Cratonia, Detritia and Volcania, which form the map pattern of Figure 62. The occurrence of an SIR of 0.7123 from the MFPC puts the complex, and hence the Dillinger terrane, within the Cratonia of Arth's terminology (in press). This suggests that cratonic basement underlies the Dillinger, and provides a further link with the Cratonia terranes north of the Denali fault system. This contrasts distinctly from the oceanic and flyschoid terranes which predominate south of the fault zone which are intruded by the calc-alkaline rocks of the typical AkR-TM belt. Thus

it seems that, although magmatism is a direct result of tectonic events, it cannot be unequivocally used as a tectonic indicator. It may, however, be useful as an indicator of crustal and/or mantle composition, hence providing clues as to the genetic associations of the intruded terranes.

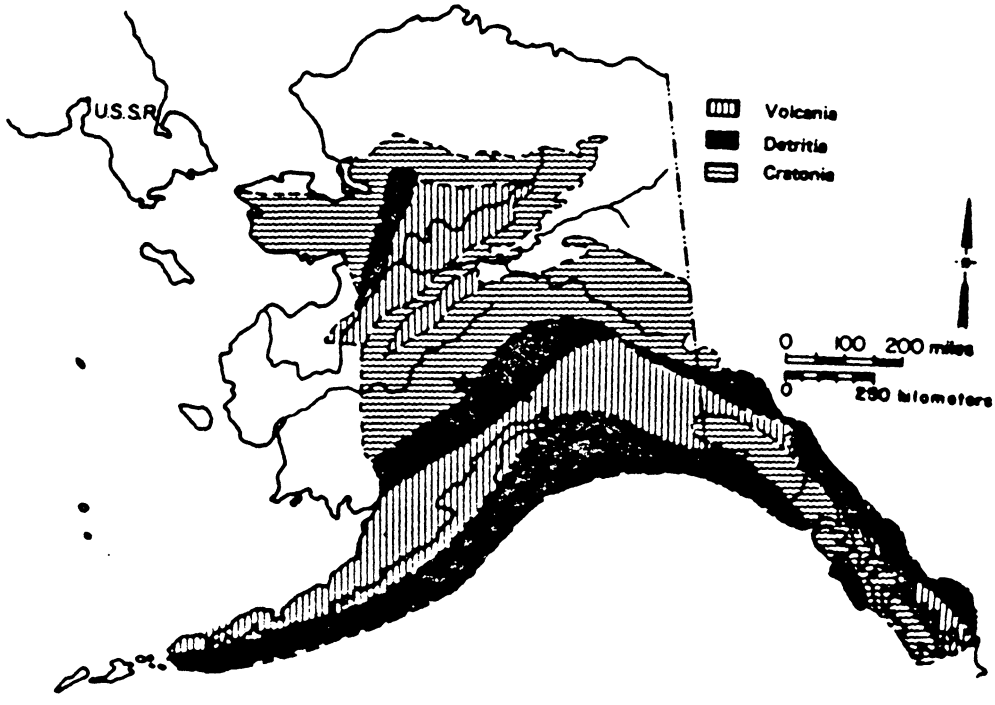

Figure 62. Map showing regional grouping on basis of SIR: Arth (in press) separates the groups into Cratonia (SIR = 0.708 - 0.725), Detritia (SIR = 0.705 - 0.708), and Volcania (SIR = 0.702 - 0.705).

References cited

Aleinikoff,J.N., Dusel-Bacon,Cynthia, Foster,H.L., and Nokleberg,W.J., 1987, Lead isotopic fingerprinting of tectono-stratigraphic terranes, east-central Alaska; Can.J.Earth Sciences, v.24, p.2089-2098.

Arana,V., Barberi,F. and Santacroce,R., 1975, Some data on the comendite type area of S. Pietro and S. Antioco Islands, Sardinia; Bull.Volc., v.38, n.3, p.725-736.

Arth,J.G., 1976, Behavior of trace elements during magmatic processes - a summary of theoretical models and their applications; U.S.G.S. J. of Research, v.4, n.1, p.41-47.

Arth,J.G., 1988, Isotopic composition of the igneous rocks of Alaska; DNAG Alaska volume, in press.

Bailey,D.K., 1974, Petrogenesis: melting in the deep crust; in Sorensen,H., ed., The alkaline rocks; John Wiley & Sons, London, p.436-442.

Baker,B.H., 1987, Outline of the petrology of the Kenya rift alkaline province; in Fitton,J.G. and Upton,B.G.J., eds., Alkaline igneous rocks; Geol.Soc.Special Pub. No 30, p.293-311.

Baker,P.E., Brosset,R., Gass,I.G. and Neary,C.R., 1973, Jebel al Abyad: a recent alkalic volcanic complex in western Saudi Arabia; Lithos, v.6, p.291-314.

Baker,P.E., Buckley,F. and Holland,J.G., 1974, Petrology and geochemistry of Easter Island; Contrib.Mineral.Petrol., v.44, p.85-100.

Barberi,F., Ferrara,G., Santacroce,R., Treuil,M. and Varet,J., 1975, A transitional basalt - pantellerite sequence of fractional crystallization, the Boina Centre (Afar Rift, Ethiopia); J.of Petrology, v.16, pt.1, p.22-56.

Barker,F., Wones,D.R., Sharp,W.N., and Desborough,G.A., 1975, The Pikes Peak batholith, Colorado Front Range, and a model for the origin of the gabbro-anorthosite-syenite-potassic granite suite; Precambrian Research, v.2, p.97-160.

Beikman,H.M., 1980, Geologic map of Alaska; U.S.Geological Survey, 1:2,500,000, 2sh.

Bence,A.E. and Albee,A.L., 1968, Empirical correction factors for the electron microanalysis of silicates and oxides; J.of Geology, v.76, p.382-403.

Bergman,S.C. and Doherty,D.J., 1986, Nature and origin of 50-75 Ma volcanism and plutonism in W. and S. Alaska; GSA Abstracts with Programs, v.18,n.6,p.539.

Bevier,M.L., Armstrong,R.L. and Souther,J.G., 1979, Miocene peralkaline volcanism in west-central British Columbia - its temporal and plate-tectonic setting; Geolgy, v.7, p.389-392.

Black,R., Lameyre,J., and Bonin,B., 1985, The structural setting of alkaline complexes; J.of African Earth Sciences, v.3, p.5-16.

Blaxland,A.B., van Breemen,Otto, Emeleus,C.H., and Anderson,J.G., 1978, Age and origin of the major syenite centers in the Gardar province of south Greenland: Rb-Sr studies; GSA Bull., v.89, p.231-244.

Blodgett,R.B., 1983, Paleobiogeographic implications of Devonian fossils from the Nixon Fork terrane, southwestern Alaska; GSA Abstracts with Programs, v.15,n.5,p.428.

Bonin,B., Grelou-Orsini,C. and Vialette,Y., 1978, Age, origin and evolution of the anorogenic complex of Evisa (Corsica): a K - Li - Rb - Sr study; Contrib.Mineral.Petrol., v.65, p.425-432.

Bowden,P. and Turner,D.C., 1974, Peralkaline and associated ring-complexes in the Nigeria-Niger Province, west Africa; in Sorensen,H., ed., The alkaline rocks; John Wiley & Sons, London, p.330-351.

Bowden,P., Black,R., Martin,R.F., Ike,E., Kinnaird,J.A., and Batchelor,R.A., 1987, Niger-Nigerian alkaline ring-complexes: a classic example of African Phanerozoic anorogenic mid-plate magmatism; in Fitton,J.G. and Upton,B.G.J., Alkaline igneous rocks; Geological Society Special Publication No.30, p.357-379.

Bowen,N.L. and Schairer,J.F., 1932, The system FeO - SiO_2; Am.J.Sci., 5th series, v.24, p.255-324.

Bowen,N.L. and Tuttle,O.F., 1950, The system $NaAlSi_3O_8$ - $KAlSi_3O_8$ - H_2O; J.of Geology, v.58, p.489-511.

Box,S.E., 1985, Early Cretaceous orogenic belt in northwestern Alaska: internal organization, lateral extent, and tectonic interpretation; in Howell,D.G.,ed., Tectonostratigraphic terranes of the circum-Pacific region; Circum-Pacific Council for Energy and Mineral Resources Earth Science Series No.1, p.137-145.

Brooks,C.K. and Gill,R.C.O., 1982, Compositional variation in the pyroxenes and amphiboles of the Kangerdlugssuaq intrusion, east Greenland: further evidence for the crustal contamination of syenite magma; Min.Mag., v.45, p.1-9.

Brown,P.E., and Becker,S.M., 1986, Fractionation, hybridisation and magma-mixing in the Kialineq centre, East Greenland; Contrib.Min.Pet., v.92, p.57-70.

Brown,G.C., Thorpe,R.S., and Webb,P.C., 1984, The geochemical characteristics of granitoids in contrasting arcs and comments on magma sources; J.geol.Soc.London, v.141, p.413-426.

Buddington,A.F., 1959, Granite emplacement with special reference to North America; GSA Bull., v.70, p.671-747.

Bundtzen,T.K., 1982, Geology and mineral resources of McGrath - Iditarod and Farewell areas, Alaska; Alaska Geological Society Symposium Program and Abstracts, p.44.

Bundtzen,T.K. and Gilbert,W.G., 1983, Outline of the geology and mineral resources of upper Kuskokwim region, Alaska; in G.Mull and K.Reed, eds., Western Alaska geology and resource potential; J. of the Alaska Geological Society, v.3, p.101-117.

Bundtzen,T.K. and Swanson,S.E., 1984, Geology and petrology of igneous rocks in Innoko River area, western Alaska; GSA Abstracts with Programs, v.16.n.5,p.273.

Bundtzen,T.K. and Swanson,S.E., in press, Geology and geochemistry of the Innoko igneous belt, western Alaska; manuscript submitted to GSA Bulletin.

Cerny,P. and Burt,D.M., 1984, Paragenesis, crystallochemical characteristics, and geochemical evolution of micas in granite pegmatites; MSA Rev. in Min., v.13, p.257-298.

Chayes,F., 1963, Relative abundance of intermediate members of the oceanic basalt-trachyte association; J.Geophys.Res., v.68, n.5, p.1519- 1534.

Churkin,Michael,Jr., Wallace,W.K., Bundtzen,T.K., and Gilbert,W.G., 1984, Nixon Fork - Dillinger terranes: a dismembered Paleozoic craton margin in Alaska displaced from Yukon Territory; GSA Abstracts with Programs, v.16, n.5, p.275.

Coe,R.S., Globerman,B.R., Plumley,P.W., and Thrupp,G.A., 1985, Paleomagnetic results from Alaska and their tectonic implications; in Howell,D.G.,ed., Tectonostratigraphic terranes of the circum-Pacific region; Circum-Pacific Council for Energy and Mineral Resources Earth Science Series No.1, p.85-108.

Collerson,K.D., 1982, Geochemistry and Rb-Sr geochronology of associated Proterozoic peralkaline and subalkaline anorogenic granites from Labrador; Contrib.Min.Pet., v.81, p.126-147.

Collins,W.J., Beams,S.D., White,A.J.R., and Chappell,B.W., 1982, Nature and origin of A-type granites with particular reference to southeastern Australia; Contrib.Mineral.Petrol., v.80, p.189-200.

Coney,P.J., Jones,D.L., and Monger,J.W.H., 1980, Cordilleran suspect terranes; Nature, v.288, p.329-333.

Coombs,D.S., 1963, Trends and affinities of basaltic magmas and pyroxenes as illustrated on the diopside-olivine-silica diagram; Min.Soc.Am.Spec. Paper 1, p.227-250.

Cox,K.G., Bell,J.D., and Pankhurst,R.J., 1979, The interpretation of igneous rocks; George Allen and Unwin, London, 450p.

Cox,K.G., Gass,I.G. and Mallick,D.I.J., 1970, The peralkaline volcanic suite of Aden and Little Aden, South Arabia; J.of Petrology, v.11, pt.3, p.433-461.

Csejtey,Bela Jr., Cox,D.P., Evarts,R.C., Stricker,G.D., and Foster,H.L., 1982, The Cenozoic Denali fault system and the Cretaceous accretionary development of southern Alaska; J.of Geophys.Res., v.87, n.B5, p.3741- 3754.

Currie,K.L., Eby,G.N. and Gittons,John, 1986, The petrology of the Mont Saint Hilaire complex, southern Quebec: an alkaline gabbro - peralkaline syenite association; Lithos, v.19, p.65-81.

Deer,W.A., Howie,R.A., and Zussman,J., 1976, An introduction to the rock-forming minerals; Longman, London, 528p.

Dickey,D.B., 1984, Cenozoic non-marine sedimentary rocks of the Farewell fault zone, McGrath quadrangle, Alaska; Sed.Geol., v. 38, p.443-463.

Dingwell,D.B., Scarfe,C.M., and Cronin,D.J., 1985, The effect of fluorine on viscosities in the system Na_2O-Al_2O_3-SiO_2: implications for phonolites, trachytes and rhyolites; Am.Min., v.70, p.80-87.

Dodson,M.H., 1973, Closure temperature in cooling geochronological and petrological systems; Contrib.Mineral.Petrol., v.40, 259-274.

Engel,A.E.J., Engel,C.G., and Havens,R.G., 1965, Chemical characteristics of oceanic basalts and the upper mantle; GSA Bull., v.76, p.719-734.

Ernst,W.G., 1962, Synthesis, stability relations, and occurrence of riebeckite and riebeckite-arfvedsonite solid solutions; J.of Geology, v.70, p.689-736.

Faure,Gunter, 1977, Principles of isotope geology; John Wiley & Sons, New York, 464p.

Faure,Gunter and Powell,J.L., 1972, Strontium isotope geology; Springer- Verlag, Berlin and Heidelberg, 188p.

Ferguson,A.K., 1978, The crystallization of pyroxenes and amphiboles in some alkaline rocks and the presence of a pyroxene compositional gap; Contrib.Mineral.Petrol., v.67, p.11-15.

Fleischer,Michael, 1987, Glossary of mineral species, 5th edition; The Mineralogical Record, Inc., Tucson, 234p.

Foland,K.A. and Friedman,Irving, 1977, Application of Sr and O isotope relations to the petrogenesis of the alkaline rocks of the Red Hill complex, New Hampshire, USA; Contrib.Mineral.Petrol., v.65, p.213-225.

Forbes,R.B., Turner,D.L., Stout,J.H., and Smith,T.E., 1973, Cenozoic offset along the Denali fault, Alaska; Transactions of the Am. Geophys. Union, v.54, p.495.

Fuhrman,M.L. and Lindsley,D.H., 1988, Ternary-feldspar modeling and thermometry; Am.Min., v.73, p.201-215.

Gemuts,I., Puchner,C.C., and Stefel,C.I., 1983, Regional geology and tectonic history of western Alaska; J.of Alaska Geol.Soc., v.3, p.67-86.

Gibson,I.L., 1975, A review of the geology, petrology and geochemistry of the volcano Fantale; Bull.Volc., v.38, n.3, p.791-802.

Gilbert,W.G., 1975, Outline of tectonic history of west-central Alaska; GSA Abstracts with Programs, v.7, p.320.

Gilbert,W.G. and Bundtzen,T.K., 1983, Paleozoic stratigraphy of Farewell area, southwest Alaska Range, Alaska; Alaska Geol. Society Symposium Program and Abstracts, p.10-11.

Gilbert,W.G. and Bundtzen,T.K., 1984, Stratigraphic relationship between Dillinger and Mystic terranes, western Alaska Range, Alaska; GSA Abstracts with Programs, v.16, n.5, p.286.

Gilbert,W.G. and Solie,D.N., 1983, Preliminary bedrock geology of McGrath A-3 quadrangle, Alaska; ADGGS Report of Investigations 83-7, 1pl.

Gilbert,W.G., Solie,D.N., and Dickey,D.B., 1982, Preliminary bedrock geology of the McGrath B-3 quadrangle, Alaska; ADGGS Open-file Report 148,1pl.

Gilbert,W.G., Solie,D.N., and Kline,J.T., 1989, Geology of the McGrath A-3 quadrangle, Alaska; ADGGS Professional Report (in press).

Gill,J.B., 1981, Orogenic andesites and plate tectonics; Springer- Verlag, New York, 390p.

Giret,Andre, Bonin,Bernard and Leger, J.-M., 1980, Amphibole compositional trends in oversaturated and undersaturated alkaline plutonic ring-complexes; Can.Min., v.18, p.481-495.

Graham,C.M. and Navrotsky,Alexandra, 1986, Thermochemistry of the tremolite-edenite amphiboles using fluorine analogues, and applications to amphibole-plagioclase-quartz equilibria; Contrib.Mineral.Petrol., v.93, p.18-32.

Gromet,L.P. and Silver,L.T., 1983, Rare earth element distributions among minerals in a granodiorite and their petrogenetic implications; Geochim. et Cosmochim. Acta, v.47, p.925-939.

Hammarstrom,J.M. and Zen,E-an, 1986, Aluminum in hornblende: an empirical geobarometer; Am. Min., v.71, p.1297-1313.

Hedge,C.E., 1970, Whole-rock Rb-Sr age of the Pikes Peak batholith, Colorado; U.S.Geological Survey Prof.Paper 700-B, p.B86-B89.

Herreid,Gordon, 1968, Geological and geochemical investigations southwest of Farewell, Alaska; Alaska Division of Geological and Geophysical Surveys Geologic Report 26, 24p.

Hollister,L.S., Grissom,G.C., Peters,E.K., Stowell,H.H., and Gisson,V.B., 1987, Confirmation of the empirical correlation of Al in hornblende with pressure of solidification of calc-alkaline plutons; Am. Min., v.71, p.231.

Hudson,Travis, 1979, Mesozoic plutonic belts of southern Alaska; Geology, v.7, p.230-234.

Hudson,T.L., in press, Crustal melting events in Alaska; DNAG Alaska volume.

Irvine,T.N. and Baragar,W.R.A., 1971, A guide to the chemical classification of the common volcanic rocks; Canadian J.of Earth Science, v.8, p.523-548.

Jacobson,R.R.E., Macleod,W.N., and Black,R., 1958, Ring-complexes in the younger granite province of northern Nigeria; Mem.Geol.Soc.London, v.1, 72p.

Jones,D.L., Silberling,N.J., Berg,H.C., and Plafker,G., 1981, Tectonostratigraphic terrane map of Alaska; USGS open-file report 81-792, 20pp.

Jones,D.L., Silberling,N.J., Gilbert,Wyatt, and Coney,Peter, 1982, Character, distribution, and tectonic significance of accretionary terranes in the central Alaska Range; J.Geophys.Res., v.87, p.3709-3717.

Kinnaird,J.A., Bowden,P., Ixer,R.A., and Odling,N.W.A., 1985, Mineralogy, geochemistry and mineralization of the Ririwai complex, northern Nigeria; J.of African Earth Sci., v.3, p.185-222.

Kline,J.T. and Bundtzen,T.K., 1986, Two glacial records from west-central Alaska; in Hamilton,T.D., Reed,K.M. and Thorson,R.M.,ed., Glaciation in Alaska - the geologic record, p.123-150.

Koritnig,S., 1978, Fluorine; in Wedepohl,K.H., ed., Handbook of geochemistry, v.II/1, Springer-Verlag, Berlin, p.9-B-1 - 9-O-4.

Kozinski,Jane, 1986, The Nutzotin Mountains sequence, Alaska and the Deazadeash Group, Yukon Teritory as offset markers for the Denali fault - new evidence from Alaska; GSA Abstracts with Programs, v.18, n.2, p.125.

LaBas,M.J., 1962, The role of aluminium in igneous rocks; Am.J.Sci., v.258, p.548-554.

Lanphere,M.A., 1978, Displacement history of the Denali fault system, Alaska and Canada; Can.J.of Earth Sciences, v.15, p.817-822.

Larsen,L.M., 1976, Clinopyroxenes and coexisting mafic minerals from the alkaline Ilimaussaq intrusion, South Greenland; J.of Petrology, v.17, pt.2, p.258-290.

Leake,B.E., 1971, On aluminous and edenitic hornblendes; Min.Mag., v.38, n.296, p.389-407.

Leake,B.E., 1978, Nomenclature of amphiboles; Canadian Mineralogist, v.16, p.501-520.

LeMaitre,R.W., 1976, The chemical variability of some common igneous rocks; J.of Petrology, v.17, p.589-637.

Lindsley,D.H. and Andersen,D.J., 1983, A two-pyroxene thermometer; J.Geophys.Res., v.88, supplement, p.A887-A906.

Lindsley,D.H. and Munoz,J.L., 1969, Subsolidus relations along the join hedenbergite - ferrosilite; Am.J.Sci., v.260A, p.255-324.

Loiselle,M.C., 1978, Geochemistry and petrogenesis of the Belknap Mountains Complex and Pliny Range, White Mountain series, New Hampshire; unpublished PhD. dissertation, M.I.T.

Loiselle,M.C. and Wones,D.R., 1979, Characteristics and origin of anorogenic granites; GSA Abstracts with Programs, v.11, p.468.

Luth,W.C., Jahns,R.H., and Tuttle,O.F., 1964, The granite system at pressures of 4 to 10 kilobars; J.of Geophysical Research, v.69, n.4, p.759-773.

Macdonald,G.A. and Katsura,T., 1964, Chemical composition of Hawaiian lavas; J.of Petrology, v.5, p.82-133.

Macdonald,R., 1974, The role of fractional crystallization in the formation of the alkaline rocks; in Sorensen,H., ed., The alkaline rocks; John Wiley & Sons, London, p.442-459.

Macdonald,R., 1975(a), Nomenclature and petrochemistry of the peralkaline oversaturated extrusive rocks; Bull.Volc., v.38, n.3, p.498-516.

Macdonald,R., 1975(b), Tectonic settings and magma associations; Bull. Volc., v.38, n.3, p.575-593.

Macdonald,R., 1987, Quaternary peralkaline silicic rocks and caldera volcanoes of Kenya; in Fitton,J.G. and Upton,B.G.J., eds., Alkaline igneous rocks; Geol.Society Special Paper No 30, p.313-333.

Mahood,G.A., 1984, Pyroclastic rocks and calderas associated with strongly peralkaline magmatism; J.Geophys.Res., v.89, n.B10, p.8540- 8552.

Manning,D.A.C., 1981, The effect of fluorine on liquidus phase relationships in the system Qz-Ab-Or with excess water at 1kb; Contrib.Mineral.Petrol., v.76, p.206-215.

Manning,D.A.C. and Henderson,C.M.B., 1981, The effect of the addition of fluorine on liquidus phase relationships in the system Qz - Ab - Or with excess water at 1 kb; NERC Progress in Experimental Petrology, v.5, p.16-23.

Manning,D.A.C. and Pichavant,M., 1983, The role of fluorine and boron in the generation of granitic melts; in Migmatites, melting and metamorphism, M.P.Atherton and C.D.Gribble,eds., Shiva Press, p.94- 109.

Mariano,A.N., 1978(a), The application of cathodoluminescence for carbonatite exploration and characterization; in Proc. of the First International Symposium on Carbonatites, June 20-27,1976, Pocos de Caldas, Brasil, p.39-57.

Mariano,A.N., 1978(b), Cathodoluminescence of feldspars from granite plutons of southeastern New England; GSA Abstracts with Programs, v.10, n.2, p.74.

Martin,R.F. and Bonin,B., 1976, Water and magma genesis: the association hypersolvus granite - subsolvus granite; Can.Min., v.14, p.228-237.

Martin,R.F. and Bowden,Peter, 1981, Peraluminous granites produced by rock - fluid interaction in the Ririwai nonorogenic ring-complex, Nigeria: mineralogic evidence; Can.Min., v.19, p.65-82.

Mitchell,R.H. and Platt,R.G., 1978, Mafic mineralogy of ferroaugite syenite from the Coldwell alkaline complex, Ontario, Canada; J.of Petrology, v.19, pt.4, p.627-651.

Moll-Stalcup,Elizabeth, in press, Cenozoic magmatism in mainland Alaska; DNAG Alaska volume.

Morrison,G.W., 1980, Characteristics and tectonic setting of the shoshonite rock association; Lithos, v.13, p.97-108.

Morse,S.A., 1980, Basalts and phase diagrams; Springer-Verlag, New York, 493p.

Naney,M.T., 1983, Phase equilibria of rock-forming ferromagnesian silicates in granitic systems; Am.J.Sci., v.283, p.993-1033.

Nelson,D.O., Nelson,K.L., Reeves,K.D., and Mattison,G.D., 1987, Geochemistry of Tertiary alkaline rocks of the eastern Trans-Pecos Magmatic Province, Texas; Contrib.Mineral.Petrol., v.97, p.72-92.

Neumann,E.-R., 1976, Compositional relations among pyroxenes, amphiboles and other mafic phases in the Oslo region plutonic rocks; Lithos, v.9, p.85-109.

Nickel,E., 1978, The present status of cathode luminescence as a tool in sedimentology; Minerals Sci.Engng., v.10, n.2, p.73-100.

Noble,D.C. and Parker,D.F., 1975, Peralkaline silicic volcanic rocks of the western United States; Bull.Volc., v.38, n.3, p.803-827.

Nokleberg,W.J., Plafker,George, and Roeske,S.M., 1986, Structural analysis and accretionary tectonics of Cretaceous and Early Tertiary flysch sequences juxtaposed along the Contact fault, eastern Chugach Mountains, Alaska; GSA Abstracts with Programs, v.18, n.2, p.164.

Norrish,K. and Chappell,B.W., 1977, X-ray fluorescence spectrometry; in Zussman,J., ed., Physical methods in determinative mineralogy, 2nd ed.; Academic Press, New York, p.201-273.

Norrish,K. and Hutton,J.T., 1969, An accurate X-ray spectrographic method for the analysis of a wide range of geological samples; Geochim. et Cosmochim. Acta, v.33, p.431-453.

Parker,D.F., 1983, Origin of the trachyte - quartz trachyte - peralkaline rhyolite suite of the Oligocene Paisano volcano, Trans-Pecos Texas; GSA Bull., v.94, p.614-629.

Patton,W.W. and Gilbert,W.G., 1982, Tectonics of west-central Alaska and the adjoining Bering Sea region; Alaska Geol.Society Symposium Program and Abstracts, p.35.

Plafker,George, Naeser,C.W., Zimmerman,R.A., Radford,Geoff, Kitson,Bill, and Hudson,Travis, 1984, Cenozoic uplift history of the Mount McKinley area, based on fission-track dating; GSA Abstracts with Programs, v.16, n.5, p.329.

Platt,R.G. and Woolley,A.R., 1986, The mafic mineralogy of the peralkaline syenites and granites of the Mulanje complex, Malawi; Min.Mag., v.50, p.85-99.

Powell,Marjorie, and Powell,Roger, 1974, An olivine-clinopyroxene geothermometer; Contrib.Mineral.Petrol., v.48, p.249-263.

Reed,B.L. and Elliott,R.L., 1968, Results of stream sediment sampling in parts of the southern Alaska Range: U.S.Geological Survey Open-File Report 310, 42p.

Reed,B.L. and Elliott,R.L., 1970, Reconnaissance geologic map, analyses of bedrock and stream sediment samples, and an aeromagnetic map of parts of the southern Alaska Range; U.S.Geological Survey Open-File Report 413.

Reed,B.L. and Lanphere,M.A., 1969, Age and chemistry of Mesozoic and Tertiary plutonic rocks in south-central Alaska; GSA Bulletin, v.80, p.23-44.

Reed,B.L. and Lanphere,M.A., 1970, Plutonic belts of central and southern Alaska Range and Alaska Peninsula; AAPG Bulletin, v.54, n.12, p.2502.

Reed,B.L. and Lanphere,M.A., 1972, Generalized geologic map of the Alaska-Aleutian Range batholith showing K-Ar ages of the plutonic rocks; U.S.Geological Survey Map MF-372.

Reed,B.L. and Lanphere,M.A., 1973, Alaska-Aleutian Range batholith: geochronology, chemistry, and relation to circum-Pacific plutonism; GSA Bulletin, v.84, p.2583-2610.

Reed,B.L. and Lanphere,M.A., 1974, Chemical variations across the Alaska-Aleutian Range batholith; J.of Research, U.S.Geological Survey, v.2, n.3, p.343-352.

Reed,B.L. and Miller,T.P., 1980, Uranium and thorium content of some Tertiary granitic rocks in the southern Alaska Range; U.S.Geological Survey open-file report 80-1052.

Reed,B.L. and Nelson,S.W., 1980, Geologic map of the Talkeetna quadrangle, Alaska; U.S.Geological Survey Map I-1174.

Robinson,Peter, 1982, The amphibole formula; in Veblen,D.R. and Ribbe, P.H., eds., Amphiboles: petrology and experimental phase relations; MSA Rev.in Min., v.9B, p.3-6.

Roeder,P.L. and Emslie,R.F., 1970, Olivine - liquid equilibrium; Contrib.Mineral.Petrol., v.29, p.275-289.

Rucklidge,J.C., 1971, Specifications of Fortran program SUPERRECAL; Department of Geology, University of Ontario.

Scofield,Nancy and Gilbert,M.C., 1982, Alkali amphiboles of the Wichita Mountains; Oklahoma Geol.Survey Guidebook 21, p.60-64.

Sheraton,J.W. and Black,L.P., 1988, Chemical evolution of granitic rocks in the East Antarctic Shield, with particular reference to post- orogenic granites; Lithos, v.21, p.37-52.

Simkin,Tom and Smith,J.V., 1970, Minor-element distribution in olivine; J.of Geology, v.78, p.304-325.

Smith,G.M., Graubard,C.M., and Keith,S.B., 1986, Pattern of Laramide magmatism and tectonics in southern Alaska: the effect of changing slab dip with increased convergence rate; GSA Abstracts with Programs, v.18, n.6, p.754.

Solberg,T.N. and Speer,J.A., 1982, QALL, a 16-element analytical scheme for efficient petrologic work on an automated ARL-SEMQ: application to mica reference samples; in Heinrich,K.F.J., ed., Microbeam Analysis; San Francisco Press, Inc., San Francisco, p.422-426.

Solie,D.M., 1983, The Middle Fork Plutonic Complex, McGrath A-3 quadrangle, southwest Alaska; Alaska Division of Geological and Geophysical Surveys Report of Investigations 83-16, 17p.

Solie,D.N, Bundtzen,T.K., and Gilbert,W.G., 1982, Upper Cretaceous - lower Tertiary volcanic rocks near Farewell, Alaska; AGU Pacific Northwest Meeting, Proceedings,33rd Alaska Science Conference, p.138.

Solie,D.N., and Su, Shu-Chun, 1987, An occurrence of Ba-rich micas from the Alaska Range; Am.Min., v.72, p.995-999.

Spencer,K.J., and Lindsley,D.H., 1981, A solution model for coexisting iron-titanium oxides; Am.Min., v.66, p.1189-1201.

Steiger,R.H. and Jaeger,E., 1977, Subcommission on geochronology: convention on the use of decay constants in geochronology and cosmochronology; Earth Planet.Sci.Letters, v.36, p.359-362.

Steiner,J.C., Jahns,R.H., and Luth,W.C., 1975, Crystallization of alkali feldspar and quartz in the haplogranite system $NaAlSi_3O_8$ - $KAlSi_3O_8$ - SiO_2 - H_2O at 4 kb; GSA Bull., v.86, p.83-93.

Stephenson,D., 1972, Alkali clinopyroxenes from nepheline syenites of the South Qoroq Centre, south Greenland; Lithos, v.5, p.187-201.

Stephenson,D. and Upton,B.G.J., 1982, Ferromagnesian silicates in a differentiated alkaline complex: Kungnat Fjeld, South Greenland; Min.Mag., v.46, p.283-300.

Stone,D.B. and Wallace,W.K., 1987, A geological framework of Alaska; Episodes, v.10, p.283-289.

Stormer,J.C. and Carmichael,I.S.E., 1971, Fluorine - hydroxyl exchange in apatite and biotite, a potential igneous geothermometer; Contrib.Mineral.Petrol., v.31, p.121-131.

Stormer,J.C.,Jr., and Nicholls,J., 1978, XLFRAC: a program for the interactive testing of magmatic differentiation models; Computers & Geosciences, v.4, p.143-159.

Stout,J.H. and Chase,C.G., 1980, Plate kinematics of the Denali fault system; Can.J.of Earth Sciences, v.17, p.1527-1537.

Streckeisen,A., 1976, To each plutonic rock it proper name; Earth Science Rev., v.12, p.1-33.

Strong,D.F. and Taylor,R.P., 1984, Magmatic-subsolidus and oxidation trends in composition of amphiboles from silica-saturated peralkaline igneous rocks; TMPM Tschermaks Min.Petr.Mitt., v.32, p.211-222.

Sutherland,D.S., 1975, Petrography and mineralogy of the peralkaline silicic rocks; Bull.Volc., v.38, n.3, p.517-547.

Taylor,R.P., Strong,D.F. and Fryer,B.J., 1981, Volatile control of contrasting trace element distributions in peralkaline granitic and volcanic rocks; Contrib.Min.Pet., v.77, p.267-271.

Thornton,C.P. and Tuttle,O.F., 1960, Chemistry of igneous rocks: I. differentiation index; Am.J.Sci., v.258, p.664-684.

Turner,D.C. and Bowden,P., 1979, The Ningi-Burra complex, Nigeria: dissected calderas and migrating magmatic centres; J.Geol.Soc.London, v.136, p.105-119.

Tuttle,O.F., and Bowen,N.L., 1958, Origin of granite in the light of experimental studies in the system $NaAlSi_3O_8$-$KAlSi_3O_8$-SiO_2-H_2O; GSA Mem.74, 154p.

Wallace,W.K. and Engebretson,D.C., 1984, Relationships between plate motions and late Cretaceous to Paleogene magmatism in southwestern Alaska; Tectonics, v.3, n.2, p.295-315.

Weaver,S.D., 1976/7, The Quaternary caldera volcano Emuruangogolak, Kenya Rift, and the petrology of a bimodal ferrobasalt - pantelleritic trachyte association; Bull.Volc., v.40, p.209-230.

Whalen,J.B., Currie,K.L., and Chappell,B.W., 1987, A-type granites: geochemical characteristics, discrimination and petrogenesis; Contrib.Min.Pet., v.95, p.407-419.

Whipple,E.R., 1974, A study of Wilson's determination of ferrous iron in silicates; Chem.Geol., v.14, p.223-238.

Wiebe,R.A., 1980, Commingling of contrasted magmas in the plutonic environment: examples from the Nain anorthositic complex; J.of Geology, v.88, p.197-209.

Williams,Howel, Turner,F.J., and Gilbert,C.M., 1982, Petrography: an introduction to the study of rocks in thin sections; W.H.Freeman and Co., San Francisco, 626p.

York,D., 1969, Least squares fitting of a straight line with correlated errors; Earth and Planet.Sci.Letters, v.5, p.320-324.

Appendix A. Physiographic setting and background information

The MFPC is located in southern Alaska, on the north-central flank of the Alaska Range. The headwaters of the Middle Fork of the Kuskokwim River originate in a glacier located within the plutonic complex. It is in the McGrath A-3 half-degree sheet. The nearest village is McGrath, about 115 km to the north. Accessibility to the complex is primarily by helicopter. The nearest fixed-wing airstrip, which is privately constructed and not reliably maintained, is about 12 km to the north, at a sheephunting camp on the Middle Fork.

The topography varies in elevation from about 1800 ft (about 550 m) at the western contact of the complex in the Big River drainage, to peaks over 6000 ft (about 1825 m). The highest peak is 6990 ft (2130 m). The MFPC is drained by several streams in glacially scoured valleys, with drift present along lower valley walls and bottoms. Above the glacial drift, bedrock exposure is good, obscured only by talus and ice. However, the rocks are often inaccessible due to extreme steepness. Of the approximately 125 km^2 which comprise the exposure of the complex, roughly 15 km^2 are covered by glacial ice. Vegetation occurs on the lower slopes and valley bottoms, and is restricted to alpine tundra and low brush. No trees are present. Wildlife observed in the MFPC includes caribou, Dall sheep, wolverine, an occasional brown bear, and abundant mosquitoes.

Climatic difficulties result in short field seasons. Snow does not melt until mid- to late June, and early snow flurries cover the high peaks by mid- to late August. Precipitation levels are high; weeks of fog and rain are not unusual. Stream levels fluctuate greatly due to the combined effects of melting glaciers and rainfall.

Mapping of the MFPC was initially undertaken by the author in 1982 as part of a mapping project by the Alaska Division of Geological and Geophysical Surveys. One goal of the project was to produce geologic maps of each of the McGrath quadrangles, at a scale of 1:63,360 (1″ = 1 mile). The only previous published work in the the MFPC was by Reed and Elliott, who reported the presence of the pluton from their regional reconnaissance mapping (Reed and Elliott, 1970). Field work for the present study entailed a total of 45 workable days in the area, spread over the course of four field seasons.

Appendix B. Petrographic and geochemical summary of samples

Representative sample suite

ADGGS suite of samples

	GABBROS						
Sample #	83DNS307	82DNS186	84DNS44a	82DNS196	84DNS34d	84DNS39a	84DNS39c
Mode %	59 olivine	45 olivine	38 plag	32 plag	52 plag	58 plag	63 plag
	15 plag	26 plag	36 olivine	22 cpx	21 cpx	24 cpx	18 cpx
	15 cpx	20 opx+cpx	12 biotite	20 biotite	13 biotite	13 biotite	9 kspar
	7 biotite	8 biotite	11 cpx	15 olivine	8 hb	3 ilm	4 ilm
	1 hb	1 opaque	1 opaque	7 opx	6 ilm	2 hb	2 olivine
	1 opaque	<1 hb	2 chlorite	2 hb	<1 olivine	1 kspar	2 biotite
	tr apatite			2 opaque	<1 opaque	<1 olivine	<1 zr/sph
				<1 apatite		tr ap, zr	<1 apatite
							<1 hb
SiO2 (wt%)	42.25	43.06	43.97	47.46	49.47	51.97	53.12
TiO2 (wt%)	0.63	0.74	0.59	1.21	3.79	2.46	2.27
Al2O3(wt%)	5.41	6.91	8.84	10.53	14.29	15.01	15.41
FeO* (wt%)	16.67	15.58	15.36	15.08	12.51	11.01	12.30
MnO(wt%)	0.20	0.19	0.24	0.20	0.17	0.22	0.18
MgO(wt%)	28.33	25.72	24.29	17.00	5.69	4.49	2.54
CaO(wt%)	3.37	4.75	4.89	6.68	9.62	8.40	6.41
Na2O(wt%)	1.05	1.04	1.31	1.74	2.66	3.24	4.10
K2O(wt%)	0.40	0.49	0.48	1.12	1.48	1.80	2.93
P2O5(wt%)	0.17	0.20	0.21	0.33	0.62	0.50	0.78
LOI (wt%)	0.94	1.63	0.64	0.00	0.30	0.26	0.00
Total(wt%)	99.42	100.31	100.82	101.35	100.60	99.36	100.04
Ba (ppm)	203.00	261.00	304.01	472.00	917.65	882.27	1849.00
Rb (ppm)	13.25	14.6	15.9	30.7	34.8	57.4	35.20
Sr (ppm)	144.10	181.4	245.2	259.2	410.00	395.70	412.2
F (ppm)	-	-	-	1000	-	-	-
CIPW Norms							
Qtz	0.00	0.00	0.00	0.00	0.00	0.00	0.00
Or	2.40	2.93	2.83	6.53	8.72	10.73	17.31
Ab	9.02	8.92	11.06	14.53	22.44	27.66	34.68
An	9.00	12.91	16.79	17.38	22.61	21.29	14.98
Di	5.52	7.78	4.89	10.75	17.43	14.65	10.04
Hy	2.44	3.89	3.17	9.11	13.87	17.31	6.24
Ol	70.00	61.67	59.65	38.69	6.322	2.48	10.63
Ilm	1.21	1.42	1.12	2.27	7.18	4.71	4.31
Ap	0.40	0.47	0.48	0.75	1.43	1.17	1.80

	DIORITES				
Sample #	82DNS74b	83DNS320d	83DNS318b	82DNS209	84DNS47c
Mode %	49 plag	35 plag	48 plag	55 plag	54 plag
	21 cpx	19 hb	11 kspar	13 cpx	12 cpx
	14 biotite	15 kspar	10 biotite	12 biotite	12 biotite
	11 hb	6 biotite	8 hb	7 hb	10 hb
	1 quartz	4 opaque	7 quartz	4 quartz	4 quartz
	1 opaque	3 quartz	4 opaque	4 opaque	3 opaque
	1 apatite	2 apatite	3 cpx	3 kspar	2 kspar
	<1 kspar	1 cpx	<1 apatite	1 apatite	1 apatite
	tr tourm	tr myrmekite	tr zircon	tr zr/sph	tr allan/sph
SiO2(wt%)	50.67	51.74	51.80	53.17	53.20
TiO2(wt%)	1.70	2.84	2.49	2.71	1.84
Al2O3(wt%)	15.30	15.14	15.37	16.39	16.01
FeO*(wt%)	9.49	12.55	10.48	9.04	9.33
MnO(wt%)	0.19	0.23	0.18	0.16	0.19
MgO(wt%)	6.22	3.57	4.19	3.96	4.89
CaO(wt%)	10.14	6.84	6.85	7.82	9.17
Na2O(wt%)	2.70	3.02	2.45	3.21	2.81
K2O(wt%)	1.62	2.05	2.35	2.04	1.61
P2O5(wt%)	0.38	0.86	0.53	0.50	0.49
LOI	0.87	1.14	1.94	0.35	0.28
Total(wt%)	99.28	99.98	98.63	99.35	99.82
Ba (ppm)	563.00	778.00	815,00	344.00	602.32
Rb (ppm)	36.40	74.40	93.00	55.10	54.50
Sr (ppm)	431.20	432.90	391.80	376.10	454.00
F (ppm)	-	1000.00	-	-	-
CIPW Norm					
Qtz	0.00	1.67	3.61	2.24	2.02
Or	9.73	12.26	14.36	12.18	9.56
Ab	23.21	25.85	21.44	27.43	23.89
An	25.24	21.95	24.82	24.53	26.44
Di	19.30	5.68	5.66	9.47	13.36
Hy	9.81	25.11	23.95	17.78	20.09
Ol	8.53	0.00	0.00	0.00	0.00
Ilm	3.28	5.46	4.89	5.20	3.51
Ap	0.89	2.01	1.27	1.17	1.14

	HB-BT GRANITES							
Sample #	84DNS33a	83DNS307d	84DNS57a	82DNS197	84DNS34a	82DNS75d	83DNS322a	84DNS63a
Mode %	42 plag	33 kspar	52 kspar	36 plag	40 plag	59 kspar	34 plag	53 kspar
	25 kspar	33 plag	23 quartz	32 kspar	30 kspar	23 quartz	33 quartz	25 quartz
	22 quartz	25 quartz	20 plag	22 quartz	17 quartz	12 plag	26 kspar	12 plag
	5 biotite	6 hb	3 biotite	5 biotite	11 biotite	6 hb (+cpx)	6 biotite	5 hb
	4 chlorite	3 biotite	2 hb	5 hb (+cpx)	1 ilmenite	<1 biotite	<1 hb	1 chlorite
	2 sericite	tr apatite	1 apatite	tr opaque	1 hb	<1 late amph	tr opaque	<1 opaque
	<1 opaque	tr opaque	<1 opaque	tr apatite	tr apatite	tr ilmenite	tr apatite	<1 cc
	tr apatite	tr allanite	tr zr	tr allan/zr	tr zr/sph	tr apatite	tr zr	<1 sericite
	tr zr/sph		tr ep, cc	tr cc	5 chlorite	tr zr	tr chlorite	1 late bt
	tr cc		tr ser, chl		3 cc		tr epidote	
	<5 alt.hb							
SiO2(wt%)	66.13	66.85	67.38	68.37	69.06	69.47	70.07	71.41
TiO2(wt%)	0.62	0.43	0.57	0.52	0.42	0.33	0.41	0.32
Al2O3(wt%)	15.95	15.34	14.93	15.48	15.71	14.55	14.70	13.24
FeO*(wt%)	3.68	4.81	4.16	3.23	2.98	3.32	2.44	2.58
MnO(wt%)	0.09	0.12	0.04	0.09	0.08	0.03	0.02	0.02
MgO(wt%)	1.17	0.69	1.11	1.02	0.97	0.55	1.19	0.54
CaO(wt%)	3.32	1.61	1.83	2.48	1.55	1.26	2.52	1.06
Na2O(wt%)	3.37	3.45	3.61	3.74	4.29	4.45	3.29	3.35
K2O(wt%)	3.89	6.49	5.70	4.83	5.04	5.77	4.22	5.96
P2O5(wt%)	0.11	0.05	0.13	0.09	0.06	0.03	0.10	0.05
LOI (wt%)	1.65	0.32	0.65	0.18	0.99	0.25	0.34	0.72
Total(wt%)	99.98	100.16	100.11	100.03	101.15	100.01	99.30	99.25
Ba (ppm)	1772.79	505.00	707.74	1432.00	988.32	3.24	1202.00	869.81
Rb (ppm)	163.70	181.10	252.00	236.60	207.50	271.70	215.80	149.70
Sr (ppm)	290.30	81.60	170.00	221.50	156.10	53.60	209.70	78.20
F (ppm)	-	-	-	1000.00	-	-	-	-
CIPW Norms								
Qtz	20.76	13.93	16.48	19.31	17.95	16.29	26.42	24.93
C	0.43	0.00	0.00	0.00	0.52	0.00	0.38	0.00
Or	23.38	38.41	33.86	28.58	29.73	34.18	25.20	35.74
Ab	29.00	29.24	30.71	31.69	36.24	37.74	28.13	28.77
An	16.02	7.21	7.74	11.20	7.29	2.69	11.97	3.54
Di	0.00	0.40	0.45	0.45	0.00	2.92	0.00	1.26
Hy	8.96	9.87	9.36	7.56	7.33	5.48	6.88	5.03
Ilm	1.20	0.82	1.09	0.99	0.80	0.63	0.79	0.62
Ap	0.26	0.12	0.30	0.21	0.14	0.07	0.23	0.12

			SYENITES			
Sample #	82DNS128	82DNS210	82DNS79	84DNS32a	84DNS32b	82DNS195b
Mode %	89 kspar	80 kspar	83 kspar	68 kspar	82 kspar	77 kspar
	7 cpx	6 plag	8 cpx	12 plag	8 plag	9 quartz
	1 olivine	4 cpx	5 olivine	8 cpx	3 hb	6 cpx
	1 opeque	2 hb	2 ilmenite	6 hb	5 quartz	4 biotite
	<1 plag	2 quartz	1 quartz	5 quartz	1 cpx	1 opeque
	<1 amph	.7 ilmenite	<1 plag	1 ilmenite	<1 olivine	1 olivine
	tr fl?	.2 biotite	<1 hb	<1 olivine	<1 opeque	<1 amph
	tr hem	tr apatite	<1 zr	<1 ap, zr	<1 biotite	<1 ap, zr
	tr zr	tr zr	<1 Fe ox.	tr biotite	<1 ap, zr	<1 Fe ox.
		tr idd,act		tr Fe ox.	<1 allanite	<1 cc
				tr act, ep	tr act, idd.	
SiO2(wt%)	60.84	61.28	62.71	61.77	62.96	64.28
TiO2(wt%)	0.66	0.59	0.47	0.60	0.55	0.56
Al2O3(wt%)	15.65	16.58	16.44	16.51	16.65	14.95
FeO*(wt%)	8.81	7.00	6.41	5.77	5.56	6.79
MnO(wt%)	0.22	0.12	0.18	0.12	0.08	0.11
MgO(wt%)	0.14	0.81	0.28	0.39	0.59	0.72
CaO(wt%)	2.70	2.52	1.92	2.19	2.08	1.99
Na2O(wt%)	5.21	4.92	5.23	4.78	4.69	5.57
K2O(wt%)	5.45	5.84	6.13	5.99	5.98	5.54
P2O5(wt%)	0.08	0.07	0.03	0.06	0.06	0.04
LOI (wt%)	0.00	0.00	0.00	0.05	0.05	0.11
Total(wt%)	99.63	99.46	99.49	98.13	99.25	100.57
Ba (ppm)	92.00	1665.00	28.00	1186.74	1405.35	165.00
Rb (ppm)	64.31	82.20	75.96	123.50	133.20	141.41
Sr (ppm)	17.76	102.20	12.83	133.40	160.80	26.56
F (ppm)	710.00	1000.00	710.00	2800.00	900.00	1600.00
CIPW Norms						
Qtz	0.00	0.00	0.54	5.43	4.05	2.86
Or	32.28	34.60	36.30	36.19	35.62	32.86
Ab	44.19	41.74	44.34	41.35	40.00	45.84
An	3.23	5.92	3.29	6.03	6.77	0.00
Di	8.60	5.36	3.35	4.03	2.82	8.35
Hy	6.70	10.19	9.23	2.56	9.54	8.96
Ol	3.57	0.90	0.00	0.00	0.00	0.00
Ilm	1.26	1.12	0.89	1.16	1.05	1.06
Ap	0.19	0.16	0.07	0.14	0.14	0.09

	ALKALI-FELDSPAR GRANITES				
Sample #	82DNS195c	84DNS61a	82DNS193	82DNS162b	83DNS321d
Mode %	76 kspar	56 kspar	56 kspar	60 kspar	56 kspar
	13 quartz	39 quartz	39 quartz	33 quartz	40 quartz
	10 Na-amph	3 arfved	5 arfved	7 Na-amph	3 arfved
	<1 opaque	2 biotite	<1 biotite	1 biotite	1 biotite
	tr fl	<1 ilmenite	tr zr	tr fl	tr plag(ab)
	tr zr	<1 fl	tr opaque	tr zr	tr fl, zr
	tr Fe ox.	<1 zr		tr opaque	tr chl(alt)
	tr zinn	<1 aenig.		tr Fe ox.	tr opaque
	tr chev?				tr Fe ox.
SiO2(wt%)	68.63	74.54	74.95	74.99	75.48
TiO2(wt%)	0.33	0.19	0.18	0.15	0.15
Al2O3(wt%)	14.29	12.38	11.74	11.45	12.01
FeO*(wt%)	3.86	1.97	2.55	2.71	2.14
MnO(wt%)	0.04	0.00	0.07	0.00	0.06
MgO(wt%)	0.59	0.58	0.25	0.46	0.02
CaO(wt%)	1.04	0.34	0.25	0.11	0.26
Na2O(wt%)	5.53	4.77	4.56	4.95	4.65
K2O(wt%)	5.34	4.72	4.57	4.46	4.66
P2O5(wt%)	0.00	0.00	0.00	0.00	0.00
LOI(wt%)	0.25	0.27	0.13	0.11	0.14
Total(wt%)	99.90	99.76	99.25	99.399	99.57
Ba(ppm)	7.00	13.38	7.00	4.00	19.00
Rb(ppm)	255.90	227.00	357.40	494.30	329.10
Sr(ppm)	3.80	2.40	10.80	3.60	6.03
F(ppm)	2800	930	3450	2600	1400
CIPW Norms					
Qtz	12.80	27.84	30.60	30.88	30.76
Or	31.67	28.03	27.24	26.55	27.69
Ab	43.93	37.59	35.25	34.31	36.04
Na-metasil	0.71	0.69	0.86	1.83	0.82
Di	4.48	1.44	1.09	0.48	1.15
Hy	5.79	4.04	4.61	5.67	3.25
Ilm	0.63	0.36	0.35	0.29	0.29

SAMPLE #	ROCK TYPE	SiO2	TiO2	Al2O3	Fe2O3	FeO	MnO
82DNS202	Host	80.46	0.42	8.57	0.00	1.22	0.08
84DNS64	Host	58.26	0.71	11.25	0.00	4.58	0.03
85DNS206	Host	64.26	0.77	16.14	0.00	6.14	0.16
82DNS62	Gabbro	50.99	2.52	16.10	1.66	6.92	0.16
82DNS105	Gabbro	47.63	3.42	14.28	0.57	11.11	0.22
82DNS145	Gabbro	48.72	1.20	11.17	1.83	10.22	0.19
82DNS170	Gabbro	46.98	1.39	15.03	2.70	10.68	0.24
82DNS178	Gabbro	43.69	0.99	7.60	2.80	13.96	0.25
82DNS196	Gabbro	46.65	1.28	10.54	2.17	12.45	0.23
82AR12	Gabbro	46.90	3.17	13.70	1.60	17.10	0.37
82DNS79	Syenite	62.79	0.66	16.07	1.52	4.87	0.17
82DNS80	Syenite	62.53	0.61	15.79	1.56	6.13	0.20
82DNS127	Syenite	65.89	0.64	15.81	0.87	2.99	0.06
82DNS125	Syenite	61.19	0.72	16.15	1.48	4.42	0.12
82DNS195b	Syenite	64.94	0.58	14.66	1.80	4.48	0.15
82DNS210	Syenite	60.62	0.64	16.00	1.17	5.30	0.16
79AR6	Syenite	63.20	0.45	16.40	1.30	4.00	0.13
82AR10	Syenite	60.80	0.57	15.00	1.62	6.94	0.22
82AR11	Syenite	60.40	0.66	16.40	1.30	5.74	0.17
82DNS162	AFgranite	72.11	0.26	11.89	1.98	1.07	0.04
82DNS193	AFgranite	74.84	0.18	11.16	1.28	1.43	0.03
82DNS64	PFqtzsy	62.22	0.95	16.31	1.21	4.54	0.12
82DNS67a	PFqtzsy	62.88	0.91	15.58	2.42	4.06	0.12
82DNS67b	PFqtzsy	66.59	0.60	15.15	0.98	3.53	0.09
82DNS208	PFqtzsy	62.44	0.61	15.29	3.83	1.85	0.12
82AR9	PFqtzsy	66.50	0.50	14.80	1.87	2.19	0.06
82DNS82	HBgranite	69.17	0.53	15.13	1.19	2.15	0.07
82DNS197	HBgranite	67.97	0.54	14.87	0.70	2.37	0.06
79AR7	HBgranite	70.60	0.38	13.80	0.95	2.40	0.04
82DNS75b	HBgranite	71.24	0.34	14.38	1.01	2.37	0.07
82DNS77b	Diorite	51.98	1.57	15.72	1.43	7.07	0.16
82DNS112b	Diorite	51.66	2.17	14.38	10.53	3.96	0.31
82DNS184	Diorite	50.64	2.04	15.28	1.24	7.67	0.16
82DNS209	Diorite	52.11	2.95	15.81	0.86	7.59	0.15
82DNS111	Diorite	53.00	1.80	15.70	0.63	7.65	0.15

SAMPLE #	ROCK TYPE	MgO	CaO	Na2O	K2O	P2O5
82DNS202	Host	2.31	1.99	2.50	0.69	0.05
84DNS64	Host	3.29	6.58	1.57	2.21	0.18
85DNS206	Host	1.78	0.43	1.50	2.77	0.16
82DNS62	Gabbro	3.00	7.26	3.16	2.66	0.62
82DNS105	Gabbro	4.39	8.77	2.97	1.78	1.36
82DNS145	Gabbro	14.95	7.91	2.11	1.15	0.28
82DNS170	Gabbro	7.26	8.11	2.72	1.24	0.35
82DNS178	Gabbro	23.27	5.60	1.31	0.80	0.23
82DNS196	Gabbro	16.78	6.92	1.83	1.19	0.35
82AR12	Gabbro	2.87	7.49	3.36	1.38	0.99
82DNS79	Syenite	0.04	2.06	5.53	6.07	0.04
82DNS80	Syenite	0.11	2.79	5.26	5.78	0.11
82DNS127	Syenite	0.89	3.14	4.25	4.20	0.13
82DNS125	Syenite	0.51	2.72	4.91	4.98	0.11
82DNS195b	Syenite	0.28	2.11	5.21	5.51	0.09
82DNS210	Syenite	0.19	2.49	4.77	5.84	0.08
79AR6	Syenite	0.16	2.00	5.40	6.10	0.06
82AR10	Syenite	0.10	3.19	4.67	5.43	0.08
82AR11	Syenite	0.19	2.72	4.80	5.99	0.08
82DNS162	AFgranite	0.12	0.85	4.52	4.84	0.02
82DNS193	AFgranite	0.05	0.28	4.41	4.63	0.00
82DNS64	PFqtzsy	0.77	3.29	4.67	5.32	0.17
82DNS67a	PFqtzsy	0.80	2.34	4.14	5.29	0.17
82DNS67b	PFqtzsy	0.52	1.95	4.34	5.62	0.09
82DNS208	PFqtzsy	0.38	1.60	4.87	5.81	0.08
82AR9	PFqtzsy	0.38	1.42	4.27	5.79	0.09
82DNS82	HBgranite	0.48	1.77	4.01	5.52	0.07
82DNS197	HBgranite	0.65	2.48	3.69	4.88	0.89
79AR7	HBgranite	0.47	1.40	3.30	5.70	0.06
82DNS75b	HBgranite	0.17	1.27	4.50	5.71	0.05
82DNS77b	Diorite	5.84	9.05	3.35	1.81	0.24
82DNS112b	Diorite	1.90	6.75	3.92	1.94	0.53
82DNS184	Diorite	5.05	8.63	3.33	2.66	0.59
82DNS209	Diorite	4.00	7.83	3.42	2.03	0.46
82DNS111	Diorite	4.61	8.62	3.06	1.90	0.50

Appendix C. Probe data

OLIVINE ANALYSES

	1	2	3	4	5	6	7	8
SIO2	30.70	30.64	39.28	39.33	39.46	39.35	38.34	38.41
AL2O3	0.03	0.03	0.0	0.0	0.0	0.02	0.0	0.0
NA2O	0.01	0.03	0.02	0.0	0.01	0.01	0.01	0.01
K2O	0.05	0.06	0.03	0.03	0.03	0.04	0.04	0.01
MGO	0.70	0.69	40.19	40.79	41.13	41.29	40.98	40.59
CL	0.0	0.01	0.0	0.0	0.0	0.0	0.0	0.0
FEO	68.10	68.18	23.09	23.18	22.15	21.91	20.86	21.51
MNO	2.08	1.96	0.40	0.40	0.39	0.34	0.36	0.37
CR2O3	0.06	0.07	0.02	0.01	0.04	0.03	0.02	0.02
TIO2	0.05	0.09	0.06	0.10	0.06	0.06	0.06	0.06
BAO	0.14	0.13	0.08	0.0	0.05	0.02	0.02	0.08
F	0.10	0.11	0.04	0.05	0.02	0.02	0.04	0.05
CAO	0.29	0.26	0.07	0.06	0.10	0.08	0.07	0.06
P2O5	0.02	0.04	0.15	0.08	0.06	0.08	0.04	0.03
SRO	0.0	0.0	0.0	0.03	0.0	0.08	0.05	0.04
SUM	102.14	102.10	103.24	103.86	103.37	103.07	100.69	101.08

SI	1.008	1.008	1.007	1.007	0.992	0.992	0.987	0.987	0.991	0.991	0.989	0.989	0.985	0.985	0.986	0.986
AL	0.001	"	0.001	"	0.0	"	0.0	"	0.0	"	0.001	"	0.0	"	0.0	"
TI	0.001	"	0.002	"	0.001	"	0.002	"	0.001	"	0.001	"	0.001	"	0.001	"
FE	1.870	"	1.874	"	0.488	"	0.486	"	0.465	"	0.461	"	0.448	"	0.462	"
MN	0.058	"	0.055	"	0.009	"	0.008	"	0.008	"	0.007	"	0.008	"	0.008	"
MG	0.034	"	0.034	"	1.513	"	1.525	"	1.539	"	1.547	"	1.569	"	1.553	"
CA	0.010	"	0.009	"	0.002	"	0.002	"	0.003	"	0.002	"	0.002	"	0.002	"
BA	0.002	1.977	0.002	1.977	0.001	2.013	0.0	2.023	0.0	2.017	0.0	2.019	0.0	2.028	0.001	2.026
O	4.000	"	4.000	"	4.000	"	4.000	"	4.000	"	4.000	"	4.000	"	4.000	"

1 82DNS210(CORE)-SYENITE
2 82DNS210(RIM)-SYENITE
3 82DNS186(CORE)-GABBRO
4 82DNS186(RIM)-GABBRO
5 82DNS186(CORE)-GABBRO
6 82DNS186(RIM)-GABBRO
7 82DNS186(IN CPX)-GABBRO
8 82DNS186(IN PLAG)-GABBRO

OLIVINE ANALYSES

	9	10	11	12
SIO2	37.08	37.02	35.75	36.94
AL2O3	0.01	0.0	0.0	0.0
NA2O	0.0	0.01	0.0	0.01
K2O	0.02	0.02	0.02	0.02
MGO	32.14	32.42	31.26	32.70
CL	0.0	0.0	0.0	0.0
FEO	32.93	32.66	31.60	32.17
MNO	0.57	0.61	0.52	0.55
CR2O3	0.03	0.03	0.03	0.03
TIO2	0.07	0.02	0.04	0.05
BAO	0.11	0.04	0.09	0.04
F	0.03	0.06	0.05	0.06
CAO	0.10	0.09	0.09	0.13
P2O5	0.07	0.03	0.05	0.05
SRO	0.06	0.0	0.0	0.01
SUM	102.99	102.88	99.40	102.58

SI	0.986	0.986	0.984	0.984	0.985	0.985	0.983	0.983
AL	0.0	"	0.0	"	0.0	"	0.0	"
TI	0.001	"	0.0	"	0.001	"	0.001	"
FE	0.733	"	0.726	"	0.728	"	0.716	"
MN	0.013	"	0.014	"	0.012	"	0.012	"
MG	1.274	"	1.285	"	1.283	"	1.297	"
CA	0.003	"	0.003	"	0.003	"	0.004	"
BA	0.001	2.025	0.0	2.028	0.001	2.028	0.0	2.030
O	4.000	"	4.000	"	4.000	"	4.000	"

9 82DNS196(IN CPX)-GABBRO
10 82DNS196-GABBRO
11 82DNS196-GABBRO
12 82DNS196-GABBRO

OLIVINE ANALYSES

	1	2	3	4	5	6
SIO2	51.22	51.22	30.95	30.79	32.32	32.43
AL2O3	0.34	0.34	0.13	0.17	0.08	0.06
K2O	0.02	0.02	0.05	0.05	0.05	0.05
NA2O	0.04	0.02	-0.01	0.02	0.02	0.02
MGO	16.55	16.29	1.28	0.13	6.30	6.45
FEO	31.83	31.82	67.50	68.36	63.08	62.59
TIO2	0.26	0.25	0.15	0.15	0.16	0.19
MNO	0.77	0.82	1.98	2.30	1.27	1.30
BAO	0.0	0.0	0.0	0.0	0.0	0.0
SRO	0.0	0.0	0.0	0.0	0.0	0.0
CL	0.04	0.09	0.14	0.15	0.12	0.18
CAO	1.49	1.50	0.24	0.29	0.16	0.11
F	0.02	0.01	0.21	0.07	0.13	0.20
SUM	102.46	102.24	102.23	102.19	103.37	103.13

SI	1.305	1.305	1.307	1.307	1.006	1.006	1.010	1.010	1.004	1.004	1.008	1.006
AL	0.010	*	0.010	*	0.005	*	0.007	*	0.003	*	0.002	*
TI	0.005	*	0.005	*	0.004	*	0.004	*	0.004	*	0.004	*
FE	0.678	*	0.679	*	1.834	*	1.875	*	1.639	*	1.624	*
MN	0.017	*	0.018	*	0.054	*	0.064	*	0.033	*	0.034	*
MG	0.628	*	0.620	*	0.062	*	0.006	*	0.292	*	0.298	*
CA	0.041	*	0.041	*	0.008	*	0.010	*	0.005	*	0.004	*
BA	0.0	1.379	0.0	1.373	0.0	1.968	0.0	1.966	0.0	1.977	0.0	1.967
O	4.000	*	4.000	*	4.000	*	4.000	*	4.000	*	4.000	*

1 84DNS34D-GABBRO
2 84DNS34D-GABBRO
3 84DNS32A-SYENITE
4 82DNS79-SYENITE
5 84DNS39C-GABBRO
6 84DNS39C-GABBRO

PYROXENE ANALYSES

	1	2	3	4	5	6	7	8
SIO2	51.36	51.11	50.91	50.46	51.49	51.49	51.52	52.61
AL2O3	1.24	0.92	2.36	1.39	1.51	1.12	1.31	0.70
K2O	0.03	0.02	0.06	0.02	0.01	0.02	0.04	0.02
NA2O	0.22	0.26	0.48	0.28	0.24	0.16	0.36	0.17
MGO	12.97	11.68	12.45	11.31	12.32	12.26	12.33	12.86
FEO	14.43	13.58	12.40	16.07	13.35	13.72	13.94	13.90
TIO2	0.41	0.40	0.86	1.11	0.65	0.39	0.46	0.36
MNO	0.38	0.37	0.35	0.51	0.39	0.47	0.45	0.40
CL	0.0	0.0	0.0	0.0	0.0	0.0	0.0	0.0
SRO	0.0	0.0	0.0	0.0	0.0	0.0	0.0	0.0
BAO	0.08	0.07	0.10	0.03	0.0	0.10	0.0	0.0
CAO	19.57	21.21	20.35	19.85	20.83	21.06	20.06	20.55
F	0.08	0.0	0.20	0.0	0.06	0.0	0.08	0.04
SUM	100.61	99.56	100.22	101.02	100.79	100.69	100.49	101.57

SI	1.943	*	1.959	*	1.920	*	1.925	*	1.941	*	1.950	*	1.951	*	1.968	*
AL	0.055	1.999	0.041	2.000	0.080	2.000	0.062	1.987	0.059	2.000	0.050	2.000	0.049	2.000	0.031	1.999
AL	0.0	*	0.001	*	0.024	*	0.0	*	0.008	*	0.0	*	0.009	*	0.0	*
TI	0.012	*	0.012	*	0.024	*	0.032	*	0.018	*	0.011	*	0.013	*	0.010	*
FE	0.457	*	0.435	*	0.391	*	0.513	*	0.421	*	0.435	*	0.441	*	0.435	*
MN	0.012	*	0.012	*	0.011	*	0.016	*	0.012	*	0.015	*	0.014	*	0.013	*
MG	0.731	1.212	0.667	1.127	0.700	1.151	0.643	1.204	0.692	1.153	0.692	1.153	0.696	1.174	0.717	1.175
CA	0.793	*	0.871	*	0.822	*	0.811	*	0.841	*	0.855	*	0.814	*	0.824	*
NA	0.016	*	0.019	*	0.035	*	0.021	*	0.018	*	0.012	*	0.026	*	0.012	*
K	0.001	*	0.001	*	0.003	*	0.001	*	0.0	*	0.001	*	0.002	*	0.001	*
SR	0.0	0.811	0.0	0.892	0.0	0.860	0.0	0.833	0.0	0.859	0.0	0.867	0.0	0.842	0.0	0.837
O	6.000	*	6.000	*	6.000	*	6.000	*	6.000	*	6.000	*	6.000	*	6.000	*

1 84DNS34D-GABBRO
2 84DNS34D-GABBRO
3 84DNS34D-GABBRO
4 84DNS39A-GABBRO
5 84DNS39A-GABBRO
6 84DNS39A-GABBRO
7 84DNS39A-GABBRO
8 84DNS47C-DIORITE

PYROXENE ANALYSES

	9	10	11	12	13	14	15	16
SIO2	52.18	52.47	49.66	49.69	49.24	48.50	47.96	48.11
AL2O3	0.54	0.50	0.62	0.66	0.80	0.31	0.71	0.48
K2O	0.02	0.02	0.03	0.02	0.10	0.03	0.03	0.04
NA2O	0.13	0.18	0.23	0.26	0.15	0.31	0.34	0.36
MGO	12.93	12.52	3.41	3.56	2.17	0.22	0.24	0.24
FEO	13.35	12.89	26.18	25.41	27.44	30.63	30.28	30.41
TIO2	0.23	0.19	0.46	0.56	0.22	0.35	0.62	0.68
MNO	0.34	0.34	0.69	0.69	0.93	0.90	0.90	0.89
CL	0.0	0.0	0.0	0.0	0.0	0.0	0.0	0.0
SRO	0.0	0.0	0.0	0.0	0.0	0.0	0.0	0.0
BAO	0.04	0.03	0.08	0.02	0.07	0.11	0.11	0.08
CAO	21.16	21.70	19.85	20.24	19.56	20.06	19.68	19.96
F	0.03	0.0	0.09	0.10	0.10	0.09	0.07	0.13
SUM	100.88	100.83	101.13	101.09	100.61	101.31	100.76	101.17

SI	1.968	*	1.978	*	1.982	*	1.979	*	1.989	*	1.983	*	1.970	*	1.969	*
AL	0.024	1.990	0.022	2.000	0.018	2.000	0.021	2.000	0.011	2.000	0.015	1.998	0.030	2.000	0.023	1.992
AL	0.0	*	0.0	*	0.011	*	0.010	*	0.027	*	0.0	*	0.004	*	0.0	*
TI	0.007	*	0.005	*	0.014	*	0.017	*	0.007	*	0.011	*	0.019	*	0.021	*
FE	0.421	*	0.406	*	0.874	*	0.846	*	0.927	*	1.047	*	1.040	*	1.041	*
MN	0.011	*	0.011	*	0.023	*	0.023	*	0.032	*	0.031	*	0.031	*	0.031	*
MG	0.726	1.164	0.703	1.126	0.203	1.125	0.211	1.108	0.131	1.124	0.013	1.103	0.015	1.109	0.015	1.107
CA	0.854	*	0.876	*	0.849	*	0.864	*	0.847	*	0.879	*	0.866	*	0.875	*
NA	0.009	*	0.012	*	0.018	*	0.020	*	0.012	*	0.025	*	0.027	*	0.029	*
K	0.001	*	0.001	*	0.002	*	0.001	*	0.005	*	0.002	*	0.002	*	0.002	*
SR	0.0	0.865	0.0	0.889	0.0	0.868	0.0	0.885	0.0	0.864	0.0	0.905	0.0	0.895	0.0	0.906
O	6.000	*	6.000	*	6.000	*	6.000	*	6.000	*	6.000	*	6.000	*	6.000	*

9 84DNS47C-DIORITE
10 84DNS47C-DIORITE
11 82DNS32A-SYENITE
12 82DNS32A-SYENITE
13 82DNS32A-SYENITE
14 82DNS79-SYENITE
15 82DNS79-SYENITE
16 82DNS79-SYENITE

PYROXENE ANALYSES

	17		18	
SIO2	51.74		51.66	
AL2O3	0.87		0.92	
K2O	0.02		0.02	
NA2O	0.24		0.27	
MGO	9.00		9.05	
FEO	19.04		19.15	
TIO2	0.39		0.41	
MNO	0.47		0.50	
CL	0.0		0.0	
SRO	0.0		0.0	
BAO	0.08		0.04	
CAO	19.90		19.74	
F	0.04		0.0	
SUM	101.67		101.72	
SI	1.978	*	1.975	*
AL	0.022	2.000	0.025	2.000
AL	0.017	*	0.017	*
TI	0.011	*	0.012	*
FE	0.609	*	0.612	*
MN	0.015	*	0.016	*
MG	0.513	1.165	0.516	1.173
CA	0.815	*	0.809	*
NA	0.018	*	0.020	*
K	0.001	*	0.001	*
SR	0.0	0.834	0.0	0.830
O	6.000	*	6.000	*

17 84DNS39C-GABBRO
18 84DNS39C-GABBRO

PYROXENE ANALYSES

	1	2	3	4	5	6	7	8
SIO2	47.67	47.89	49.07	51.30	55.52	55.75	55.91	54.60
AL2O3	0.64	0.59	0.18	0.86	0.50	0.61	0.40	0.39
NA2O	0.30	0.33	0.12	0.12	0.01	0.0	0.0	0.02
K2O	0.03	0.03	0.04	0.02	0.02	0.02	0.02	0.04
MGO	1.37	1.46	2.25	14.23	29.93	30.20	30.30	29.59
CL	0.0	0.01	0.0	0.0	0.01	0.0	0.0	0.0
FEO	29.12	29.00	27.26	10.99	13.63	13.31	13.21	12.98
MNO	0.85	0.79	0.84	0.38	0.39	0.35	0.36	0.34
CR2O3	0.03	0.06	0.05	0.12	0.02	0.03	0.05	0.03
TIO2	0.72	0.45	0.07	0.38	0.26	0.27	0.25	0.27
BAO	0.06	0.08	0.10	0.16	0.04	0.02	0.05	0.0
F	0.08	0.07	0.03	0.03	0.04	0.0	0.03	0.01
CAO	20.17	20.27	21.54	20.20	1.09	1.15	1.16	1.13
P2O5	0.01	0.01	0.03	0.02	0.0	0.01	0.04	0.0
SRO	0.07	0.03	0.0	0.0	0.0	0.0	0.0	0.0
SUM	100.94	100.84	101.37	98.49	101.35	101.66	101.61	99.36

SI	1.949	*	1.957	*	1.980	*	1.958	*	1.961	*	1.960	*	1.965	*	1.964	*
AL	0.031	1.980	0.028	1.986	0.009	1.989	0.039	1.996	0.021	1.981	0.025	1.985	0.017	1.982	0.017	1.981
AL	0.0	*	0.0	*	0.0	*	0.0	*	0.0	*	0.0	*	0.0	*	0.0	*
TI	0.022	*	0.014	*	0.002	*	0.011	*	0.007	*	0.007	*	0.007	*	0.007	*
FE	0.996	*	0.991	*	0.920	*	0.351	*	0.403	*	0.391	*	0.388	*	0.390	*
MN	0.029	*	0.027	*	0.029	*	0.012	*	0.012	*	0.010	*	0.011	*	0.010	*
MG	0.083	1.131	0.089	1.121	0.135	1.086	0.809	1.183	1.575	1.997	1.583	1.992	1.587	1.993	1.586	1.995
CA	0.884	*	0.888	*	0.931	*	0.826	*	0.041	*	0.043	*	0.044	*	0.044	*
NA	0.024	*	0.026	*	0.009	*	0.009	*	0.001	*	0.0	*	0.0	*	0.001	*
K	0.002	*	0.002	*	0.002	*	0.001	*	0.001	*	0.001	*	0.001	*	0.002	*
SR	0.002	0.911	0.001	0.916	0.0	0.942	0.0	0.836	0.0	0.043	0.0	0.045	0.0	0.045	0.0	0.046
O	6.000	*	6.000	*	6.000	*	6.000	*	6.000	*	6.000	*	6.000	*	6.000	*

1 82DNS210-SUBSOLVUS SYENITE
2 82DNS210-SUBSOLVUS SYENITE
3 82DNS210-SUBSOLVUS SYENITE
4 82DNS197-HB GRANITE
5 82DNS186-GABBRO
6 82DNS186-GABBRO
7 82DNS186-GABBRO
8 82DNS186-GABBRO

PYROXENE ANALYSES

	9	10	11	12	13	14	15	16
SIO2	54.61	50.97	52.13	50.32	51.43	50.97	53.68	54.19
AL2O3	0.47	2.48	1.34	2.90	0.60	2.28	0.66	0.54
NA2O	0.01	0.25	0.40	0.27	0.16	0.41	0.0	0.02
K2O	0.03	0.03	0.03	0.03	0.04	0.03	0.01	0.01
MGO	29.90	17.19	17.28	17.01	12.90	14.93	25.86	26.24
CL	0.0	0.0	0.0	0.0	0.0	0.0	0.0	0.0
FEO	12.90	5.56	5.36	5.71	14.12	7.11	18.77	18.48
MNO	0.40	0.21	0.16	0.21	0.39	0.23	0.50	0.54
CR2O3	0.03	0.51	0.35	0.39	0.02	0.49	0.05	0.05
TIO2	0.31	0.97	0.73	1.39	0.23	0.81	0.22	0.18
BAO	0.01	0.04	0.03	0.04	0.03	0.08	0.02	0.06
F	0.08	0.06	0.01	0.04	0.03	0.07	0.06	0.01
CAO	1.17	20.68	21.34	20.78	19.74	20.95	1.27	1.20
P2O5	0.0	0.06	0.03	0.01	0.04	0.02	0.02	0.0
SRO	0.0	0.06	0.03	0.0	0.0	0.02	0.06	0.0
SUM	99.81	98.41	98.80	98.62	99.61	97.75	101.03	101.43

SI	1.955	*	1.902	*	1.938	*	1.878	*	1.965	*	1.929	*	1.952	*	1.959	*
AL	0.020	1.975	0.098	2.000	0.059	1.997	0.122	2.000	0.027	1.992	0.071	2.000	0.028	1.980	0.023	1.982
AL	0.0	*	0.011	*	0.0	*	0.006	*	0.0	*	0.030	*	0.0	*	0.0	*
TI	0.008	*	0.027	*	0.020	*	0.039	*	0.007	*	0.023	*	0.006	*	0.005	*
FE	0.386	*	0.174	*	0.167	*	0.178	*	0.451	*	0.225	*	0.571	*	0.559	*
MN	0.012	*	0.007	*	0.005	*	0.007	*	0.013	*	0.007	*	0.015	*	0.017	*
MG	1.596	2.002	0.956	1.175	0.957	1.150	0.946	1.178	0.735	1.205	0.842	1.128	1.401	1.994	1.414	1.994
CA	0.045	*	0.827	*	0.850	*	0.831	*	0.808	*	0.849	*	0.049	*	0.046	*
NA	0.001	*	0.018	*	0.029	*	0.020	*	0.012	*	0.030	*	0.0	*	0.001	*
K	0.001	*	0.001	*	0.001	*	0.001	*	0.002	*	0.001	*	0.000	*	0.000	*
SR	0.0	0.047	0.001	0.848	0.001	0.881	0.0	0.852	0.0	0.822	0.000	0.881	0.001	0.051	0.0	0.048
O	6.000	*	6.000	*	6.000	*	6.000	*	6.000	*	6.000	*	6.000	*	6.000	*

9 82DNS186-GABBRO
10 82DNS186-GABBRO
11 82DNS186-GABBRO
12 82DNS186-GABBRO
13 82DNS209-DIORITE
14 82DNS196-GABBRO
15 82DNS196-GABBRO
16 82DNS196-GABBRO

PYROXENE ANALYSES

	17	18	19
SIO2	52.32	52.02	51.15
AL2O3	1.12	2.00	1.57
NA2O	0.15	0.33	0.47
K2O	0.01	0.03	0.04
MGO	16.03	16.81	9.38
CL	0.0	0.0	0.0
FEO	7.02	8.64	18.12
MNO	0.26	0.31	0.53
CR2O3	0.04	0.31	0.04
TIO2	0.43	0.74	0.69
BAO	0.01	0.04	0.05
F	0.06	0.01	0.25
CAO	22.05	19.42	19.90
P2O5	0.0	0.02	0.0
SRO	0.02	0.0	0.02
SUM	99.42	100.30	101.87

SI	1.948	*	1.923	*	1.944	*
AL	0.049	1.997	0.077	2.000	0.056	2.000
AL	0.0	*	0.010	*	0.014	*
TI	0.012	*	0.021	*	0.020	*
FE	0.219	*	0.267	*	0.576	*
MN	0.008	*	0.010	*	0.017	*
MG	0.890	1.129	0.926	1.234	0.531	1.158
CA	0.880	*	0.769	*	0.810	*
NA	0.011	*	0.024	*	0.035	*
K	0.000	*	0.001	*	0.002	*
SR	0.000	0.891	0.0	0.794	0.000	0.847
O	6.000	*	6.000	*	6.000	*

17 82DNS196-GABBRO
18 82DNS196-GABBRO
19 82DNS75D-HB GRANITE

AMPHIBOLE ANALYSES

	1	2	3	4	5	6	7	8
SIO2	50.27	50.88	50.94	50.91	51.17	47.55	47.07	47.64
AL2O3	0.76	0.70	0.75	0.89	0.70	1.66	1.78	1.72
NA2O	5.91	4.99	5.37	6.39	5.42	4.38	4.33	4.19
K2O	0.93	0.65	0.64	0.44	0.44	1.12	1.12	1.11
MGO	0.13	0.15	0.14	0.12	0.14	0.21	0.22	0.23
CL	0.05	0.04	0.04	0.01	0.03	0.08	0.08	0.09
FEO	35.62	36.04	35.93	36.29	36.38	35.06	35.51	35.56
MNO	0.69	0.61	0.65	0.49	0.70	0.78	0.78	0.83
CR2O3	0.02	0.05	0.03	0.04	0.05	0.02	0.06	0.09
TIO2	0.41	0.37	0.40	0.40	0.21	1.90	1.96	1.79
BAO	0.04	0.06	0.04	0.03	0.03	0.10	0.08	0.10
F	0.67	0.49	0.50	0.25	0.34	0.88	0.86	0.98
CAO	2.00	1.86	1.64	0.35	1.54	5.18	5.34	5.47
P2O5	0.0	0.04	0.0	0.03	0.0	0.01	0.0	0.02
SRO	0.02	0.14	0.07	0.0	0.0	0.0	0.0	0.0
H2O	1.52	1.61	1.60	1.73	1.69	1.41	1.42	1.37
SUM	98.98	98.53	98.68	98.27	98.76	100.21	100.47	100.98
-O= F+CL	0.29	0.22	0.22	0.11	0.15	0.39	0.38	0.43
SUM	98.68	98.31	98.46	98.16	98.61	99.82	100.09	100.55

SI	8.168	*	8.254	*	8.250	*	8.260	*	8.271	*	7.721	*	7.648	*	7.694	*
AL	0.0	8.168	0.0	8.254	0.0	8.250	0.0	8.260	0.0	8.271	0.279	8.000	0.341	7.989	0.306	8.000
AL	0.146	*	0.134	*	0.143	*	0.170	*	0.133	*	0.039	*	0.0	*	0.021	*
TI	0.050	*	0.045	*	0.049	*	0.049	*	0.026	*	0.232	*	0.239	*	0.217	*
FE	4.840	*	4.890	*	4.866	*	4.924	*	4.918	*	4.761	*	4.825	*	4.803	*
MN	0.095	*	0.084	*	0.089	*	0.067	*	0.096	*	0.107	*	0.107	*	0.114	*
MG	0.031	5.162	0.036	5.189	0.034	5.181	0.029	5.239	0.034	5.206	0.051	5.180	0.053	5.225	0.055	5.210
CA	0.348	*	0.323	*	0.285	*	0.061	*	0.267	*	0.901	*	0.930	*	0.946	*
NA	1.862	*	1.570	*	1.686	*	2.010	*	1.698	*	1.379	*	1.364	*	1.312	*
K	0.193	*	0.134	*	0.132	*	0.091	*	0.091	*	0.232	*	0.232	*	0.229	*
SR	0.002	2.404	0.013	2.040	0.007	2.110	0.0	2.162	0.0	2.056	0.0	2.512	0.0	2.526	0.0	2.487
CL	0.014	*	0.011	*	0.011	*	0.003	*	0.008	*	0.022	*	0.022	*	0.025	*
F	0.344	*	0.251	*	0.258	*	0.128	*	0.174	*	0.452	*	0.442	*	0.501	*
H	1.647	2.005	1.742	2.005	1.729	1.996	1.872	2.003	1.822	2.004	1.527	2.001	1.539	2.003	1.476	2.001
O	24.000	*	24.000	*	24.000	*	24.000	*	24.000	*	24.000	*	24.000	*	24.000	*

1 82DNS195C-AF GRANITE
2 82DNS195C-AF GRANITE
3 82DNS195C-AF GRANITE
4 82DNS195C-AF GRANITE
5 82DNS195C-AF GRANITE
6 82DNS195C-AF GRANITE
7 82DNS195C-AF GRANITE
8 82DNS195C-AF GRANITE

AMPHIBOLE ANALYSES

	9	10	11	12	13	14	15	16
SIO2	47.23	47.63	48.99	47.55	47.46	40.80	41.12	48.23
AL2O3	1.92	1.56	1.21	1.70	1.58	7.61	7.50	1.28
NA2O	4.17	3.91	4.29	4.32	3.93	2.01	1.86	0.26
K2O	1.17	1.15	1.04	1.10	1.10	1.25	1.22	0.31
MGO	0.24	0.33	0.27	0.27	0.20	1.21	1.20	0.70
CL	0.10	0.09	0.06	0.10	0.09	0.45	0.45	0.16
FEO	35.56	34.85	34.68	35.71	35.47	32.97	32.93	37.33
MNO	0.80	0.80	0.78	0.74	0.74	0.61	0.51	0.98
CR2O3	0.05	0.05	0.04	0.05	0.07	0.05	0.05	0.05
TIO2	1.95	1.95	0.90	1.91	1.88	1.99	1.98	0.10
BAO	0.11	0.11	0.12	0.14	0.08	0.14	0.09	0.06
F	0.95	0.90	0.68	0.94	0.91	0.76	0.81	0.04
CAO	5.88	5.45	4.57	5.56	5.22	10.25	10.22	9.28
P2O5	0.01	0.03	0.02	0.03	0.01	0.01	0.01	0.02
SRO	0.08	0.0	0.12	0.0	0.0	0.17	0.03	0.0
H2O	1.39	1.40	1.51	1.39	1.39	1.38	1.35	1.79
SUM	101.44	100.02	99.10	101.29	99.97	101.46	101.18	100.46
-O= F+CL	0.42	0.40	0.30	0.42	0.40	0.42	0.44	0.05
SUM	101.02	99.62	98.80	100.87	99.57	101.04	100.74	100.41

SI	7.612	*	7.736	*	7.972	*	7.664	*	7.729	*	6.618	*	6.670	*	7.794	*
AL	0.365	7.976	0.264	8.000	0.028	8.000	0.323	7.986	0.271	8.000	1.382	8.000	1.330	8.000	0.206	8.000
AL	0.0	*	0.035	*	0.204	*	0.0	*	0.032	*	0.073	*	0.104	*	0.037	*
TI	0.236	*	0.238	*	0.110	*	0.231	*	0.230	*	0.243	*	0.242	*	0.012	*
FE	4.793	*	4.734	*	4.719	*	4.813	*	4.831	*	4.473	*	4.467	*	5.045	*
MN	0.109	*	0.110	*	0.108	*	0.101	*	0.102	*	0.084	*	0.070	*	0.134	*
MG	0.058	5.196	0.080	5.197	0.065	5.206	0.065	5.210	0.049	5.244	0.293	5.165	0.290	5.173	0.169	5.397
CA	1.015	*	0.948	*	0.797	*	0.960	*	0.911	*	1.781	*	1.776	*	1.607	*
NA	1.303	*	1.231	*	1.353	*	1.350	*	1.241	*	0.632	*	0.585	*	0.081	*
K	0.241	*	0.238	*	0.216	*	0.226	*	0.228	*	0.259	*	0.252	*	0.064	*
SR	0.007	2.566	0.0	2.418	0.011	2.377	0.0	2.536	0.0	2.390	0.016	2.688	0.003	2.616	0.0	1.752
CL	0.027	*	0.025	*	0.017	*	0.027	*	0.025	*	0.124	*	0.124	*	0.044	*
F	0.484	*	0.462	*	0.350	*	0.479	*	0.469	*	0.390	*	0.416	*	0.020	*
H	1.494	2.006	1.517	2.004	1.639	2.006	1.494	2.001	1.510	2.004	1.493	2.007	1.461	2.000	1.930	1.994
O	24.000	*	24.000	*	24.000	*	24.000	*	24.000	*	24.000	*	24.000	*	24.000	*

9 82DNS195C-AF GRANITE
10 82DNS195C-AF GRANITE
11 82DNS195C-AF GRANITE
12 82DNS195C-AF GRANITE
13 82DNS195C-AF GRANITE
14 82DNS210-SYENITE
15 82DNS210-SYENITE
16 82DNS210-SYENITE

AMPHIBOLE ANALYSES

	17	18	19	20	21	22	23	24
SIO2	48.35	40.41	44.85	44.16	46.77	49.60	50.32	49.58
AL2O3	1.25	8.19	6.85	6.88	5.92	0.63	0.73	0.70
NA2O	0.24	1.90	1.35	1.32	1.45	8.13	8.28	7.31
K2O	0.25	1.43	0.88	0.83	0.66	0.72	0.59	0.42
MGO	0.65	1.25	6.66	6.62	10.07	0.33	0.28	0.35
CL	0.15	0.57	0.13	0.07	0.07	0.03	0.02	0.04
FEO	38.64	32.69	25.15	25.36	21.46	35.34	35.30	36.10
MNO	1.09	0.56	0.69	0.76	0.82	0.72	0.80	0.86
CR2O3	0.04	0.05	0.04	0.04	0.04	0.04	0.05	0.04
TIO2	0.08	2.23	1.56	1.60	1.22	0.86	0.60	0.25
BAO	0.07	0.08	0.05	0.13	0.02	0.08	0.08	0.04
F	0.08	0.80	0.78	0.73	0.56	2.12	2.15	2.13
CAO	8.45	10.42	10.73	10.39	10.34	0.83	0.52	0.67
P2O5	0.01	0.0	0.01	0.03	0.01	0.02	0.02	0.02
SRO	0.0	0.09	0.05	0.07	0.0	0.0	0.0	0.0
H2O	1.78	1.34	1.54	1.56	1.70	0.85	0.86	0.83
SUM	101.01	101.88	101.22	100.35	101.04	100.16	100.45	99.24
-O= F+CL	0.07	0.47	0.36	0.32	0.25	0.90	0.91	0.91
SUM	100.94	101.41	100.87	100.03	100.79	99.26	99.54	98.34

SI	7.796	*	6.530	*	6.919	*	6.882	*	7.060	*	8.061	*	8.122	*	8.128	*
AL	0.204	8.000	1.470	8.000	1.081	8.000	1.118	8.000	0.940	8.000	0.0	8.061	0.0	8.122	0.0	8.128
AL	0.033	*	0.090	*	0.164	*	0.145	*	0.113	*	0.121	*	0.139	*	0.135	*
TI	0.010	*	0.271	*	0.181	*	0.188	*	0.138	*	0.105	*	0.073	*	0.031	*
FE	5.210	*	4.418	*	3.245	*	3.305	*	2.709	*	4.803	*	4.765	*	4.949	*
MN	0.149	*	0.077	*	0.090	*	0.100	*	0.105	*	0.099	*	0.109	*	0.119	*
MG	0.156	5.558	0.301	5.156	1.531	5.211	1.538	5.276	2.266	5.330	0.080	5.208	0.067	5.153	0.086	5.320
CA	1.460	*	1.804	*	1.773	*	1.735	*	1.672	*	0.145	*	0.090	*	0.118	*
NA	0.075	*	0.595	*	0.404	*	0.399	*	0.424	*	2.562	*	2.591	*	2.323	*
K	0.051	*	0.295	*	0.173	*	0.165	*	0.127	*	0.149	*	0.121	*	0.088	*
SR	0.0	1.586	0.008	2.703	0.004	2.355	0.006	2.305	0.0	2.224	0.0	2.856	0.0	2.803	0.0	2.529
CL	0.041	*	0.156	*	0.034	*	0.018	*	0.018	*	0.008	*	0.005	*	0.011	*
F	0.041	*	0.409	*	0.381	*	0.360	*	0.267	*	1.090	*	1.098	*	1.104	*
H	1.915	1.998	1.444	2.009	1.585	1.999	1.622	2.000	1.712	1.997	0.922	2.019	0.926	2.029	0.908	2.023
O	24.000	*	24.000	*	24.000	*	24.000	*	24.000	*	24.000	*	24.000	*	24.000	*

17 82DNS210-SYENITE
18 82DNS210-SYENITE
19 82DNS197-HB GRANITE
20 82DNS197-HB GRANITE
21 83DNS322A-HB GRANITE
22 83DNS321-AF GRANITE
23 83DNS321-AF GRANITE
24 83DNS321-AF GRANITE

AMPHIBOLE ANALYSES

	25	26	27	28	29	30	31	32
SIO2	49.30	50.25	50.08	50.66	51.07	44.85	50.13	42.65
AL2O3	0.82	1.77	2.46	1.35	1.44	5.46	2.30	7.53
NA2O	6.79	0.37	0.49	0.25	0.26	0.29	0.27	1.64
K2O	0.41	0.18	0.19	0.14	0.14	1.96	0.23	1.24
MGO	0.39	10.78	10.72	10.82	10.78	8.68	10.09	2.66
CL	0.02	0.19	0.20	0.20	0.16	0.73	0.27	0.23
FEO	38.89	21.55	22.52	25.95	24.87	28.57	25.28	30.51
MNO	0.87	0.40	0.48	0.65	0.58	0.42	0.57	0.61
CR2O3	0.04	0.05	0.04	0.05	0.03	0.04	0.05	0.04
TIO2	0.11	0.37	0.42	0.27	0.23	1.10	0.32	1.76
BAO	0.06	0.07	0.06	0.02	0.06	0.16	0.07	0.12
F	2.20	0.22	0.12	0.11	0.14	0.10	0.16	0.43
CAO	0.50	11.13	10.44	7.61	8.74	6.75	8.33	10.30
P2O5	0.01	0.01	0.02	0.01	0.0	0.03	0.0	0.01
SRO	0.0	0.07	0.02	0.08	0.0	0.0	0.02	0.02
H2O	0.80	1.82	1.87	1.86	1.87	1.68	1.82	1.62
SUM	99.10	99.10	100.01	99.95	100.28	98.57	99.79	101.20
-O= F+CL	0.93	0.14	0.10	0.09	0.10	0.21	0.13	0.23
SUM	98.17	98.96	99.92	99.86	100.19	98.36	99.66	100.97

SI	6.109	*	7.651	*	7.571	*	7.716	*	7.724	*	7.103	*	7.645	*	6.780	*
AL	0.0	8.109	0.318	7.968	0.429	8.000	0.242	7.958	0.257	7.980	0.897	8.000	0.355	8.000	1.220	8.000
AL	0.159	*	0.0	*	0.009	*	0.0	*	0.0	*	0.122	*	0.059	*	0.191	*
TI	0.014	*	0.042	*	0.048	*	0.031	*	0.026	*	0.131	*	0.037	*	0.210	*
FE	5.074	*	2.744	*	2.847	*	3.305	*	3.146	*	3.519	*	3.224	*	4.058	*
MN	0.121	*	0.052	*	0.061	*	0.084	*	0.074	*	0.056	*	0.074	*	0.082	*
MG	0.096	5.464	2.446	5.284	2.416	5.382	2.456	5.877	2.430	5.676	2.049	5.877	2.294	5.687	0.682	5.000
CA	0.068	*	1.816	*	1.691	*	1.242	*	1.416	*	1.145	*	1.361	*	1.754	*
NA	2.165	*	0.109	*	0.144	*	0.074	*	0.076	*	0.089	*	0.080	*	0.505	*
K	0.086	*	0.035	*	0.037	*	0.027	*	0.027	*	0.396	*	0.045	*	0.251	*
SR	0.0	2.340	0.008	1.968	0.002	1.873	0.007	1.350	0.0	1.519	0.0	1.630	0.002	1.487	0.002	2.512
CL	0.008	*	0.049	*	0.051	*	0.052	*	0.041	*	0.196	*	0.070	*	0.062	*
F	1.144	*	0.108	*	0.057	*	0.053	*	0.067	*	0.050	*	0.077	*	0.216	*
H	0.878	2.028	1.848	2.003	1.886	1.995	1.890	1.994	1.887	1.995	1.754	2.000	1.852	1.999	1.718	2.000
O	24.000	*	24.000	*	24.000	*	24.000	*	24.000	*	24.000	*	24.000	*	24.000	*

25 83DNS321-AF GRANITE
26 83DNS320D-DIORITE
27 83DNS320D-DIORITE
28 83DNS320D-DIORITE
29 83DNS320D-DIORITE
30 83DNS320D-DIORITE
31 83DNS320D-DIORITE
32 82DNS75D-HB GRANITE

AMPHIBOLE ANALYSES

	1	2	3	4	5	6	7	8
SIO2	49.94	50.98	46.82	42.78	43.24	45.68	45.09	45.24
TIO2	0.65	0.44	1.54	1.72	1.62	1.69	1.65	1.56
AL2O3	4.33	3.06	6.07	9.05	7.93	8.87	8.92	8.67
FEO	18.84	19.32	23.72	26.17	27.24	17.26	17.22	17.36
MNO	0.32	0.30	0.45	0.45	0.45	0.70	0.64	0.68
MGO	11.97	11.31	8.04	5.66	5.05	11.15	11.08	10.84
CAO	11.69	12.30	10.47	10.07	10.32	11.70	11.70	11.70
BAO	0.06	0.13	0.06	0.06	0.09	0.04	0.07	0.06
NA2O	0.68	0.38	1.84	1.89	1.93	1.17	1.21	1.11
K2O	0.33	0.24	0.70	1.26	1.28	1.13	1.11	1.10
F	0.32	0.18	1.15	1.39	1.21	0.26	0.18	0.22
CL	0.0	0.0	0.0	0.0	0.0	0.0	0.0	0.0
H2O	1.88	1.93	1.45	1.28	1.35	1.90	1.93	1.90
SUM	101.01	100.57	102.33	101.78	101.71	101.55	100.80	100.44
-O= F+CL	0.13	0.08	0.48	0.59	0.51	0.11	0.08	0.09
SUM	100.88	100.49	101.85	101.19	101.20	101.44	100.72	100.35

SI	7.372	*	7.583	*	7.066	*	6.634	*	6.746	*	6.751	*	6.719	*	6.768	*
AL	0.628	8.000	0.437	8.000	0.934	8.000	1.366	8.000	1.254	8.000	1.249	8.000	1.281	8.000	1.232	8.000
AL	0.126	*	0.098	*	0.146	*	0.288	*	0.204	*	0.296	*	0.285	*	0.296	*
TI	0.072	*	0.049	*	0.175	*	0.201	*	0.190	*	0.188	*	0.185	*	0.175	*
FE	2.326	*	2.397	*	2.994	*	3.394	*	3.554	*	2.133	*	2.146	*	2.172	*
MN	0.040	*	0.038	*	0.058	*	0.059	*	0.059	*	0.088	*	0.081	*	0.086	*
MG	2.634	5.197	2.501	5.083	1.809	5.180	1.308	5.249	1.174	5.183	2.456	5.181	2.461	5.158	2.417	5.147
CA	1.849	*	1.955	*	1.693	*	1.673	*	1.725	*	1.853	*	1.868	*	1.875	*
NA	0.195	*	0.109	*	0.538	*	0.568	*	0.584	*	0.335	*	0.350	*	0.322	*
K	0.062	*	0.045	*	0.135	*	0.249	*	0.255	*	0.213	*	0.211	*	0.210	*
BA	0.003	2.109	0.008	2.117	0.005	2.371	0.004	2.494	0.006	2.569	0.002	2.403	0.004	2.433	0.004	2.411
CL	0.0	*	0.0	*	0.0	*	0.0	*	0.0	*	0.0	*	0.0	*	0.0	*
F	0.149	*	0.084	*	0.549	*	0.682	*	0.597	*	0.122	*	0.085	*	0.104	*
H	1.851	2.001	1.910	1.994	1.460	2.009	1.324	2.006	1.405	2.002	1.873	1.995	1.919	2.003	1.896	2.000
O	24.000	*	24.000	*	24.000	*	24.000	*	24.000	*	24.000	*	24.000	*	24.000	*

1 84DNS39A-GABBRO
2 84DNS47C-DIORITE
3 84DNS34A-HB GRANITE
4 84DNS57A-DIORITE
5 84DNS57A-HB GRANITE
6 84DNS44A-GABBRO
7 84DNS44A-GABBRO
8 84DNS44A-GABBRO

AMPHIBOLE ANALYSES

	9	10	11	12	13	14	15	16
SIO2	45.60	41.71	41.92	41.82	41.49	41.78	41.81	44.19
TIO2	1.22	1.93	1.92	1.99	1.99	2.11	2.01	0.83
AL2O3	8.59	8.01	7.85	7.88	8.00	8.22	8.12	5.77
FEO	16.94	29.97	29.87	31.22	30.70	30.72	30.25	32.22
MNO	0.71	0.48	0.47	0.52	0.45	0.54	0.48	0.52
MGO	11.39	2.84	2.83	2.28	2.76	2.61	2.77	2.48
CAO	11.79	10.29	10.35	10.44	10.44	10.44	10.38	10.20
BAO	0.09	0.12	0.05	0.13	0.08	0.11	0.03	0.04
NA2O	1.00	1.61	1.76	1.58	1.39	1.66	1.68	1.12
K2O	0.92	1.29	1.28	1.19	1.25	1.24	1.23	1.24
F	0.23	1.01	1.16	0.95	0.82	1.16	1.16	0.53
CL	0.0	0.0	0.0	0.0	0.0	0.0	0.0	0.0
H2O	1.90	1.40	1.33	1.43	1.49	1.35	1.34	1.62
SUM	100.38	100.66	100.79	101.43	100.88	101.94	101.26	100.76
-O= F+CL	0.10	0.43	0.49	0.40	0.35	0.49	0.49	0.22
SUM	100.28	100.23	100.30	101.03	100.51	101.45	100.77	100.54

SI	6.802	*	6.678	*	6.702	*	6.677	*	6.642	*	6.629	*	6.659	*	7.072	*
AL	1.198	8.000	1.322	8.000	1.298	8.000	1.323	8.000	1.358	8.000	1.371	8.000	1.341	8.000	0.928	8.000
AL	0.312	*	0.189	*	0.181	*	0.160	*	0.151	*	0.165	*	0.183	*	0.160	*
TI	0.137	*	0.232	*	0.231	*	0.239	*	0.240	*	0.252	*	0.241	*	0.100	*
FE	2.113	*	4.013	*	3.994	*	4.169	*	4.110	*	4.076	*	4.029	*	4.312	*
MN	0.090	*	0.065	*	0.084	*	0.070	*	0.081	*	0.073	*	0.065	*	0.070	*
MG	2.532	5.184	0.678	5.176	0.674	5.144	0.543	5.180	0.659	5.221	0.617	5.183	0.658	5.176	0.592	5.233
CA	1.884	*	1.765	*	1.773	*	1.786	*	1.791	*	1.775	*	1.771	*	1.749	*
NA	0.289	*	0.500	*	0.546	*	0.489	*	0.431	*	0.511	*	0.519	*	0.347	*
K	0.175	*	0.263	*	0.261	*	0.242	*	0.255	*	0.251	*	0.250	*	0.253	*
BA	0.005	2.354	0.008	2.536	0.003	2.583	0.008	2.526	0.005	2.482	0.007	2.543	0.002	2.542	0.003	2.352
CL	0.0	*	0.0	*	0.0	*	0.0	*	0.0	*	0.0	*	0.0	*	0.0	*
F	0.109	*	0.511	*	0.587	*	0.480	*	0.415	*	0.582	*	0.584	*	0.268	*
H	1.891	1.999	1.495	2.007	1.419	2.005	1.523	2.003	1.591	2.006	1.429	2.011	1.424	2.008	1.729	1.998
O	24.000	*	24.000	*	24.000	*	24.000	*	24.000	*	24.000	*	24.000	*	24.000	*

9 84DNS44A-GABBRO
10 84DNS32A-SUBSOLVUS SYENITE
11 84DNS32A-SUBSOLVUS SYENITE
12 84DNS32A-SUBSOLVUS SYENITE
13 84DNS32A-SUBSOLVUS SYENITE
14 84DNS32B-SUBSOLVUS SYENITE
15 84DNS32B-SUBSOLVUS SYENITE
16 84DNS32B-SUBSOLVUS SYENITE

AMPHIBOLE ANALYSES

	17	18	19	20
SIO2	50.86	49.95	51.68	51.03
TIO2	0.89	0.89	0.47	0.39
AL2O3	1.06	1.06	0.81	0.64
FEO	34.25	35.06	34.65	36.26
MNO	0.70	0.76	0.65	0.65
MGO	1.00	0.89	1.10	0.01
CAO	1.25	1.55	2.49	0.22
BAO	0.04	0.10	0.07	0.11
NA2O	6.22	6.06	5.73	7.51
K2O	0.66	0.54	0.73	1.05
F	1.44	1.83	1.15	1.94
CL	0.0	0.0	0.0	0.0
H2O	1.20	1.00	1.35	0.96
SUM	99.57	99.69	100.86	100.77
-O= F+CL	0.61	0.77	0.48	0.82
SUM	98.96	98.92	100.38	99.95

SI	8.152	*	8.070	*	8.175	*	8.210	*
AL	0.0	8.152	0.0	8.070	0.0	8.175	0.0	8.210
AL	0.200	*	0.202	*	0.151	*	0.121	*
TI	0.107	*	0.108	*	0.056	*	0.047	*
FE	4.591	*	4.737	*	4.586	*	4.879	*
MN	0.095	*	0.104	*	0.087	*	0.089	*
MG	0.239	5.232	0.214	5.365	0.259	5.139	0.002	5.138
CA	0.215	*	0.268	*	0.422	*	0.038	*
NA	1.933	*	1.898	*	1.758	*	2.343	*
K	0.135	*	0.111	*	0.147	*	0.215	*
BA	0.003	2.285	0.006	2.284	0.004	2.332	0.007	2.603
CL	0.0	*	0.0	*	0.0	*	0.0	*
F	0.730	*	0.935	*	0.576	*	0.987	*
H	1.283	2.013	1.078	2.013	1.425	2.001	1.030	2.018
O	24.000	*	24.000	*	24.000	*	24.000	*

17 82DNS162-AF GRANITE
18 82DNS162-AF GRANITE
19 82DNS162-AF GRANITE
20 84DNS61A-AF GRANITE

BIOTITE ANALYSES

	1	2	3	4	5	6	7	8
SIO2	34.93	35.73	35.78	38.03	37.77	38 25	36.68	36.75
AL2O3	10.11	8.67	13.22	14.25	12.34	7 02	13.06	13.01
NA2O	0.00	0.02	0.03	1.15	0.10	0 27	0.07	0.30
K2O	8.88	8.48	9.23	7 63	9.42	8.50	9.14	9.04
MGO	0.53	0 69	6.85	19.75	10.13	0.45	9.16	10 83
CL	1.56	0.69	0.20	0 03	0.13	0 09	0.18	0 04
FEO	39.59	41.25	26.85	8 09	22.83	39.53	23.87	20 87
MNO	0.30	0.40	0.31	0 04	0 31	0.73	0.14	0.15
CR2O3	0.06	0.07	0.04	0.03	0.05	0.05	0.06	0.03
TIO2	2.34	1.39	4.30	6.27	4.60	0.33	5.65	6.19
BAO	0.27	0.09	0.14	0.47	0.39	0.12	0.83	1.06
F	0.16	0.10	1.20	0.26	1.08	3.54	0.36	0.72
CAO	0.08	0.08	0.09	0.02	0.06	0.14	0.09	0.06
P2O5	0.01	0.01	0.01	0.00	0.02	0.00	0 01	0 01
SRO	0.00	0.01	0.00	0.10	0.00	0.00	0.09	0.00
H2O	3.11	3.33	3.21	4.04	3.41	1.90	3.73	3.63
SUM	101.86	100.92	101.41	100.03	102.57	100.87	102.96	102.65
-O= F+CL	0.42	0.20	0.55	0 12	0.48	1.51	0.19	0.31
SUM	101.44	100.72	100.86	99.91	102.09	99.36	102.77	102.34

SI	5.854	*	6.033	*	5.606	*	5 465	*	5 728	*	6.481	*	5 566	*	5.535	*
AL	1 996	7.850	1.725	7.758	2.394	8.000	2.413	7.877	2.205	7.934	1.402	7.882	2.335	7.901	2.309	7.844
AL	0.0	*	0.0	*	0.047	*	0 0	*	0 0	*	0 0	*	0 0	*	0 0	*
TI	0.295	*	0.176	*	0.507	*	0.678	*	0.525	*	0 042	*	0 645	*	0.701	*
FE	5.548	*	5.824	*	3.518	*	0.972	*	2.896	*	5.601	*	3.029	*	2.629	*
MN	0.043	*	0.057	*	0.041	*	0.005	*	0.040	*	0.105	*	0 018	*	0 019	*
MG	0.132	6.018	0.174	6.232	1.600	5.713	4.230	5.884	2 290	5.750	0.114	5.862	2.072	5.763	2.431	5.780
CA	0.014	*	0 014	*	0.015	*	0 003	*	0.010	*	0 025	*	0.015	*	0 010	*
NA	0.0	*	0.007	*	0 009	*	0.320	*	0 029	*	0 089	*	0 021	*	0 088	*
K	1.898	*	1 826	*	1.845	*	1.398	*	1 822	*	1.837	*	1 769	*	1.737	*
BA	0.018	1.930	0 006	1.853	0.009	1.877	0.026	1.748	0.023	1.885	0.008	1.959	0 049	1.854	0.063	1.896
CL	0.443	*	0.197	*	0.053	*	0.007	*	0.033	*	0 026	*	0.046	*	0 010	*
F	0.085	*	0.053	*	0.595	*	0.118	*	0.518	*	1 897	*	0.173	*	0.343	*
H	3.477	4.005	3.751	4.001	3.355	4.003	3.873	3.998	3.450	4.001	2.147	4.070	3.776	3.995	3.647	4.000
O	24.000	*	24.000	*	24.000	*	24.000	*	24.000	*	24.000	*	24.000	*	24.000	*

1 82DNS210-SUBSOLVUS SYENITE
2 82DNS210-SUBSOLVUS SYENITE
3 82DNS197-HB GRANITE
4 82DNS186-GABBRO
5 83DNS322A-HB GRANITE
6 83DNS321D-AF GRANITE
7 83DNS320D-DIORITE
8 83DNS320D-DIORITE

BIOTITE ANALYSES

	9
SIO2	37.82
AL2O3	14.85
NA2O	0.75
K2O	8.76
MGO	17.95
CL	0.04
FEO	10.95
MNO	0.06
CR2O3	0.07
TIO2	4.91
BAO	0.27
F	0.56
CAO	0.03
P2O5	0.0
SRO	0.03
H2O	3.86
SUM	100.81
-O= F+CL	0.24
SUM	100.56

SI	5.485	*
AL	2.515	8.000
AL	0.022	*
TI	0.535	*
FE	1.328	*
MN	0.007	*
MG	3.880	5.773
CA	0.005	*
NA	0.211	*
K	1.620	*
BA	0.015	1.851
CL	0 010	*
F	0.257	*
H	3.734	4.001
O	24.000	*

9 82DNS196-GABBRO

BIOTITE ANALYSES

	1	2	3	4	5	6	7	8
SIO2	36.15	35.69	36.42	36.95	36.63	36 09	36.24	35.64
TIO2	6.27	6.31	5.88	7.02	6.74	7.04	5.21	5.03
AL2O3	14.29	14.50	14.30	13.77	13.80	14.04	14.16	14.18
FEO	21.72	21.61	20.68	19.73	19.88	21.40	22.10	21.68
MNO	0.13	0.13	0.11	0.12	0 09	0 11	0.17	0.13
MGO	9.65	9.73	10.50	10.52	10 80	9 40	9.89	10.10
CAO	0.04	0.03	0.06	0.03	0.03	0.04	0.04	0.09
BAO	1.25	1.48	0.81	0.67	0.50	0.94	0 71	0.50
NA2O	0.18	0.17	0.13	0.21	0.23	0 14	0.07	0.10
K2O	8.68	8.74	8.83	8.92	8.91	8.81	8.99	8.78
F	0.44	0.38	0.25	0.39	0 43	0.45	0.56	0.66
CL	0.0	0.0	0.0	0.0	0 0	0 0	0.0	0.0
H2O	3.77	3.78	3.86	3.83	3.79	3.76	3.68	3.59
SUM	102.57	102.55	101.83	102.16	101 83	102.22	101.82	100.48
-O= F+CL	0.19	0.16	0.11	0.16	0 18	0.19	0.24	0.28
SUM	102.38	102.39	101.72	102.00	101.65	102.03	101.58	100.20

SI	5.451	*	5.395	*	5.483	*	5.519	*	5.493	*	5 447	*	5 505	*	5.475	*
AL	2.539	7.990	2.583	7.978	2.517	8.000	2.424	7.943	2.438	7.931	2 497	7.944	2 495	8 000	2.525	8.000
AL	0 0	*	0 0	*	0.020	*	0 0	*	0 0	*	0 0	*	0 039	*	0 042	*
TI	0.711	*	0 717	*	0 666	*	0.789	*	0 760	*	0 799	*	0 595	*	0 581	*
FE	2.739	*	2.732	*	2 604	*	2 465	*	2.493	*	2.701	*	2 807	*	2.785	*
MN	0.017	*	0.017	*	0.014	*	0 015	*	0 011	*	0 014	*	0 022	*	0 017	*
MG	2.169	5.635	2.192	5.659	2.356	5.659	2.342	5.611	2.414	5.678	2 115	5.629	2 239	5.702	2 313	5.738
CA	0.006	*	0 005	*	0 010	*	0 005	*	0 005	*	0 006	*	0 007	*	0 015	*
NA	0.053	*	0 050	*	0 038	*	0 061	*	0 067	*	0 041	*	0 021	*	0 030	*
K	1.669	*	1 685	*	1 696	*	1.699	*	1.704	*	1 696	*	1 742	*	1.720	*
BA	0.074	1.802	0.088	1.828	0.048	1.791	0.039	1.804	0 029	1.805	0 056	1.799	0 042	1 811	0 030	1.795
CL	0.0	*	0.0	*	0.0	*	0.0	*	0.0	*	0 0	*	0 0	*	0.0	*
F	0.210	*	0.182	*	0.119	*	0.184	*	0 204	*	0 215	*	0 269	*	0 321	*
H	3.792	4.002	3.812	3.994	3.876	3.996	3 816	4.001	3 791	3.995	3.786	4 000	3 729	3 998	3.679	4 000
O	24.000	*	24.000	*	24 000	*	24.000	*	24.000	*	24.000	*	24 000	*	24.000	*

1 84DNS34D-GABBRO
2 84DNS34D-GABBRO
3 84DNS34D-GABBRO
4 84DND34D-GABBRO
5 84DNS34D-GABBRO
6 84DNS34D-GABBRO
7 84DNS39A-GABBRO
8 84DNS39AGABBRO

BIOTITE ANALYSES

	9	10	11	12	13	14	15	16
SIO2	36.37	37.70	37 56	37.81	36 79	36.33	37.14	35.22
TIO2	5.01	4.97	6.08	4.57	6 51	5.69	5.35	2.25
AL2O3	14.14	13.85	13.85	13.75	13.86	13 82	13.59	12.35
FEO	21.09	20.23	19.68	21 43	20.71	24 81	25 11	35 30
MNO	0.10	0.16	0 13	0.18	0 12	0 25	0 20	0 42
MGO	10.51	11.57	11.22	11 02	10 37	7 58	7 62	1.97
CAO	0.11	0 04	0 02	0 08	0.03	0.06	0 05	0 12
BAO	0.55	0.19	0.54	0 10	1 41	1.19	0 22	0 18
NA2O	0.09	0.09	0.14	0 09	0.18	0 13	0 10	0 0
K2O	8.76	9.28	9.08	9 10	8.65	8.72	9.07	8.20
F	0.47	0.44	0 48	0 53	0.46	0.78	0.94	0.26
CL	0.0	0 0	0 0	0 0	0 0	0 0	0.0	0 0
H2O	3.70	3.82	3.81	3.76	3.79	3.56	3.51	3.52
SUM	100.90	102.34	102.59	102.42	102.88	102 92	102.90	99.79
-O= F+CL	0.20	0.19	0.20	0.22	0.19	0.33	0.40	0.11
SUM	100.70	102.15	102.39	102.20	102.69	102.59	102.50	99.68

SI	5.533	*	5.612	*	5.576	*	5.647	*	5.505	*	5.545	*	5.638	*	5.787	*
AL	2.467	8.000	2.388	8.000	2.423	7.998	2.353	8.000	2.444	7.948	2.455	8.000	2 362	8.000	2.213	8.000
AL	0.068	*	0.041	*	0.0	*	0.066	*	0.0	*	0 031	*	0 069	*	0.179	*
TI	0.573	*	0.556	*	0 679	*	0 513	*	0.732	*	0.653	*	0.611	*	0 278	*
FE	2.683	*	2.518	*	2.443	*	2.676	*	2.591	*	3.167	*	3.188	*	4.851	*
MN	0.013	*	0.020	*	0.016	*	0 023	*	0 015	*	0.032	*	0 026	*	0 058	*
MG	2.383	5.720	2.567	5.704	2.483	5.621	2.453	5.732	2.313	5.652	1.724	5.608	1.724	5.617	0 482	5.848
CA	0.018	*	0.006	*	0.003	*	0 013	*	0 005	*	0.010	*	0.008	*	0.021	*
NA	0.027	*	0.026	*	0.040	*	0.026	*	0.052	*	0 038	*	0.029	*	0.0	*
K	1.700	*	1.762	*	1.719	*	1.733	*	1.651	*	1 698	*	1 756	*	1.719	*
BA	0.033	1.777	0.011	1.805	0.031	1.794	0 006	1.778	0.083	1.790	0.071	1.817	0 013	1.807	0.012	1.751
CL	0.0	*	0.0	*	0.0	*	0.0	*	0.0	*	0.0	*	0 0	*	0.0	*
F	0.226	*	0.207	*	0.225	*	0.250	*	0.218	*	0.377	*	0 451	*	0 135	*
H	3.755	3.981	3.793	4.000	3.773	3.998	3.746	3.996	3.783	4.001	3.625	4.001	3.554	4.006	3.858	3.994
O	24.000	*	24.000	*	24.000	*	24.000	*	24.000	*	24.000	*	24.000	*	24.000	*

9 84DNS39A-GABBRO
10 84DNS47C-DIORITE
11 84DNS47C-DIORITE
12 84DNS47C-DIORITE
13 84DNS47C-DIORITE
14 84DNS34A-HB GRANITE
15 84DNS34A-HB GRANITE
16 84DNS32A-SUBSOLVUS SYENITE

BIOTITE ANALYSES

	17	18	19
SIO2	40.33	40.03	38.46
TIO2	3.73	4.13	4.32
AL2O3	6.71	6.77	12.88
FEO	35.99	35.89	22.34
MNO	0.42	0.44	0.08
MGO	0.08	0.10	11.13
CAO	0.07	0.07	0.06
BAO	0.04	0.09	0.27
NA2O	0.24	0.18	0.09
K2O	8.38	8.55	8.85
F	3.03	3.25	0.98
CL	0.0	0.0	0.0
H2O	2.27	2.18	3.56
SUM	101.29	101.68	103.02
-O= F+CL	1.28	1.37	0.41
SUM	100.01	100.31	102.61

SI	6.596	*	6.539	*	5.738	*
AL	1.293	7.889	1.303	7.842	2.262	8.000
AL	0.0	*	0.0	*	0.003	*
TI	0.459	*	0.507	*	0.485	*
FE	4.923	*	4.903	*	2.787	*
MN	0.058	*	0.061	*	0.010	*
MG	0.020	5.459	0.024	5.495	2.475	5.760
CA	0.012	*	0.012	*	0.010	*
NA	0.076	*	0.057	*	0.026	*
K	1.748	*	1.781	*	1.684	*
BA	0.003	1.839	0.006	1.856	0.016	1.736
CL	0.0	*	0.0	*	0.0	*
F	1.567	*	1.679	*	0.462	*
H	2.477	4.044	2.375	4.054	3.543	4.006
O	24.000	*	24.000	*	24.000	*

17 84DNS61A-AF GRANITE
18 84DNS61A-AF GRANITE
19 84DNS39C-GABBRO

PLAGIOCLASE ANALYSES

	1	2	3	4	5	6	7	8
SIO2	54.07	60.49	58.97	55.19	60.00	59.44	56.50	57.33
TIO2	0.10	0.03	0.05	0.10	0.05	0.04	0.05	0.03
AL2O3	29.48	25.66	26.03	29.12	25.75	25.66	27.93	27.55
FEO	0.10	0.15	0.08	0.14	0.11	0.06	0.04	0.06
MNO	0.0	0.0	0.0	0.0	0.0	0.0	0.0	0.0
MGO	0.01	0.0	0.01	0.02	0.0	0.02	0.01	0.0
CAO	11.45	6.61	7.10	10.86	6.75	7.09	9.64	9.01
BAO	0.04	0.02	0.0	0.10	0.01	0.06	0.02	0.0
NA2O	4.99	7.62	7.08	5.37	6.57	6.65	5.46	6.02
K2O	0.28	0.23	0.48	0.28	0.43	0.43	0.32	0.33
SUM	100.52	100.81	99.80	101.18	99.67	99.45	99.97	100.33

SI	2.433	*		2.672	*		2.637	*		2.464	*		2.673	*		2.661	*		2.535	*		2.560	*	
AL	1.563	*		1.335	*		1.372	*		1.532	*		1.352	*		1.354	*		1.477	*		1.450	*	
TI	0.003	3.999		0.001	4.008		0.002	4.011		0.003	3.999		0.002	4.027		0.001	4.016		0.002	4.013		0.001	4.011	
FE	0.004	*		0.006	*		0.003	*		0.005	*		0.004	*		0.002	*		0.002	*		0.002	*	
MN	0.0	*		0.0	*		0.0	*		0.0	*		0.0	*		0.0	*		0.0	*		0.0	*	
MG	0.001	*		0.0	*		0.001	*		0.001	*		0.0	*		0.001	*		0.001	*		0.0	*	
CA	0.552	*		0.313	*		0.340	*		0.519	*		0.322	*		0.340	*		0.463	*		0.431	*	
BA	0.001	*		0.0	*		0.0	*		0.002	*		0.0	*		0.001	*		0.0	*		0.0	*	
NA	0.435	*		0.653	*		0.614	*		0.465	*		0.568	*		0.577	*		0.475	*		0.521	*	
K	0.016	1.009		0.013	0.984		0.027	0.985		0.016	1.008		0.024	0.918		0.025	0.947		0.018	0.959		0.019	0.973	
O	8.000	*		8.000	*		8.000	*		8.000	*		8.000	*		8.000	*		8.000	*		8.000	*	

1 84DNS34D-GABBRO
2 84DNS34D-GABBRO
3 84DNS34D-GABBRO
4 84NDS34D-GABBRO
5 84DNS39A-GABBRO
6 84DNS39A-GABBRO
7 84DNS47C-DIORITE
8 84DNS47C-DIORITE

PLAGIOCLASE ANALYSES

	9	10	11	12	13	14	15	16
SIO2	59.79	62.24	52.59	61.90	64.11	64.04	58.70	62.45
TIO2	0.01	0.02	0.03	0.0	0.01	0.02	0.02	0.03
AL2O3	26.54	25.22	28.51	24.55	23.93	23.93	26.76	24.13
FEO	0.08	0.07	0.07	0.06	0.01	0.04	0.11	0.21
MNO	0.0	0.0	0.0	0.0	0.0	0.0	0.0	0.0
MGO	0.0	0.0	0.01	0.0	0.0	0.0	0.0	0.0
CAO	7.66	6.05	15.46	5.45	4.70	4.60	8.25	5.48
BAO	0.13	0.08	0.0	0.03	0.0	0.08	0.0	0.06
NA2O	7.02	7.90	3.45	7.60	8.39	8.94	6.33	7.36
K2O	0.26	0.25	0.10	0.31	0.20	0.16	0.34	0.41
SUM	101.49	101.83	100.21	99.90	101.35	101.81	100.51	100.13

SI	2.631	*		2.714	*		2.395	*		2.742	*		2.790	*		2.782	*		2.609	*		2.759	*	
AL	1.376	*		1.296	*		1.530	*		1.281	*		1.227	*		1.225	*		1.402	*		1.256	*	
TI	0.0	4.007		0.001	4.010		0.001	3.926		0.0	4.023		0.0	4.017		0.001	4.008		0.001	4.011		0.001	4.017	
FE	0.003	*		0.003	*		0.003	*		0.002	*		0.0	*		0.001	*		0.004	*		0.008	*	
MN	0.0	*		0.0	*		0.0	*		0.0	*		0.0	*		0.0	*		0.0	*		0.0	*	
MG	0.0	*		0.0	*		0.001	*		0.0	*		0.0	*		0.0	*		0.0	*		0.0	*	
CA	0.361	*		0.283	*		0.754	*		0.259	*		0.219	*		0.214	*		0.393	*		0.259	*	
BA	0.002	*		0.001	*		0.0	*		0.001	*		0.0	*		0.001	*		0.0	*		0.001	*	
NA	0.599	*		0.668	*		0.305	*		0.653	*		0.708	*		0.753	*		0.545	*		0.630	*	
K	0.015	0.980		0.014	0.968		0.006	1.069		0.018	0.931		0.011	0.939		0.009	0.979		0.019	0.962		0.023	0.922	
O	8.000	*		8.000	*		8.000	*		8.000	*		8.000	*		8.000	*		8.000	*		8.000	*	

9 84DNS34A-HB GRANITE
10 84DNS34A-HB GRANITE
11 84DNS34A-HB GRANITE
12 84DNS34A-HB GRANITE
13 84DNS34A-HB GRANITE
14 84DNS34A-HB GRANITE
15 84DNS57A-HB GRANITE
16 84DNS39C-GABBRO

PLAGIOCLASE ANALYSES

	1	2	3	4	5	6	7	8
SIO2	68.14	65.04	65.68	64.62	64.64	64.99	54.88	62.92
AL2O3	19.16	20.99	21.42	21.47	21.44	21.26	28.31	22.56
NA2O	9.96	9.37	9.56	9.27	8.26	8.59	4.27	6.92
K2O	0.11	1.14	0.69	0.66	0.91	0.84	0.13	0.22
MGO	0.0	0.04	0.02	0.04	0.04	0.04	0.18	0.06
CL	0.01	0.0	0.0	0.0	0.0	0.0	0.0	0.0
FEO	0.42	0.14	0.13	0.15	0.16	0.13	0.17	0.10
MNO	0.0	0.0	0.0	0.0	0.01	0.01	0.10	0.02
CR2O3	0.0	0.01	0.0	0.0	0.0	0.02	0.09	0.03
TIO2	0.0	0.04	0.03	0.02	0.01	0.01	0.07	0.03
BAO	0.0	0.0	0.0	0.02	0.01	0.09	0.11	0.01
F	0.0	0.01	0.0	0.01	0.02	0.04	0.02	0.04
CAO	0.0	2.19	2.34	2.77	2.86	2.51	10.82	4.19
P2O5	0.0	0.0	0.01	0.0	0.01	0.02	0.0	0.02
SRO	0.0	0.0	0.0	0.02	0.03	0.0	0.07	0.0
SUM	97.81	98.98	99.88	99.07	98.40	98.47	99.13	97.04

SI	3.025	*		2.898	*		2.894	*		2.875	*		2.887	*		2.898	*		2.490	*		2.838	*	
AL	1.002	*		1.102	*		1.112	*		1.126	*		1.128	*		1.117	*		1.513	*		1.199	*	
TI	0.0	4.027		0.001	4.001		0.001	4.007		0.001	4.001		0.0	4.016		0.0	4.018		0.002	4.006		0.001	4.038	
FE	0.018	*		0.005	*		0.005	*		0.006	*		0.006	*		0.005	*		0.006	*		0.004	*	
MN	0.0	*		0.0	*		0.0	*		0.0	*		0.0	*		0.0	*		0.004	*		0.001	*	
MG	0.0	*		0.003	*		0.001	*		0.003	*		0.003	*		0.003	*		0.012	*		0.004	*	
CA	0.0	*		0.105	*		0.110	*		0.132	*		0.137	*		0.120	*		0.526	*		0.202	*	
BA	0.0	*		0.0	*		0.0	*		0.0	*		0.0	*		0.002	*		0.002	*		0.0	*	
NA	0.857	*		0.809	*		0.817	*		0.800	*		0.715	*		0.743	*		0.376	*		0.605	*	
K	0.006	*		0.065	*		0.039	*		0.037	*		0.052	*		0.048	*		0.008	*		0.013	*	
SR	0.0	0.879		0.0	0.986		0.0	0.972		0.001	0.978		0.001	0.914		0.0	0.920		0.002	0.935		0.0	0.829	
O	8.000	*		8.000	*		8.000	*		8.000	*		8.000	*		8.000	*		8.000	*		8.000	*	

1 82DNS195C-AF GRANITE
2 82DNS210-SUBSOLVUS SYENITE
3 82DNS210-SUBSOLVUS SYENITE
4 82DNS210-SUBSOLVUS SYENITE
5 82DNS210-SUBSOLVUS SYENITE
6 82DNS210-SUBSOLVUS SYENITE
7 82DNS197-HB GRANITE
8 82DNS197-HB GRANITE

PLAGIOCLASE ANALYSES

	9	10	11	12	13	14	15	16
SIO2	62.99	60.36	60.85	61.93	52.08	49.70	50.91	49.22
AL2O3	22.81	24.19	24.50	23.54	30.90	29.74	31.58	31.07
NA2O	7.14	6.38	6.88	7.31	3.18	2.35	2.74	2.50
K2O	0.29	0.22	0.18	0.26	0.06	0.07	0.07	0.08
MGO	0.07	0.10	0.10	0.07	0.26	0.33	0.30	0.27
CL	0.0	0.0	0.0	0.0	0.0	0.0	0.0	0.0
FEO	0.11	0.12	0.12	0.09	0.11	0.12	0.09	0.16
MNO	0.01	0.03	0.0	0.03	0.02	0.04	0.03	0.02
CR2O3	0.0	0.03	0.03	0.0	0.03	0.02	0.0	0.0
TIO2	0.0	0.03	0.01	0.02	0.08	0.08	0.10	0.12
BAO	0.09	0.04	0.03	0.03	0.06	0.04	0.01	0.05
F	0.01	0.01	0.0	0.0	0.03	0.04	0.0	0.02
CAO	4.18	5.96	6.02	4.89	13.35	16.93	14.29	14.20
P2O5	0.01	0.0	0.02	0.0	0.01	0.04	0.0	0.02
SRO	0.03	0.0	0.04	0.15	0.11	0.14	0.07	0.13
SUM	97.73	97.44	98.74	98.34	100.22	99.55	100.23	97.82

SI	2.829	*		2.736	*		2.726	*		2.779	*		2.354	*		2.294	*		2.309	*		2.290	*	
AL	1.207	*		1.292	*		1.294	*		1.245	*		1.646	*		1.617	*		1.688	*		1.704	*	
TI	0.0	4.035		0.001	4.030		0.0	4.020		0.001	4.024		0.003	4.003		0.003	3.914		0.003	4.000		0.004	3.998	
FE	0.004	*		0.005	*		0.004	*		0.003	*		0.004	*		0.005	*		0.003	*		0.006	*	
MN	0.0	*		0.001	*		0.0	*		0.001	*		0.001	*		0.002	*		0.001	*		0.001	*	
MG	0.005	*		0.007	*		0.007	*		0.005	*		0.018	*		0.023	*		0.020	*		0.019	*	
CA	0.201	*		0.289	*		0.289	*		0.235	*		0.647	*		0.837	*		0.694	*		0.708	*	
BA	0.002	*		0.001	*		0.001	*		0.001	*		0.001	*		0.001	*		0.0	*		0.001	*	
NA	0.622	*		0.561	*		0.598	*		0.636	*		0.279	*		0.210	*		0.241	*		0.226	*	
K	0.017	*		0.013	*		0.010	*		0.015	*		0.003	*		0.004	*		0.004	*		0.005	*	
SR	0.001	0.851		0.0	0.873		0.001	0.910		0.004	0.899		0.003	0.955		0.004	1.085		0.002	0.966		0.004	0.968	
O	8.000	*		8.000	*		8.000	*		8.000	*		8.000	*		8.000	*		8.000	*		8.000	*	

9 82DNS197-HB GRANITE
10 82DNS197-HB GRANITE
11 82DNS197-HB GRANITE
12 82DNS197-HB GRANITE
13 82DNS186-GABBRO
14 82DNS186-GABBRO
15 82DNS186-GABBRO
16 82DNS186-GABBRO

PLAGIOCLASE ANALYSES

	17	18	19	20	21	22	23	24
SIO2	52.79	54.32	59.18	55.87	59.77	60.20	55.82	56.00
AL2O3	28.48	28.49	25.33	27.46	25.15	24.72	27.51	27.76
NA2O	3.67	4.48	6.18	4.98	6.85	6.78	5.15	5.48
K2O	0.20	0.22	0.47	0.42	0.30	0.44	0.34	0.34
MGO	0.20	0.19	0.14	0.17	0.11	0.12	0.18	0.20
CL	0.0	0.0	0.0	0.0	0.0	0.0	0.0	0.0
FEO	0.17	0.15	0.12	0.18	0.15	0.19	0.17	0.16
MNO	0.0	0.0	0.0	0.02	0.0	0.02	0.0	0.0
CR2O3	0.03	0.0	0.0	0.0	0.0	0.03	0.04	0.0
TIO2	0.05	0.10	0.09	0.08	0.01	0.03	0.08	0.06
BAO	0.05	0.01	0.0	0.08	-0.02	0.0	0.05	0.05
F	0.02	0.01	0.01	0.01	0.0	0.0	0.0	0.01
CAO	11.21	10.98	7.24	9.61	6.82	6.54	9.72	9.78
P2O5	0.0	0.0	0.01	0.01	0.02	0.01	0.0	0.04
SRO	0.07	0.06	0.14	0.21	0.03	0.14	0.09	0.10
SUM	96.90	99.02	98.90	99.09	99.20	99.19	99.13	99.96

SI	2.452	*		2.471	*		2.664	*		2.534	*		2.679	*		2.699	*		2.530	*		2.521	*	
AL	1.559	*		1.527	*		1.344	*		1.468	*		1.329	*		1.306	*		1.469	*		1.473	*	
TI	0.002	4.013		0.003	4.002		0.003	4.010		0.003	4.004		0.0	4.008		0.001	4.006		0.003	4.002		0.002	3.996	
FE	0.007	*		0.006	*		0.005	*		0.007	*		0.006	*		0.007	*		0.006	*		0.006	*	
MN	0.0	*		0.0	*		0.0	*		0.001	*		0.0	*		0.001	*		0.0	*		0.0	*	
MG	0.014	*		0.013	*		0.009	*		0.011	*		0.007	*		0.008	*		0.012	*		0.013	*	
CA	0.558	*		0.535	*		0.349	*		0.467	*		0.328	*		0.314	*		0.472	*		0.472	*	
BA	0.001	*		0.0	*		0.0	*		0.001	*		0.0	*		0.0	*		0.001	*		0.001	*	
NA	0.331	*		0.395	*		0.539	*		0.438	*		0.595	*		0.589	*		0.453	*		0.478	*	
K	0.012	*		0.013	*		0.027	*		0.024	*		0.017	*		0.025	*		0.020	*		0.020	*	
SR	0.002	0.923		0.002	0.963		0.004	0.933		0.006	0.955		0.001	0.953		0.004	0.948		0.002	0.966		0.003	0.993	
O	8.000	*		8.000	*		8.000	*		8.000	*		8.000	*		8.000	*		8.000	*		8.000	*	

17 82DNS209-DIORITE
18 82DNS209-DIORITE
19 82DNS209-DIORITE
20 82DNS209-DIORITE
21 82DNS209-DIORITE
22 82DNS209-DIORITE
23 82DNS209-DIORITE
24 82DNS209-DIORITE

PLAGIOCLASE ANALYSES

	25	26	27	28	29	30	31	32
SIO2	59.49	54.29	59.81	59.85	55.99	69.05	58.13	58.31
AL2O3	25.68	28.74	25.21	25.41	28.26	19.13	26.45	25.97
NA2O	7.28	4.96	7.47	7.28	5.46	10.43	5.28	5.46
K2O	0.38	0.18	0.28	0.30	0.27	0.14	0.38	0.63
MGO	0.14	0.18	0.11	0.12	0.18	0.0	0.14	0.15
CL	0.0	0.0	0.0	0.0	0.0	0.0	0.0	0.0
FEO	0.26	0.14	0.08	0.11	0.11	0.84	0.15	0.17
MNO	0.0	0.0	0.0	0.0	0.0	0.01	0.02	0.02
CR2O3	0.01	0.02	0.03	0.0	0.0	0.01	0.0	0.01
TIO2	0.04	0.09	0.0	0.02	0.03	0.0	0.06	0.03
BAO	0.04	0.04	0.0	0.04	0.05	0.03	0.10	0.17
F	0.02	0.01	0.01	0.04	0.01	0.0	0.02	0.02
CAO	7.10	11.01	6.77	6.83	10.01	0.0	8.20	7.73
P2O5	0.0	0.0	0.01	0.0	0.0	0.0	0.0	0.0
SRO	0.0	0.09	0.04	0.0	0.0	0.0	0.25	0.19
SUM	100.41	99.74	99.77	100.00	100.39	99.66	99.17	98.84

SI	2.647	*		2.458	*		2.671	*		2.667	*		2.509	*		3.022	*		2.615	*		2.633	*	
AL	1.346	*		1.533	*		1.327	*		1.334	*		1.492	*		0.986	*		1.402	*		1.382	*	
TI	0.001	3.994		0.003	3.994		0.0	3.998		0.001	4.001		0.001	4.002		0.0	4.008		0.002	4.019		0.001	4.016	
FE	0.010	*		0.005	*		0.003	*		0.004	*		0.004	*		0.031	*		0.006	*		0.006	*	
MN	0.0	*		0.0	*		0.0	*		0.0	*		0.0	*		0.0	*		0.001	*		0.001	*	
MG	0.009	*		0.012	*		0.007	*		0.008	*		0.012	*		0.0	*		0.009	*		0.010	*	
CA	0.338	*		0.534	*		0.324	*		0.326	*		0.481	*		0.0	*		0.395	*		0.374	*	
BA	0.001	*		0.001	*		0.0	*		0.001	*		0.001	*		0.001	*		0.002	*		0.003	*	
NA	0.628	*		0.435	*		0.647	*		0.629	*		0.474	*		0.885	*		0.461	*		0.478	*	
K	0.022	*		0.010	*		0.016	*		0.017	*		0.015	*		0.008	*		0.022	*		0.036	*	
SR	0.0	1.007		0.002	1.000		0.001	0.998		0.0	0.985		0.0	0.988		0.0	0.924		0.007	0.902		0.005	0.914	
O	8.000	*		8.000	*		8.000	*		8.000	*		8.000	*		8.000	*		8.000	*		8.000	*	

25 82DNS209-DIORITE
26 83DNS322A-HB GRANITE
27 83DNS322A-HB GRANITE
28 83DNS322A-HB GRANITE
29 83DNS322A-HB GRANITE
30 83DNS321-AF GRANITE
31 83DNS320D-DIORITE
32 83DNS320D-DIORITE

PLAGIOCLASE ANALYSES

	33	34	35	36	37	38	39	40
SIO2	54.27	59.80	54.69	56.79	57.03	63.67	66.04	65.88
AL2O3	28.41	25.34	28.68	27.39	27.06	22.17	21.98	21.04
NA2O	4.29	6.57	4.64	5.56	5.75	8.48	8.59	8.43
K2O	0.33	0.52	0.30	0.34	0.10	0.22	0.29	0.55
MGO	0.19	0.11	0.20	0.17	0.18	0.06	0.04	0.03
CL	0.0	0.0	0.0	0.0	0.0	0.0	0.0	0.0
FEO	0.14	0.10	0.14	0.13	0.11	0.13	0.16	0.07
MNO	0.01	0.01	0.02	0.01	0.02	0.01	0.0	0.02
CR2O3	0.02	0.01	0.0	0.0	0.01	0.0	0.03	0.0
TIO2	0.10	0.05	0.09	0.05	0.06	0.0	0.0	0.0
BAO	0.11	0.20	0.11	0.15	0.02	0.0	0.03	0.01
F	0.01	0.04	0.03	0.03	0.02	0.01	0.0	0.02
CAO	10.51	6.53	10.63	8.96	8.64	2.93	3.08	2.26
P2O5	0.0	0.01	0.03	0.01	0.03	0.0	0.0	0.0
SRO	0.15	0.19	0.16	0.12	0.13	0.02	0.0	0.0
SUM	98.52	99.42	99.67	99.68	99.10	97.71	100.23	98.34

SI	2.479	*	2.677	*	2.473	*	2.555	*	2.572	*	2.857	*	2.889	*	2.927	*
AL	1.529	*	1.337	*	1.528	*	1.452	*	1.438	*	1.172	*	1.133	*	1.102	*
TI	0.003	4.012	0.002	4.016	0.003	4.004	0.002	4.008	0.002	4.012	0.0	4.030	0.0	4.022	0.0	4.029
FE	0.005	*	0.004	*	0.005	*	0.005	*	0.004	*	0.005	*	0.006	*	0.003	*
MN	0.0	*	0.0	*	0.001	*	0.0	*	0.001	*	0.0	*	0.0	*	0.001	*
MG	0.013	*	0.007	*	0.013	*	0.011	*	0.012	*	0.004	*	0.003	*	0.002	*
CA	0.514	*	0.313	*	0.515	*	0.432	*	0.417	*	0.141	*	0.144	*	0.108	*
BA	0.002	*	0.004	*	0.002	*	0.003	*	0.0	*	0.0	*	0.001	*	0.0	*
NA	0.380	*	0.570	*	0.407	*	0.485	*	0.503	*	0.738	*	0.729	*	0.726	*
K	0.019	*	0.030	*	0.017	*	0.020	*	0.006	*	0.013	*	0.016	*	0.031	*
SR	0.004	0.938	0.005	0.933	0.004	0.965	0.003	0.959	0.003	0.947	0.001	0.901	0.0	0.899	0.0	0.871
O	8.000	*	8.000	*	8.000	*	8.000	*	8.000	*	8.000	*	8.000	*	8.000	*

33 83DNS320D-DIORITE
34 83DNS320D-DIORITE
35 83DNS320D-DIORITE
36 83DNS320D-DIORITE
37 82DNS196-GABBRO
38 82DNS75D-HB GRANITE
39 82DNS75D-HB GRANITE
40 82DNS75D-HB GRANITE

PLAGIOCLASE ANALYSES

	41
SIO2	70.70
AL2O3	18.57
NA2O	8.62
K2O	0.08
MGO	0.01
CL	0.0
FEO	0.03
MNO	0.0
CR2O3	0.0
TIO2	0.05
BAO	0.02
F	0.04
CAO	0.85
P2O5	0.03
SRO	0.01
SUM	98.94

SI	3.079	*
AL	0.953	*
TI	0.002	4.033
FE	0.001	*
MN	0.0	*
MG	0.001	*
CA	0.040	*
BA	0.0	*
NA	0.728	*
K	0.004	*
SR	0.0	0.774
O	8.000	*

41 82DNS75D-HB GRANITE

ALKALI FELDSPAR ANALYSES

	1		2		3		4		5		6		7		8	
SIO2	64.59		63.61		65.17		66.29		65.61		67.72		68.62		65.45	
TIO2	0.05		0.04		0.04		0.02		0.04		0.01		0.01		0.03	
AL2O3	19.25		19.46		19.01		18.60		18.94		19.03		20.08		18.46	
FEO	0.0		0.02		0.01		0.02		0.05		0.17		0.35		0.13	
MNO	0.0		0.0		0.02		0.0		0.0		0.0		0.0		0.01	
MGO	0.0		0.0		0.0		0.0		0.0		0.0		0.0		0.0	
CAO	0.23		0.16		0.0		0.11		0.14		0.0		0.0		0.0	
BAO	0.91		0.91		0.88		0.15		0.33		0.02		0.0		0.0	
NA2O	2.11		1.76		0.33		2.82		2.25		6.43		9.39		0.36	
K2O	12.43		12.88		15.39		12.02		11.62		5.85		0.21		15.47	
SUM	99.57		98.84		100.85		100.03		98.98		99.23		98.66		99.91	
SI	2.972	*	2.957	*	2.988	*	3.012	*	3.005	*	3.023	*	3.013	*	3.011	*
AL	1.044	*	1.066	*	1.027	*	0.996	*	1.022	*	1.001	*	1.039	*	1.001	*
TI	0.002	4.018	0.001	4.024	0.001	4.016	0.001	4.009	0.001	4.029	0.000	4.025	0.000	4.053	0.001	4.013
FE	0.0	*	0.001	*	0.000	*	0.001	*	0.002	*	0.006	*	0.013	*	0.005	*
MN	0.0	*	0.0	*	0.001	*	0.0	*	0.0	*	0.0	*	0.0	*	0.0	*
MG	0.0	*	0.0	*	0.0	*	0.0	*	0.0	*	0.0	*	0.0	*	0.0	*
CA	0.011	*	0.008	*	0.0	*	0.005	*	0.007	*	0.0	*	0.0	*	0.0	*
BA	0.016	*	0.017	*	0.016	*	0.003	*	0.006	*	0.0	*	0.0	*	0.0	*
NA	0.188	*	0.159	*	0.029	*	0.248	*	0.200	*	0.557	*	0.799	*	0.032	*
K	0.730	0.946	0.764	0.948	0.900	0.946	0.697	0.954	0.679	0.893	0.333	0.897	0.012	0.821	0.908	0.946
O	8.000	*	8.000	*	8.000	*	8.000	*	8.000	*	8.000	*	8.000	*	8.000	*

1 84DNS47C-DIORITE
2 84DNS47C-DIORITE
3 84DNS34A-HB GRANITE
4 84DNS57A-HB GRANITE
5 84DNS32B-SUBSOLVUS SYENITE
6 82DNS162A-AF GRANITE
7 82DNS162A- AF GRANITE
8 84DNS61A-AF GRANITE

ALKALI FELDSPAR ANALYSES

	9	
SIO2	65.55	
TIO2	0.08	
AL2O3	20.20	
FEO	0.06	
MNO	0.0	
MGO	0.0	
CAO	0.89	
BAO	0.77	
NA2O	3.85	
K2O	9.39	
SUM	100.79	
SI	2.948	*
AL	1.070	*
TI	0.003	4.021
FE	0.002	*
MN	0.0	*
MG	0.0	*
CA	0.043	*
BA	0.014	*
NA	0.336	*
K	0.539	0.933
O	8.000	*

9 84DNS39C-GABBRO

ILMENITE ANALYSES

	1	2	3	4	5	6	7	8
SIO2	0.12	0.12	0.17	0.07	0.09	0.13	0.26	0.21
AL2O3	0.03	0.06	0.06	0.10	0.20	0.04	0.07	0.08
K2O	0.05	0.05	0.06	0.06	0.05	0.06	0.17	0.06
NA2O	0.02	0.01	0.02	0.02	0.03	0.05	0.05	0.01
MGO	0.10	0.07	0.05	0.13	0.34	0.20	0.05	0.03
FEO	47.14	47.37	47.11	46.65	47.14	46.63	45.31	47.36
TIO2	53.91	51.88	51.15	51.76	50.54	51.80	52.01	47.91
MNO	1.52	1.62	1.74	1.50	1.06	1.54	2.78	2.05
CL	0.0	0.0	0.0	0.0	0.0	0.0	0.0	0.0
BAO	0.39	0.38	0.32	0.43	0.33	0.45	0.42	0.37
CAO	0.10	0.09	0.13	0.11	0.10	0.11	0.18	0.20
F	0.07	0.08	0.16	0.14	0.12	0.12	0.19	0.20
SUM	102.80	101.09	100.24	100.25	99.38	100.32	100.40	97.63

TI	0.995	*	0.980	*	0.975	*	0.983	*	0.970	*	0.983	*	0.985	*	0.947	*
AL	0.001	0.996	0.002	0.982	0.002	0.977	0.003	0.986	0.006	0.976	0.001	0.984	0.002	0.987	0.002	0.950
MG	0.004	*	0.003	*	0.002	*	0.005	*	0.013	*	0.008	*	0.002	*	0.001	*
FE	0.968	*	0.995	*	0.998	*	0.985	*	1.007	*	0.984	*	0.954	*	1.041	*
MN	0.032	*	0.034	*	0.037	*	0.032	*	0.023	*	0.033	*	0.059	*	0.046	*
CA	0.003	1.006	0.002	1.034	0.004	1.041	0.003	1.025	0.003	1.045	0.003	1.027	0.005	1.020	0.006	1.094
O	3.000	*	3.000	*	3.000	*	3.000	*	3.000	*	3.000	*	3.000	*	3.000	*

1 84DNS34D-GABBRO
2 84DND34D-GABBRO
3 84DNS34D-GABBRO
4 84DNS39A-GABBRO
5 84DNS39A-GABBRO
6 84DNS47C-DIORITE
7 84DNS34A-HB GRANITE
8 84DNS57A-HB GRANITE

ILMENITE ANALYSES

	9	10	11	12	13
SIO2	0.11	0.08	0.08	0.09	0.08
AL2O3	0.03	0.03	0.02	0.04	0.03
NA2O	0.01	0.06	0.00	0.02	0.01
K2O	0.06	0.05	0.06	0.07	0.07
MGO	0.11	0.11	0.11	5.54	5.54
CL	0.01	0.02	0.01	0.01	0.01
FEO	46.51	46.86	47.52	40.61	39.34
MNO	1.90	2.11	1.75	0.70	0.73
CR2O3	0.07	0.07	0.09	0.21	0.23
TIO2	53.18	52.69	52.82	56.23	55.37
BAO	0.35	0.36	0.32	0.26	0.29
F	0.06	0.06	0.05	0.10	0.08
CAO	0.10	0.10	0.10	0.10	0.09
P2O5	0.04	0.03	0.03	0.0	0.02
SUM	101.85	101.91	102.34	103.22	101.10

TI	0.992	*	0.985	*	0.984	*	0.993	*	0.997	*
AL	0.001	0.993	0.001	0.986	0.001	0.985	0.001	0.994	0.001	0.997
MG	0.004	*	0.004	*	0.004	*	0.194	*	0.198	*
FE	0.965	*	0.974	*	0.985	*	0.798	*	0.787	*
MN	0.040	*	0.044	*	0.037	*	0.014	*	0.015	*
CA	0.003	1.012	0.003	1.028	0.003	1.028	0.003	1.008	0.002	1.002
O	3.000	*	3.000	*	3.000	*	3.000	*	3.000	*

9 82DNS195C-AF GRANITE
10 82DNS210-SYENITE
11 82DNS210-SYENITE
12 82DNS186-GABBRO
13 82DNS186-GABBRO

CHEVKINITE(?) ANALYSES
82DNS195C

	1	2
SIO2	18.30	18.20
AL2O3	0.19	0.16
NA2O	0.07	0.06
K2O	0.10	0.11
MGO	0.28	0.26
CL	0.03	0.03
FEO	11.81	12.34
MNO	0.33	0.42
CR2O3	0.23	0.23
TIO2	21.54	20.92
BAO	0.33	0.38
F	0.65	0.58
CAO	3.84	3.57
P2O5	0.08	0.10
SR3	0.0	0.09
SUM	57.14	56.74
-O= F+CL	0.28	0.25
SUM	56.86	56.49

PROBE ANALYSES FROM CONTACT ROCK CONTAINING BARIUM-RICH MICA
SAMPLE 82DNS151C, FROM MIDDLE FORK PLUTON AREA, ALASKA

PYROXENE ANALYSES

	82-151Cpyx	82-151Cpyx	82-151Cpyx
SIO2	49.77	50 02	51.15
TIO2	0.26	0.13	0.04
AL2O3	5.66	6.07	5.24
FEO	4.35	3 89	3.69
MNO	0.11	0.07	0.11
MGO	14.24	14 80	15.14
CAO	25.83	25.66	25.96
BAO	0.0	0.0	0 06
NA2O	0.03	0.03	0.02
K2O	0 01	0.01	0.01
F	0.08	0 08	0.08
CL	0.0	0.0	0.0
SUM	100.26	100.68	101.42

SI	1.835	*	1.830	*	1.856	*
AL	0.165	2.000	0.170	2.000	0.144	2.000
AL	0 081	*	0 092	*	0.080	*
TI	0.007	*	0 004	*	0.001	*
FE	0.134	*	0.119	*	0.112	*
MN	0 003	*	0.002	*	0.003	*
MG	0.783	1.008	0 807	1.024	0.819	1.015
CA	1.020	*	1.006	*	1 009	*
BA	0.0	*	0 0	*	0 001	*
O	6.000	*	6.000	*	6.000	*

OTHER PROBE ANALYSES FROM 82DNS151C

	82-151C spinel	82-151C spinel	82-151C "opaque"	82-151C calcite
SIO2	0.07	0.06	39.46	0.07
TIO2	0.04	0.04	0.04	0.01
AL2O3	63.98	63.94	0.14	0 0
FEO	14.03	12.14	17.32	0 0
MNO	0.33	0.21	0.75	0.03
MGO	19.76	21.69	10.59	0.16
CAO	0.07	0.09	27 26	52.23
BAO	0.0	0.05	0 02	0 02
NA2O	0.01	0 02	0 01	0 0
K2O	0 00	0 00	0 02	0 01
F	0.03	0.04	0.28	0 09
SUM	98.32	98.28	95.89	52.62

Appendix D. Analytical procedures

Major and trace element geochemistry

Samples analysed for bulk rock geochemistry at VPI&SU (ranging from 0.2 - 20 kg, depending of grain size and availability) were carefully cleaned of weathering rinds using sledgehammer and/or water-lubricated rock saw. Specimens were preserved for hand sample and thin sections. The remaining sample was crushed, split using the cone and quarter method, and shattered in a tungsten carbide mill. Samples for mineral separates were rolled, and processed in heavy liquids (acetylene tetrabromide or methylene iodide), further separated with a Franz magnetic separator, and finally hand-picked for purity. Fused glass discs and pressed powder pellets were made from the same sample splits. Fused discs were analysed for all major elements but Na_2O ; pellets were analysed for Na_2O, Rb, Sr and Ba (Norrish and Chappell, 1977). Analyses were done on a Philips Sequential X-ray Analysis Spectrometer Model 1450 wavelength dispersive unit using the techniques of Norrish and Hutton (1969). Calibrations were done by H. Pendrak on 4/24/86 for major oxides and on 5/20/85 for trace elements, using USGS rock powder standards PCC-1, GSP-1, BCR-1, AVG-1 and G-2.

Whole rock samples in the Alaska Division of Geological and Geophysical Surveys, Fairbanks, Alaska laboratory, under the direction of Milton Wiltse, were also run on an XRF using the methods of Norrish and Hutton (1969). Of the nine samples which were run in both laboratories, results are within less than 3 % relative to each other for the major elements. Analysis of whole rock fluorine was done using wet chemical methods by X-Ray Assay Laboratories Ltd., Ontario, Canada.

Isotope geochemistry

Rb and Sr concentrations were determined on the XRF as described above. Mineral separates and samples containing less than 10 ppm Rb or Sr were reanalyzed using isotope dilution techniques. Rb and Sr isotopic compositions were measured on a 35 cm - radius solid source mass spectrometer interfaced to a PDP/1123+ minicomputer. Sample powders were dissolved in HF and HNO_3 acid in Savillex bombs; Sr and Rb were separated on bromide resin cation exchange columns, in a 2.5 N HCl solution. Concentrates were loaded on single rhenium filaments with phosphoric acid on a film of tantallum oxide. All Sr isotopic analyses were normallized to $^{86}Sr/^{88}Sr$ of 0.1194. The average measured Eimer and Amend $SrCO_3$ $^{87}Sr/^{86}Sr$ value over the period of analysis was 0.70813 $\pm$.00003. All analyses were adjusted by 0.99982 to correct to the absolute value of the Eimer and Amend value of 0.70800. Total blanks during the time of analysis were less than 800 pg Sr and 600 pg Rb.

Regressions were calculated according to the method of York (1969), using Model II ages and MSRS values. All standard errors of the mean are stated at the

two sigma confidence level. Age calculation were made using a ^{87}Rb decay constant of 1.42 x $10^{-11}yr^{-1}$ (Steiger and Jaeger, 1977).

Mineral chemistry

Mineral chemistry was analyzed using the ARL-SEMQ, 9-channel microprobe at VPI&SU, with accelerating voltage of 15 KeV and a 20 na beam current. Analytical methods are described in Solberg and Spear (1982). The data were reduced following the method of Bence and Albee (1968). The Fortran SUPERRECAL program (Rucklidge, 1971) was used to recalculate mineral compositions and H_2O content.

Mineral cathodoluminescence was observed on a Technosyn cold cathode luminescence microscope, using an accelerating voltage of 15 - 16 KeV, and a beam current of 350 - 450 μa.

Appendix E. Calculation of Bulk Distribution Coefficient (D)

Gabbro sample 82DNS196

$$D = \sum_{i=1}^{n} \omega_i K_{Di}$$

Mineral	Mode x	G =	ω
plagioclase	32	2.7	28.3
olivine	15	3.2	15.6
c-pyroxene	22	3.3	23.7
o-pyroxene	7	3.4	7.8
biotite	20	3.0	19.5
opaque	2	4.7	3.1
hornblende	2	3.1	2.0

D_K

$= (28.3x0.17) + (15.6x0.0068) + (23.7x0.038) +$

$(7.8x0.014) + (19.5x2.7) + (3.1x0.01) + (2.0x0.17)$

$= 0.5895$

(1.12 wt% K_2O in 82DNS196)/(X wt% K_2Oin parent liquid) $= 0.5895$

X = (1.90 wt% K_{2O} in parent liquid)(0.83) = 1.58 wt% K in parent liquid

D_{Rb}

$= (28.3x0.05) + (15.6x0.0) + (23.7x0.03) + (7.8x0.013) +$

$(19.5x3.06) + (3.1x0.0) + (2.0x0.2)$

$= 0.623$

(30.7 ppm Rb in 82DNS196)/(X ppm Rb in parent liquid) = 0.623

X = 49.27 ppm Rb in parent liquid

$(K/Rb)_{liquid}$

$= 320.68$

Appendix F. An occurrence of barium-rich micas from the Alaska Range

Introduction

The following paper, by D.N.Solie and S.-C.Su, has been published in American Mineralogist, 1987, volume 72, pages 995 - 999. It is included here complete as published.

Abstract

Two compositionally different groups of Ba-rich micas are present within one rock sample from the contact aureole of the Middle Fork plutonic complex, northwest Alaska Range. The more Ba-rich group has pale green to colorless pleochroism, up to 18 wt% BaO, and the average formula

$(Ba_{0.55}K_{0.40}Na_{0.03})(Mg_{2.57}Al_{0.16}Fe^{2+}_{0.23}Fe^{3+}_{0.04}Ti_{0.01})(Si_{2.24}Al_{1.76})O_{10.00}[(OH)_{1.30}F_{0.70}]$.

The other is pale brown to colorless, contains up to 13 wt % BaO, and has an average formula of

$(Ba_{0.40}K_{0.54}Na_{0.03})(Mg_{2.57}Al_{0.07}Fe^{2+}_{0.24}Ti_{0.10})(Si_{2.40}Al_{1.60})O_{10.00}[(OH)_{1.40}F_{0.60}]$.

Optically the two are similar, with $0° < 2V_x < 5°$ and birefringences of 0.018 (green mica) and 0.022 (brown mica). Compositionally, they most closely approximate the brittle mica kinoshitalite,

$(Ba_{0.58}K_{0.35}Na_{0.11}Ca_{0.01})(Mg_{2.06}Al_{0.22}Mn^{2+}_{0.52}Mn^{3+}_{0.21}Fe^{3+}_{0.05}Ti_{0.01})(Si_{2.05}Al_{1.95})O_{10.00}[(OH)_{1.61}F_{0.06}O_{0.33}]$.

However, in comparison with reported kinoshitalites, the Middle Fork specimens are not manganiferous, are considerably richer in Mg and Fe, and have different optical properties.

Geologic setting and petrography

The barian mica-bearing sample is from the southwest contact zone of the early Tertiary Middle Fork plutonic complex (Solie, 1983), where hedenbergite-fayalite-($\pm$ quartz) syenite intrudes thinly bedded Paleozoic calc-phyllites and marbles. Thin syenitic dikes and sills are abundant within the contact zone. The profoundly recrystallized contact rocks from which the micaceous sample was taken retain crude sedimentary layering. The presence of wollastonite in samples from within 10 m of the mica-bearing specimen is indicative of high temperature ($\geq$600°C) contact metamorphism (Harker and Tuttle, 1956; Greenwood, 1967). The pressure of contact metamorphism is probably about 1-2 kbar, based on estimated thickness of overlying stratigraphy (Bundtzen and Gilbert, 1983).

The green and white calc-silicate sample contains the barian micas, diopside, calcite (< 0.2 wt% MgO), green spinel (MgO > FeO), hematite, and alkali feldspar. Grain size of all the phases is fine to medium with some mica grains as large as 1 mm in diameter. Spinel occurs as inclusions in barian micas and diopside, diopside and calcite occur as symplectic intergrowths in some layers, and a semi-opaque al-

teration product is prevalent in areas of the rock. Texturally, both green and brown barian micas appear to be in equilibrium. Green mica comprises up to about ten modal percent of the sample and brown mica up to about two modal percent. Brown mica occurs as cores within some green mica grains, as rims around other green micas, and as monochromatic brown grains. In some cases, one side of a crystal is brown and the other side is green, with no apparent rimming relationship.

Analytical procedures

Electron microprobe analyses were performed on (001) cleavage surfaces of mineral separates using the ARL-SEMQ, 9-channel microprobe at Virginia Polytechnic Institute and State University. The data were reduced following the method of Bence and Albee (1968). Mineral separations were done using methylene iodide, were further cleaned by use of a magnetic separator, and then were hand-picked for purity. Spinel inclusions in micas were released by grinding and subsequently magnetically removed. Ferrous iron determinations were performed using Whipple's (1974) titration method, on 0.125 grams of green mica separate and 0.019 grams of brown mica separate. Precision of measurements is estimated to be better than ± 0.1 wt% FeO, based on replicate analyses of a whole rock sample and blanks. Ba concentrations in the whole rock were analyzed using X-ray fluorescence spectrometry on pelletized rock powders.

Composition and optical properties

Green mica

The pale green mica has an average compositional formula of

$(Ba_{0.55}K_{0.40}Na_{0.03})(Mg_{2.57}Al_{0.16}Fe_{0.27}Ti_{0.01})(Si_{2.24}Al_{1.76})O_{10.00}[(OH)_{1.30}F_{0.70}]$,

based on nine electron microprobe analyses of individual grains (Table 7) Included in the microprobe analytical scheme were Cr, Zn, Ni, P, Sr, Rb, Mn, and Cl. All were close to or below analytical detection limits. A ferrous iron determination on the bulk mica separate yielded 3.46 wt% FeO; that is, 86% of the average total iron by weight is Fe^{2+}.

The pleochroism of the green mica is weak, with a formula of X = colorless, Y = Z = pale green. The optic sign is (-), and $2V_x$ is between 0° and 5°. Refractive indices are $\alpha = 1.598(2)$, and $\beta \simeq \gamma = 1.615(2)$. Crystals commonly have pseudohexagonal form and a perfect (001) cleavage.

Brown mica

The brown mica has a lower Ba concentration than the green variety, with the average compositional formula of

$(Ba_{0.40}K_{0.54}Na_{0.03})(Mg_{2.57}Al_{0.07}Fe_{0.24}Ti_{0.10})(Si_{2.40}Al_{1.60})O_{10.00}[(OH)_{1.40}F_{0.60}]$,

based on nine electron microprobe analyses (Table 8). Titration of the bulk mineral separate yielded a ferrous iron content of 3.76 wt%. This is greater than the average total iron from the nine microprobe analyses, though some individual grains contain > 3.76 wt% total Fe. Thus, within the error of the iron determi-

Table 7. Representative green barium mica compositions

	1	2	3	4	5	6	7	8	9
SiO_2	27.66	27.74	27.88	28.00	28.27	28.12	28.09	27.90	28.15
TiO_2	0.20	0.20	0.18	0.13	0.15	0.14	0.17	0.19	0.21
Al_2O_3	20.13	20.71	20.22	20.41	20.12	19.95	20.17	20.14	20.19
FeO^x	4.29	4.13	3.81	4.20	4.03	3.63	4.40	4.23	3.50
MnO	0.15	0.17	0.17	0.16	0.15	0.13	0.18	0.18	0.12
MgO	21.22	21.78	21.45	21.29	21.73	21.81	21.20	21.30	22.02
CaO	0.09	0.08	0.08	0.08	0.08	0.09	0.08	0.09	0.07
BaO	17.59	17.24	17.40	17.01	17.73	18.24	17.32	16.99	18.06
Na_2O	0.13	0.11	0.15	0.16	0.20	0.14	0.17	0.18	0.12
K_2O	3.95	3.96	4.03	3.88	3.95	3.92	3.97	4.03	3.80
F	2.62	2.82	2.69	2.76	3.01	3.11	2.66	2.37	2.82
H_2O	2.50	2.46	2.49	2.47	2.38	2.32	2.51	2.63	2.46
Sum	99.43	100.21	99.42	99.39	100.53	100.29	99.80	99.23	100.33
FeO^x = Total Fe reported as FeO									
Si	4.465	4.421	4.483	4.490	4.503	4.502	4.504	4.489	4.488
Al^{IV}	3.535	3.579	3.517	3.510	3.497	3.498	3.496	3.511	3.512
Al^{VI}	0.294	0.310	0.314	0.348	0.279	0.265	0.315	0.308	0.282
Ti	0.024	0.024	0.022	0.016	0.018	0.017	0.020	0.023	0.025
Fe	0.579	0.550	0.512	0.563	0.537	0.486	0.590	0.569	0.467
Mn	0.021	0.023	0.023	0.022	0.020	0.018	0.024	0.025	0.016
Mg	5.106	5.173	5.141	5.089	5.159	5.204	5.067	5.108	5.233
Ca	0.016	0.014	0.014	0.014	0.014	0.015	0.014	0.016	0.012
Na	0.041	0.034	0.047	0.050	0.062	0.043	0.053	0.056	0.037
K	0.813	0.805	0.826	0.794	0.803	0.800	0.812	0.827	0.773
Ba	1.113	1.077	1.096	1.069	1.107	1.144	1.088	1.071	1.128
F	1.338	1.421	1.368	1.400	1.516	1.575	1.349	1.206	1.422
H	2.692	2.615	2.671	2.642	2.529	2.478	2.685	2.823	2.617

Note: Number of cations on the basis of 24 anions. H_2O was not analyzed but is added into total oxides based on the calculated mineral formula.

nation, essentially all of the iron is ferrous. Trace elements included in the microprobe analyses resulted in near or below analytical detection limits for Cr, Zn, Ni, P, Sr, Rb, Mn and Cl. The pleochroic scheme of the brown micas is X = colorless, Y = Z = pale brown. The $2V_x$ ranges from 0° to 5°, the optic sign is (-), and the refractive indices are $\alpha = 1.592(2)$, and $\beta \simeq \gamma = 1.614(2)$.

Discussion

The Ba-rich micas of this occurrence are compositionally and optically different from Ba-rich micas reported in nephelinites from Hawaii (Mansker et al., 1979), in pyroxene leucitites from the Alban Hills, Italy (Thompson, 1977), in manganese-rich contact rocks from the Noda-Tamagawa mine, Iwate Prefecture, Japan (Yoshii et al., 1973b), and from Kyoto Prefecture, Japan (Yoshii et al., 1973a). The latter two occurrences have been described as kinoshitalite. Yoshii and Maeda (1975) concluded from their study of physical and optical properties of the Ba-rich manganoan micas from Japan that the boundary between manganoan phlogopite and kinoshitalite is near the ratio Ba : K = 1 : 2; that is, kinoshitalite contains Ba $\geq$ 0.5 K. Using this criterion, both the green and brown micas of this study can be considered as kinoshitalite, since Ba : K = 1.37 : 1 for the green micas and 0.74 : 1 for the brown. However, when compared to the kinoshitalite from Japan, (Yoshii et al., 1973a,b; Yoshii and Maeda, 1975; Kato et al., 1979; Guggenheim and Kato, 1984) the Middle Fork micas are notably manganese deficient, and correspondingly higher in both Fe_{total} and MgO. Also, the Middle Fork specimens are richer in fluorine. Thus, the description of kinoshitalite as the barian analog of manganoan phlogopite (Yoshii et al., 1973b) is unsuitable

Table 8. Representative brown barium mica compositions.

	1	2	3	4	5	6	7	8	9
SiO_2	31.36	30.96	31.32	30.79	30.90	30.78	31.10	31.36	30.36
TiO_2	1.38	1.36	1.47	1.47	2.00	2.06	1.89	1.99	2.08
Al_2O_3	18.07	18.01	18.40	18.43	18.22	17.87	18.11	18.00	18.14
FeO^x	3.12	3.14	3.15	3.96	4.09	3.47	4.16	3.66	3.61
MnO	0.11	0.11	0.13	0.14	0.17	0.10	0.13	0.14	0.18
MgO	22.66	22.61	22.78	21.86	21.90	22.16	21.88	21.91	22.00
CaO	0.06	0.07	0.07	0.06	0.08	0.06	0.07	0.08	0.07
BaO	13.08	12.92	13.13	12.79	13.07	12.91	12.22	12.90	13.38
Na_2O	0.21	0.17	0.21	0.19	0.23	0.23	0.19	0.18	0.12
K_2O	5.48	5.40	5.33	5.39	5.37	5.38	5.53	5.46	5.12
F	2.54	2.38	2.17	2.42	2.49	2.25	2.68	2.31	2.52
H_2O	2.70	2.74	2.89	2.73	2.72	2.80	2.63	2.81	2.67
Sum	99.70	98.87	100.14	99.21	100.19	99.12	99.46	99.83	99.19
FeO^x = Total Fe reported as FeO									
Si	4.851	4.829	4.819	4.798	4.782	4.799	4.820	4.849	4.748
Al^{IV}	3.149	3.171	3.181	3.202	3.218	3.201	3.180	3.151	3.252
Al^{VI}	0.146	0.139	0.155	0.182	0.104	0.081	0.128	0.129	0.090
Ti	0.161	0.160	0.170	0.172	0.233	0.242	0.220	0.231	0.245
Fe	0.404	0.410	0.405	0.516	0.529	0.452	0.539	0.473	0.472
Mn	0.014	0.015	0.017	0.018	0.022	0.013	0.017	0.018	0.024
Mg	5.225	5.256	5.224	5.077	5.051	5.149	5.054	5.050	5.128
Ca	0.010	0.012	0.012	0.010	0.013	0.010	0.012	0.013	0.012
Na	0.063	0.051	0.063	0.057	0.069	0.070	0.057	0.054	0.036
K	1.081	1.074	1.046	1.071	1.060	1.070	1.093	1.077	1.021
Ba	0.793	0.790	0.792	0.781	0.792	0.789	0.742	0.782	0.820
F	1.243	1.174	1.056	1.193	1.219	1.109	1.314	1.130	1.246
H	2.786	2.851	2.966	2.838	2.808	2.912	2.719	2.899	2.785

Note: Number of cations on the basis of 24 anions. H_2O was not analyzed but is added into total oxides based on the calculated mineral formula.

when applied to the Middle Fork micas. They do, however, approximate the definition of kinoshitalite (Yoshii et al., 1973a) as being the magnesian analog of anandite [$BaFe_3(Si_3Fe^{3+})O_{10}(OH)S$] (Guggenheim, 1984).

The differences in optical properties among the various barian micas is apparent in Table 9. The $2V_x$ of the measured Japanese specimens is 23° to 25°. It is 0° to 5° in the Middle Fork samples. This is probably due to substitutions of Mg, Ti, and Fe for Mn in the octahedral sites of the Middle Fork micas. Color differences probably can be attributed to this substitution as well. The Japanese kinoshitalites are light yellowish brown (Yoshii and Maeda, 1975) or colorless (Yoshii et al., 1973a), whereas of the Middle Fork samples the less Ba-rich mica is light brown (not yellowish), and the more Ba-rich mica is a pale light green. These idiomatic colors, caused by transition-metal constituents, are a result of crystal-field transitions (Nassau, 1978).

The differences between the two Middle Fork micas are the different Ba : K ratios, the higher Ti content of the brown micas, and the greater Fe_{total} and Fe^{3+} contents of the green micas. It is probably the differences in Fe and Ti which lead to the color differences between the two compositions. Single grains in which both compositions (and colors) are present commonly have a sharp color interface. Electron microprobe analyses at this intersection yield intermediate compositions, probably as a result of averaging the two compositions under the electron beam, rather than a graded zonation between compositions. Within each composition, Ba distribution is homogeneous. Substitutions between the two groups appear to include the coupled substitution proposed by Mansker et al. (1979) and Yoshii et al. (1973b): $Ba^{2+} + Al^{(IV)3+} = K^+ + Si^{4+}$. The correlation coefficient for this substitution is -0.992, and charge balance is attained by the substitution of Al for Si in the tetrahedral sites. In contrast to the Hawaiian micas, however, Ti^{4+} concen-

Table 9. Comparison of optical properties with kinoshitalites from Japan.

	Green Ba-mica	Brown Ba-mica	Kinoshitalite	Kinoshitalite	
α	1.598(2)	1.592(2)	1.621	1.619	1.615(2)
β	1.616(2)	1.614(2)	1.639	1.633	1.630(2)
γ	1.616(2)	1.614(2)	1.641	1.635	1.630(2)
γ-α	0.018	0.022	0.020	0.016	0.015
2vx	0°	0-5°	25°	23°	very small
Absorption	X < Y = Z	X < Y = Z	X < Y≃Z	X < Y≃Z	colorless

[1] This study.

[2] Iwate Prefecture, Japan (Yoshii and Maeda, 1975).

[3] Kyoto Prefecture, Japan (Yoshii et al., 1973a).

tration is higher in the less Ba-rich Middle Fork micas, with a correspondingly lower Al^{3+} and Fe^{3+} content in the octahedral sites.

The lack of gradational composition change between the two Middle Fork micas is suggestive of a possible solvus relationship between them. However, it is not clear from the available data which of the compositional variables would be the controlling factor in such a relationship, if it exists. The different chemistries could simply reflect growth in small scale local environments of different bulk and/or fluid composition. The correlation of fluorine content with barium content in the micas (Figure 63) suggests that fluid composition may have been a controlling factor in the mica compositions.

Contrary to the suggestion that high pressure is requisite for high Ba content in micas (Shmakin, 1984), the Middle Fork micas probably formed at moderately low pressures (1 - 2 kbar). However, it does seem probable that high temperature is important in the formation of these Ba-micas. Indeed, Hatch et al. (1957) found the fluorine analog of kinoshitalite, $BaMg_3Al_2Si_2O_{10}F_2$, to have the highest melting temperature (about 1450°C) of any of their synthetically produced fluorine micas.

The Ba in the micas could have had either a magmatic source or it may originally have been present in the metasedimentary country rock. Within the adjacent Middle Fork plutonic complex, syenites, gabbros and late hornblende-biotite-granites have whole rock Ba contents > 1000 ppm. An alkali feldspar from the syenite has 0.33 wt% BaO; alkali feldspars from monzodiorites and a quartz monzonite have BaO up to 0.91 wt%. The adjacent syenite appears to have been a dry magma; there is no evidence from miarolitic cavities or pegmatites of barium concentration in any late stage magmatic fluids. If Ba were mobilized from the pluton into the surrounding contact aureole, it had to be dissolved and transported by hydrothermal fluids derived from the metasediments.

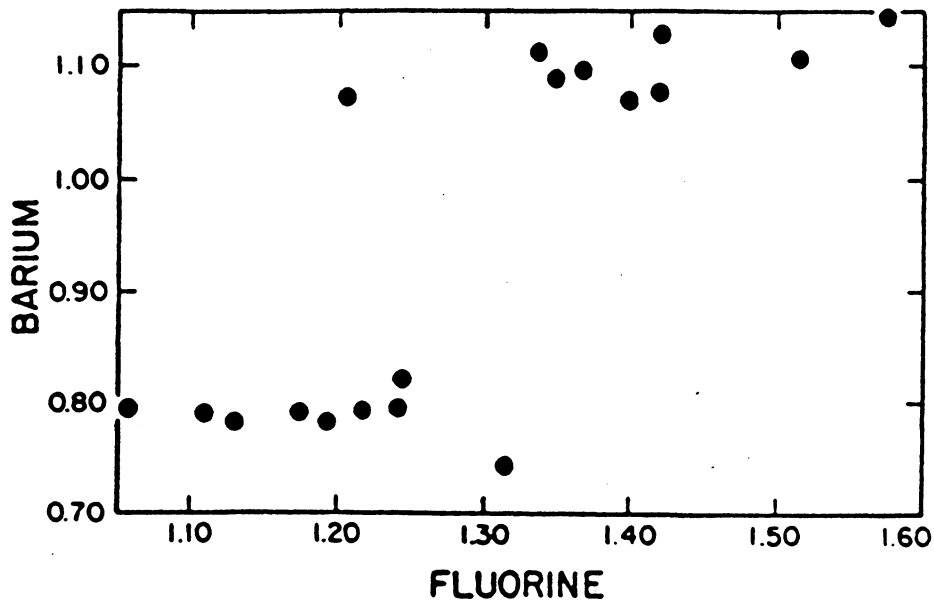

Figure 63. Atomic contents of Ba plotted against F, based on 24 anions: The more Ba-rich green micas are more F-rich than the brown micas, with little overlap in compositions.

Because the partition coefficient of Ba between alkali feldspar (the dominant Ba-bearing mineral in the plutonic rocks) and hydrothermal solution at 700-800°C strongly favors the feldspar (Carron and Lagache, 1980), it seems unlikely that the plutonic rocks were the source. Furthermore, in the presumably CO_2-rich fluids generated during contact metamorphism of calcareous sediments, the solubility of $BaCO_3$ decreases with increasing temperature (Holland and Malinin, 1979). Therefore, Ba mobilization is commonly considered to be negligible during metamorphism (Barbey and Cuney, 1982), and even during anatexis (Lee and Doering, 1974). It seems most likely that the source of Ba was within the metasediments of the contact zone. Country rocks surrounding the pluton which have not been recrystallized by contact metamorphism have been analyzed, and contain up to about 2000 ppm Ba, thus providing a viable source for the Ba.

Conclusion

Two different compositions of Ba-rich micas from the Alaska Range are present in apparent equilibrium in a contact-metamorphosed calcareous metasediment. Though most closely approximating the Ba-Mg-rich brittle mica kinoshitalite, the end-member composition of which has never been observed in nature, the specimens reported herein both have significantly different compositions and optical properties from previously reported barian micas. The Middle Fork samples have lower Mn, higher Mg, smaller $2V_x$, and different color than other known kinoshitalites. Petrologically, they seem to have formed at fairly high temperatures (≥600°C), but not necessarily at high pressure. The barium was probably present within the recrystallizing metasediments, and became incorpo-

rated into the micas as a function of very localized whole rock and fluid composition control during contact metamorphism.

Acknowledgments

Samples were collected for this study by D.N.S. during a regional mapping project of the Alaska Division of Geological and Geophysical Surveys. Support and encouragement from W.G. Gilbert, T.K. Bundtzen, and J.T. Kline are gratefully acknowledged. Whole rock and mineral analyses were done at VPI&SU. Thanks are due to T.N. Solberg for assistance on the microprobe, A.K. Sinha and F.D. Bloss for their helpful discussions, P.H. Ribbe and D.A. Hewitt for comments on early versions of this paper, and P. Cerny for his review.

References

Barbey, P. and Cuney, M. (1982) K, Rb, Sr, Ba, U and Th geochemistry of the Lapland granulites (Fennoscandia). LILE fractionation controlling factors. Contributions to Mineralogy and Petrology, 81, 304-316.

Bence, A.E. and Albee, A.L. (1968) Empirical correction factors for the electron microanalysis of silicates and oxides. Journal of Geology, 76, 382-403.

Bundtzen, T.K. and Gilbert, W.G. (1983) Outline of geology and mineral resources of upper Kuskokwim region, Alaska. In G. Mull and K. Reed, Eds., Western Alaska geology and resource potential. Journal of the Alaska Geological Society, 3, 101-117.

Carron, J.-P. and Lagache, M. (1980) Etude experimentale du fractionnement des elements Rb, Cs, Sr et Ba entre feldspaths alcalins, solutions hydrothermales et liquides silicates dans le systeme Q.Ab.Or.H_2O a 2 kbar entre 700 et 800°C. Bulletin de Mineralogie, 103, 571-578.

Greenwood, H.J. (1967) Wollastonite: stability in H_2O - CO_2 mixtures and occurrences in a contact-metamorphic aureole near Salmo, British Columbia, Canada. American Mineralogist, 52, 1669-1680.

Guggenheim, S. (1984) The brittle micas. In S.W. Bailey, Ed., Micas. Mineralogical Society of America, Reviews in Mineralogy, 13, 61-104.

Guggenheim, S. and Kato, T. (1984) Kinoshitalite and Mn phlogopites: trial refinements in subgroup symmetry and further refinement in ideal symmetry. Mineralogical Journal, 12, 1-5.

Harker, R.I. and Tuttle, O.F. (1956) Experimental data on the P_{CO2} - T curve for the reaction: calcite + quartz = wollastonite + carbon dioxide. American Journal of Science, 254, 239-256.

Hatch, R.A., Humphrey, R.A., Eitel, W. and Comeforo, J.E. (1957) Synthetic mica investigations IX: review of progress from 1947 to 1955. United States Bureau of Mines, R.I.5337.

Holland, H.D. and Malinin, S.D. (1979) The Solubility and Occurrence of Non-ore Minerals. In H.L. Barnes, Ed., Geochemistry of Hydrothermal Ore Deposits, 461-508. John Wiley & Sons, New York.

Kato, T., Miura,Y., Yoshii,M. and Maeda,K. (1979) The crystal structures of 1M-kinoshitalite, a new barium brittle mica and 1M-manganese trioctahedral micas. Mineralogical Journal, 9, 392-408.

Lee, D.E. and Doering, W.P. (1974) Barium in hybrid granitoid rocks of the southern Snake Range, Nevada. Journal of Research, United States Geological Survey, 2, 761-675.

Mansker, W.L., Ewing, R.C. and Keil, K. (1979) Barian-titanian biotites in nephelinites from Oahu, Hawaii. American Mineralogist, 64, 156-159.

Nassau, K. (1978) The origins of color in minerals. American Mineralogist, 63, 219-229.

Shmakin, B.M. (1984) Causes and consequences of high contents of barium in sheet muscovite and phlogopite. In Non-metallic Mineral Ores. Proceedings of the 27th International Geological Congress, Moscow, USSR, 261-271, VNU Science Press, Utrecht, The Netherlands.

Solie, D.N. (1983) The Middle Fork plutonic complex, McGrath A-3 quadrangle, southwest Alaska. Alaska Division of Geological and Geophysical Surveys, RI 83-16.

Thompson, R.N. (1977) Primary basalts and magma genesis. Contributions to Mineralogy and Petrology, 60, 91-108.

Whipple, E.R. (1974) A study of Wilson's determination of ferrous iron in silicates. Chemical Geology, 14, 223-238.

Yoshii, M. and Maeda,K. (1975) Relations between barium content and the physical and optical properties in the manganoan phlogopite-kinoshitalite series. Mineralogical Journal, 8, 58-65.

Yoshii, M., Maeda, K., Kato, T., Watanabe, T., Yui, S., Kato, A. and Nagashima, K. (1973a) Kinoshitalite, a new mineral from the Noda-Tamagawa mine, Iwate Prefecture. Chigaku Kenkyu, 24, 181-190. (not seen; extracted from New Mineral Names, American Mineralogist, 60, 486-487).

Yoshii,M., Togashi,Y. and Maeda,K. (1973b) On the intensity changes of basal reflections with relation to barium content in manganoan phlogopites and kinoshitalite. Bulletin of the Geological Society of Japan, 24, 543-550.

The vita has been removed from the scanned document

ALASKA DIVISION OF GEOLOGICAL & GEOPHYSICAL SURVEYS

PROFESSIONAL REPORT 92

Base by U.S. Geological Survey, 1958.

Bedrock geology by W.G. Gilbert, 1982-83, and T.N. Solie, 1982-86; surficial geology by J.T. Kline, 1982-83. Assisted by Kristin Kline, 1982; John Ebel and M.S. Lockwood, 1982; Daniel Solie, 1984; and K.H. Clautice, 1986. Cartography by A.G. Sturmann and G.M. Laird.

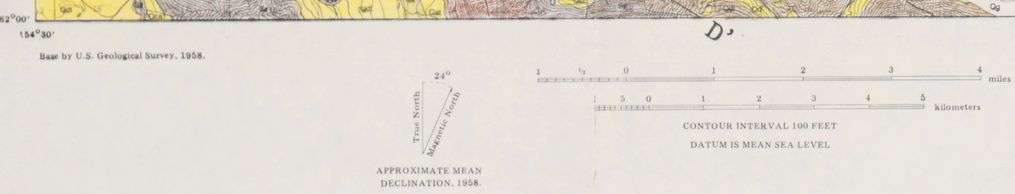

APPROXIMATE MEAN DECLINATION, 1958.

CORRELATION OF MAP UNITS

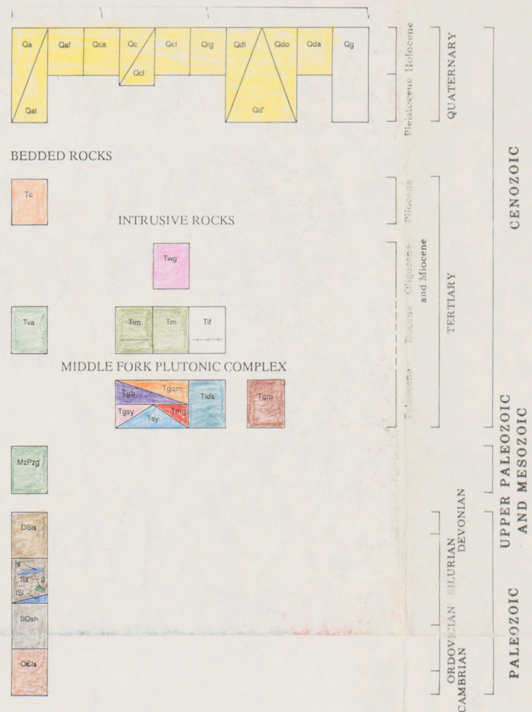

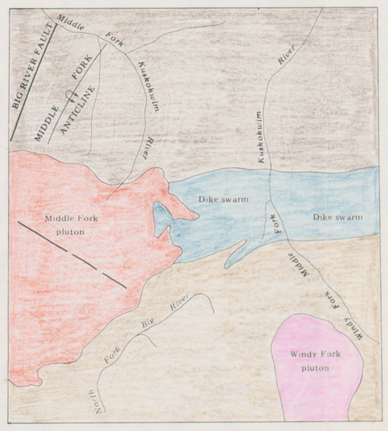

Figure 1. Major structural elements in McGrath A-3 Quadrangle, southwestern Alaska. Scale 1:25,000.

MAP SYMBOLS

- Contact
- High-angle fault - Dashed where inferred; dotted where concealed; queried where doubtful
- Thrust fault - Sawteeth on upper block; dashed where inferred
- Anticline, showing trace of axial plane
- Overturned anticline, showing trace of axial plane and direction of dip of limbs. Dotted where concealed
- Syncline, showing trace of axial plane. Dotted where concealed
- Overturned syncline, showing trace of axial plane and direction of dip of limbs. Dotted where concealed
- Minor fold axis, showing plunge of axial plane
- Strike and dip of beds - Commonly parallel to foliation
- Inclined
- Vertical
- Horizontal
- Overturned (lower limbs of Middle Fork and North Fork anticlines)
- Strike and dip of foliation in igneous rocks
- Strike and dip of joints in igneous rocks
- Fossil locality (table 2)
- K-Ar sample locality (table 3)
- Mineral prospect (table 4)

DESCRIPTION OF MAP UNITS

Qa — ALLUVIUM, UNDIFFERENTIATED—Fluvial silt, sand, and gravel that form fans, terraces, and flood plains. Thickness varies from a few feet to several tens of feet. (See table 1 for engineering properties.)

Qaf — TERRACE ALLUVIUM—Fluvial silt, sand, and gravel of various ages that compose fill and cut terraces; may also include strath terraces. In some places, mantled by an appreciable thickness of colluvial silt and a thick vegetation mat, especially where permafrost limits drainage. Older terrace deposits commonly contain highly weathered clasts in a silty matrix; thus the deposits may not be suitable as a source of construction materials. (See table 1 for engineering properties.)

Qaf — ALLUVIAL-FAN DEPOSITS—Poorly to moderately sorted fluvial silt, sand, and gravel that form deltoid fans where tributaries join higher order streams. In mountain trunk valleys, tend to be coarse grained and poorly sorted due to steep stream gradients and drastic seasonal fluctuations in stream energy. (See table 1 for engineering properties.)

Qca — COLLUVIAL-ALLUVIAL DEPOSITS—Poorly to moderately sorted silt, sand, gravel, and diamicton of colluvial and locally alluvial origin; commonly form alternating or interfingering stratified and unstratified lenses. Sediments usually issue from gulleys and steep minor tributaries with intermittent stream flow to form relatively small, steep fans along valley walls. Fans generally most active in early to late spring when intense freeze-thaw cycles produce copious meltwater. (See table 1 for engineering properties.)

Qc — COLLUVIUM, UNDIFFERENTIATED—Typically unconsolidated, unsorted deposits derived primarily from mass-wasting processes, such as creep and solifluction; earthflow, mudflow, and debris flow; and rockslide, snowslide, and rockfall. Includes primary products of bedrock erosion and retransported surficial deposits. Colluvium is widespread throughout quadrangle but is mapped only where appreciable thickness masks bedrock lithology and structure. (See table 1 for engineering properties.)

Qcl — LANDSLIDE DEPOSITS—Chaotically deformed colluvium derived from slow and continuous or sudden mass movement of bedrock or surficial deposits along planes of failure. Surface of landslide deposits are characteristically very hummocky and lack integrated drainages. Recent landslides show additional surface disturbances, such as randomly tilted trees and torn vegetation mats. Unit also includes rockfalls, which, in some cases, contain blocks to 40-ft (12-m) wide. In western part of quadrangle, where glacially oversteepened headwalls occur, rockfalls result from spalling along joints of massive rock.

Qct — TALUS—Angular, frost-riven bedrock transported by gravity down cirque headwalls, avalanche chutes, and steep slopes and gullies. Forms cones or aprons at or near angle of repose along valley walls. Distal ends may grade into rock glaciers.

Qrg — ROCK GLACIERS AND ROCK-GLACIER DEPOSITS—Unsorted, angular, frost-shattered cobbles and boulders, commonly containing considerable interstitial ice (up to 55 percent in active rock glaciers). Generally originate at 3,500 to 5,000 ft (1,100 to 1,500 m) in north-facing cirques and along steep valley walls of blocky-weathering, relatively resistant rock; may head in true glaciers or talus cones. Front of active rock glaciers very steep and unstable.

Qdt — TILL AND TILLITES—Unsorted to poorly sorted clay- to boulder-size material deposited directly by glacial ice; calcite locally cements older tills, forming tillite. Cobble and boulder clasts are commonly striated, subangular to subrounded, and polyhedrally faceted. On plateau in northwestern part of quadrangle, moraines locally contain permafrost and are overlain by thick accumulations of peat. (See table 1 for engineering properties.)

Qdf — THIN DRIFT OVER BEDROCK—Patchy, thin drift, including till and glaciofluvial deposits. Delineates former ice positions along valley walls but does not obscure underlying bedrock. Geochemical analyses of unit may be affected by presence of mineralized material moved long distances from parent sources.

Qdo — OUTWASH—Stratified drift consisting of coarse, subrounded gravel with sand and silt lenses and partings deposited by sidelacial and proglacial meltwater streams. Deposits tend to fine down valley from former side and terminal glacial positions. Distal part of outwash bodies typically interfinger or merge gradationally with other alluvial deposits. (See table 1 for engineering properties.)

Qda — ABANDONED OUTWASH-CHANNEL DEPOSITS—Moderately sorted sand and gravel deposits formed in channels that were cut into bedrock or drift by meltwater from glaciers of predominantly late Wisconsin age. Locally may be good source for small to moderate amounts of aggregate materials.

Qg — ACTIVE GLACIERS—Occur in cirques with base levels above 4,800 to 5,200 ft (1,500 to 1,600 m; elevations vary with aspect); termini are generally between 4,300 and 5,000 ft (1,300 to 1,500 m). Most glaciers in quadrangle appear to be in gradual retreat.

BEDDED ROCKS

Tc — CONGLOMERATE—Crudely stratified beds (15- to 50-ft thick; 5- to 15-m thick) of orange-weathering, gray-green, moderately indurated granule-pebble conglomerate. Composed of subangular, very poorly sorted clasts to 0.75-in. (2-cm) diam., with scattered (>5 percent), subrounded pebbles and cobbles to 3-in. (8-cm) diam. Unit locally derived, containing roughly equal amounts of igneous clasts from Tids unit and phyllitic calcareous-sandstone clasts from Ss unit. Unit occurs in fault sliver in northeastern part of T. 23 N., R. 27 W. Age uncertain but assigned to Tertiary by Herreid (1968) on basis of restricted occurrence and clast types.

Tva — ANDESITE FLOWS—Mafic to intermediate volcanic rocks in northeast corner of quadrangle. Display columnar jointing.

MzPzg — GREENSTONE—Altered, olive-green, locally schistose mafic volcanic flows, agglomerate, and tuff(?). Includes subordinate thin, lenticular beds of gray marble.

DSls — LIMESTONE, CALCAREOUS SANDSTONE, AND SHALE—Very thinly bedded, orange- to buff-weathering calcareous siltstone to fine-grained sandstone (30 percent); cross-bedded silty limestone (30 percent); and dark-gray phyllitic shale (30 percent). Includes scattered lenses of dark-gray laminated limestone to 6-ft (2-m) thick (5 percent) and fine- to medium-grained calcareous sandstone, as in Ss unit, to 6-ft (2-m) thick (5 percent). Isoclinally folded on all scales and commonly sheared. Equivalent to DSls unit of Bundtzen and others (1987) to the east and DSls and Dls units of Gilbert (1981) to the southwest. Top of unit not exposed in McGrath A-3 Quadrangle, but to east Bundtzen and others (1987) estimated unit reaches maximum thickness of 1,200 ft (400 m).

Ss — PHYLLITIC CALCAREOUS SANDSTONE—Very thinly to very thickly bedded, buff- to orange-weathering, gray to gray-green phyllitic calcareous sandstone; interbedded with lesser amounts of thinly laminated to thinly bedded, orange- to brown-weathering, black to gray or gray-green slate and phyllitic calcareous siltstone. Locally contains partings of thinly laminated, silver-weathering gray phyllite and intervals of very thinly to thinly bedded, gray silty limestone.

The phyllitic calcareous sandstone is a very fine to very coarse grained micaceous feldspathic litharenite (Folk, 1968) with abundant secondary minerals. Original detrital mineralogy and texture is evident in thin section in some samples (Gilbert and others, 1988), but the coarser clasts are commonly flattened and stretched. The sandstone displays pervasive foliation defined by elongate, partially recrystallized framework grains and cataclastic shear planes. In the north-central part of the quadrangle, the sandstone exhibits graded bedding, oscillation ripple marks, and planar cross-bedding. The phyllitic siltstone commonly grades into the calcareous sandstone or siltstone and occasionally displays cross-beds and pyrite crystals on partings.

In general, unit contains subparallel, crosscutting quartz and calcite veinlets and is typically hornfelsed parallel to contacts with igneous units. From outcrop- to nappe-scale, unit is subisoclinally to isoclinally folded. Correlative with mSs, mSs, mSl, uSl, Ss, and uSsl units of Bundtzen and others (1987). Thickness unknown due to structural repetitions and faulting.

ls - Thinly to very thickly bedded, medium-gray weathering, dark-gray laminated limestone. Generally included as part of Ss unit but locally mapped separately as lSl unit.

g - Medium-grained chlorite-hornblende-augite greenstone.

lSl — LIMESTONE—Thinly laminated, gray limestone that locally marks base of Ss unit; may contain very thin layers of black chert. Correlative with lSl unit of Bundtzen and others (1987). Varies from 0-to 90-ft (0- to 30-m) thick.

SSlsh — BLACK SHALE—Black to dark-gray, locally pyritic shale, siltstone, argillite, phyllite, and very fine grained sandstone in northwest and southwest parts of quadrangle. Includes beds of fine- to medium-grained sandstone and occasional layers of silty limestone. Also includes scattered beds (0- to 2-in. thick; 0- to 5-cm thick) of dark-gray limestone in basal 20 m that overlie silty limestone unit (OCls). Shale unit slightly to intensely sheared and folded. Contains Upper Ordovician to Lower Silurian graptolite-bearing horizons (table 2). In McGrath A-3 Quadrangle, unit is about 800-ft (250-m) thick but is structurally thickened in cores of Middle Fork and North Fork anticlines.

OCls — SILTY LIMESTONE—Very thin to medium (up to 10-in. thick; up to 25-cm thick), lenticular beds of orange-weathering, light-gray silty limestone in northwest and southwest parts of quadrangle; interbedded with thin (0.5- to 2-in. thick; 1-to 5-cm thick) beds of gray siltstone and gray carbonaceous phyllite. Silty laminae commonly cross-bedded in several stacked cosets. Unit rarely cut by calcite veinlets. Generally sheared along limestone-siltstone contacts and siltstone-phyllite partings. Deformed into tight chevron and subisoclinal folds that range from crenulations to nappes. Base of unit not exposed in map area; however, in adjacent quadrangles to southwest, Gilbert (1981) estimated minimum thickness for unit of 3,000 ft (1,000 m).

INTRUSIVE ROCKS

Twg — WINDY FORK GRANITE—White to pink and blue-gray medium- to coarse-grained, hypidiomorphic-granular peralkaline arfvedsonite granite of Windy Fork pluton. Composed of perthite (40 to 60 percent), quartz (25 to 45 percent), and arfvedsonite (5 to 10 percent), with accessory riebeckite (<2 percent); may contain minor plagioclase and red-brown biotite. Accessory minerals include opaque grains, zircon, fluorite, apatite, monazite(?), and carbonate. Presence of uranothorite or thorianite may cause radioactivity to 2,500 cps in Windy Fork pluton (Reed and Miller, 1980). Eudialyte and aegirine-augite occur in veins that cut granite and adjacent country rock. One sample of aegirine-augite from margin of Windy Fork pluton (table 3, site 7) yielded K-Ar age of 23.5 ± 0.7 m.y. Reed and Lanphere (1972) reported K-Ar ages from biotite and hornblende in the Windy Fork pluton of 30.1 ± 0.9 m.y. and 29.0 ± 0.9 m.y., respectively.

Tim — MAFIC DIABASE—Diabase intrusion of the Chip Loy prospect (located in northeast quadrant of map). Composed of unaltered labradorite laths (<50 percent), clinopyroxene (25 percent), tremolite (20 percent), magnetite (3 percent), biotite (1 percent), and apatite (1 percent) (Herreid, 1968). Includes 39-ft (12-m)-thick sulfide-rich zone along iron-stained contact between diabase and phyllitic calcareous sandstone unit (Ss). Sulfide zone consists of pyrrhotite (50 to 70 percent) with minor chalcopyrite, pentlandite, magnetite, and possible bravoite (table 4; W.S. Roberts, written commun., 1984). Age of intrusion uncertain, although assigned to Tertiary on basis of similarities to Tertiary pyrrhotite-rich intrusions in McGrath B-2 Quadrangle (Bundtzen and others, 1982).

Tm — MONZONITE—Medium-grained, hypidiomorphic-granular clinopyroxene-hornblende monzonite that intrudes greenstone unit (MzPzg) in northwest corner of quadrangle. Contains pyroxene (pink in thin section) surrounded by hornblende (35 to 40 percent), labradorite (30 to 40 percent), alkali feldspar (20 to 25 percent), anhedral opaque minerals (3 to 5 percent), minor biotite, and apatite. Secondary minerals include white mica and green amphibole after hornblende.

Tif — FELSIC SILLS AND DIKES—Generally light pink-tan to white, aphanitic to fine-grained felsic sills and dikes to 15-ft (5-m) thick. Commonly altered to and coated with brown-orange gossan.

Tgqm — QUARTZ MONZONITE—Fine- to medium-grained, hypidiomorphic-granular biotite quartz monzonite that composes small plug in northwest corner of quadrangle. Alkali feldspars are perthitic. Hornblende is present in minor amounts. Accessory minerals include zircon, titanite, and apatite. Biotite from K-Ar sample (table 3, site 1) yielded age of 56.6 ± 1.7 m.y. Reed and Lanphere (1972) reported K-Ar age of 56.0 ± 1.6 m.y. from biotite of same intrusion.

MIDDLE FORK PLUTONIC COMPLEX

Tgqm — GRANITE, QUARTZ MONZONITE, AND MONZODIORITE—Fine- to medium-grained, hypidiomorphic-granular biotite- and hornblende-bearing plutonic rocks with variable quartz contents and feldspar ratios; predominantly quartz monzonite and monzodiorite (Streckeisen, 1973). Plagioclase composition ranges from andesine to labradorite; minor clinopyroxene generally present and rimmed by hornblende; locally contains alkali feldspar phenocrysts. Accessory zircon, apatite, and opaque minerals ubiquitous; tourmaline present in some areas. Fine-grained mafic enclaves common; most have wholly igneous texture, though some retain layering of sedimentary origin. Intruded locally by leucocratic veinlets of quartz and alkali feldspar. In places, includes alkali gabbro unit (Tgb) and underlying syenite unit (Tsy). Contact with syenite (Tsy) on peak at 6,375 ft (1,980 m) is sharp and near horizontal. Elsewhere, contact with syenite unit (Tsy) is diffuse, possibly due to mixing of units in semicrystalline state. Three K-Ar samples (table 3, sites 2, 3, and 4) yielded ages of 56.1 ± 1.7 m.y., 56.6 ± 1.7 m.y., and 57.2 ± 1.7 m.y., respectively.

Tgb — ALKALI GABBRO—Dark-green-brown, fine- to medium-grained, subophitic biotite-olivine-pyroxene gabbro. Typically composed of andesine (30 to 55 percent), clinopyroxene (10 to 25 percent), biotite (2 to 30 percent), olivine (5 to 20 percent), and green to brown hornblende after pyroxene (1 to 2 percent). Minor constituents include opaque minerals (1 to 10 percent), alkali feldspar (0 to 5 percent), orthopyroxene (0 to 5 percent), and accessory apatite. Secondary minerals include chlorite, iddingsite, serpentine, actinolite, carbonate, and apophyllite. Crystallization sequence: olivine-pyroxene-plagioclase-biotite-hornblende. Locally layered due to segregation of mafic minerals. Unit commonly intruded by crosscutting leucocratic veinlets of quartz and alkali feldspar, locally in graphic intergrowth, with traces of biotite and opaque minerals. Gabbro typically weathers to brown grus, which forms rounded outcrops. In places, unit includes small bodies of granite, quartz monzonite, and monzodiorite (Tgqm). Layered gabbro in sec. 1, T. 23 N., R. 28 W. intrudes syenite (Tsy) at sharp contact; elsewhere, contacts generally gradational.

Tg — GRANITE—Fine- to coarse-grained, hypidiomorphic-granular granite to quartz syenite of Middle Fork pluton. Color index = < 25. Contains hornblende (0 to 10 percent), clinopyroxene (0 to 10 percent), and biotite (0 to 5 percent), with minor opaque minerals, apatite, and zircon; arfvedsonite and riebeckite present locally. Alkali feldspar generally perthitic and commonly pink in hand specimen. Modal quartz ranges from 10 to 25 percent. Locally contains fine-grained, pyroxene-rich mafic enclaves. Unit typically weathers to white grus.

Tsy — SYENITE—Green-gray, white-gray weathering, medium- to coarse-grained, hypidiomorphic-granular olivine-clinopyroxene syenite of Middle Fork pluton; locally iron stained. Composed of perthitic alkali feldspar (45 to 90 percent), green-brown hornblende after pyroxene (1 to 20 percent), clinopyroxene (3 to 10 percent), plagioclase (3 to 10 percent), olivine with magnetite alteration rims (1 to 7 percent), and interstitial quartz (0 to 10 percent). Minor constituents are biotite (0 to 3 percent), opaque minerals (1 to 2 percent), rutile needles (< 1 percent), apatite (<1 percent), zircon (< 1 percent), fluorite(?), and monazite(?). Secondary minerals include chlorite, carbonate, iddingsite, actinolite, and epidote. Typically forms massive, jointed cliffs. At several localities, includes bedded country rock and plutonic bodies of Tgqm unit.

Tmg — MIDDLE FORK GRANITE—Medium- to coarse-grained, hypidiomorphic-granular peralkaline granite of southeast margin of Middle Fork pluton. Color index = 8 to 10. Middle Fork granite is very similar in mineralogy to Windy Fork granite (Twg) and appears gradational with syenite unit (Tsy). Eudialyte noted in granite talus at two locations. Outcrops typically massive and weather in large blocks. Amphibole from K-Ar samples (table 3, sites 5 and 6) yielded ages of 57.7 ± 1.7 m.y. and 55.6 ± 1.7 m.y., respectively.

Tids — DIKE SWARM—Swarm of subparallel mafic dikes and minor felsic dikes; slivers of Ss are particularly abundant within 1,500 ft (500 m) of Tids-Ss contact. Dikes commonly consist of fine-grained andesine laths, biotite, clinopyroxene (titanaugite in some mafic dikes), olivine, and opaque minerals with pervasive chlorite and carbonate alteration.

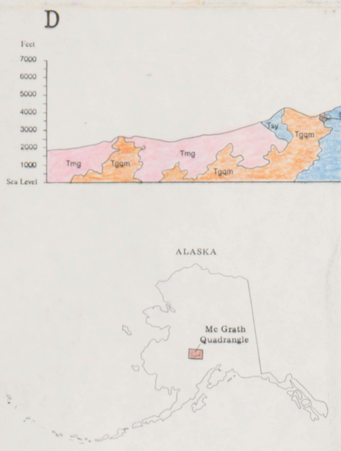

GEOLOGIC MAP OF THE MC GRATH A-3 QUADRANGLE, ALASKA

By

Wyatt G. Gilbert, Diana N. Solie and Jeffrey T. Kline

1988

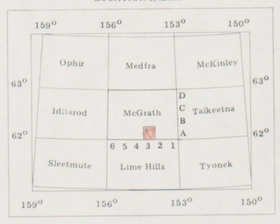

Available from Alaska Division of Geological and Geophysical Surveys, 3700 Airport Way, Fairbanks, 99709, 400 Willoughby Avenue (3rd floor), Juneau, 99801, U.S. Geological Survey, Public Information Office, 701 C Street, Anchorage, 99513, and Information Specialist, U.S. Geological Survey, 4230 University Drive, Rm. 101, Anchorage, 99508. Mail orders should be addressed to the DGGS office in Fairbanks. Cost $5.

154°30'
62°15'
154°00'
62°15'

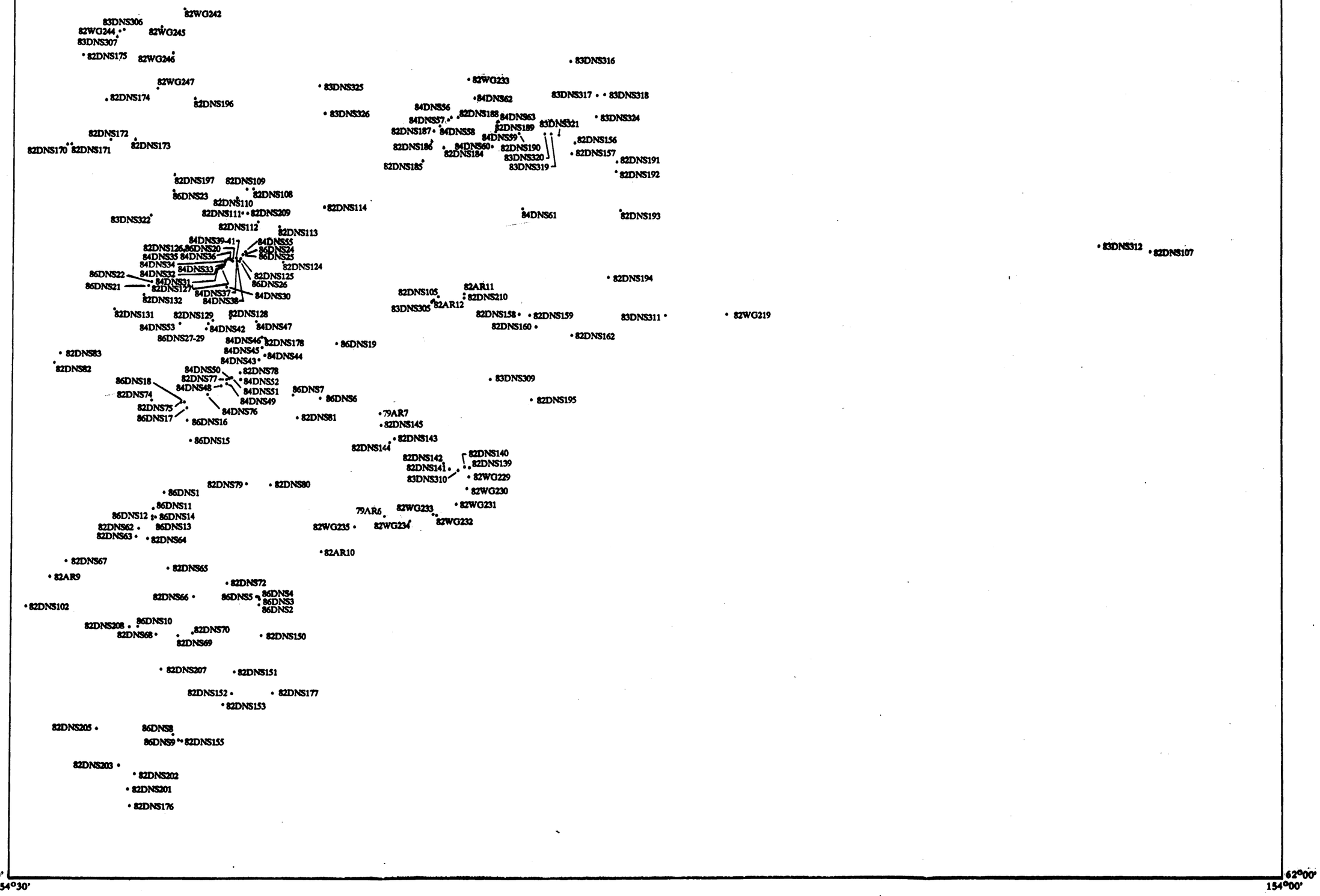

62°00'
154°30'
62°00'
154°00'

MIDDLE FORK PLUTONIC COMPLEX
SAMPLE LOCATION MAP OVERLAY
MC GRATH A-3 QUADRANGLE